**735**

**2019**

# Berichte

zur Polar- und Meeresforschung

**Reports on Polar and Marine Research**

## The Expedition PS118
## of the Research Vessel POLARSTERN
## to the Weddell Sea in 2019

Edited by

Boris Dorschel

with contributions of the participants

**HELMHOLTZ**

*Titel: FS Polarstern in schweren Meereisbedingungen kurz vor dem südlichsten Punkt der Expedition (Foto: Boris Dorschel, AWI).*

*Cover: RV Polarstern in heavy sea ice conditions close to the southern-most position of the Expedition (Photo: Boris Dorschel, AWI).*

# The Expedition PS118
# of the Research Vessel POLARSTERN
# to the Weddell Sea in 2019

**Edited by**
**Boris Dorschel**
**with contributions of the participants**

# PS118

## 9 February 2019 - 10 April 2019

## Punta Arenas (Chile) - Punta Arenas (Chile)



**Chief scientist**
**Boris Dorschel**

**Coordinator**
**Rainer Knust**

# Contents

1

# 1. ÜBERBLICK UND FAHRTVERLAUF

Boris Dorschel                                        AWI

Die Antarktische Halbinsel ist eine der sich am schnellsten erwärmenden Regionen dieser Welt (Bentley et al., 2009; Rignot et al., 2008; Scambos et al., 2000; Vaughan et al., 2003). Als mögliche Folge dessen sind in den Jahren 1995 und 2002 erst der Larsen A Eisschelf und später der Larsen B Eisschelf fast vollständig zerfallen (De Angelis and Skvarca, 2003; Domack et al., 2005; Gutt et al., 2011; Pudsey et al., 2001; Rebesco et al., 2014; Rott et al., 1996; Shepherd et al., 2003; Skvarca and De Angelis, 2003; Wendel and Kumar, 2017). Dadurch verbleibt – als letzter großer Eisschelf im westlichen Weddellmeer – nur noch der Larsen C Eisschelf. Im Juli 2017 hat der Larsen C Eisshelf den Eisberg A68 gekalbt. Mit ca. 5.800 km$^2$ ist A68 einer der größten Eisberge, die jemals erfasst worden sind. Die Verlagerung der Schelfeiskante landwärts hat einen erheblichen Einfluss auf die Umweltfaktoren und Ökosysteme in dem ehemals vom Schelfeis bedeckten Gebiet. Eisschelfe entkoppeln die darunter befindliche Wassersäule und den Meeresboden von dem direkten Einfluss der Atmosphäre und des Sonnenlichts (Gutt et al., 2011). In Folge des Abbruchs von A68 kommt es sowohl zu Austauschprozessen zwischen Ozean und Atmosphäre als auch zur Primärproduktion in der oberen Wassersäule in den vormals von einem Eisschelf bedeckten Gebieten. Diese Veränderungen finden in einem sehr kurzen Zeitraum statt, was zu schnellen Anpassungserscheinungen der Ökosysteme führt.

Das Hauptziel der *Polarstern* Expedition PS118 war das Gebiet, in dem der Eisberg A68 vom Larsen C Eisschelf abgebrochen war, wodurch ein ehemals von Schelfeis bedecktes Gebiet potentiell für die Forschung zugänglich wurde. Das Ziel der Expedition war es, in dem A68 Abbruchgebiet möglichst zeitnah Informationen über verschiedene Basisparameter, wie z.B. Umweltfaktoren und Organismenverteilungen aufzunehmen, um so die Zustände, wie sie unter dem Eisschelf herrschten zu erfassen. Weitere Zielgebiete waren die Bereiche der desintegrierten Eisschelfe Larsen A und B bzw. Canyons auf dem Larsen Kontinentalhang. Als alternative Arbeitsgebiete wurden das Powell- und das Jane-Becken ausgewählt (Abb. 1.1).

Aufgrund der Eisbedingungen gelang es nicht, das Zielgebiet zu erreichen. Auch die alternativen Arbeitsgebiete waren wegen der Eissituation nicht erreichbar. Stattdessen wurden Stationen im nordwestlichen Weddellmeer zwischen Snowhill Island und Joinville Island, im Powell Becken und am westlichen Ende des südwestlichen Scotia Rückens angefahren.

Während PS118 wurden Sediment-, Benthos-, Wasser- und Eisproben gewonnen (Abb. 1.2). Zusätzlich wurden bathymetrische und sedimentakustische Daten aufgezeichnet. Anhand der Proben und Daten sollten Fragestellungen zur Eisschilddynamik, zu Ozean – Kryosphärenwechselwirkungen, Ozeanzirkulation, biologischen Prozessen und einer Vielzahl von Umweltprozessen untersucht werden. Hierzu gehört die Funktion von Ökosystemen, Habitatverteilungen und Populationsdynamiken/-verbreitungen. Die Diversität an Disziplinen wurde auch durch die Expeditionsteilnahme von insgesamt 13 Arbeitsgruppen aus den Wissenschaftsbereichen Bathymetrie/Hydroakustik, Biologie, Geologie, Geophysik, Ozeanographie, Meereisphysik und Meereisbiologie widergespiegelt.

Die Expedition PS118 mit *Polarstern* begann offiziell am 9. Februar 2019 in Punta Arenas und endete am 10. April 2019 ebenfalls in Punta Arenas. Wetterbedingt und durch die Vorgaben

der Hafenbehörden konnte *Polarstern* erst am 18. Februar Punta Arenas verlassen. Am 21. Februar passierte *Polarstern* den Antarktis Sund und gelangte in das Weddellmeer. Dort traf sie auf schwere Eisbedingungen, konnte allerdings trotzdem weiter nach Süden vordringen, und es wurde an dem Ziel festgehalten, das A68 Abbruchgebiet am Larsen C Eisschelf zu erreichen. Am 3. März bei 65°17'S/58°4'W (Abb. 1.1) wurde der Versuch, das Larsen C Eisschelf zu erreichen aufgegeben, da bei einem weiteren Vordringen nach Süden bei den vorherrschenden Eisbedingungen eine pünktliche Rückkehr nach Punta Arenas zum Expeditionsende nicht mehr gewährleistet war.

Auf Grund der Eissituation war es auch nicht möglich, die alternativen Arbeitsgebiete in den Bereichen der ehemaligen Eisschelfe Larsen A und B zu erreichen. Stattdessen wurden Arbeitsgebiete im nordwestlichen Weddellmeer angefahren. In diesen wurden durch Umweltgradienten definierte Benthosstationen beprobt (Abb. 1.2). Nach Abschluss dieser Arbeiten verließ *Polarstern* das Weddellmeer am 16. März durch den Antarctic Sund. Während der verbleibenden Zeit wurden Forschungsarbeiten im Powell Becken und auf dem südwestlichen Scotia Rückens durchgeführt. Am 4. April wurden die Forschungsarbeiten eingestellt, und am 8. April lief *Polarstern* wieder in Punta Arenas ein, wo die Expedition PS118 offiziell am 10. April endete.
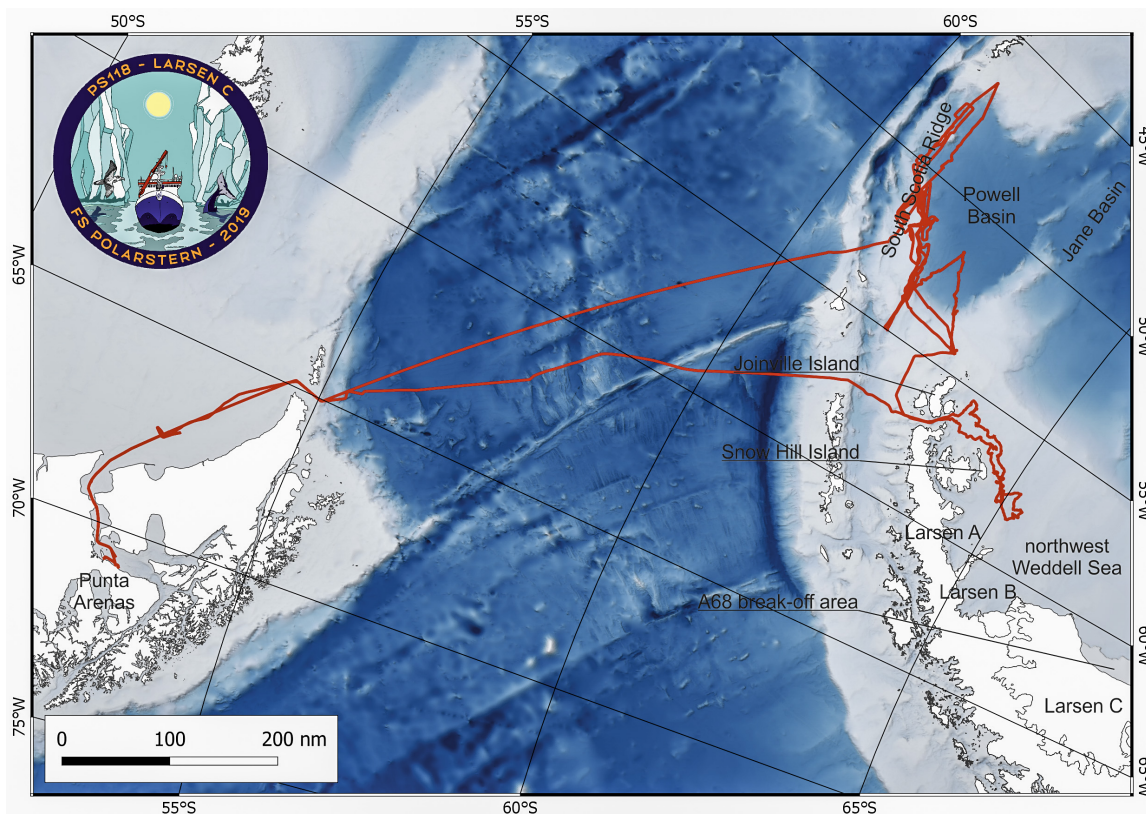


*Abb. 1: Polarstern Expedition PS118 Fahrtverlauf. Siehe https://doi.pangaea.de/10.1594/ PANGAEA.901319 für eine Darstellung des master tracks in Verbindung mit der Stationsliste für PS118*

*Fig. 1: Polarstern Expedition PS118 cruise track. See https://doi.pangaea.de/10.1594/ PANGAEA.901319 to display the master track in conjunction with the list of stations for PS118*
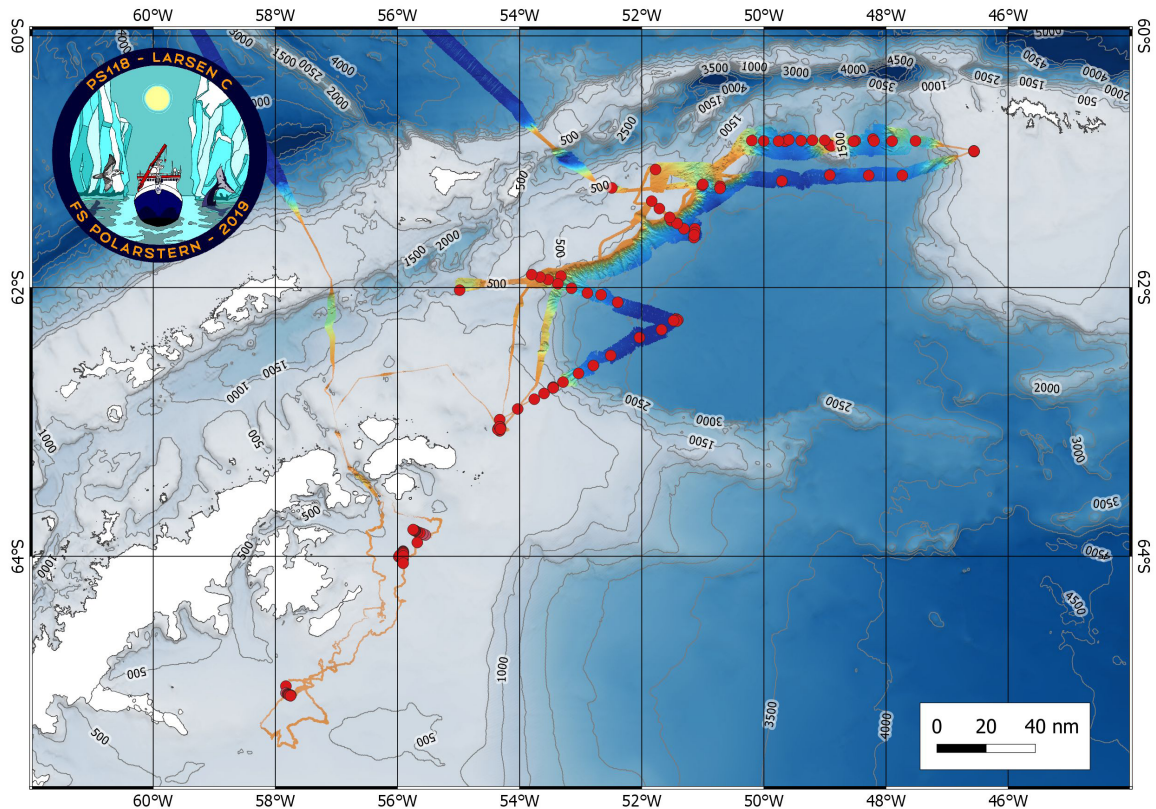
*Abb. 2: Übersicht der Beprobungsstationen. Für detaillierte Informationen siehe Expeditionsbericht.*

*Fig. 2: Overview of sampling sites. See cruise report for detailed information.*

## SUMMARY AND ITINERARY

The Antarctic Peninsula is among the fastest warming regions of the world (Bentley et al., 2009; Rignot et al., 2008; Scambos et al., 2000; Vaughan et al., 2003). The Larsen A and Larsen B ice shelves disintegrated almost entirely in 1995 and 2002, respectively, leaving the Larsen C ice shelf as the last remaining large ice shelf in the west Weddell Sea (De Angelis and Skvarca, 2003; Domack et al., 2005; Gutt et al., 2011; Pudsey et al., 2001; Rebesco et al., 2014; Rott et al., 1996; Shepherd et al., 2003; Skvarca and De Angelis, 2003; Wendel and Kumar, 2017). In July 2017 the Larsen C ice shelf calved iceberg A68, with ca. 5,800 km[2] one of the largest icebergs ever recorded. The resulting landward shift of the ice-edge has a profound effect on environmental factors and ecosystems in the previous ice-shelf covered areas. Ice shelves decouple the underlying water column and seafloor from the direct influence of the atmosphere and sunlight (Gutt et al., 2011). Consequently, the break-off of A68 allows for ocean-atmosphere exchange processes and the penetration of sunlight in the upper water column in the former ice-shelf covered area. These changes happen in a very short time frame triggering a rapid ecosystem response.

The main target area for the *Polarstern* expedition PS118 was the break-off area of A68 in the Larsen C ice shelf, where the retreat of the ice shelf made the seafloor potentially accessible for research. The main goal of the expedition was to collect information on basic parameters, such as environmental factors and organism distribution from the A68 break-off area as early as possible to document under ice shelf conditions. Additional target areas were the Larsen A and B embayment and canyons on the continental slope of the west Weddell Sea. Alternative study areas were Powell and Jane Basin (Fig. 1.1)

Sea ice conditions, however, prevented *Polarstern* from reaching the main target area. Furthermore, it was also impossible to reach the alternative study areas Larsen A and B and the Larsen continental slope. Instead, locations were visited in the northwest Weddell Sea between Snowhill Island and Joinville Island, in the Powell Basin and on the western South Scotia Ridge to collect sediment, benthos, water, and ice samples (Fig. 1.2). For the whole period bathymetric and sediment acoustic data were recorded. Based on samples and data, research questions on ocean-cryosphere interactions, ocean circulation and on a variety of biological and environmental processes were addressed. The diversity in disciplines was reflected by 13 different working groups, from bathymetry/hydroacoustics, biology, geology, geophysics, oceanography, sea ice physics, and sea ice biology that took part in expedition PS118.

Officially, expedition PS118 started in Punta Arenas on 9 February and ended in Punta Arenas on 10 April. Due to weather-related issues and requirements of the harbour authorities, *Polarstern* was only able to leave Punta Arenas on 18 February. On 21 February, *Polarstern* passed through the Antarctic Sound entering the Weddell Sea. There, she encountered heavy sea ice conditions, nevertheless continuing her southward journey to the break-off area of A68 at the Larsen C ice shelf. At 65°17'S/58°4'W (Fig. 1.1), on 3 March, the attempt to reach Larsen C was aborted. It became obvious that a continuation of the southward travel bore the risk of not making it back to Punta Arenas in time. At this stage, the sea ice conditions also ruled out the Larsen A and B embayment as alternative study areas. Instead, sites in the northwest Weddell Sea were visited, where benthic sampling took place along a profile defined by environmental gradients (Fig. 1.2). Once this was completed, *Polarstern* left the Weddell Sea through the Antarctic Sound on 16 March. The remaining research time was spent in the Powell Basin and on the western South Scotia Ridge. On 4 April, all research activities were stopped and *Polarstern* headed for Punta Arenas where she arrived on 8 April. The expedition PS118 officially ended on 10 April.

## References

Bentley MJ, Hodgson DA, Smith JA, Cofaigh CÓ, Domack EW, Larter RD, Roberts SJ, Brachfeld S, Leventer A, Hjort C, Hillenbrand C-D & Evans J (2009) Mechanisms of Holocene palaeoenvironmental change in the Antarctic Peninsula region. The Holocene, 19, 51-69.

De Angelis H & Skvarca P (2003) Glacier Surge After Ice Shelf CollapsE Science, 299, 1560-1562.

Domack EW, Duran D, Leventer A, Ishman S, Doane S, McCallum S, Amblas D, Ring J, Gilbert R & Prentice M (2005) Stability of the Larsen B ice shelf on the Antarctic Peninsula during the Holocene epoch. Nature, 436, 681-685. http://dx.doi.org/10.1038/nature03908

Gutt J, Barratt I, Domack EW, d'Udekem d'Acoz C, Dimmler W, Grémare A, Heilmayer O, Isla E, Janussen D, Jorgensen E, Kock K-H, Lehnert LS, López-Gonzáles P, Langner S, Linse K, Manjón-Cabeza ME, Meißner M, Montiel A, Raes M, Robert H, Rose A, Schepisi ES, Saucède T, Scheidat M, Schenke H-W, Seiler J & Smith CR (2011) Biodiversity change after climate-induced ice-shelf collapse in the Antarctic. Deep Sea Research Part II: Topical Studies in Oceanography, 58, 74-83. http://dx.doi.org/10.1016/Jdsr2.2010.05.024

Pudsey CJ, Evans J, Domack EW, Morris P & del Valle RA (2001) Bathymetry and acoustic facies beneath the former Larsen-A and Prince Gustav ice shelves, north-west Weddell Sea. Antarctic Science, 13, 312-322. https://doi.org/10.1017/S095410200100044X

Rebesco M, Domack EW, Zgur F, Lavoie C, Leventer A, Brachfeld S, Willmott V, Halverson G, Truffer, TA Scambos M, Smith J & Pettit E (2014) Boundary condition of grounding lines prior to collapse, Larsen-B Ice Shelf. Antarctica Science, 345, 1354-1358.

Rignot E, Bamber JL, van den Broeke MR, Davis C, Li Y, van de Berg WJ & van Meijgaard E (2008) Recent Antarctic ice mass loss from radar interferometry and regional climate modelling. Nature Geoscience, 1, 106-110.

Rott H, Skvarca P & Nagler T (1996) Rapid Collapse of Northern Larsen Ice Shelf. Antarctica Science, 271, 788-792.

Scambos TA, Hulbe C, Fahnestock MA & Bohlander J (2000) The link between climate warming and break-up of ice shelves in the Antarctic Peninsula. Journal of Glaciology, 46, 516-530.

Shepherd A, Wingham DJ, Payne T & Skvarca P (2003) Larsen Ice Shelf has progressively thinned. Science, 203, 856-859.

Skvarca P & De Angelis H (2003) Impact assessment of regional climatic warming on glaciers and ice shelves of the northeastern Antarctic Peninsula. Antarctic Research Series, 79, 69-78.

Vaughan DG, Marshall GJ, Connolley WM, Parkinson CL, Mulvaney R, Hodgson DA, King JC, Pudsey CJ & Turner J (2003) Recent Rapid Regional Climate Warming on the Antarctic Peninsula. Climatic Change, 60, 243-274.

Wendel J & Kumar M (2017) Six points of perspective on Larsen C's huge new iceberg EOS 98. https://doi.org/10.1029/2017EO077735

## 2. WEATHER CONDITIONS DURING PS118

Michael Knobelsdorf, Christian.Rohleder          DWD


*09.02.-17.02.2019 Punta Arenas*

During this period, *Polarstern* remained alternately at the pier or on anchor. On Monday morning (18.02.), the pilot came on board and the expedition PS118 of *Polarstern* began.

*18.02. -24.02.*

The first part of the voyage led through the eastern part of the Strait of Magellan into the South Atlantic on course Antarctic Sound with fine weather and moderate westerly winds. After passing Islas Estados and Cape Horn on Tuesday (19.02.), *Polarstern* steamed through the Drake Strait to Antarctica. On Tuesday (19.02.) and Wednesday (20.02.) a storm low of 968 hPa swept across the Cape Horn region towards Falkland Island. It affected *Polarstern* with south-easterly winds of up to 12Bft, with a significant wave height of 7 to 8 m. On Wednesday afternoon (20.02.) the storm subsided, southerly winds of 4 to 5 Bft prevailed. High air pressure expanded with a light to moderate swell of up to 2 m. Until Sunday (24.02.) the high-pressure influence with up to 1,009 hPa continued. Within a weak pressure gradient there were southerly winds of strength 4 to 5 Bft experienced, at times it was calm without any wind. Occasionally there was fog and some snow.

*25.02.-03.03.*

From Monday (25.02.) to Wednesday (27.02.), the sailing area of *Polarstern* was located between high-pressure ridges to the west of the peninsula and an extensive low pressure system in the Weddell Sea. Mostly moderate southerly winds up to 6 Bft were experienced, at times accompanied by some snow and fog patches with light and variable winds. Until Friday (01.03.), a high-pressure ridge over the Drake Passage strengthened to an independent high (1015 hPa) near the Falkland Islands, which extended a ridge (1,005 hPa) into the southern Weddell Sea. Mostly north-easterly winds with 4 to 5 Bft prevailed. The weather changed from Sunday (03.03.) onwards, as a secondary low (985 hPa) approached the working area. In the wake of the low, south-westerly winds of 5 Bft set in.

*04.03.-10.03.*

From Monday (04.03.) to Wednesday (06.03.), the region was influenced by a low (975 hPa) over the Drake Passage. Secondary lows formed, which subsequently moved across the working area. Depending on their locations, north-easterly or south-westerly winds with a maximum wind force of 5 to 6 Bft set in. Mostly good visibility prevailed, at times some snow contributed to the deterioration of visibility. On Thursday (07.03.) and Friday (08.03.), a high-pressure ridge (990 hPa) brought mainly sunny weather with often weak winds in the local area. On Friday afternoon, surprisingly deep stratus passed by. This probably had been formed due to sea smoke over a Polyna about 35 nm away and was driven to us within a north-easterly airflow with the visibility deteriorating. On the weekend (9.03./10.03.), flat depressions passed

north of the working area and brought at times freezing fog and snow at times. Mostly easterly to north-easterly winds of 5 Bft dominated. In the wake of the low-pressure systems, south-westerly winds of 8 Bft built up.

*11.03.-17.03.*

After a storm low crossed the working area on Monday (11.03.), high-pressure conditions followed with sunny weather prevailing. Initial south-westerly winds of 7 to 8 Bft decreased rapidly to 3 Bft. On Wednesday (13.03.) and Thursday (14.03.), a low west of the Antarctic Peninsula provoked north-westerly to westerly winds of up to 7 Bft. From Friday (15.03.) to Sunday (17.03.), storm lows with their associated troughs moved rapidly over the region. The north-westerly wind increased at times to 9 to 10 Bft, in the wake of the respective lows, the wind turned to west to southwest with initially similar wind forces. Snow and rainfall were widespread.

18.03.-24.03.

On Monday (18.03.) and Tuesday (19.03.), a depression passed south of the working area into the Weddell Sea. Thus, north-westerly winds of 7 Bft prevailed, the significant wave height was 3 m at times, accompanied by snow and rain with poor visibility. Subsequently, a weak high-pressure influence set in, accompanied by southerly winds. On Thursday (21.03.), a shallow depression with 985 hPa formed south of the working area. It influenced the weather with westerly to south-westerly winds of 4 to 5 Bft and temporary snow. On the weekend (23/24.03.), high-pressure ridges alternated with shallow depressions. Mostly moderate southerly winds prevailed. On Sunday (24.03.), high-pressure of 1017 hPa brought mostly sunny weather with only weak winds.

*25.03.-31.03.*

On Monday (25.03.) and Tuesday (26.03.), a storm low (984 hPa) swept across the region into the Weddell Sea. The northerly wind increased up to 8 Bft. At times, the visibility was poor due to snow or rain. On Wednesday (27.03.) and Thursday (28.03.), high-pressure ridges alternated with low-pressure systems. In the open water, a sea state developed with a swell of 3 to 4 m. On Friday (29.03.), a secondary low split off from a hurricane vortex (960 hPa) in the Bellingshausen Sea. During the night, the region was hit by a hurricane force low (950 hPa) with 11 Bft winds from the southwest. The wind-sea produced a significant wave height of up to 7 m. As of Saturday (30.03.), the south-westerly winds with a high-pressure ridge moving in rapidly decreased. At the same time, the wind sea dropped significantly. However, the swell increased to 3 to 4 m. On Sunday (31.03.), weak high-pressure dominated with mostly weak southerly winds.

*01.04.-07.04.*

On Monday (01.04.) and Tuesday (02.04.), high-pressure of 996 hPa still dominated over the region. Partly cloudy conditions with a little snowfall and some sunshine prevailed with a swell of 2 to 3 m. On Wednesday (03.04.) and Thursday (04.04.), *Polarstern* was influenced by a storm low (960 hPa) over the southern Drake Passage. The sky was mostly overcast with heavy snowfall and bad visibility due to fog. Subsequently *Polarstern* made her way back through Drake Passage. On Saturday (06.04.), first calm conditions dominated however the trough of a hurricane force low (950 hPa) over the central Drake Passage reached us with a significant wave height building up to 7 m. Hurricane force winds were experienced with 11 to 12 Bft. On Sunday (07.04.), the wind decreased noticeably to 4 to 5 Bft, as a high-pressure area (1015 hPa) spread over to the Strait of Magellan.

On Monday afternoon (08.04.) *Polarstern* entered Punta Arenas with moderate north-easterly winds.

# 3. INTEGRATED MACRO- AND MEGABENTHIC CHARACTERISATION OF THE WEDDELL SEA

Angelika Brandt[1,2], Davide Di Franco[1,2], Huw Griffiths[3], Kerstin Jerosch[4], Marie Verheye[5,6] Filip Volckaert[7], Henrik Christiansen[7] (not on board), Bruno Danis[8] (not on board), Gilles Lepoint[6] (not on board), Katrin Linse[3] (not on board), Isa Schön[5] (not on board), Anton Van de Putte[5] (not on board)

[1] Senckenberg
[2] Goethe University, Frankfurt, Germany
[3] BAS
[4] AWI Bremerhaven
[5] RBINS, Brussels, Belgium
[6] ULg
[7] KU Leuven
[8] ULB, Brussels, Belgium

**Grant-No. AWI_PS118_07**

**Grant-No. AWI_PS118_10**

**Grant-No. AWI_PS118_15**

## Objectives

The Southern Ocean is productive and rich in biodiversity, from the shelf to the deep seafloor, but faces environmental changes that occur at unprecedented rates (see e.g. Meredith, 2005; Gutt et al., 2014; Griffiths et al., 2017; Kaiser et al., 2013) especially in shallow water. Therefore, many organisms that are under threat face the challenge to either adapt or migrate to avoid extinction (Brandt & Gutt, 2011; Ellingsen et al., 2007). Which option is feasible for specific species or populations depends on both abiotic and biotic factors. The latter includes traits that species naturally exhibit (including physiological potential to cope with environmental changes and mobility), the potential to change these traits in a given population over time (adaptation) and the interplay between species for example through predation and competition. Biodiversity assessments throughout the animal phyla can be used as benchmark studies against which changes in the ecosystem can be measured (e.g. Linse et al., 2007).

It is therefore important to assess biodiversity at all levels, from species to populations to ecosystems. We therefore focus on:

- Biodiversity census data at the species level. Occurrence data form an important baseline for spatial and temporal comparisons and any work that builds on such data (cf. associated research projects of M. Holtappels, D. Piepenburg, A. Purser, C. Richter and U. Webb).

- Genomic diversity at the population level

- Trophic diversity at the ecosystem/community level

In the overarching objective of improving the understanding of the distribution and (genetic and trophic) diversity of marine Antarctic fauna, as well as how these might change in the future, we perform the following complementary analyses:

- Integrative taxonomy: specimens of the target taxa are identified morphologically to species level (whenever possible). In addition, as species identity can be difficult to establish based on morphology only, increasingly standard molecular techniques (e.g.

"barcoding" or the sequencing of other gene fragments depending on the scientific question) is used to facilitate identification to species level (Grant et al., 2010; Riehl et al., 2014).

- Genomics: as a single species is not necessarily a homogenous, invariable unit, but mostly comprised of different individuals and populations with differing genetic background and spatial connections (Volckaert et al., 2012), we employ state of the art genomic methods to characterize the population genetic status, the identification of species ranges, sympatric or allopatric distributions and the direction of gene-flow between populations of selected species (connectivity).

- Ecology: (i) General ecology: we identify functional groups of selected taxa by means of morphological analyses of mouthparts, as well as gut content analyses, for the assessment of dietary preferences and adaptations to potential shifts in the occurrence of species. (ii) Trophodynamics: in addition we apply stable isotope analyses to determine trophic niche width, plasticity and overlap of the same taxa (as in e.g. Michel et al., 2016). (iii) Community analyses helps us understand turnover, succession and which groups dominate in areas characterized by different environmental conditions.

The analyses are embedded into the SCAR-AntEco (State of the Antarctic Ecosystem) and Ant-ERA (Antarctic Thresholds - Ecosystem Resilience and Adaptation) programs. A focus of the ongoing projects is peracarid crustaceans (especially isopods and amphipods). Moreover, the Belgian research projects, vERSO and RECTO (Belgian Science Policy), focus particularly on Antarctic target species across the animal kingdom: birds (*Pagodroma* spp.), fish (Notothenioidei), starfish (Asteroidea), feather stars (Crinoidea), and crustaceans (Amphipoda and Ostracoda).

**Work at sea**
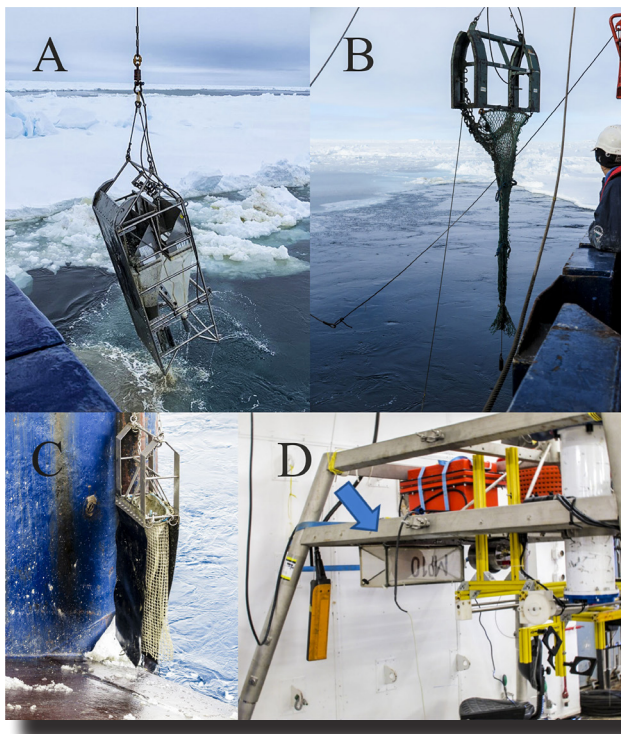


*Fig. 3.1: Sampling gear: A. Epibenthic sledge, B. Agassiz trawl, C. Rauschert dredge and D. Amphipod traps attached to the underside of the lander's platform (photo credits: H. Griffiths, F. Volckaert and M. Verheye).*

At each station a preliminary site exploration was organised with the Ocean Floor Observation and Bathymetry System (OFOBS), including video, high-resolution photo and bathymetry information (see Seabed Habitat Mapping - Chapter 11)

Four types of gear were used to collect benthic animals: the Agassiz trawl (AGT) with a mesh size of 1 cm and a mouth width of 2 m, the Rauschert dredge with a mesh size of 1 mm (RD), the epibenthic sledge (EBS), consisting of a supra- and an epinet with a mesh size of 300 µm, and an amphipod trap (AT) (Fig. 3.1).

All gear was deployed in a standardized way, in order to allow the best possible comparability across expeditions. The deployment of the EBS followed that described by Brenke (2005). The AGT was deployed in a similar way, but with slightly more speed when deploying in order to avoid the net to flip over the frame of the trawl. The RD was attached with a cable behind the AGT for each deployment.

The AGT (with attached RD) and the EBS were deployed at a total of 5 stations (6, 9, 12, 38 & 77) for a duration of 5 to 10 min per trawl, with 1 or 2 EBS and up to 3 AGT-RD replicates at each station (Fig. 3.2 and Tab. 3.1). Deployment of the AT was opportunistic as the original planned method of deployment was not possible because it would have required good weather and ice free conditions with depths of less than 500 m. The traps were instead attached on the platform of the lander system (see Bentho-pelagic processes – Chapter 6) at station 38 (Tab. 3.1).
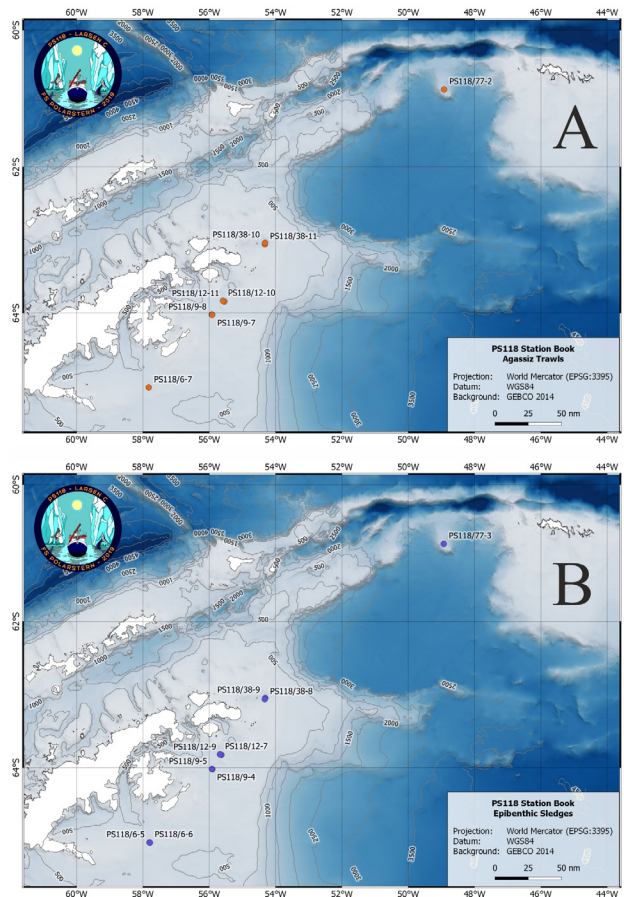


*Fig. 3.2: Maps of all sampling events of the a) Agassiz trawl coupled with the Rauschert dredge and b) Epibenthic sledge (credit: S. Dreutter)*

**Tab. 3.1:** List of the sampling stations in the Weddell Sea and Powell Basin with indication of Longitude, latitude, Epibenthic Sledge (EBS), Agassiz Trawl (AGT), Rauschert Dredge (RD) and Amphipod Trap (AT). Duration: * 5 min; ** 10 min; *** 4 days.

| PS118 # | Station | Lat Lon | Depth [m] | EBS | AGT | RD | AT |
|---|---|---|---|---|---|---|---|
| 1 | 6 | 64°57'S; 57°50'W | 430 | 6-5, 6-6 | 6-7* | 6-7* | |
| 2 | 9 | 64°01'S; 55°54'W | 405 | 9-4, 9-5 | 9-6* (failed), 9-7**, 9-8* | 9-6* (failed), 9-7**, 9-8* | |
| 3 | 12 | 63°50'S; 55°36'W | 411-434 | 12-9 | 12-10**, 12-11* | 12-10**, 12-11* | |
| 4 | 38 | 63°04'S; 54°19'W | 416-427 | 38-8, 38-9 | 38-10*, 38-11* | 38-10*, 38-11* | 38-6 Lander recovered*** |
| 5 | 77 | 60°52'S; 48°56'W | 1035-1048 | 77-3** | 77-2** | 77-2** (failed) | |

When the catch was on deck, it was photographed, and sieved when required (Fig. 3.3). The EBS catches were sieved with a mesh size of 300 μm and/or directly transferred into precooled (-20°) 96 % ethanol, following Riehl (2014). The AGT catch was sieved with a mesh size of 1 mm and sorted to major taxa, which were each weighed and directly stored in 96 % precooled ethanol or frozen (the latter in preparation for stable isotope analyses). The RD catch was sieved with mesh sizes of 500 μm and 300 μm in succession, and immediately transferred to a tub of 96% ethanol. All ethanol-preserved samples were stored at -20°C for at least 48 h before further processing, to avoid DNA degradation.
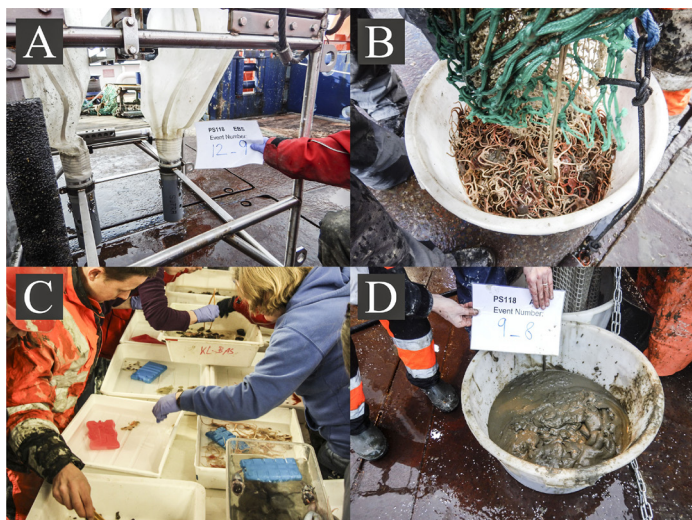


*Fig. 3.3: Photographs of the sorting of macro- and megabenthos on deck of Polarstern. A. EBS sample ready to collect; B. AGT sample being collected; C. sorting of AGT sample and D. RD ready to collect (photo credits: A. Brandt and H. Griffiths).*

In the laboratory, selected ethanol-preserved specimens were further sorted to species, genus or class level (depending on time, taxa and available taxonomic expertise on board) and counted. Examples of typical macro- and megafauna found in the catches are presented in Fig. 3.4. These basic biodiversity data will be shared with the other biology groups, facilitating the creation of a comprehensive biodiversity dataset for the entire expedition, which all users can build upon for further in-depth studies.
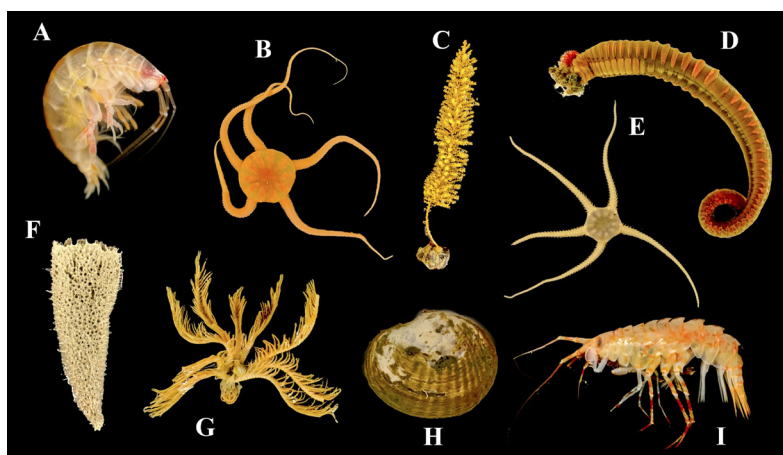


*Fig. 3.4: Representative macro- and megabenthos collected with the AGT. A: Amphipoda, Ampeliscidae B: Ophiuroidea, Ophionotus victoriae C: Polinoida; D: Polychaeta; E: Ophiuroidea; F: Porifera; G: Crinoidea; H: Bivalvia; I: Amphipoda, Eusiridae (photo credit: H. Griffiths).*

Some target taxa were processed further in view of future work:

- Amphipods: tissue samples (pleopods) of target taxa (Eusirus, Epimeria, Iphimediidae) have been taken for further DNA analyses

- Fishes: detailed ancillary data (pictures in lateral view, length, weight, sex, maturity) were collected. A tissue sample was taken (fin clip) and preserved in absolute ethanol for further DNA analysis. A muscle biopsy was taken for isotope analysis and directly frozen. The entire stomach was isolated and frozen for prey identification with DNA barcoding. The gill chamber was dissected and stored in ethanol for further extractions of parasites (Platyhelminthes). The gonad was preserved in a Dietrich solution for further histological examination.

Other sorted and preserved target taxa will be dispatched to project partners not on board, for further analyses later from the home laboratories.

High quality contextual environmental data are indispensable for statistical analyses aiming to evaluating potential drivers of genetic or trophic diversity. Here we will depend on the oceanographic work conducted during current and previous *Polarstern* expeditions. Subsequent laboratory procedures (DNA-sequencing, morphological and gut content analyses, stable isotope analyses…) and statistical analyses are foreseen at the respective institutions in Belgium, Germany and the UK.

**Preliminary (expected) results**

Ice conditions in the western Weddell Sea determined our sampling schedule to such an extent that sites were reorganized between 65° and 61°N. Generally, stations at 500 m depth were characterized by fine mud, while the 1,000 m station showed a pebbles on fine sediment (Tab. 3.2). All stations were located in sites with cold (approximately -1.8°C) Weddell Sea shelf or bottom water.

Epibenthic sledge: All supranets from 4 of the 5 stations were fully sorted (station 77 was sampled too near to the end of the expedition with no time to sort the samples), as well as two epinet samples. A total of 39,291 individuals of 35 taxa were sorted (some examples are given in Fig. 3.5). Of the identified taxa, Copepoda Calanoidea were the most frequent with 15,820 (41 %) individuals; followed by Cumacea (4,276, 11 %); Polychaeta (3,551, 9 %); Isopoda (3,384, 9 %) and Euphausiacea (2,887, 7 %) (Fig. 3.6; Tab. 3.2). As expected more typical suprabenthic organisms (e.g. calanoid copepods and euphasiaceans) were usually caught in the supranet, whereas the epinet caught more epi- and inbenthic invertebrates such as polychaetes, crustaceans and bivalves. Considering the supranet data only, station 38 was most abundant in terms of number
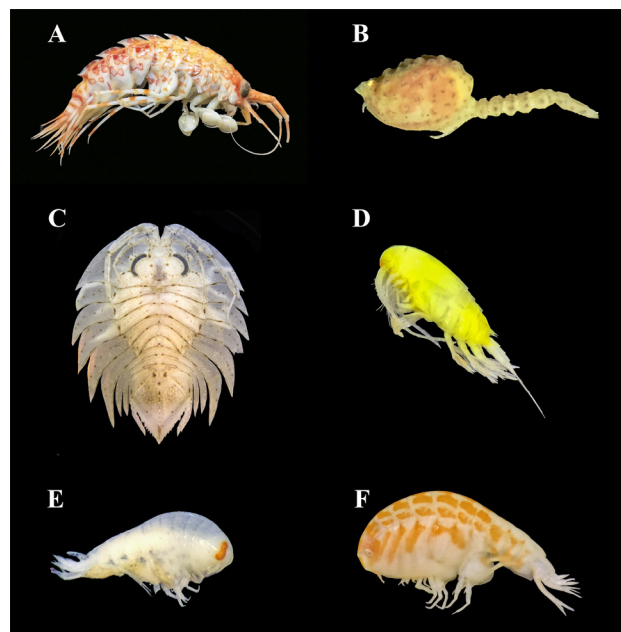


*Fig. 3.5: Photographs of representative crustaceans collected with the EBS. A: Amphipoda, Eusirus perdentatus; B: Cumacea, Campylaspidae; C: Serolidae, Ceratoserolis trilobitoides; D: Calanoida, Calanus sp.; E: Amphipoda, Lysianassidae; F: Amphipoda, Stegocephalidae (photo credit: D. Di Franco).*

of individuals (11,725) but had the lowest diversity, whereas station 9 yielded the lowest number of individuals (4,390) but had the highest diversity with a total of 25 taxa identified so far.
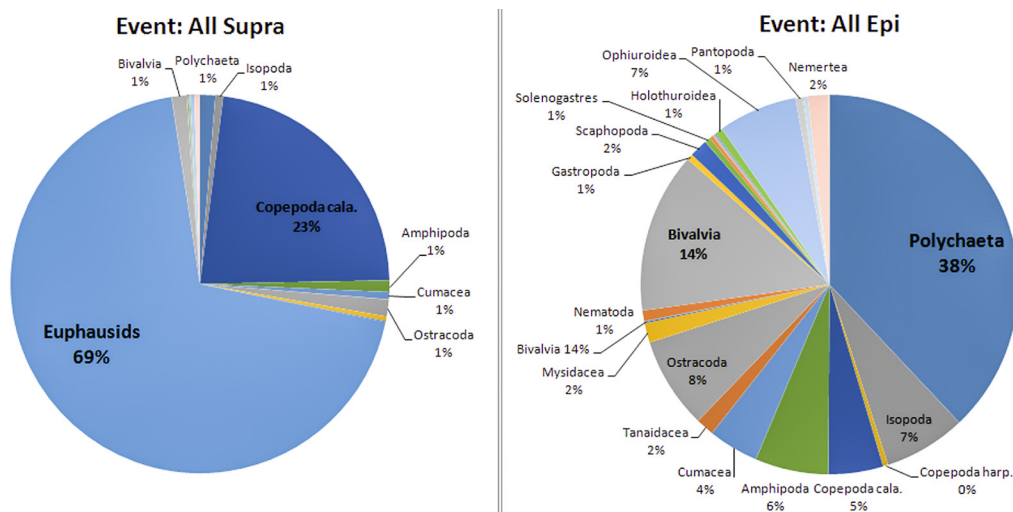


*Fig. 3.6: Pie chart of the taxa collected with the EBS in the supra- and epinet.*

*Agassiz trawl*

On each AGT deployment, mega- and macrobenthic biodiversity samples were collected. A total of 4774 individuals belonging to 11 phyla were sampled. Arthropoda were the most abundant (39.5 %), followed by Echinodermata (36 %), Mollusca (13.8 %), Annelida (5.3 %) and fishes (2.6 %) (Fig. 3.7; Tab. 3.2). The majority of the samples were collected at during event 12_10 (a 10 min trawl), during which 43.2% of the total number of individuals were collected. Trawl 12_11 (a 5 min trawl) collected 20.7%. At all other stations, less than 10 % of the total number of specimens were collected.
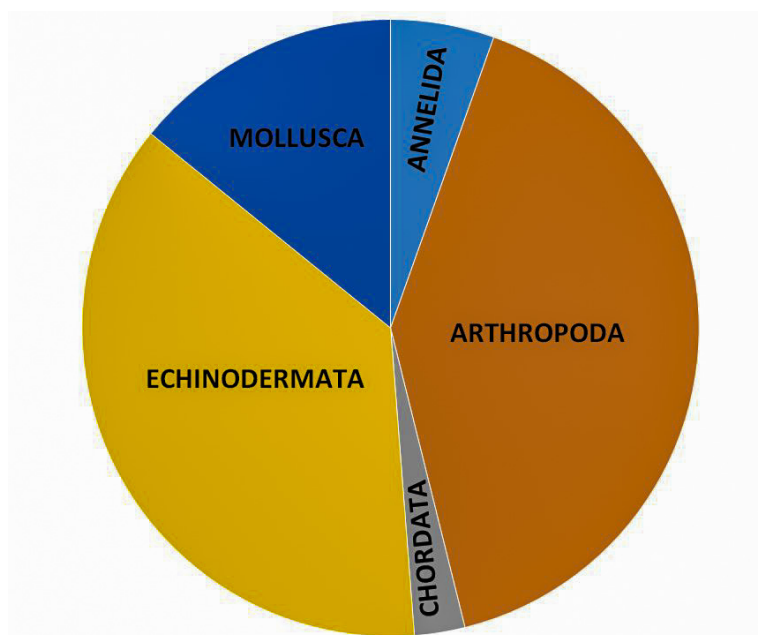


*Fig. 3.7: Pie chart of the taxa present at >1% of the individuals collected with the AGT.*

In total 51 fish were caught, most of them in the AGT at stations 12 and 77, and occasionally in the EBS. At least eleven species of the families Nototheniidae of the subfamily Pleuragramminae (*Pleuragramma antarctica*), Trematominae (e.g. *Trematomus scottii, T. bernachii* and *Lepidonotothen* sp.), Artedidraconinae (*Pogonophryne* sp.), Channichthyinae (e.g. *Champsocephalus gunnari* and *Cryodraco antarcticus*), Zoarcidae, Liparidae (*Paraliparis antarcticus*), and Macrouridae (*Marcrourus caml*) were collected.

*Rauschert dredge*

The coarse fractions (sieved with 500 μm mesh size) of the RD were completely sorted, for 4 out of the 5 stations (events # 6-7, 9-7, 9-8, 12-10, 12-11 and 38-11). The first sample (6-7) being relatively poor in organisms, both fractions (500 and 300 μm) were sorted completely under the microscope. In the coarse fraction (500 μm) of event 38-11, many ostracods were observed. As this is a taxon of specific interest, this fraction was completely sorted under the microscope. A total of 3,976 individuals belonging to 22 taxa were sorted, excluding Polychaeta for which we estimated >2,500 individuals were present. The second most abundant taxon in our sample, after the Polychaeta, was the Ostracoda with 979 individuals (24.6 % of total number of specimens), followed by Cumacea (19.3 %), Bivalvia (14.9%), Ophiuroidea (12.6 %), Foraminifera (9.6 %) and Amphipoda (5.9 %). All remaining taxa accounted for less than 5 % of the total number of specimens.

*Amphipod trap*

More than 1,000 amphipods of the superfamily Lysianassoidea were collected with two amphipod traps baited with pieces of fish and attached on the underside of the lander for 5 days.

All these biodiversity samples will contribute to the major research questions we have about taxonomy, ecology, genetic population structure, connectivity, adaptive potential, trophic plasticity, and niche partitioning.

**Tab. 3.2:** Characteristics of the five sampling stations by sediment type and key macro- and megabenthic organisms.

| # | Station | Sediment | Key organisms |
|---|---------|----------|---------------|
| 1 | 6 | Fine mud | Polychaetes, bivalves, ophiuroids, cnidarians |
| 2 | 9 | Fine mud | Gastropods, ophiuroids, polychaetes, scaphopods |
| 3 | 12 | Fine mud | Ophiuroids (dominant), mysids, decapods, isopods, amphipods, Nototheniidae fishes |
| 4 | 38 | Fine mud (anoxic) | Bivalves, scaphopods, ophiuroids, polychaetes, nemerteans - generally at a low diversity |
| 5 | 77 | Pebbles on mud | Ophiuroids, ascidians, holothurians |

**Data management**

Macro- and megabenthic identifications will be deposited in suitable SCAR databases (e.g. Biodiversity.aq) and linked to the World Data Center PANGAEA Data Publisher for Earth & Environmental Science (www.pangaea.de). Genetic data will be deposited in appropriate online databases (BOLD – The Barcode of Life Data System; SRA – The Sequence Read Archive of NCBI).

Samples will be physically stored at the Royal Belgian Institute of Natural Sciences (RBINS, B), the Senckenberg Institute (D) and the British Antarctic Survey (BAS, UK).

**References**

Brandt A & Gutt J (2011) Biodiversity of a unique environment: the Southern Ocean benthos threat by climate change. In: Zachos, F. & J. C. Habel, Biodiversity hotspots, 25, pp. 503-526, Springer Publishers, Heidelberg. DOI 10.1007/978-3-642-20992-5.

Brökeland W, Choudhury M & Brandt, A (2007) Composition, abundance and distribution of Peracarida from the Southern Ocean deep sea. Deep-Sea Research II, 54: 1752-1759.

Brenke N (2005) An epibenthic sledge for operations on marine soft bottom and bedrock. Marine Technological Society Journal, 39, 10–21.

Ellingsen K, Brandt A, Hilbig B & Linse K (2007) The diversity and spatial distribution of polychaetes, isopods and bivalves in the Atlantic sector of the deep Southern Ocean. Polar Biology, 30, 1265-1273.

Grant RA, Griffiths HJ, Steinke D, Wadley V & Linse K (2010) Antarctic DNA barcoding; a drop in the ocean? Polar Biology, 34, 775–780.

Griffiths HJ, Meijers AJS & Bracegirdle TJ (2017) More losers than winners in a century of future Southern Ocean seafloor warming. Nature Climate Change, 7, 749–754.

Gutt J, Bertler N, Bracegirdle T, Buschmann A, Comiso J, Hosie G, Isla E, Schloss IR, Smith CR, Tournadre J & Xavier JC (2014) The Southern Ocean ecosystem under multiple climate change stresses - an integrated circumpolar assessment. Global Change Biology, 21, 1434–1453.

Kaiser S, Brandão SN, Brix S, Barnes DKA, Bowden D, Ingels J, Leese F, Linse K, Schiaparelli S, Arango C, Bax N, Blazewicz-Paszkowycz M, Brandt A, Catarino AI, Danis B, David B, De Ridder C, Dubois P, Ellingsen KE, Glover A, Griffiths HJ, Gutt J, Halanych K, Havermans C, Held C, Janussen D, Lörz A-N, Pearce D, Pierrat B, Riehl T, Rose A, Sands CJ, Soler i Membrives A, Schüller M, Strugnell J, Vanreusel A, Veit-Köhler G, Wilson N & Yasuhara M (2013) Pattern, process and vulnerability of Southern Ocean benthos - a decadal leap in knowledge and understanding. Marine Biology, 160, 2295-2317.

Linse K, Brandt A, Bohn J, Danis B, De Broyer C, Heterier V, Hilbig B, Janussen D, López González PJ, Schwabe E & Thomson M (2007) Macro- and megabenthic communities in the abyssal Weddell Sea (South Atlantic). Deep-Sea Research II, 54:1848–1863.

Meredith MP (2005) Rapid climate change in the ocean west of the Antarctic Peninsula during the second half of the 20th century. Geophysical Research Letters, 32,1-5.

Michel LN, David B, Dubois P, Lepoint G & De Ridder C (2016) Trophic plasticity of Antarctic echinoids under contrasted environmental conditions. Polar Biology, 39, 913–923.

Riehl T, Brenke N, Brix S, Driskell A, Kaiser S & Brandt A (2014) Field and laboratory methods for DNA studies on deep-sea isopod crustaceans. Polar Research, 35, 205–226.

Volckaert FAM, Rock J & Van de Putte AP (2012) Connectivity and molecular ecology of Antarctic fishes. In: Adaptation and Evolution in Marine Environments, Volume 1 (eds. di Prisco G & Verde C), 75–96. Springer, Berlin.

# 4. DIPLONEMIDS: AN EMERGING MAJOR PLAYER AMONG PLANKTONIC MICROEUKARYOTES

Olga Flegontova[1]
Pavel Flegontov[2] (not on board), Ales Horak[1] (not on board), Julius Lukes[1] (not on board)

[1]Czech Academy of Sciences
[2]University of Ostrava

## Objectives

Until recently, biodiversity of marine microeukaryotes (protists) remained understudied, as compared to that of bacteria and macroscopic organisms. This situation has changed with the advent of metabarcoding techniques, the development of universal eukaryotic primers and finding the most informative gene regions. Recent studies have mapped protist biodiversity on the global scale: de Vargas et al. (2015), Massana et al. (2015), Pernice et al. (2016), among others. A large set of metabarcodes (the V9 region of the 18S rRNA gene) was generated for planktonic eukaryotes by the Tara Oceans project (de Vargas et al., 2015). Unexpectedly, in that dataset diplonemids emerged among the most abundant and diverse (i.e. rich in operational taxonomic units, OTUs) clades of eukaryotes in the plankton. Diplonemids (Diplonemea) used to be a very small and obscure group of protists, belonging to the Euglenozoa phylum, alongside with much better studied kinetoplastids and euglenids. Diplonemids are marine heterotrophs of unknown lifestyle and include just few formally described genera (Tashyreva et al., 2018). We analyzed an extended Tara Oceans metabarcoding dataset (850 size-fractionated plankton communities sampled at 123 globally distributed sites) and revealed that diplonemids surpass all other eukaryotic phyla in diversity and are among the most abundant phyla in the mesopelagic zone (Flegontova et al., 2016). Members of by far the most diverse diplonemid family Eupelagonemidae (also known as deep-sea pelagic diplonemids or the DSPD I clade, Lara et al., 2009) remain uncultured, and their trophic mode remains unknown (Gawryluk et al., 2016). We believe that diplonemids experienced a relatively recent speciation burst, potentially via neutral speciation mechanisms (Suzuki & Chiba, 2016), after entering a new ecological niche.

During PS118, the key objective of our study was the biogeography and diversity of diplonemids and other microbial eukaryotes in the Southern Ocean. Based on our previous studies, we know that diplonemids are especially abundant in the mesopelagic and deeper layers, and that they range in size from about 1 to 20 μm.

During the cruise, we collected numerous samples for later laboratory analysis aimed at:

1. studying the distribution of diplonemids within the bathypelagic zone (1,000-4,000 m), an understudied region at present;

2. constructing detailed depth profiles of abundance, OTU richness and community structure (surface to bottom) by sampling nearby locations;

3. obtaining independent estimates of relative abundance for diplonemids using the metabarcoding and fluorescent in situ hybridization (FISH) approaches.

**Work at sea**

We collected 110 planktonic DNA samples (Tab. 4.1) and 65 samples of fixed cells (Tab. 4.2) on 0.8 μm filters, both coming from the 0.8-20 μm size fraction. The samples were collected at 17 stations, at depths ranging from 40 m to 3,300 m, with up to 17 samples collected per station, and with approximate depth spacing steps of 200 m. Each planktonic sample was collected using a 12 l Niskin bottle fired at a predetermined depth by the oceanographic team (See section 9). For DNA analysis, 10 l of seawater per sample were filtered through a system of two filters (20 and 0.8 μm) using a Cole-Palmer Masterflex benchtop peristaltic pump. The finer filters (0.8 μm) were preserved in a cell lysis buffer and stored at 0°C for subsequent metabarcoding analysis. For FISH analysis, 400 ml of water per sample were filtered through a 20 μm filter and diluted with formaldehyde to a final concentration of 1 % formaldehyde, stored for 24 hours at 0°C, and than filtered through a 0.8 μm filter. The filters were dried and stored at -20°C for subsequent FISH analysis.

**Tab. 4.1:** Table showing locations and depths of samples to be returned for DNA analysis

| Sample | Station | Date | UTC time | Latitude | Longitude | Depth [m] |
|---|---|---|---|---|---|---|
| 1 | PS118_004_1 | 2019-02-22 | 18:47:58 | 63°49.17'S | 056°28.38'W | 500 |
| 2 | PS118_004_1 | 2019-02-22 | 18:53:17 | 63°49.17'S | 056°28.38'W | 300 |
| 3 | PS118_004_1 | 2019-02-22 | 18:58:43 | 63°49.17'S | 056°28.38'W | 100 |
| 4 | PS118_005_1 | 2019-03-04 | 15:34:10 | 64°59.05'S | 057°44.90'W | 350 |
| 5 | PS118_005_1 | 2019-03-04 | 15:37:23 | 64°59.05'S | 057°44.90'W | 250 |
| 6 | PS118_005_1 | 2019-03-04 | 15:40:25 | 64°59.05'S | 057°44.90'W | 150 |
| 7 | PS118_006_1 | 2019-03-05 | 12:25:40 | 64°58.80'S | 057°46.63'W | bottom |
| 8 | PS118_006_1 | 2019-03-05 | 12:26:38 | 64°58.80'S | 057°46.63'W | 400 |
| 9 | PS118_006_1 | 2019-03-05 | 12:29:12 | 64°58.80'S | 057°46.63'W | 300 |
| 10 | PS118_006_1 | 2019-03-05 | 12:32:00 | 64°58.80'S | 057°46.63'W | 200 |
| 11 | PS118_006_1 | 2019-03-05 | 12:34:35 | 64°58.80'S | 057°46.63'W | 100 |
| 12 | PS118_008_2 | 2019-03-11 | 16:38:57 | 63°59.98'S | 055°54.40'W | bottom |
| 13 | PS118_008_2 | 2019-03-11 | 16:46:42 | 63°59.98'S | 055°54.40'W | 300 |
| 14 | PS118_008_2 | 2019-03-11 | 16:50:30 | 63°59.98'S | 055°54.40'W | 200 |
| 15 | PS118_008_2 | 2019-03-11 | 16:55:01 | 63°59.98'S | 055°54.40'W | 100 |
| 16 | PS118_010_1 | 2019-03-13 | 11:55:55 | 64°00.17'S | 055°58.57'W | bottom |
| 17 | PS118_010_1 | 2019-03-13 | 11:59:00 | 64°00.17'S | 055°58.57'W | 300 |
| 18 | PS118_010_1 | 2019-03-13 | 12:01:56 | 64°00.17'S | 055°58.57'W | 200 |
| 19 | PS118_010_1 | 2019-03-13 | 12:04:23 | 64°00.17'S | 055°58.57'W | 100 |
| 20 | PS118_011_1 | 2019-03-13 | 18:36:45 | 63°54.00'S | 055°40.56'W | 200 |
| 21 | PS118_011_1 | 2019-03-13 | 18:40:00 | 63°54.00'S | 055°40.56'W | 100 |
| 22 | PS118_012_1 | 2019-03-14 | 07:03:11 | 63°48.34'S | 055°44.73'W | bottom |
| 23 | PS118_012_1 | 2019-03-14 | 07:04:44 | 63°48.34'S | 055°44.73'W | 400 |
| 24 | PS118_012_1 | 2019-03-14 | 07:08:33 | 63°48.34'S | 055°44.73'W | 300 |
| 25 | PS118_012_1 | 2019-03-14 | 07:11:02 | 63°48.34'S | 055°44.73'W | 200 |
| 26 | PS118_012_1 | 2019-03-14 | 07:14:17 | 63°48.34'S | 055°44.73'W | 100 |
| 27 | PS118_013_1 | 2019-03-17 | 11:32:24 | 63°04.09'S | 054°18.76'W | bottom |
| 28 | PS118_013_1 | 2019-03-17 | 11:37:54 | 63°04.09'S | 054°18.76'W | 300 |
| 29 | PS118_013_1 | 2019-03-17 | 11:40:36 | 63°04.09'S | 054°18.76'W | 200 |

| Sample | Station | Date | UTC time | Latitude | Longitude | Depth [m] |
|--------|---------|------|----------|----------|-----------|-----------|
| 30 | PS118_013_1 | 2019-03-17 | 11:43:33 | 63°04.09'S | 054°18.76'W | 100 |
| 31 | PS118_015_2 | 2019-03-18 | 19:01:02 | 62°01.00'S | 054°59.51'W | bottom |
| 32 | PS118_015_2 | 2019-03-18 | 19:08:10 | 62°01.00'S | 054°59.51'W | 1200 |
| 33 | PS118_015_2 | 2019-03-18 | 19:12:39 | 62°01.00'S | 054°59.51'W | 1000 |
| 34 | PS118_015_2 | 2019-03-18 | 19:18:04 | 62°01.00'S | 054°59.51'W | 800 |
| 35 | PS118_015_2 | 2019-03-18 | 19:22:29 | 62°01.00'S | 054°59.51'W | 600 |
| 36 | PS118_015_2 | 2019-03-18 | 19:27:04 | 62°01.00'S | 054°59.51'W | 400 |
| 37 | PS118_015_2 | 2019-03-18 | 19:32:28 | 62°01.00'S | 054°59.51'W | 200 |
| 38 | PS118_015_2 | 2019-03-18 | 19:36:09 | 62°01.00'S | 054°59.51'W | 55 |
| 39 | PS118_020_1 | 2019-03-19 | 07:10:53 | 61°59.86'S | 053°09.52'W | bottom |
| 40 | PS118_020_1 | 2019-03-19 | 07:15:10 | 61°59.86'S | 053°09.52'W | 2000 |
| 41 | PS118_020_1 | 2019-03-19 | 07:19:56 | 61°59.86'S | 053°09.52'W | 1800 |
| 42 | PS118_020_1 | 2019-03-19 | 07:25:07 | 61°59.86'S | 053°09.52'W | 1600 |
| 43 | PS118_020_1 | 2019-03-19 | 07:29:37 | 61°59.86'S | 053°09.52'W | 1400 |
| 44 | PS118_020_1 | 2019-03-19 | 07:34:50 | 61°59.86'S | 053°09.52'W | 1200 |
| 45 | PS118_020_1 | 2019-03-19 | 07:39:34 | 61°59.86'S | 053°09.52'W | 1000 |
| 46 | PS118_020_1 | 2019-03-19 | 07:44:22 | 61°59.86'S | 053°09.52'W | 800 |
| 47 | PS118_020_1 | 2019-03-19 | 07:49:11 | 61°59.86'S | 053°09.52'W | 600 |
| 48 | PS118_020_1 | 2019-03-19 | 07:54:22 | 61°59.86'S | 053°09.52'W | 400 |
| 49 | PS118_020_1 | 2019-03-19 | 07:59:01 | 61°59.86'S | 053°09.52'W | 200 |
| 50 | PS118_020_1 | 2019-03-19 | 08:02:23 | 61°59.86'S | 053°09.52'W | 60 |
| 51 | PS118_024_4 | 2019-03-20 | 09:56:20 | 62°14.54'S | 051°25.52'W | bottom |
| 52 | PS118_024_4 | 2019-03-20 | 10:01:27 | 62°14.54'S | 051°25.52'W | 3000 |
| 53 | PS118_024_4 | 2019-03-20 | 10:06:25 | 62°14.54'S | 051°25.52'W | 2800 |
| 54 | PS118_024_4 | 2019-03-20 | 10:11:27 | 62°14.54'S | 051°25.52'W | 2600 |
| 55 | PS118_024_4 | 2019-03-20 | 10:16:02 | 62°14.54'S | 051°25.52'W | 2400 |
| 56 | PS118_024_4 | 2019-03-20 | 10:21:17 | 62°14.54'S | 051°25.52'W | 2200 |
| 57 | PS118_024_4 | 2019-03-20 | 10:26:09 | 62°14.54'S | 051°25.52'W | 2000 |
| 58 | PS118_024_4 | 2019-03-20 | 10:30:53 | 62°14.54'S | 051°25.52'W | 1800 |
| 59 | PS118_024_4 | 2019-03-20 | 10:35:59 | 62°14.54'S | 051°25.52'W | 1600 |
| 60 | PS118_024_4 | 2019-03-20 | 10:40:32 | 62°14.54'S | 051°25.52'W | 1400 |
| 61 | PS118_024_4 | 2019-03-20 | 10:45:28 | 62°14.54'S | 051°25.52'W | 1200 |
| 62 | PS118_024_4 | 2019-03-20 | 10:50:02 | 62°14.54'S | 051°25.52'W | 1000 |
| 63 | PS118_024_4 | 2019-03-20 | 10:55:00 | 62°14.54'S | 051°25.52'W | 800 |
| 64 | PS118_024_4 | 2019-03-20 | 10:59:17 | 62°14.54'S | 051°25.52'W | 600 |
| 65 | PS118_024_4 | 2019-03-20 | 11:04:09 | 62°14.54'S | 051°25.52'W | 400 |
| 66 | PS118_024_4 | 2019-03-20 | 11:09:28 | 62°14.54'S | 051°25.52'W | 200 |
| 67 | PS118_024_4 | 2019-03-20 | 11:12:56 | 62°14.54'S | 051°25.52'W | 50 |
| 68 | PS118_032_1 | 2019-03-21 | 21:54:45 | 62°45.96'S | 053°26.99'W | bottom |
| 69 | PS118_032_1 | 2019-03-21 | 21:59:10 | 62°45.96'S | 053°26.99'W | 700 |
| 70 | PS118_032_1 | 2019-03-21 | 22:04:18 | 62°45.96'S | 053°26.99'W | 500 |

| Sample | Station | Date | UTC time | Latitude | Longitude | Depth [m] |
|---|---|---|---|---|---|---|
| 71 | PS118_032_1 | 2019-03-21 | 22:08:48 | 62°45.96'S | 053°26.99'W | 300 |
| 72 | PS118_032_1 | 2019-03-21 | 22:17:18 | 62°45.96'S | 053°26.99'W | 40 |
| 73 | PS118_049_2 | 2019-03-26 | 18:39:43 | 61°28.66'S | 051°30.42'W | bottom |
| 74 | PS118_049_2 | 2019-03-26 | 18:45:11 | 61°28.66'S | 051°30.42'W | 1000 |
| 75 | PS118_049_2 | 2019-03-26 | 18:50:43 | 61°28.66'S | 051°30.42'W | 800 |
| 76 | PS118_049_2 | 2019-03-26 | 18:55:58 | 61°28.66'S | 051°30.42'W | 600 |
| 77 | PS118_049_2 | 2019-03-26 | 19:00:49 | 61°28.66'S | 051°30.42'W | 400 |
| 78 | PS118_049_2 | 2019-03-26 | 19:05:54 | 61°28.66'S | 051°30.42'W | 200 |
| 79 | PS118_049_2 | 2019-03-26 | 19:09:35 | 61°28.66'S | 051°30.42'W | 40 |
| 80 | PS118_054_1 | 2019-03-27 | 13:17:46 | 60°50.60'S | 049°35.78'W | bottom |
| 81 | PS118_054_1 | 2019-03-27 | 13:25:05 | 60°50.60'S | 049°35.78'W | 2400 |
| 82 | PS118_054_1 | 2019-03-27 | 13:29:30 | 60°50.60'S | 049°35.78'W | 2200 |
| 83 | PS118_054_1 | 2019-03-27 | 13:34:01 | 60°50.60'S | 049°35.78'W | 2000 |
| 84 | PS118_054_1 | 2019-03-27 | 13:38:49 | 60°50.60'S | 049°35.78'W | 1800 |
| 85 | PS118_054_1 | 2019-03-27 | 13:45:20 | 60°50.60'S | 049°35.78'W | 1500 |
| 86 | PS118_054_1 | 2019-03-27 | 13:51:47 | 60°50.60'S | 049°35.78'W | 1200 |
| 87 | PS118_054_1 | 2019-03-27 | 13:56:06 | 60°50.60'S | 049°35.78'W | 1000 |
| 88 | PS118_054_1 | 2019-03-27 | 14:01:44 | 60°50.60'S | 049°35.78'W | 750 |
| 89 | PS118_054_1 | 2019-03-27 | 14:06:40 | 60°50.60'S | 049°35.78'W | 550 |
| 90 | PS118_054_1 | 2019-03-27 | 14:10:45 | 60°50.60'S | 049°35.78'W | 400 |
| 91 | PS118_054_1 | 2019-03-27 | 14:15:51 | 60°50.60'S | 049°35.78'W | 200 |
| 92 | PS118_054_1 | 2019-03-27 | 14:20:03 | 60°50.60'S | 049°35.78'W | 40 |
| 93 | PS118_059_1 | 2019-03-28 | 03:03:22 | 60°50.78'S | 048°11.74'W | bottom |
| 94 | PS118_059_1 | 2019-03-28 | 03:10:47 | 60°50.78'S | 048°11.74'W | 2400 |
| 95 | PS118_059_1 | 2019-03-28 | 03:16:25 | 60°50.78'S | 048°11.74'W | 2200 |
| 96 | PS118_059_1 | 2019-03-28 | 03:21:28 | 60°50.78'S | 048°11.74'W | 2000 |
| 97 | PS118_059_1 | 2019-03-28 | 03:27:25 | 60°50.78'S | 048°11.74'W | 1800 |
| 98 | PS118_059_1 | 2019-03-28 | 03:32:40 | 60°50.78'S | 048°11.74'W | 1600 |
| 99 | PS118_059_1 | 2019-03-28 | 03:51:37 | 60°50.78'S | 048°11.74'W | 700 |
| 100 | PS118_060_1 | 2019-03-28 | 06:27:35 | 60°50.73'S | 047°53.83'W | 1600 |
| 101 | PS118_060_1 | 2019-03-28 | 06:32:40 | 60°50.73'S | 047°53.83'W | 1400 |
| 102 | PS118_060_1 | 2019-03-28 | 06:37:47 | 60°50.73'S | 047°53.83'W | 1200 |
| 103 | PS118_060_1 | 2019-03-28 | 06:42:48 | 60°50.73'S | 047°53.83'W | 1000 |
| 104 | PS118_060_1 | 2019-03-28 | 06:49:00 | 60°50.73'S | 047°53.83'W | 760 |
| 105 | PS118_060_1 | 2019-03-28 | 06:53:32 | 60°50.73'S | 047°53.83'W | 600 |
| 106 | PS118_060_1 | 2019-03-28 | 07:00:00 | 60°50.73'S | 047°53.83'W | 400 |
| 107 | PS118_071_2 | 2019-03-31 | 20:26:40 | 61°04.67'S | 051°46.06'W | 700 |
| 108 | PS118_071_2 | 2019-03-31 | 20:33:00 | 61°04.67'S | 051°46.06'W | 500 |
| 109 | PS118_071_2 | 2019-03-31 | 20:38:40 | 61°04.67'S | 051°46.06'W | 300 |
| 110 | PS118_071_2 | 2019-03-31 | 20:44:55 | 61°04.67'S | 051°46.06'W | 100 |

**Tab. 4.2:** Table showing locations and depths of samples to be returned for FISH analysis

| Sample | Station | Date | UTC time | Latitude | Longitude | Depth [m] |
|---|---|---|---|---|---|---|
| 1 | PS118_005_1 | 2019-03-04 | 15:34:10 | 64°59.05'S | 057°44.90'W | 350 |
| 2 | PS118_005_1 | 2019-03-04 | 15:37:23 | 64°59.05'S | 057°44.90'W | 250 |
| 3 | PS118_005_1 | 2019-03-04 | 15:40:25 | 64°59.05'S | 057°44.90'W | 150 |
| 4 | PS118_006_1 | 2019-03-05 | 12:26:38 | 64°58.80'S | 057°46.63'W | 400 |
| 5 | PS118_006_1 | 2019-03-05 | 12:29:12 | 64°58.80'S | 057°46.63'W | 300 |
| 6 | PS118_006_1 | 2019-03-05 | 12:32:00 | 64°58.80'S | 057°46.63'W | 200 |
| 7 | PS118_008_2 | 2019-03-11 | 16:38:57 | 63°59.98'S | 055°54.40'W | bottom |
| 8 | PS118_008_2 | 2019-03-11 | 16:46:42 | 63°59.98'S | 055°54.40'W | 300 |
| 9 | PS118_008_2 | 2019-03-11 | 16:50:30 | 63°59.98'S | 055°54.40'W | 200 |
| 10 | PS118_008_2 | 2019-03-11 | 16:55:01 | 63°59.98'S | 055°54.40'W | 100 |
| 11 | PS118_010_1 | 2019-03-13 | 11:55:55 | 64°00.17'S | 055°58.57'W | bottom |
| 12 | PS118_010_1 | 2019-03-13 | 11:59:00 | 64°00.17'S | 055°58.57'W | 300 |
| 13 | PS118_010_1 | 2019-03-13 | 12:01:56 | 64°00.17'S | 055°58.57'W | 200 |
| 14 | PS118_010_1 | 2019-03-13 | 12:04:23 | 64°00.17'S | 055°58.57'W | 100 |
| 15 | PS118_012_1 | 2019-03-14 | 07:03:11 | 63°48.34'S | 055°44.73'W | bottom |
| 16 | PS118_012_1 | 2019-03-14 | 07:04:44 | 63°48.34'S | 055°44.73'W | 400 |
| 17 | PS118_012_1 | 2019-03-14 | 07:08:33 | 63°48.34'S | 055°44.73'W | 300 |
| 18 | PS118_012_1 | 2019-03-14 | 07:11:02 | 63°48.34'S | 055°44.73'W | 200 |
| 19 | PS118_012_1 | 2019-03-14 | 07:14:17 | 63°48.34'S | 055°44.73'W | 100 |
| 20 | PS118_013_1 | 2019-03-17 | 11:40:36 | 63°04.09'S | 054°18.76'W | 200 |
| 21 | PS118_013_1 | 2019-03-17 | 11:37:54 | 63°04.09'S | 054°18.76'W | 300 |
| 22 | PS118_013_1 | 2019-03-17 | 11:32:24 | 63°04.09'S | 054°18.76'W | bottom |
| 23 | PS118_013_1 | 2019-03-17 | 11:43:33 | 63°04.09'S | 054°18.76'W | 100 |
| 24 | PS118_015_2 | 2019-03-18 | 19:08:10 | 62°01.00'S | 054°59.51'W | 1200 |
| 25 | PS118_015_2 | 2019-03-18 | 19:12:39 | 62°01.00'S | 054°59.51'W | 1000 |
| 26 | PS118_015_2 | 2019-03-18 | 19:18:04 | 62°01.00'S | 054°59.51'W | 800 |
| 27 | PS118_015_2 | 2019-03-18 | 19:22:29 | 62°01.00'S | 054°59.51'W | 600 |
| 28 | PS118_015_2 | 2019-03-18 | 19:32:28 | 62°01.00'S | 054°59.51'W | 200 |
| 29 | PS118_020_1 | 2019-03-19 | 07:15:10 | 61°59.86'S | 053°09.52'W | 2000 |
| 30 | PS118_020_1 | 2019-03-19 | 07:25:07 | 61°59.86'S | 053°09.52'W | 1600 |
| 31 | PS118_020_1 | 2019-03-19 | 07:34:50 | 61°59.86'S | 053°09.52'W | 1200 |
| 32 | PS118_020_1 | 2019-03-19 | 07:44:22 | 61°59.86'S | 053°09.52'W | 800 |
| 33 | PS118_020_1 | 2019-03-19 | 07:54:22 | 61°59.86'S | 053°09.52'W | 400 |
| 34 | PS118_024_4 | 2019-03-20 | 10:11:27 | 62°14.54'S | 051°25.52'W | 2600 |
| 35 | PS118_024_4 | 2019-03-20 | 10:26:09 | 62°14.54'S | 051°25.52'W | 2000 |
| 36 | PS118_024_4 | 2019-03-20 | 10:40:32 | 62°14.54'S | 051°25.52'W | 1400 |
| 37 | PS118_024_4 | 2019-03-20 | 10:55:00 | 62°14.54'S | 051°25.52'W | 800 |
| 38 | PS118_024_4 | 2019-03-20 | 11:09:28 | 62°14.54'S | 051°25.52'W | 200 |
| 39 | PS118_032_1 | 2019-03-21 | 21:54:45 | 62°45.96'S | 053°26.99'W | bottom |
| 40 | PS118_032_1 | 2019-03-21 | 21:59:10 | 62°45.96'S | 053°26.99'W | 700 |
| 41 | PS118_032_1 | 2019-03-21 | 22:04:18 | 62°45.96'S | 053°26.99'W | 500 |
| 42 | PS118_032_1 | 2019-03-21 | 22:08:48 | 62°45.96'S | 053°26.99'W | 300 |

| Sample | Station | Date | UTC time | Latitude | Longitude | Depth [m] |
|---|---|---|---|---|---|---|
| 43 | PS118_032_1 | 2019-03-21 | 22:17:18 | 62°45.96'S | 053°26.99'W | 40 |
| 44 | PS118_049_2 | 2019-03-26 | 18:39:43 | 61°28.66'S | 051°30.42'W | bottom |
| 45 | PS118_049_2 | 2019-03-26 | 18:45:11 | 61°28.66'S | 051°30.42'W | 1000 |
| 46 | PS118_049_2 | 2019-03-26 | 18:50:43 | 61°28.66'S | 051°30.42'W | 800 |
| 47 | PS118_049_2 | 2019-03-26 | 18:55:58 | 61°28.66'S | 051°30.42'W | 600 |
| 48 | PS118_049_2 | 2019-03-26 | 19:00:49 | 61°28.66'S | 051°30.42'W | 400 |
| 49 | PS118_049_2 | 2019-03-26 | 19:05:54 | 61°28.66'S | 051°30.42'W | 200 |
| 50 | PS118_049_2 | 2019-03-26 | 19:09:35 | 61°28.66'S | 051°30.42'W | 40 |
| 51 | PS118_054_1 | 2019-03-27 | 13:17:46 | 60°50.60'S | 049°35.78'W | bottom |
| 52 | PS118_054_1 | 2019-03-27 | 13:29:30 | 60°50.60'S | 049°35.78'W | 2200 |
| 53 | PS118_054_1 | 2019-03-27 | 13:38:49 | 60°50.60'S | 049°35.78'W | 1800 |
| 54 | PS118_054_1 | 2019-03-27 | 13:51:47 | 60°50.60'S | 049°35.78'W | 1200 |
| 55 | PS118_054_1 | 2019-03-27 | 14:01:44 | 60°50.60'S | 049°35.78'W | 750 |
| 56 | PS118_054_1 | 2019-03-27 | 14:10:45 | 60°50.60'S | 049°35.78'W | 400 |
| 57 | PS118_054_1 | 2019-03-27 | 14:20:03 | 60°50.60'S | 049°35.78'W | 40 |
| 58 | PS118_059_1 | 2019-03-28 | 03:03:22 | 60°50.78'S | 048°11.74'W | bottom |
| 59 | PS118_059_1 | 2019-03-28 | 03:16:25 | 60°50.78'S | 048°11.74'W | 2200 |
| 60 | PS118_059_1 | 2019-03-28 | 03:27:25 | 60°50.78'S | 048°11.74'W | 1800 |
| 61 | PS118_059_1 | 2019-03-28 | 03:51:37 | 60°50.78'S | 048°11.74'W | 700 |
| 62 | PS118_060_1 | 2019-03-28 | 06:27:35 | 60°50.73'S | 047°53.83'W | 1600 |
| 63 | PS118_060_1 | 2019-03-28 | 06:37:47 | 60°50.73'S | 047°53.83'W | 1200 |
| 64 | PS118_060_1 | 2019-03-28 | 06:49:00 | 60°50.73'S | 047°53.83'W | 760 |
| 65 | PS118_060_1 | 2019-03-28 | 07:00:00 | 60°50.73'S | 047°53.83'W | 400 |

**Preliminary (expected) results**

For samples collected during the PS118 cruise, the V4 and V9 metabarcodes will be amplified with universal eukaryotic primers for all samples and sequenced using technologies and read length (Illumina HiSeq or MiSeq, paired reads up to 300 nt long) appropriate for the shorter V9 region (about 130 nt in length) and for the longer V4 region of the 18S rRNA gene (up to 600 nt and longer). An OTU delimitation approach and analysis pipeline tested in our previous studies will be used (Flegontova et al., 2016, 2018). The results of this work will be used in a comparative study along with metabarcodes previously generated by our working group for a collection of 37 Arctic samples. Combining the Arctic and Antarctic datasets, we will perform a detailed investigation of diplonemid biodiversity in polar regions. Since community composition data would be generated using universal primers, diplonemids would be studied in the context of other eukaryotes. In summary, we plan to study this neglected but important group in the polar regions, particularly their occurence within the bathypelagic zone, a region under-investigated at present. We hope that the PS118 data on correlation of diplonemid abundance with environmental factors and on co-occurrence with other organisms will help us to propose hypotheses concerning their trophic strategies, which remain elusive to date. This information is crucial for bringing diplonemids of the most important Eupelagonemidae family into culture, which would allow further studies of their biology.

**Data management**

Results of our project will be published in peer-reviewed journals (at least one publication planned). Sample meta-data will be deposited at the World Data Center PANGAEA Data

Publisher for Earth & Environmental Science ([www.pangaea.de](http://www.pangaea.de)). Plankton samples on filters will be used for DNA extraction, and DNA will be stored at -70 °C at the Institute of Parasitology, Czech Academy of Sciences, and made available upon request. All metabarcoding sequences (raw reads) generated during the project will be submitted to public databases: the European Nucleotide Archive and EukBank (unieuk.org), where they will be freely available.

## References

de Vargas C, Audic S, Henry N, Decelle J, Mahe F, Logares R, Lara E, Berney C, Le Bescot N, Probert I, Carmichael M, Poulain J, Romac S, Colin S, Aury JM, Bittner L, Chaffron S, Dunthorn M, Engelen S, Flegontova O, Guidi L, Horák A, Jaillon O, Lima-Mendez G, Lukeš J, Malviya S, Morard R, Mulot M, Scalco E, Siano R, Vincent F, Zingone A, Dimier C, Picheral M, Searson S, Kandels-Lewis S; Tara Oceans Coordinators, Acinas SG, Bork P, Bowler C, Gorsky G, Grimsley N, Hingamp P,Iudicone D, Not F, Ogata H, Pesant S, Raes J, Sieracki ME, Speich S, Stemmann L, Sunagawa S,Weissenbach J, Wincker P & Karsenti E (2015) Eukaryotic plankton diversity in the sunlit ocean. Science, 348, 1261605.

Flegontova O, Flegontov P, Malviya S, Audic S, Wincker P, de Vargas C, Bowler C, Lukeš J & Horák A (2016) Extreme diversity of diplonemid eukaryotes in the ocean. Current Biology, 26, 3060-3065.

Flegontova O, Flegontov P, Malviya S, Poulain J, de Vargas C Bowler C, Lukeš J & Horák A (2018) Neobodonids are dominant kinetoplastids in the global ocean. Environmental Microbiology, 20, 878-889.

Gawryluk RMR, del Campo J, Okamoto N, Strassert JFH, Lukeš J, Richards TA, Worden AZ, Santoro AE & Keeling PJ (2016) Morphological identification and single-cell genomics of marine diplonemids. Current Biology, 26, 3053-3059.

Lara E, Moreira D, Vereshchaka A & Lopez-Garcia P (2009) Pan-oceanic distribution of new highly diverse clades of deep-sea diplonemids. Environmental Microbiology, 11, 47-55.

Massana R, Gobet A, Audic S, Bass D, Bittner L, Boutte C, Chambouvet A, Christen R, Claverie JM, Decelle J, Dolan JR, Dunthorn M, Edvardsen B, Forn I, Forster D, Guillou L, Jaillon O, Kooistra WH, Logares R, Mahe F, Not F, Ogata H, Pawlowski J, Pernice MC, Probert I, Romac S, Richards T, Santini S, Shalchian-Tabrizi K, Siano R, Simon N, Stoeck T, Vaulot D, Zingone A & de Vargas C (2015) Marine protist diversity in European coastal waters and sediments as revealed by highthroughput sequencing. Environmental Microbiology, 17, 4035-4049.

Pernice MC, Giner CR, Logares R, Perera-Bel J, Acinas SG, Duarte CM, Gasol JM & Massana R (2016) Large variability of bathypelagic microbial eukaryotic communities across the world's oceans. ISME Journal, 10, 945-958.

Suzuki TM & Chiba S (2016) Dynamics of evolutionary radiation under ecological neutrality. Journal of Theoretical Biology, 406, 1-7.

Tashyreva D, Prokopchuk G, Yabuki A, Kaur B, Faktorová D, Votýpka J, Kusaka C, Fujikura K, Shiratori T, Ishida K-I, Horák A & Lukeš J (2018) Phylogeny and morphology of new diplonemids from Japan. Protist, 169, 158-179.

# 5. INFLUENCE OF ICE COVER AND PRIMARY PRODUCTIVITY ON BENTHIC FOOD-WEB STRUCTURE AND ECOSYSTEM FUNCTIONING

Ursula Witte[1], Gritta Veit-Köhler[2], Kirsten MacSween[1],Friederike Säring[3], Ben Behrend[3], Heike Link[3] (not on board)

[1]University of Aberdeen
[2]SaM-DZMB
[3]University of Rostock

**Grant-No. AWI_PS118_06**

**Grant-No. AWI_PS118_08**

## Objectives

More than 60 % of the earth's surface is covered by deep seafloor below more than 200 m of water. Marine sediments are a major reservoir in the global carbon cycle and the formation, cycling or burial of organic matter (OM) in marine sediments are key terms in the global C, N and P cycles, linked to ocean nutrient budgets and productivity. The flux of particulate organic carbon (POC) sinking from the euphotic zone is the main food source for deep-water benthic communities and due to this close pelagic-benthic coupling, observed and projected climate-induced changes in upper-ocean conditions are likely to rapidly cascade to the deep seabed. Food supply to the benthos, in turn, exerts control on benthic community structure (Ruhl & Smith, 2004; Smith et al., 2009; Wei et al., 2010), and the efficiency of the recycling of organic matter through benthic food webs (e.g. Witte et al., 2003; Hunter et al., 2012). Ecosystem functioning represented by benthic boundary fluxes such as oxygen consumption and the release of inorganic nutrients (e.g., nitrate, phosphate, silicic acid) depends on composition and activity of benthic communities (Link et al., 2011). Climate-driven changes in upper ocean primary productivity and export flux will therefore directly affect the recycling of POC by seafloor communities and, subsequently, C sequestration and nutrient release.

Climate change has initiated major upheavals for polar biodiversity and ecosystem functioning (e.g. Wassmann et al., 2011), and the Antarctic Peninsula is one of the areas most affected, which *inter alia*, has led to the retreat of glaciers as well as to large-scale ice-shelf destabilization and disintegration. Additionally, opposing trends of increase and decrease of sea-ice cover have been detected for different regions of the Southern Ocean (King, 2014). Major ecosystem shifts related to these large-scale processes have already been reported from both Arctic and Antarctic coastal waters (Grebmeier et al., 2006; Moline et al., 2004). Due to financial and logistical constraints, however, our knowledge of the ecology of benthic organisms and the interplay between POC characteristics, biodiversity and the early diagenesis of POC as well as nutrient fluxes in the remote Southern Ocean is poorly constrained. The lack of adequate knowledge about these processes therefore severely hampers global C modelling and an assessment of the consequences of climate change for these important ecosystems.

Food-web structure is a key ecosystem characteristic, and profound knowledge of energy flow and organic matter cycling through and ecological interactions within an ecosystem is an essential prerequisite for the prediction of ecosystem-level response to perturbation and change. Isotope tracing experiments (ITEs) have in recent years provided a major step forward

in attempts to describe the structure and functioning of benthic food webs (e.g. Witte et al., 2003; Aberle et al., 2003; Gontikaki et al., 2011a). For organisms large enough to be identified and analysed individually (macro-, mega- and some meiofauna) they allow to directly link diversity to function on species or genus level and have great potential to enhance food-web models (e.g. Gontikaki et al., 2011b). They have also proven particularly successful in assessing the impact of food supply and quality, or oxygen availability, on rates and pathways of deep-sea carbon cycling (e.g. Witte et al., 2003; Bühring et al., 2006; Hunter et al. 2012).

The original objectives of our proposals were to compare and document benthic ecosystem functioning and food webs inside and outside the area formerly covered by shelf ice, as a proxy for the rapid transition of benthic ecosystems following major environmental change. Due to the inaccessibility of Larsen C, as well as Larsen A & B areas, the research objectives were modified to focus on the influence of sea-ice cover and primary productivity (PP) on benthic food webs and ecosystem functioning. Phytoplankton supply to the seafloor is considerably lower at under sea-ice locations than it is in open water owing to lower productivity and sedimentation rates. However, ice algae, when released from melting sea ice, may considerably enhance the input of organic matter to the seafloor (Bathmann et al., 1991).

To achieve this, we focussed on 4 alternative stations (Fig. 5.1) located along a gradient of sea-ice cover and primary productivity (see chapter 6). In order to maximise synergies, stations for incubation experiments were chosen in close cooperation with the teams working on benthic-pelagic coupling and benthic megafauna.
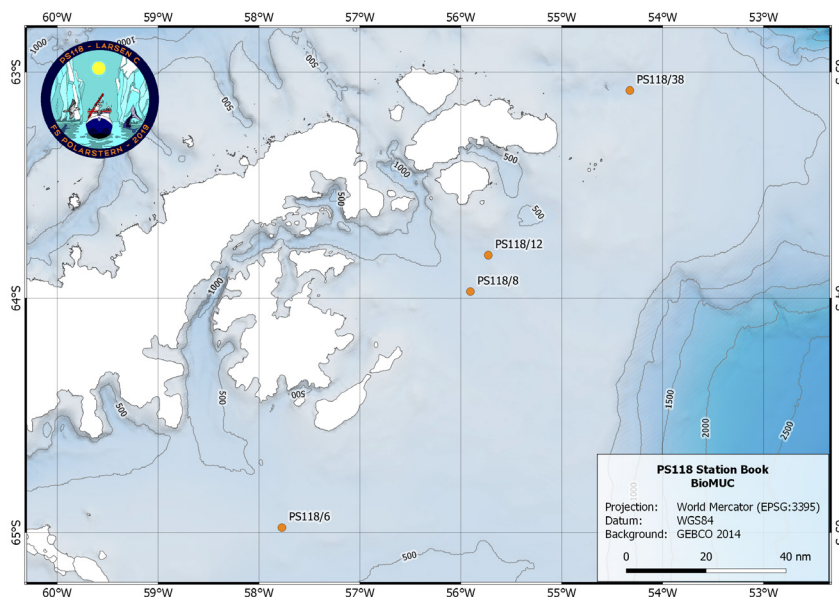


*Fig. 5.1: Stations sampled for benthic incubation experiments during Polarstern expedition PS118 were situated along a productivity and sea-ice cover gradient in the Weddell Sea (map created by Simon Dreutter).*

Specifically, we aimed to investigate whether and how changes in food supply, and subsequent changes in benthic community composition affect the rates and pathways of C and N cycling through and nutrient recycling by the benthic communities, addressing the following main objectives:

- Quantification of the rate of organic C degradation and nutrient recycling (benthic boundary fluxes), and corresponding standing stock of benthic meio- and macrofauna

- Quantification of rates and pathways of C and N cycling through the benthic community compartments by means of isotope tracing experiments (ITEs)

- Determination of the trophic structure of the benthic food web through bulk stable isotope analysis

- Reconstruction of the benthic food web at our study sites through formulation of a linear inverse model based on data generated in 1. and 2., to further elucidate differences in food-web flows along gradients of ice cover and PP.

**Work at sea**

A multiple corer (MUC10, inner diameter of Plexiglas core liners 94 mm, surface 0.007 m²) was used to retrieve sediment cores for incubation experiments and for determination of background parameters at 4 working areas, st. 6, 8, 12 and 38 (see Tables 5.1 and 5.2 for details). Water from two depths (closest to the bottom and at the fluorescence maximum) was collected with the rosette water sampler and provided by the CTD-team (see chapter 9).

*Sediment and water column background parameters*

At each station, the sediment cores that were mainly used for meiofauna for objective 3 (see below) were subsampled for environmental parameters. In each core three cut-off 20 ml syringes were pushed down to 5 cm in order to obtain sediment samples for chlorophyll-a and phaeopigment content, grain size and stable isotopic composition ($\delta^{13}C$ and $\delta^{15}N$). Complete syringes/and or cut off 1 cm slices were stored at -80° C for further analyses in the home lab.

Water from the rosette water sampler collected at the fluorescence maximum (representing the Chl-a maximum) and at the bottom (close to the ground) was sieved over a 100 µm sieve in order to remove larger particles and fauna. Filtering was carried out at 200 mbar to avoid rupture of cells. For each depth one GF/C (for Chl-a) and one GF/F filter (for $\delta^{13}C$ and $\delta^{15}N$) were prepared and stored at -80°C.



*Fig. 5.2: Incubation of sediment cores in temperature controlled laboratory container*

*Benthic boundary fluxes (objective 1)*

Shipboard incubations of sediment microcosms were run in a dark, temperature-controlled room (0.8 to 2°C) for 72–96 h (Fig. 5.2). Total sediment oxygen flux was determined as the decrease in oxygen concentrations in the water phase and was measured periodically (2 to 8 h intervals) with a non-invasive optical probe (Fibox 3 LCD, PreSens, Regensburg, Germany).

To determine changes in nutrient concentrations (nitrate, phosphate, silicic acid), samples of the overlying water phase were taken at three times during the incubation, including the onset and end. Oxygen and nutrient fluxes are determined as the slope of the linear regression of the oxygen and nutrient concentration on incubation time and corrected for solute concentration in the replacement water. A more detailed description of this method can be found in Link et al. (2011) and Link et al. (2012).

*Isotope tracing experiments (objective 2)*

Isotope tracing experiments with freeze-dried $^{13}$C/$^{15}$N-labelled algal biomass were performed in order to determine the rates and pathways of C and N cycling by the benthic community as described for example in Mäkelä et al. (2017a,b). At best, 6 control cores without algal addition, and five cores amended with freeze-dried algae were incubated for 96 h. Oxygen concentration in the water phase was measured periodically (2 to 8 h intervals) with a non-invasive optical probe (Fibox 3 LCD, PreSens, Regensburg, Germany). Water samples were taken daily for analysis of DIC/ DI$^{13}$C concentrations. At the end of the experiments, sediment cores were sampled for analysis (in the home laboratory) of the amount of tracer $^{13}$C and $^{15}$N taken up by the different benthic organisms (bacteria, meiofauna, macrofauna).

*Macro- and meiofauna natural stable isotope signatures (objective 3)*

Macrofauna: 3 sediment cores per station were sliced at 0-2, 2-5 and 5-10 cm intervals, sieved over 500 μm mesh size and preserved in 5% buffered formaldehyde for analysis of faunal community structure and background stable isotope signatures (Mäkelä et al., 2017a,b).

Meiofauna: 3 sediment cores per station were sliced at 0–1, 1–2 and 2–3 cm intervals and stored frozen. In the home laboratory specimens will be sorted to the lowest taxonomic level possible and processed for determination of natural $\delta^{13}$C and $\delta^{15}$N stable isotope ratios as described in Veit-Köhler et al. (2013).

**Tab. 5.1:** Stations sampled for benthic incubation experiments during *Polarstern* expedition PS118. Deployments of multicorer (MUC10) and CTD (depths at Chl-a maximum and bottom) given

| Station | Date | Device | Latitude | Longitude | Depth [m] |
|---|---|---|---|---|---|
| PS118_6-1 | 2019-03-05 | CTD | 64° 58.805' S | 057° 46.560' W | 6 / 424 |
| PS118_6-2 | 2019-03-05 | MUC10 | 64° 58.724' S | 057° 46.379' W | 423 |
| PS118_6-3 | 2019-03-05 | MUC10 | 64° 58.612' S | 057° 46.363' W | 425 |
| | | | | | |
| PS118_8-2 | 2019-03-11 | CTD | 63° 59.836' S | 055° 54.365' W | 2.5 / 412 |
| PS118_8-4 | 2019-03-11 | MUC10 | 63° 58.525' S | 055° 54.293' W | 414 |
| PS118_8-5 | 2019-03-11 | MUC10 | 63° 58.264' S | 055° 54.322' W | 413 |
| PS118_8-6 | 2019-03-11 | MUC10 | 63° 58.105' S | 055° 54.384' W | 415 |
| PS118_8-7 | 2019-03-11 | MUC10 | 63° 57.882' S | 055° 54.469' W | 415 |
| PS118_8-8 | 2019-03-11 | MUC10 | 63° 57.742' S | 055° 54.495' W | 415 |

| PS118_12-1 | 2019-03-14 | CTD | 63° 48.397' S | 055° 44.660' W | 20 / 456 |
| PS118_12-3 | 2019-03-14 | MUC10 | 63° 48.751' S | 055° 43.677' W | 453 |
| PS118_12-4 | 2019-03-14 | MUC10 | 63° 48.777' S | 055° 43.145' W | 453 |
| PS118_12-5 | 2019-03-14 | MUC10 | 63° 48.838' S | 055° 42.700' W | 454 |
| | | | | | |
| PS118_38-1 | 2019-03-22 | CTD | 63° 04.352' S | 054° 21.431' W | 50 / 445 |
| PS118_38-2 | 2019-03-22 | MUC10 | 63° 04.956' S | 054° 19.490' W | 414 |
| PS118_38-3 | 2019-03-22 | MUC10 | 63° 04.480' S | 054° 20.226' W | 427 |
| PS118_38-5 | 2019-03-22 | MUC10 | 63° 04.972' S | 054° 19.717' W | 415 |

**Tab. 5.2:** Use of sediment and water column samples during PS118. A: algae addition; B: control and benthic functioning; Env: environmental background data, 1 syringe subsample each for chlorophyll a, grain size, sediment stable isotope ratios (SI; δ13C and δ15N); Meio: subsamples for natural SI ratios of meiofauna; Macro: macrofauna communities and natural SI ratios. The CTD-team provided water samples from the chlorophyll maximum and near-bottom depths, water was filtered for analyses of chlorophyll-a and POC-SI ratios.

| Station | Sediment Core Replicates | | | Water Column Samples | |
|---|---|---|---|---|---|
| | Exp | Env + Meio | Macro | Chl-a | POC-SI |
| PS118_6 | 5 A, 5 B | 3 | 3 | x | x |
| PS118_8 | 5 A, 6 B | 3 | 3 | x | x |
| PS118_12 | 6 B | 3 | 3 | x | x |
| PS118_38 | 5 A, 6 B | 3 | 3 | x | x |

**Expected results**

In general, we did not produce publishable results during the cruise, as the vast majority of samples taken have yet to be analysed in the lab (water samples for nutrient concentrations, sediment samples for C/N ratios, stable isotopes, pigment content, porosity and grain size as well as the abundance, biomass, composition and diversity of meiofauna and macrofauna assemblages).

*Benthic boundary fluxes (objective 1)*

In the home laboratory, water samples will be analysed for their nutrient contents (nitrate, phosphate, silicic acid) and nutrient fluxes will be determined. Along with the measured oxygen fluxes, the quantification of these remineralisation products will provide a complex assessment of benthic functions along the investigated ice-cover gradient. We expect remineralisation rates to be higher in areas with less sea-ice cover, since we observed higher faunal densities at these stations.

*Isotope tracing experiments (objective 2)*

In the home laboratory, the amount of labelled POC respired or incorporated into bacterial or faunal biomass will be determined via IRMS or GC-c-IRMS (following biomarker extraction). We expect respiration (DI$^{13}$C) and incorporation rates to be higher and label entrainment into the sediment to be faster and deeper at stations with longer exposition to open water conditions.

Results will help understand and predict to what extent the loss of sea ice and subsequent exposure to open water conditions will change benthic food webs and the efficiency with which they recycle organic matter reaching the seafloor – on the deep Antarctic shelf and in the benthos in general.

*Macro- and meiofauna natural stable isotope signatures (objective 3)*

*Macrofauna*: In the home laboratory, specimens will be sorted to the lowest taxonomic level possible and processed for determination of C and N stable isotope ratios as described in Mäkelä et al (2017a, b). A lipid correction will be performed where applicable, and δ$^{15}$N values will be obtained from non-acidified samples to avoid acidification impacts on δ$^{15}$N values. Stable isotope data will be used to determine the trophic structure of the benthic community and mixing models will be applied to elucidate the relative importance of available food sources.

*Meiofauna*: In the home laboratory, specimens will be sorted and processed for determination of C and N stable isotope ratios. Copepods and nematodes will be the main groups for analyses since they reveal the highest abundances in the meiofauna. We expect copepods and nematodes to make use of differently degraded material (Veit-Köhler et al., 2013) and nematodes to dominate absolute uptake of provided algal material in the meiofauna.

*Comparative reconstruction of the benthic food web along a gradient of ice cover and primary productivity (objective 4)*

The above data will be used to formulate and improve a linear inverse model to reconstruct the benthic food webs at our study sites, further elucidating the role of the different food sources for Weddell Sea benthic food webs. The incorporation of $^{13}$C uptake data within linear inverse models is a relatively new development that has significantly reduced the uncertainty accompanying "traditional" food-web models (Gontikaki et al., 2011).

**Data management**

All data collected during the expedition will be stored in the the World Data Center PANGAEA Data Publisher for Earth & Environmental Science ([www.pangaea.de](www.pangaea.de)), and/ or the BODC. Metadata will be made available throughout the project as and when data sets are complete, and any temporarily embargoed data will be publically available once manuscripts are accepted for publication.

**References**

Aberle N & Witte U (2003) Deep-sea macrofauna exposed to a simulated sedimentation event in the abyssal NE Atlantic: in situ pulse chase experiments using $^{13}$C labeled phytodetritus (2003). Marine Ecology Progress Series, 251, 37-47.

Bathmann U, Fischer G, Müller PJ & Gerdes D (1991) Short-term variations in particulate matter sedimentation off Kapp Norvegia, Weddell Sea, Antarctica: relation to water mass advection, ice cover, plankton biomass and feeding activity. Polar Biology, 11, 185-195.

Bühring SI, Lampadariou N, Moodley L, Tselepides T & Witte U (2006) Benthic microbial and whole-

community responses to different amounts of 13C-enriched algae: In situ experiments in the deep Cretan Sea (Eastern Mediterranean). Limnology & Oceanography, 51,157-165.

Grebmeier JM, Overland JE, Moore SE, Farley EV, Carmack EC, Cooper LW, Frey KE, Helle JH, McLaughlin FA & McNutt LS (2006) A major ecosystem shift in the northern Bering Sea. Science, 311, 1461-1464.

Gontikaki E, Mayor DJ, Narayanaswami BE & Witte U (2011a) Feeding strategies of deep-sea sub-Arctic macrofauna of the Faroe-Shetland Channel: Combining natural stable isotopes and enrichment techniques. Deep-Sea Research I, 58, 160-172.

Gontikaki E, van Oevelen D, Soetaert K & Witte U (2011b) Food web flows through a sub-arctic deep-sea benthic community. Progress in Oceanography, 91, 245-259. doi:10.1016/ j.pocean.2010.12.014

King J (2014) A resolution of the Antarctic paradox. Nature, 505, 491-492.

Link H (2012) Studying the functioning of benthic hotspot and cold spot ecosystems in the Canadian Arctic. PhD thesis, Université du Québec à Rimouski, Canada, 171pp.

Link H, Archambault P, Tamelander T, Renaud PE & Piepenburg D (2011) Spring-to-summer changes and regional variability of benthic processes in the western Canadian Arctic. Polar Biology, 34, 2024-2038.

Hunter WR, Veuger B & Witte U (2012) Competition by metazoans and retention of labile organic matter regulate heterotrophic bacterial activity in oxygen minimum zone sediments. The ISME Journal, 6, 2140-2151.

Mäkelä A, Witte U & Archambault P (2017) Benthic macroinfaunal community structure, resource utilisation and trophic relationships in two Canadian Arctic Archipelago polynyas. *PloS one*, 12(8), e0183034. doi:10.1371/ JOURNAL.PONE.0183034

Mäkelä A, Witte U & Archambault P (2017) Ice algae vs. phytoplankton: resource utilization by Arctic deep sea macroinfauna revealed through isotope labelling experiments. *Marine Ecology Progress Series*, 572, 1-18. doi:10.3354/ MEPS12157

Moline MA, Claustre H, Frazer TK, et al. (2004) Alteration of the food web along the Antarctic Peninsula in response to a regional warming trend. Global Change Biology, 10, 1973-1980.

Ruhl H & Smith K (2004) Shifts in deep-sea community structure linked to climate and food supply. Science, 305(5683), 513-514.

Smith K Jr, Ruhl HA, Bett BJ, et al. (2009) Climate, carbon cycling, and deep-ocean ecosystems. PNAS, 106(46), 19211-19218.

Veit-Köhler G, Guilini K, Peeken I, Quillfeldt P & Mayr C (2013) Carbon and nitrogen stable isotope signatures of deep-sea meiofauna follow oceanographical gradients across the Southern Ocean. Progress in Oceanography, 110, 69-79. doi: 10.1016/j.pocean.2013.01.001

Wassmann P, Duarte CM, Agusti S, et al. (2011) Footprints of climate change in the Arctic marine ecosystem. Global Change Biology, 17(2), 1235-1249.

Wei JL, Rowe G, Escobar-Briones E, et al. (2010) Global patterns and predictions of seafloor biomass using random forests. PloS one, 5(12), e15323.

Witte U, Wenzhöfer F, Sommer S., et al (2003) In situ experimental evidence of the fate of a phytodetritus pulse at the abyssal sea floor. Nature, 424, 763-766.

# 6.    BENTHO-PELAGIC PROCESSES

Claudio Richter[1], Marwa Baloza[1], Moritz Holtappels[1], Nils Owsianowski[1], Henning Schröder[1]

[1]AWI

**Grant-No. AWI_PS118_05**

## Objectives

On Antarctic shelves, sponges and other filter-feeders often dominate the megabenthic epifauna (Arntz et al., 1994), but the factors governing their distribution and patchiness are only poorly understood. Food supply and iceberg scour are believed to play antagonistic roles in the build-up and removal of benthic biomass, explaining much of the observed patchiness (Clarke et al., 2004). In the Larsen A embayment following the 1995 collapse of the ice shelf, glass sponge biomass and abundance increased 2- and 3-fold between 2007 and 2011 (Fillinger et al., 2013), while locally abundant ascidians disappeared during the same period (Gutt et al., 2013). Prior to this shift in filter-feeder dominance, deposit feeding holothurians experienced an extreme population growth between 2000/2001 and 2005. The causes for these ecological changes and their extremely rapid pace, by Antarctic standards (Barnes, 2013), are so far only poorly understood. The community shifts suggest changes in benthic ecosystem functioning of similar magnitude in carbon and silicon sequestration by habitat forming sponges, degradation of organic matter and associated remineralisation of carbon and inorganic nutrients. Very little is known about these fundamental processes in polar regions, and even less on their dynamics – how they have changed and will change in response to the continuing decline of ice shelves off the Antarctic Peninsula.

Benthic oxygen uptake rate measurements are important to characterize the various habitats and estimate their demand for organic matter (Glud, 2008). Considering the existing data on fauna abundance for the Weddell Sea shelf, it is timely and highly relevant to investigate the community respiration also as a function of biomass and diversity. The Weddell Sea shelf offers contrasting sites of benthic biomass with high values along its eastern margin and lower values in the western and southern areas (Voß, 1988; Pineda-Metz et al., 2019). It is crucial for our understanding of bentho-pelagic coupling to measure how much the patchy primary production is imprinted on the benthic carbon mineralization below and to supplant current P/B estimates with community respiration measurements. Preferably, benthic oxygen uptake rates are measured *in-situ* using benthic Lander technology. In combination with the Eddy Covariance technique (Berg et al., 2003; Holtappels et al., 2013; Holtappels et al., 2015) this allows quantifying the integrated benthic oxygen uptake of large areas (10-100 m$^2$), i.e. on ecosystem level. The Eddy Covariance technique has been successfully deployed also in polar regions (Donis et al., 2016) where oxygen uptake rates as low as 0.5 mmol m$^{-2}$ d$^{-1}$ have been measured.

*Polarstern* cruise PS77 (ANT-XXVII/3) showed specimens of scleractinian corals in the icy waters in the vicinity of the former Larsen ice shelves. The likely old age of the corals and putative potential of the skeletons to provide proxies for the environmental history of their habitat (temperature, pH) in the skeletons shall be investigated as part of the AWI Strategy Fund DACCOR led by G. Schmidt-Grieb at AWI. PS77 (ANT-XXVII/3) also showed clusters of

the hexactinellid sponge *Rossella villosa* of different sizes. The close vicinity of the individuals raises the question of reproductive strategies employed by this rapidly expanding group in the Larsen area, namely the relative importance of clonal *vs* aclonal growth.

An exploratory remotely operated vehicle (ROV) survey during the PS96 ice-camp in Drescher Inlet led to the discovery of a community of arcturid isopods living on the underside of the >80 m thick shelf-ice. It is not known so far, how these benthic filter-feeders have populated their peculiar habitat, what role they play in the Antarctic ecosystem and to what extent the measured densities are representative for other parts of the Weddell Sea ice shelf and beyond.

The objectives of this study were five-fold:

1. to repeat the surveys carried out in previous *Polarstern* cruises to the Larsen area [PS69 (ANT-XXIII/8), PS77 (ANT-XXVII/3)] and control areas to assess the dynamics of Antarctic benthic communities

2. to carry out surveys in the Larsen C area previously covered by iceberg A68 to assess the community shortly after exposure to cryo-pelagic production

3. to collect corals and sponges in the Larsen areas to study the environmental archive in the skeleton (corals) and population genetics (sponges)

4. to carry out benthic process studies relating benthic biomass to oxygen uptake and remineralization, and

5. to explore the "hanging gardens" discovered in Drescher Inlet in other parts of the Weddell Sea in relation to potential factors governing the "seeding" of the shelf-ice with benthic organisms (e.g. rising platelet ice) and food supply (e.g. tidal currents).

Particularly, we aimed:

- to assess the status of the colonization of benthic communities in areas of differential exposure to cryo-pelagic production (Larsen A: 24 years, Larsen B: 17 years, Larsen C: 1.5 years), in comparison with the benthic community dynamics outside permanent ice-shelf cover.

- to collect sponges and corals in the Larsen area for geochemical and genetic analyses.

- to measure the benthic oxygen fluxes ex-situ and in-situ using sediment cores in addition to an Eddy-covariance Lander, and relating the fluxes to benthic biomass and water column productivity.

- to identify the abundance and spatial distribution of *Antarcturus spinacoronatus* on the face and underside of the shelf-ice in relation to bottom-up (food concentration, currents) and top-down factors (supply by platelet ice, removal by predators) governing the occurrence of "hanging gardens" at local and regional scales.

**Work at sea**

Due to heavy ice conditions, the cruise failed its main target to visit the former Larsen ice shelves. In addition, Larsen A was impossible to reach. As a consequence, three of our four main aims, above, were not fulfilled.

We re-adjusted our work plan focussing on the benthic oxygen fluxes and sediment oxygen profiles on the Antarctic Peninsula continental shelf in relation to a cryo-pelagic productivity gradient from year-round heavy ice conditions (location 1, Fig. 6.1) through the marginal ice zone (locations 2 through 5) to mainly ice-free conditions (locations 6 and 7). Sampling was

standardized to 1) a depth range of 350-450 m depth to account for depth related differences in organic matter reaching the seafloor 2) modelled tidal velocities below 5 cm s$^{-1}$ to ensure the accumulation of soft sediments, and 3) slight topographic depressions to minimize iceberg scours.
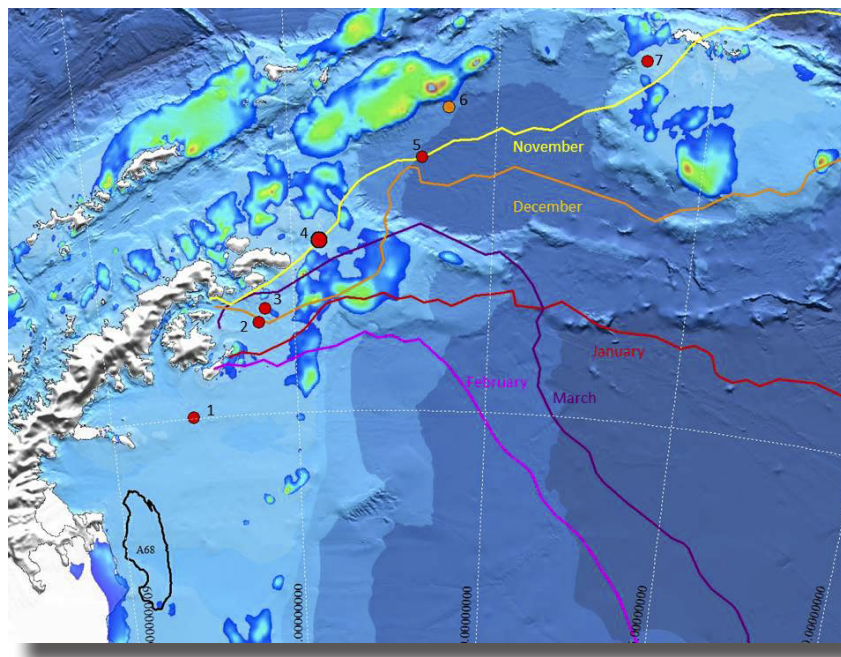


*Fig. 6.1: Map showing the 7 locations that were studied by our team along a gradient of decreasing sea ice cover (see Table 6.1 for station numbers). Coloured areas indicate modelled tidal current speeds on the shelf (<500 m) ranging between 8 cm/s (blue) and 100 cm/s (red). The coloured lines mark the climatological monthly mean sea ice extent. Sediment was retrieved at all locations (at location 6 only 3 cores). The ROV was deployed at location 2 and the lander-mooring was deployed at location 4. CTD casts were performed at all locations except for location 6.*

Our tasks consisted of

1.    the collection of sediment cores

2.    the collection of water samples in the benthic boundary layer and the water column aloft

3.    an assessment of oxygen consumption, dissolved inorganic carbon (DIC) production and nutrient remineralization in the sediment in relation to organic matter/pigment content and bacterial communities

4.    the measurement of *in-situ* oxygen fluxes and microprofiles in relation to ambient flows in the benthic boundary layer and water column. A side-aspect of our revised work programme was

5.    the imaging of the seafloor for macro- and megafauna.

Sediment cores were taken with the MUC in cooperation with the geology team (*cf*. chapter 7). Seven locations were covered (Tab. 6.1). Six locations yielded 8-9 cores used for the full set of experiments (red circles, Fig. 6.1). Five of the stations were situated in locations on the shelf that fulfilled the criteria described above (350-450 m depth, low tide, slight depression), whereas one station was situated in the deep-sea (3,290 m depth) and served as reference.

Another deep-sea station (2910 m) was sampled yielding only three cores allowing only a reduced set of experiments (orange circle, Fig. 6.1). Due to problems with the connector on the telemetry system on board *Polarstern*, it was advisable not to swap connections between OFOBS (see chapter 10) and the multicorer. As a result, MUC deployments were carried out blindfolded. Although it was planned to reduce the risk of hitting dropstones by carrying out OFOBS surveys before the deployment of the MUC, this precautionary measure was not realized.

**Tab. 6.1:** List of stations occupied by the Bentho-Pelagic Processes team during PS118 for observations, measurements and samples collected with conductivity temperature depth probe (CTD) mounted on a rosette, multicorer (MUC) and Remotely Operated Vehicle (ROV). At MUC stations 13-4 and 13-5, the sediment was so soft that the cores were filled to the brim which rendered them useless for the experiments (shaded lines). The first of the two ROV dives had technical difficulties and was aborted (shaded line).

| Gear | Station | Location | Date Time (UTC) | Latitude | Longitude | Depth [m] |
|---|---|---|---|---|---|---|
| CTD | PS118_4-1 | Test | 2019-02-22 18:30 | -63.8195 | -56.4729 | 534 |
| CTD | PS118_5-1 | 1 | 2019-03-04 15:29 | -64.9837 | -57.7516 | 445 |
| CTD | PS118_8-2 | 2 | 2019-03-11 16:38 | -63.9973 | -55.9061 | 412 |
| CTD | PS118_12-1 | 3 | 2019-03-14 07:04 | -63.8066 | -55.7443 | 456 |
| CTD | PS118_13-1 | 4 | 2019-03-17 11:31 | -63.0686 | -54.3124 | 423 |
| CTD | PS118_24-1 | 5 | 2019-03-20 01:25 | -62.2535 | -51.4796 | 3270 |
| CTD | PS118_62-1 | 7 | 2019-03-28 13:22 | -60.9307 | -46.5586 | 327 |
|  |  |  |  |  |  |  |
| MUC | PS118_5-3 | 1 | 2019-03-04 19:51 | -64.9834 | -57.7529 | 428 |
| MUC | PS118_5-4 | 1 | 2019-03-04 20:43 | -64.9795 | -57.7461 | 428 |
| MUC | PS118_8-5 | 2 | 2019-03-11 20:19 | -63.9711 | -55.9054 | 413 |
| MUC | PS118_8-6 | 2 | 2019-03-11 21:03 | -63.9684 | -55.9064 | 415 |
| MUC | PS118_8-7 | 2 | 2019-03-11 21:53 | -63.9684 | -55.9064 | 415 |
| MUC | PS118_12-2 | 3 | 2019-03-14 07:45 | -63.8089 | -55.7396 | 455 |
| MUC | PS118_12-3 | 3 | 2019-03-14 08:40 | -63.8125 | -55.7280 | 453 |
| MUC | PS118_12-5 | 3 | 2019-03-14 10:54 | -63.8140 | -55.7117 | 454 |
| MUC | PS118_12-6 | 3 | 2019-03-14 11:41 | -63.8165 | -55.7043 | 453 |
| MUC | PS118_13-3 | 4 | 2019-03-17 14:18 | -63.0528 | -54.3295 | 447 |
| MUC | PS118_13-4 | 4 | 2019-03-17 15:05 | -63.0533 | -54.3275 | 446 |
| MUC | PS118_13-5 | 4 | 2019-03-17 15:58 | -63.0538 | -54.3158 | 440 |
| MUC | PS118_24-2 | 5 | 2019-03-20 04:11 | -62.2575 | -51.4280 | 3289 |
| MUC | PS118_24-3 | 5 | 2019-03-20 06:45 | -62.2488 | -51.4090 | 3295 |
| MUC | PS118_48-2 | 6 | 2019-03-26 12:04 | -61.5724 | -51.1331 | 2908 |
| MUC | PS118_62-2 | 7 | 2019-03-28 13:57 | -60.9336 | -46.5587 | 329 |
|  |  |  |  |  |  |  |
| ROV | PS118_6-8 |  | 2019-03-06 00:56 | -64.9533 | -57.7954 | 430 |
| ROV | PS118_9-10 | 2 | 2019-03-13 03:41 | -64.0189 | -55.9182 | 404 |
|  |  |  |  |  |  |  |
| Lander Mooring | PS118_38-6 | 4 | 2019-03-22 17:22 | -63.0680 | -54.3130 | 423 |

Upon retrieval, cores were transferred to the temperature-controlled lab container (0°C) in F-Deck, stored in a water bath at near ambient temperature (-1.0 ± 0.3°C) until initiating the measurements (generally without delay). To determine the diffusive oxygen uptake of the sediments, oxygen profiles were measured using optical microsensors (Optodes, Pyroscience). For deep oxygen penetration depths, 430 µm bare fiber optodes glued into 20 cm long needles were used, while 50 µm thin retractable needle optodes were used for shallow oxygen penetration depths to increase the spatial resolution. Optodes were two-point calibrated in water at -1.0 ± 0.3°C at 100% $O_2$ saturation (air-bubbled MilliQ) and 0% $O_2$ saturation (saturated dithionite solution in seawater) and mounted on a micromanipulator (MU1, Pyroscience) using an adaptor rod. A minimum of three profiles per core at randomly chosen positions were carried out in 100-500 µm steps from 4 mm above the sediment water interface down to 10-160 mm into the sediment. Profile data (depth, oxygen concentration) were logged electronically using the "Profix" software (Pyroscience). Oxygen microprofiles were measured in 3-5 sediment cores per station.

At each station, two sediment cores were used for whole core incubations to determine the total oxygen uptake. For this, a plastic stopper was introduced into the core liner and pushed to a position at 8-12 cm above the sediment surface. The stopper was perforated with a hole to allow introducing a mini-optode (Pyroscience) from above. In the water column underneath the stopper, a magnetic stirrer was mounted which was driven by a rotating magnet outside the cores. The cores were incubated in the water bath at controlled temperatures for at least 12 hours. The oxygen concentrations were measured every 5 seconds using the 4-channel Firsting oxygen meter (Pyroscience) and the software Pyro Oxygen Logger.

At each station, three sediment cores were dedicated for pore water sampling. Rhizones were introduced through pre-drilled holes into the sediment core with a vertical spacing of samples of 1 cm from 0-10 cm depth. Below 10 cm, samples were spaced every 2 cm down to a maximum depth of 30 cm (20 samples). The pore water was retrieved in 20 ml syringes and subsampled for dissolved inorganic carbon (DIC), nutrients, dissolved metals (Fe/Mn), and sulphide.

Another three sediment cores per station were sampled for solid phase (C/N/S, grain size), microbial cells, DNA and RNA. Each core was sliced in 1 cm layers from 0-10 cm and below in 2 cm layers up to a depth of 30 cm. A subsample from each layer was collected in a Petri dish and stored frozen at -20°C. Subsamples for microbial cell counts, DNA and RNA were taken at 6 depths: 0-1, 1-2, 2-3, 3-5, 5-7, and 14-16 cm. DNA and RNA samples were stored frozen at -20°C and -80°C respectively. Samples for microbial cell counts were fixed in formaldehyde and a subsample was taken after 12 hours, washed with PBS-Buffer and stored at -20°C for later Fluorescent-In-situ-Hybridization (FISH). Finally, 3-5 cores per station (usually cores used for pore water cores and incubations) were size-fractioned through 1,000 µm, 500 µm and 300 µm sieves and the macrofauna (plus larger grains/stones) fixed in borax-buffered formaline (4% final concentration) for later analysis of biomass.

For *in-situ* measurements of benthic oxygen fluxes, the Eddy-Covariance lander was deployed. A mooring was attached to the Lander with a subsurface buoy at 30 m below the sea surface to avoid sea ice contact. The system was depth rated to 700 m. Attached to the Lander were two laterally mounted Eddy-Covariance systems oriented perpendicular to each other. This allowed at least one system to record currents unobstructed by the Lander legs in tidally shifting currents. An oxygen profiler was mounted in the centre of the lander. It was equipped with a lance holding four needle-type oxygen optodes that were pushed into the sediment. The Lander was also equipped with a CTD (Seabird), an upward looking current profiler (ADCP, 150 kHz, RDI) and a camera taking time lapse images of the sea floor. Finally, two small amphipod traps were mounted to the lander in cooperation with the Macrobenthic Biodiversity Group (see chapter 3). The mooring above was equipped with two CTDs, one at the top with

additional fluorescence and PAR sensors, and one in mid-water. Furthermore, two ADCPs (300 kHz, RDI, one upward and one downward looking) were attached near the upper buoy to measure the currents above and below. The Lander mooring was configured to be retrieved by either, a pair of deep sea releasers situated just above the mooring which would give free 200 m of additional mooring line, or by a pop-up buoy at the top of the mooring. The lander-mooring could be deployed only at location 4 (Fig. 6.1), where it was retrieved after a period of 5 days. Heavy sea ice conditions and the fact that we did not reach any Polynyas prevented a deployment during the first part of the expedition. Ice cover and strong currents at the Powell Basin prevented another deployment during the second part of the expedition.

For the collection of water samples, the CTD-rosette was used at seven stations (Tab. 6.1). It was operated by the CTD team (see chapter 10) who kindly provided Niskin samples from six standard depths: 0 m, 20 m, 40 m, 60 m, 80 m and 10 m above bottom). The 12 l bottles were released during the up-cast, and 1-2.5 l aliquots were transferred by tygon tubing to Nalgene bottles, stored in a cool-box and processed without delay.

For all depths, suspended organic carbon and nitrogen (POC and PON, 1 l) was filtered through pre-weighed and pre-combusted GF/F filters (25 mm Ø) and stored frozen at -20°C. For all depths Chl-*a* pigments (1 l) were filtered through GF/F filters (25 mm Ø) and stored frozen at -20°C. For three depths (surface, 20 m (or Chl *a* maximum) and bottom boundary layer) 0.5 l aliquots were fixed (37% formalin, end concentration 2%), stored for 4 h at 4°C and filtered through 0.2 μm polycarbonate filters (45 mm Ø). Filters were stored in individual petri dishes, filter side facing upward, sealed with parafilm and stored at -20°C for later FISH analyses. For three depths (surface, 20 m (or Chl *a* maximum) and bottom boundary layer) 1-4 l aliquots were filtered through 0.2 μm polycarbonate filters (45 mm Ø) using the inline peristaltic pump system, courtesy of the ice-group (Ilka Peeken, Erika Allhusen). Filters were folded (filter facing inward) and stored in Eppendorf caps at -80°C for subsequent bacterial DNA analyses. System was flushed with 2N-HCl-washed and milliQ between filtrations, and forceps subjected to 70 % ethanol cleaning to minimize contamination.

Seabed imaging was carried out on two stations only (Tab. 6.1) with a remotely operated vehicle (ROV, Ocean Modules, model V8 Sii) equipped with two video cameras (HD, Kongsberg oe14-502 and 4K, SubC Mk6) in front and a standard wide-angle camera (Bowtech L3C-550) to observe the tether in the back. The SubC Mk6 also has the option of taking 16.6 MPx still images. The 4K and HD cameras were equipped with red lasers triplets marking the edges of a reference triangle on the videos (10 cm horizontal, 10 cm vertical). Laser, altimeter and inclination data will allow to scale the images for abundance and size estimates. The lighting was provided by dimmable LED lights (Bowtech LED-2400 aluminium), four in the front and one in the back. ROV navigation was ensured by a compass, an orientation sensor, an altimeter (Tritech Micron Echo Sounder), a Doppler Velocity Log (RDI EXP600-FAM5SC/EXPCP, an obstacle avoidance sonar (Tritech Micron) and an Ultra Short Baseline (USBL) system (IXSea, GAPS) linked to the GPS system of *Polarstern*. A CTD (SeaBird SBE19 plus) equipped with sensors for temperature, conductivity, pressure, pH, oxygen, photosynthetically active radiation, and chlorophyll fluorescence was mounted on the ROV, and the ensemble of video, CTD, navigation and ROV system data recorded on terabyte hard drives.

The ROV was deployed from the starboard side of *Polarstern* using a 550 m cable mounted on a winch (CORMAC 5, MacArtney). A 50 kg depressor weight kept the line taught and out of reach of the vessel's propellers and thrusters. A neutrally buoyant tether was connected to the winch cable allowing the ROV to move freely about a radius of 50 m around the weight.

During the transects both cameras were looking forward in parallel, the ROV moving at an angle of 40-45° relative to the ground. A distance of 1-2 m was kept from the bottom to avoid sediment resuspension caused by the ROV's thrusters.

## Preliminary (expected) results

The bentho-pelagic processes team occupied seven locations (Tab. 6.1, Fig. 6.1). Corresponding water samples were collected from the CTD. All seven MUC stations sampled yielded sediment cores for microprofiles, oxygen incubations, pore water profiles, solid phase and microbiology sampling. The ROV was deployed at two stations, the lander at one.

*Benthic oxygen fluxes*

A total of 69 oxygen profiles were performed in altogether 23 cores. Whole cores incubations were performed in 12 cores. Porewater profiles were retrieved from 19 cores and solid phase and microbiology samples were retrieved from 20 cores. Preliminary results of the oxygen profiles and incubations are shown (Fig. 6.2). There was a significant difference between the sea ice covered location 1 and the ice-free location 4 as oxygen penetration depth decreased ten-fold and oxygen fluxes increased more than 4-fold for both diffusive and total oxygen uptake. We expect further differences between locations in pore water concentrations of dissolved iron and sulphide and also with regard to the microbial community.
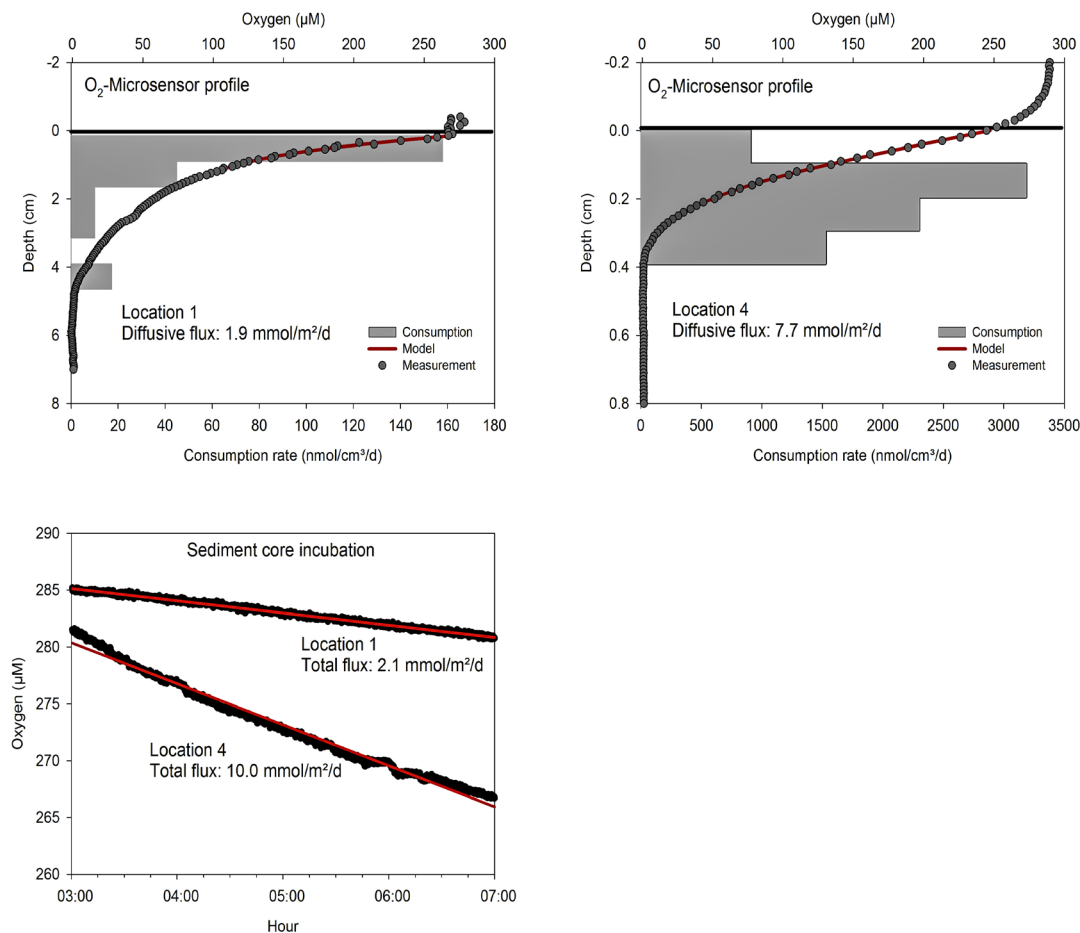


*Fig. 6.2: Oxygen microprofiles at location 1 and 4 (upper panels). Note the order of magnitude difference in the scaling of the axes between locations for both, sediment depth and consumption rate. The oxygen consumption rates in specific depth layers (grey bars) have been inversely modelled from oxygen profiles using the program PROFILE (Berg et al 1998). The overall diffusive flux was calculated by integrating the consumption rates over the entire oxic layer. Similar results were calculated when applying the Fick's first law to the oxygen gradient at the sediment-water interface. The lower panel shows a comparison of the oxygen decrease in the incubated sediment cores. The water column heights above the sediment were 8.5cm and 10.5 cm for locations 1 and 4, respectively.*

*Benthic Lander*

During the single lander-mooring deployment, all instruments were recording except the upward looking 300 kHz ADCP. Because the light of the time-lapse camera and the amphipod traps attracted benthic fish some of the fragile oxygen sensors of the Eddy-covariance device broke during the deployment. Altogether, we could retrieve 120 hours of ADCP and CTD measurements and about 40 hours of Eddy-covariance measurements. Although the Eddy covariance data first have to be analysed thoroughly, preliminary covariance statistics already show significant fluxes.

*Water column*

The CTD profiles showed overall low chl-a fluorescence readings in the water column, in the SW part of the transect and gradually higher values in the course of the sampling programme, supporting the existence of the hypothesized productivity gradient. Chl-*a* maxima were absent or weakly developed, and generally in the upper 20 m. Only on one occasion (location 7), we found a bimodal fluorescence profile with a maximum at 20 m and a secondary maximum at 60 m, suggesting partial sinking of the fall bloom. Interestingly, bottom boundary layer filters were often discoloured greenish-grey, suggesting resuspension of bedload material (inorganic and organic) by currents. However, according to Tidal Model Driver currents were generally weak in the southern part of the transect (<10 cm s$^{-1}$ major tidal ellipse of the K1 tide), but near Powell Basin currents were stronger (up to 100 cm s$^{-1}$).

*Seafloor biota*

Two ROV stations were carried out, including one (location 2) with seafloor observations. We found very soft sediment with abundant brittle stars and decapod shrimp (Fig. 6.3.A). A surprising feature of the station was the occurrence of numerous rhodaliids, a rare benthic family of siphonophores anchored like a hot air balloon above the sediment (Fig. 6.3.B). Previous surveys during PS77 (ANT-XXVII/3) had shown occasional rhodaliids in the Larsen A/B area. At the end of the dive we could observe a sea-anemone feeding on the abundant krill attracted by the ROV lights (Fig. 6.3.C) and an iridescent comb jelly (Fig. 6.3.D).
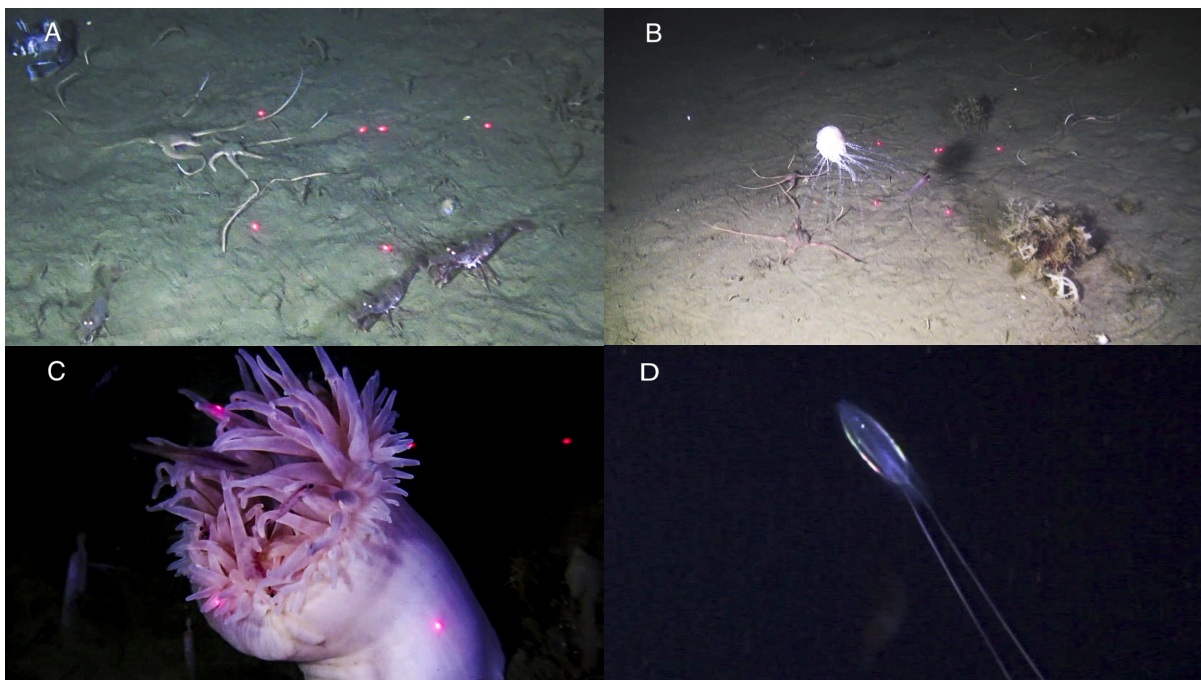


*Fig. 6.3: Video frames captured from the ROV on location 2. See text for explanation*

## Data management

Data and related information will be made available in the World Data Center PANGAEA Data Publisher for Earth & Environmental Science (www.pangaea.de).

## References

Arntz WE, Brey T, Gallardo VA (1994) Antarctic zoobenthos. Oceanography and Marine Biology: an Annual Review, 32, 241-304.

Barnes DKA (2013) Marine Biology: New Light on Growth in the Cold. Current Biology 23, (14), R609–R611, doi: 10.1016/j.cub.2013.05.058.

Berg P, Risgaard-Petersen N, Rysgaard S (1998) Interpretation of measured concentration profiles in sediment pore water. Limnology and Oceanography, 43(7), 1500-1510

Berg P, Roy H, Janssen F, Meyer V, Jorgensen BB, Huettel M, de Beer D (2003) Oxygen uptake by aquatic sediments measured with a novel non-invasive eddy-correlation technique. Marine Ecology-Progress Series, 261, 75-83.

Clarke A, Aronson RB, Crame JA, Gili JM, Blake DB (2004) Evolution and diversity of the benthic fauna of the Southern Ocean continental shelf. Antarctic Science, 16(4), 559-568.

Donis D, McGinnis DF, Holtappels M, Felden J, Wenzhoefer F (2016), Assessing benthic oxygen fluxes in oligotrophic deep-sea sediments (HAUSGARTEN observatory). Deep Sea Research Part I: Oceanographic Research Papers, 111, 1-10, doi:http://dx.doi.org/10.1016/j.dsr.2015.11.007.

Fillinger L, Janussen D, Lundälv T, Richter C (2013) Rapid Glass Sponge Expansion after Climate-Induced Antarctic Ice Shelf Collapse. Current Biology, 23, 1-5, doi: 10.1016/j.cub.2013.05.051.

Glud RN (2008) Oxygen dynamics of marine sediments. Marine Biology Research, 4, 243-289.

Gutt J, Cape M, Dimmler W, Fillinger L, Isla E, Lieb V, Lundälv T, Pulcher C (2013) Shifts in Antarctic megabenthic structure after ice-shelf disintegration in the Larsen area east of the Antarctic Peninsula. Polar Biology, 36, (6), 895-906, doi: 10.1007/s00300-013-1315-7.

Holtappels M, Glud RN, Donis D, Liu B, Hume A, Wenzhoefer F, Kuypers MMM (2013) Effects of transient bottom water currents and oxygen concentrations on benthic exchange rates as assessed by eddy correlation measurements. Journal of Geophysical Research-Oceans, 118(3), 1157-1169, doi:10.1002/jgrc.20112.

Holtappels M, Noss C, Hancke K, Cathalot C, McGinnis DF, Lorke A, Glud RN (2015) Aquatic Eddy Correlation: Quantifying the Artificial Flux Caused by Stirring-Sensitive O2 Sensors. Plos One, 10(1), e0116564, doi:10.1371/journal.pone.0116564.

Pineda-Metz S, Isla E, Gerdes D (2019) Benthic communities of the Filchner Region (Weddell Sea, Antarctica). Marine Ecology Progress Series (in review).

Voß J (1988) Zoogeographie und Gemeinschaftsanalyse des Makrozoobenthos des Weddellmeeres (Antarktis). Berichte zur Polarforschung, 45.

# 7. MARINE GEOLOGY

Frank Niessen[1], Michael Schreck[1], Sabine Hanisch[1],
Nele Lamping[1], Shuzhuang Wu[1], Huang Huang[2]
Gerhard Kuhn[1](not on board), Juliane Müller[1] (not on board), Markus Gutjahr[2] (not on board)

[1]AWI
[2]GEOMAR

## Introduction

Observations made over the past years indicate impacts of climatic changes along the Weddell Sea side of the Antarctic Peninsula (AP). In particular focus are the almost complete collapse of the ice shelves Larsen A and B and the vulnerability of the Larsen C with the recent brake-off of giant iceberg A68. However, of similar importance are observations of an increased sea-ice cover in the western Weddell Sea during the last years and the driving factors of the area for thermohaline deep-water production. Due to the intense sea-ice coverage even during austral summer months, the entire shelf area east of the Antarctic Peninsula is still largely under-sampled with respect to the sediment surface and sedimentary records. As the main target area of the cruise PS118, the Larsen ice selves A, B and C could not be reached during PS118 due to heavy sea ice conditions and inaccessibility, the central Robertson Trough area off Larsen A and B was the most southerly geological sampling location. Accordingly, the main target area shifted to the shelf north of Robertson Trough and the Powell Basin. The latter is known as an important pathway of Weddell Sea deep-water masses into the Scotia Sea and further north. With these modifications the objectives of the Marine Geology research of PS118 maintained as much as possible of what was planned originally, and were extended/modified as far as necessary:

- Search for palaeo subglacial lake or sub-ice-shelf cavern sediments in sedimentary shelf basins or troughs.

- Quantification of the relative contributions of various regional Weddell Sea Deep Water masses that form Weddell Sea Antarctic Bottom Water in space and time using Nd and Hf isotope compositions of water and sediment samples.

- Extension of Antarctic surface sediment data sets for geochemical proxy calibrations.

- Search for intra-shelf basins with high accumulation of Holocene sediments

- Search for deep-sea records indicative of Pleistocene climatic changes and variation of deep-water current activity

- However, the number of geological stations in the area remained relatively small for reasons of heavy sea-ice coverage east of the Antarctic Peninsula and related problems with geological sampling together with large sea-floor areas of the shelf being ploughed by icebergs.

## 7.1    Sedimentary environments and sampling

**Objectives**

Due to the unknown extents of ice shelves east of the Antarctic Peninsula in the past, it is critical to reconstruct and discriminate between past coverage by sea ice (Belt et al., 2016) and shelf ice by means of biomarker analyzes of sediments. Thus, taking surface samples from MUC at as many locations as possible shall be used to compare the present sea-ice situation with the youngest geological record. For the temporal context, it is essential to determine the ages of the sediments recovered by gravity cores. Dating of the shelf sediments is, however, difficult, due to the sparse distribution of dateable carbonate material and unknown $^{14}$C reservoir ages, but newer technologies need less amount of carbon for dating (Klages et al., 2014). One major target of PS118 is the discovery of depressions in shelf areas, which act as natural sediment traps to provide high resolution post-glacial and Holocene sediment records of the natural dynamics of shelf and sea ice distributions along the AP since the Last Glacial Maximum. Moreover, shelf depressions can preserve lacustrine sediments deposited in subglacial lakes at times when the AP ice sheet covered the entire shelves (Kuhn et al., 2017). This can only be distinguished after sediment coring and analysis. In addition, the few previously retrieved cores from the abyssal area of the Powell Basin indicate distinct interglacial-glacial cyclicity making the basin sediments interesting for studies of climatic changes close to the Antarctic Peninsula (Bak et al., 2018). More cores from areas with different accumulation rates are necessary to constrain the preliminary results available from recent publications (Bak et al., 2018).

**Work at sea**

*Site survey*

The selection of gravity cores (GC) and MUC samples is based on sub-bottom acoustic pattern surveyed by PARASOUND along the ship track. The deep-water coring locations at the northern end of the Powell Basin were selected after a PARASOUND survey was carried out between locations 60°50.725' S, 50°11.893' W and 60°50.856' S, 47°32.114'W combined with CTD stations (see chapter Oceanography of this report). Along this profile, the western shelf slope and deep-sea margin exhibit limited penetration and diffuse backscatter. This may indicate coarse-grained sediments induced by currents travelling along the slope in a northerly direction. We avoided this area for sampling, because GC penetration would have failed. On the other hand, the abyssal-plain sediments are well stratified and appear



*Fig. 7.1.1: Locations of gravity-coring (GC) stations of PS118*

mostly pelagic (stations PS118_75 and -79, Fig. 7.1.1, Tab. 7.1.1), whereas PS118_78 was selected from the high accumulation area of a contourite. Cores PS118_63-1 to 66-1 (Fig. 7.1.1, Tab. 7.1.1) are from pelagic sediments selected from PARASOUND data of *Polarstern* expedition ANT-XIX/5 (PS61).

**Tab. 7.1.1:** Coring-Station PARASOUND-Survey Summary

| Core No PS118 | Device | Water Depth (m) | Area | Para-sound survey | Acoustic Pattern | Variability in lateral accum. | Comments | Fig. 6.1. |
|---|---|---|---|---|---|---|---|---|
| 5-2 | SL | 4961 | C' PG/RT | PS118 | transp. / Cbr | very high | Trough fill below ice-berg ploughing depth | 3 |
| 8-3 | SL | 1696 | EaTG | PS118 | strat./till | medium | subglacial till overlain by melt-phase deposits, below ice-berg ploughing depth | 3 |
| 9-9 | SL | 1701 | EaTG | PS118 | strat./till | medium | - " - | |
| 10-2 | SL | 1706 | EaTG | PS118 | strat./till | medium | - " - | |
| 25-1 | SL | 777 | W' PB | PS118 | well strat. | low | lower end of cont. Slope | 6 |
| 38-4 | SL | 1504 | NE' APS | PS118 | well strat. | high | org. rich Holocene / melt-phase deposits | 5 |
| 38-7 | SL | 1603 | NE' APS | PS118 | well strat. | high | - " - | 5 |
| 48-3 | SL | 1569 | NW' PB | PS118 | diffuse backsc. | medium | "sandy" pelagic (lag) | |
| 62-4 | SL | 1534 | W' SOMCS | PS118 | well strat. | high | org. rich Holocene | |
| 63-1 | SL | 1731 | NE' PB | PS61-5 | well strat. | low | low accum. | |
| 64-1 | SL | 3875 | N' PB | PS61-5 | well strat. | low | medium accum. | |
| 65-1 | SL | 3904 | N' PB | PS61-5 | well strat. | low | low accum. | |
| 66-1 | SL | 2390 | N' PB | PS118 | well strat. | low | medium accum. | |
| 75-2 | SL | 1636 | N' PB | PS118 | well strat. | low | medium accum. | 7 |
| 78-1 | SL | 1237 | N' PB | PS118 | well strat. | high | max. accum. rates in contourite | |
| 79-1 | SL | 2649 | N'PB | PS118 | well strat. | very low | medium accum. | |

| Color Code | Description | | | | | | | |
|---|---|---|---|---|---|---|---|---|
| | Intra shelf depr. with undisturbed proglacial/postglacial drape | | | | | | | |
| | Intra shelf basin with high post-glacial (Holocene) accum. | | | | | | | |
| | Current-induced accum. | | | | | | | |
| | and contourite-drift | | | | | | | |
| | Undisturbed pelagic accum. | | | | | | | |
| | Glacial shelf trough with acoustically transp. Cover | | | | | | | |

Abbreviations

| APS | Antarctic Peninsula Shelf | accum. | accumulation | E' Eastern | |
|---|---|---|---|---|---|
| PG/RT | Prince Gustav/Robertsen Trough | backsc. | backscatter | N' Northern | |
| | | Cbr | Cenosoic bed rock | NW' North-Western | |
| EaTG | Erebus and Terror Gulf | strat. | stratified | NE' North-Eastern | |
| SOMCS | South Orkney Micro Continent Shelf | / | over | | |
| | | depr. | depression | W' Western | |
| PB | Powell Basin | trans. | transparent | C' Central | |

*Multi-corer sampling*

During PS118, the MUC was deployed at 9 stations (Fig. 7.1.2, Tab. 7.1.2). It was deployed parallel with the gravity corer (see below) at 8 out of these 9 stations in order to provide a complementary undisturbed surface, which is usually destroyed during gravity coring.
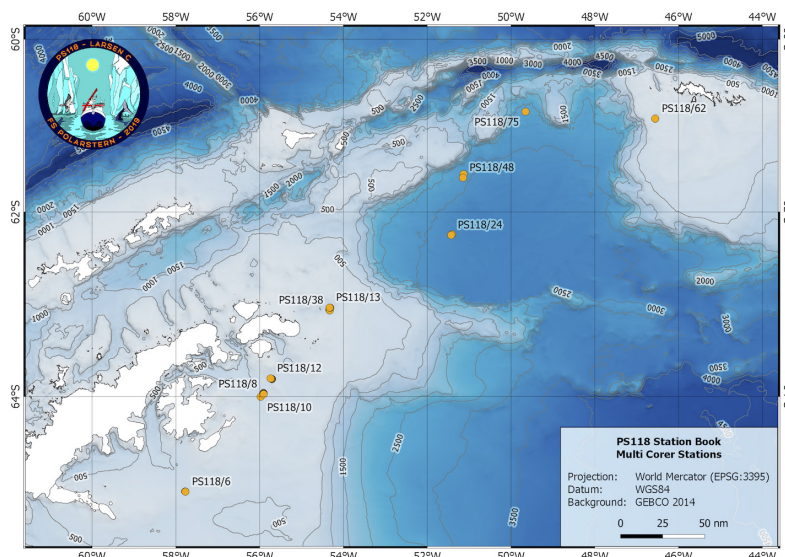


*Fig. 7.1.2: Locations of multi-coring (MUC) stations of PS118*

**Tab. 7.1.2:** Multi-Core sampling list of the Marine Geology programme

| Station | Date | Latitude | Longitude | Water Depths [m] |
|---|---|---|---|---|
| PS118_5-3 | 2019-03-04 | 64°59.00 S | 57°45.17 W | 428 |
| PS118_8-4 | 2019-03-11 | 63°58.522 S | 55°54.295 W | 413 |
| PS118_8-5 | 2019-03-11 | 63°58.260 S | 55°54.324 W | 413 |
| PS118_8-8 | 2019-03-11 | 63°57.74 S | 55°54.50 W | 415 |
| PS118_10-3 | 2019-03-13 | 64°00.150 S | 55°56.609 W | 416 |
| PS118_12-2 | 2019-03-14 | 63°48.537 S | 55°44.374 W | 455 |
| PS118_24-2 | 2019-03-20 | 62°15.450 S | 51°25.680 W | 3288 |
| PS118_38-5 | 2019-03-22 | 63°04.97 S | 54°19.72 W | 415 |

| Station | Date | Latitude | Longitude | Water Depths [m] |
|---------|------|----------|-----------|------------------|
| PS118_48-2 | 2019-03-26 | 61°34.343 S | 51°07.987 W | 2907 |
| PS118_62-3 | 2019-03-28 | 60°56.092 S | 64°33.484 W | 327 |
| PS118_75-1 | 2019-04-01 | 60°51.160 S | 49°39.245 W | 2653 |

At Station 62, the MUC had no recovery as it most likely triggered already within the water column, and thus the deployment had to be repeated. The excess water in the MUC tubes were sampled for Nd isotope analyses at five stations. Thereafter, one tube was designated for each of the following analyses:

• Archive

• Biomarkers

• Sedimentology

• Micropaleontology

The tube designated as archive was immediately frozen and later wrapped in plastic foiled and stored away frozen at -20°C. For biomarker analyses, sedimentology and micropaleontology, however, sampling was carried out in 1 cm increments on-board. Biomarker samples have been stored frozen (-20°C) in combusted glass vials, while sedimentological and micropaleontological samples are stored in 'Whirlpack' bags at +4°C.

*Gravity core sampling*

Long sediment cores were obtained at 16 stations (Fig. 7.1.1, Tab. 7.1.3) using the 1.5t-gravity corer (GC; Kiel/Hydrowerkstätten type, 12 cm Ø). Only at station PS118_5, the gravity corer was equipped with a 5 m core barrel while it was equipped with 10 m core barrel at all other stations. Despite high sediment penetration at all sites recovery varied between 94 and 993 cm. At station PS118_48, the core barrel was destroyed due to unfavourable sediments close to the sediment surface. During the station time the vessel drifted into an area with more sandy sediments limiting GC penetration. This could not be avoided due to ice conditions.

**Tab. 7.1.3:** Gravity-Core sampling list of the Marine Geology programme

| Core No. | Date Time UTC | Latitude | Longitude | Water Depth [m] | Reco-very [cm] | Pene-tration [cm] |
|----------|---------------|----------|-----------|-----------------|----------------|-------------------|
| PS118_5-2 | 2019-03-04 16:04 | 64° 59.006' S | 057° 45.068' W | 444.2 | 219 | 480 |
| PS118_8-3 | 2019-03-11 18:20 | 63° 58.973' S | 055° 54.295' W | 417.0 | 502 | 500 |
| PS118_9-9 | 2019-03-12 23:42 | 64° 01.155' S | 055° 55.891' W | 405.0 | 100 | 800 |
| PS118_10-2 | 2019-03-13 12:41 | 64° 00.181' S | 055° 58.615' W | 414.0 | 200 | 900 |
| PS118_25-1 | 2019-03-20 14:16 | 62° 19.361' S | 051° 40.550' W | 3200.1 | 675 | 900 |
| PS118_38-4 | 2019-03-22 14:45 | 63° 03.784' S | 054° 20.971' W | 447.0 | 835 | 1000 |
| PS118_38-7 | 2019-03-22 19:29 | 63° 04.865' S | 054° 19.656' W | 416.0 | 789 | 900 |
| PS118_48-3 | 2019-03-26 14:28 | 61° 32.638' S | 051° 07.746' W | 2883.6 | 94 | 250 |
| PS118_62-4 | 2019-03-28 15:38 | 60° 55.739' S | 046° 33.708' W | 327.0 | 875 | 10000 |

| Core No. | Date Time UTC | Latitude | Longitude | Water Depth [m] | Reco-very [cm] | Pene-tration [cm] |
|---|---|---|---|---|---|---|
| PS118_63-1 | 2019-03-28 21:11 | 61° 07.421' S | 047° 44.028' W | 2626.5 | 988 | 10000 |
| PS118_64-1 | 2019-03-29 01:43 | 61° 07.441' S | 048° 17.012' W | 2748.5 | 702 | 10000 |
| PS118_65-1 | 2019-03-29 05:37 | 61° 07.347' S | 048° 55.211' W | 2850.4 | 875 | 10000 |
| PS118_66-1 | 2019-03-29 13:06 | 61° 10.100' S | 049° 42.352' W | 2943.6 | 852 | 10000 |
| PS118_75-2 | 2019-04-01 13:22 | 60° 51.140' S | 049° 39.104' W | 2653.2 | 903 | 10000 |
| PS118_78-1 | 2019-04-02 06:11 | 60° 50.896' S | 048° 30.284' W | 2077.7 | 545 | 6000 |
| PS118_79-1 | 2019-04-02 09:42 | 60° 50.101' S | 048° 12.841' W | 2577.3 | 993 | 10000 |

On board the gravity core liners have been cut into 1 m sections and labelled accordingly as archive and working half. After 24 hours, the 1 m sections have been logged at room temperature for physical properties using the Multi Sensor Core Logger (for details see subchapter 7.2). Subsequently, the logged sections have been stored away at 4°C for detailed analyses in the home laboratories.

**Preliminary results**

For the area under investigation, we can largely distinguish between three different sedimentary environments and their distinctive acoustic sub-bottom pattern based on PARASOUND data:

•       The shelf area of the western Weddell Sea east of the Antarctic Peninsula

•       Small intra-shelf basins with more than 10 m thick fills of likely Holocene sediments on the shelves north-east of the Antarctic Peninsula and at the western end of the South Orkney micro continent

•       Deep-sea areas of the Powell Basin

•       The gravity cores and their acoustic facies based on PARASOUND are summarised in Table 7.2.1.

For the different sampling locations (examples are given in Fig. 7.1.3 to 7.1.7), the following observations are important to note: For area (i) the sediments cored at station PS118_5-2 from the Prince Gustav/Robertsen Trough are not significantly different from what is described in Reinhardy et al. (2011). Cores PS118_8-3, 9-9 and 10-2 are from similar acoustic facies (Fig. 7.1.3) and close to each other (Fig. 7.1.1). However, core penetration was similar and close to 10 m while recovery was extraordinarily low for two of the cores (Tab. 7.1.3). Low recovery was related to coring of an extremely stiff horizon at about 1 m sediment depth exposed in the core catcher, which blocked further recovery. Core analysis has to be carried out to interpret the environment and sediments as subglacial-lacustrine overlain by till, proglacial and/or postglacial marine. Other than shown in Fig. 7.1.3, where youngest sediments are well-stratified or transparent, the entire rest of the area (i) was found intensively ploughed by icebergs with no regular stratification visible. An area with high postglacial accumulation rates was profiled in Erebus and Terror Gulf of area (i) (Vega Drift, Fig. 7.1.4) but could not be cored due to heavy ice on the way out of the area.
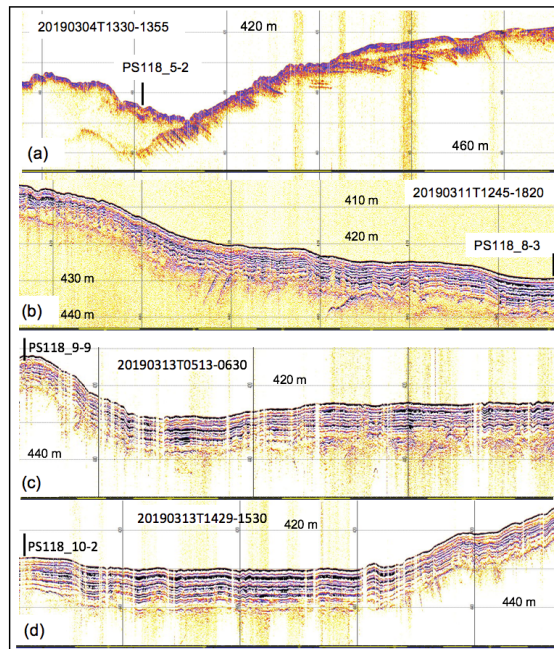
Fig. 7.1.3: PARASOUND profiles of bathymetric depressions on the eastern shelf of the Antarctic Peninsula with gravity-coring stations 5-2 (a), 8-3 (b), 9-9 (c) and 10-2 (d). Color bars at bottom of profiles give lateral distances with 1 km per yellow or black bar. Data time reference (left to right end): yyyymmddT(ime)hhmm-hhmm (UTC).
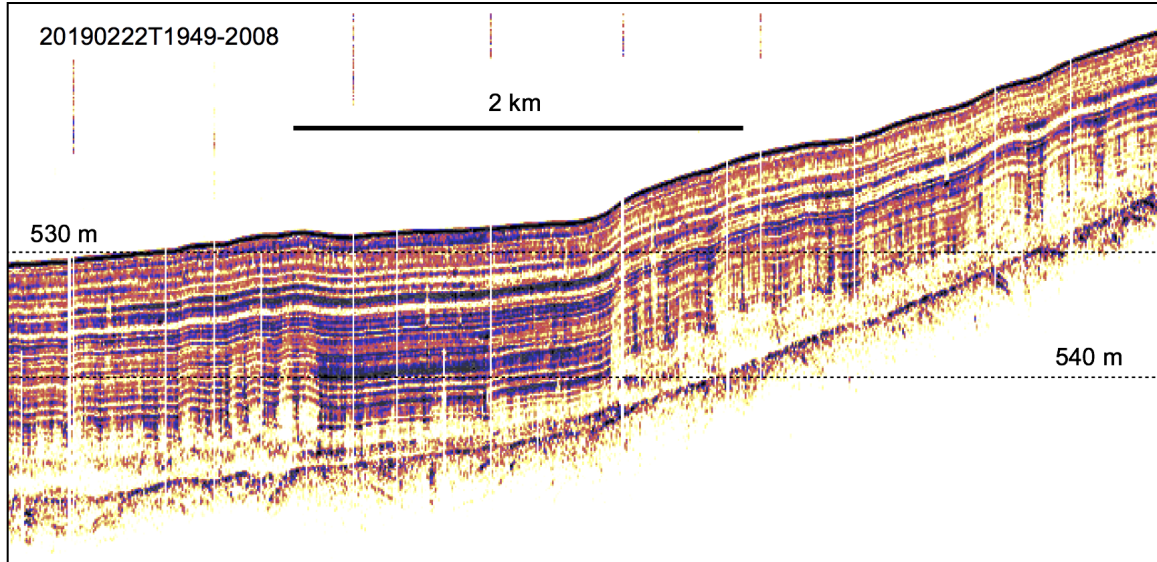


Fig. 7.1.4: PARASOUND profile of the Vega Drift near the Antarctic Sound (left and right end: 63°49.24' S / 56°29.78' W and 63°51.23' S / 56°27.55' W, respectively). Data time reference (left to right end): yyyymmddT(ime)hhmm-hhmm (UTC)
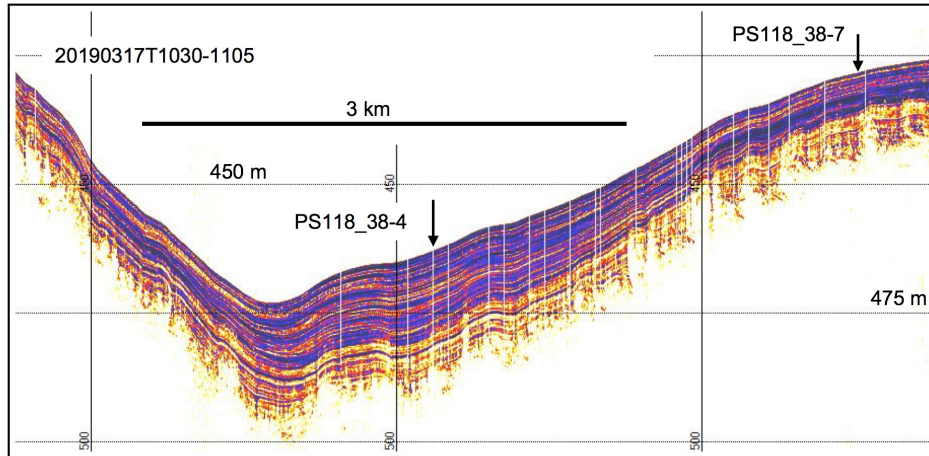
Fig. 7.1.5: PARASOUND profiles of a bathymetric depression on the northern shelf of the Antarctic Peninsula with gravity-coring stations 38-4 and 38-7. Data time reference (left to right end): yyyymmddT(ime)hhmm-hhmm (UTC)
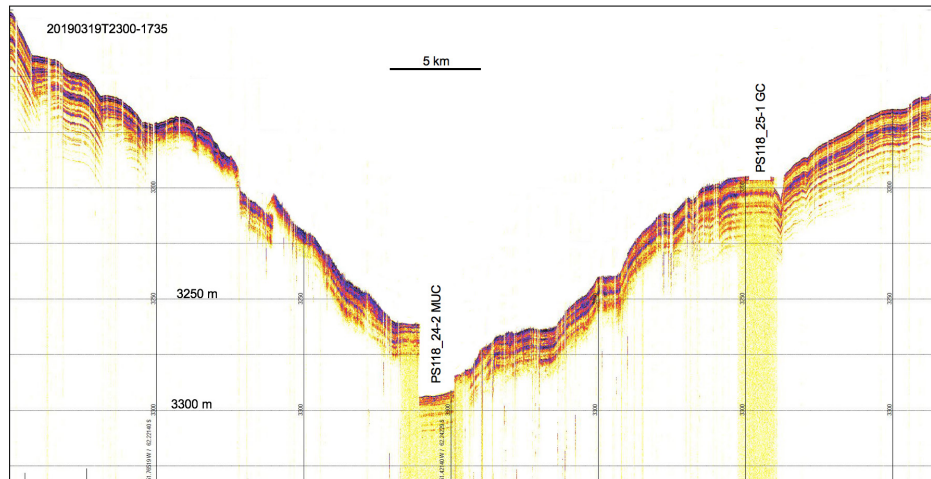


Fig. 7.1.6: PARASOUND profile of the deep-sea area of the western Powell Basin with coring stations 24 (MUC) and 25 (GC), Data time reference (left to right end): yyyymmddT(ime)hhmm-hhmm (UTC)
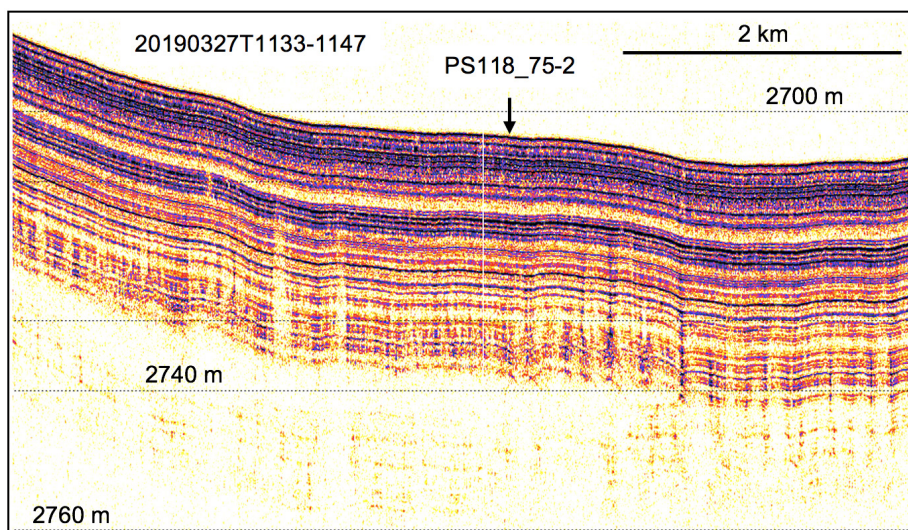


Fig. 7.1.7: PARASOUND profile of the deep-sea area of the northern Powell Basin with gravity-coring station 75 Data time reference (left to right end): yyyymmddT(ime)hhmm-hhmm (UTC)

Except for physical-property data, no analytical results are available from the MUC and GC cores so far.

**Data Management**

Data management of PARASOUND obtained during PS118 are described in Chapter 9 of this report. Management of core data determined by logging of physical properties is described in sub-chapter 7.2 below.

## 7.2 Core-physical properties (Multi-Sensor-Logging)

**Objectives**

Physical properties of sediments provide data for initial core characterisation with a very high vertical resolution. They can be used to define and interpret stratigraphic patterns, including a comparison with lithology. In combination with other data, down-core patterns of physical properties provide a powerful tool for lateral core correlation. During PS118, a Multi Sensor Core Loggers (MSCL) manufactured by GEOTEK Ltd. (UK) was used to determine physical properties non-destructively on all whole gravity cores. MSCL data are also useful to link these cores to high-resolution echosounding profiles obtained by PARASOUND DSIII-P70 thereby aiding the projection of core data from a single spot of a coring station into larger spatial and temporal scales. In combination with existing age models and core physical-property results from previous expeditions, MSCL data can provide an excellent stratigraphic-chronological framework for regional correlation of cores within the working area of PS118.

**Work at sea**

A standard MSCL-S track (GEOTEK - Ltd., UK, Ser. No. 25) was used to measure temperature, core diameter, P-wave travel time, p-wave receiver amplitude, gamma-ray attenuation, magnetic susceptibility (MS) and temperature on all gravity cores GC) in 10 mm depth intervals (Fig. 7.2.1). Based on calibration and processing, secondary parameters were calculated including Vp, WBD, volume-specific MS, porosity and impedance. In the year 2017, the right-hand "pushing" side of the AWI MSCL-25 track has been replaced by up-to-date GEOTEK hardware including the processor unit and PC now using GEOTEK software Version 6. The active pushing element is connected to a ball screw, driven by a stepper motor which can position a core to an accuracy of better than 0.5 mm. The detection of the reference point is automated using a laser unit. The technical specifications of the MSCL system are summarized in Table 7.2.1. The principle of logging cores is described in more detail in the GEOTEK manual "Multi-Sensor Core Logging", which can be downloaded from the web (http://www.geotek.co.uk).
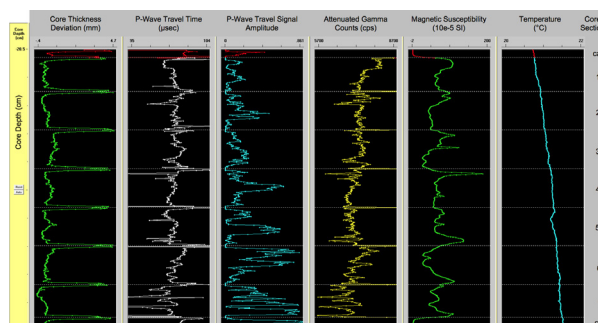


*Fig. 7.2.1: Screenshot of GEOTEK Software display with logging raw data of core PS118_25-1. Calibration sections on top and at bottom (cal) are liners filled with water.*

**Tab. 7.2.1:** Technical specifications of the GEOTEK MSCL-25 used during PS115/2.

Displacement transducer orientation: horizontal

Transducer Type: Standard Geotek Rolling

Transmitter pulse frequency: 230 kHz

Received pulse resolution: 50 ns

Seismogram sampling frequency: 12.5 MHz

Density

Radiation beam orientation: horizontal

Gamma ray source:  Cs-137, Ser. No. 0875/13

Activity: 356 Mbq (year 2013)

Energy:  0.662 MeV

Collimator diameter: 5.0 mm (GC, GKG), 2.5 mm (KAL)

Gamma detector: Gammasearch2, Model SD302D, Ser. Nr. 3114, John Count Scientific Ltd.,

10 s counting time

Temperature

Sensor: PT-100

Magnetic susceptibility

Loop sensor:  BARTINGTON MS-2C

Loop sensor diameter: 14 cm

Alternating field frequency: 565 Hz, counting time 10 s, precision 0.1 * 10-5 (SI)

Magnetic field intensity: ca. 80 A/m RMS

Point sensor: BARTINGTON MS-2F

Counting time: 10

The orientation of the P-wave and gamma sensors was horizontal. GC were measured in coring liners including end caps. Different parameters are defined and were measured as follows:

*Geometry*

The core diameter is measured as the distance between the faces of the Vp-transducers by using pre-calibrated lasers linked to transducer displacement mechanics. For GC, a standard plastic cylinder is used as the Reference Core Thickness (RCT) of known geometries (see equation below). It is mandatory by the MSCL system that the RCT is captured prior to each core-logging run in order to "zero" the measurements of core-thickness deviations from the RCT. The sediment thickness is calculated using the following equation of the GEOTEK processing software module:

X = RCT - W + CTD/10;

with RCT = Reference Core Thickness (GC=125 mm);

W = total wall thickness of liner (GC=5 mm);

CTD = core thickness deviation (raw data in mm, see above).

For GC logging the thickness deviation caused by section caps is added to the sediment thickness, because W is assumed to be constant. The software does not allow an extra input

for wall thickness of the caps (plus tape). This induces an error to WBD calculations using GEOTEK processing software (see 'Density' below). The GEOTEK processing software adds the thickness of the caps to the sediment thickness although the actual sediment core diameter will hardly vary at the caps compared to the rest of the core. A correction for this error is described in detail in the MSCL cruise report of PS87 (Stein 2014) and is applied to the density data as summarized under 'Density' below.

*Density*

Wet Bulk Density (WBD) was determined from attenuation of a gamma-ray beam transmitted from a radioactive source ($^{137}$Cs). A collimator was used to focus the radiation through the core-centre into a gamma detector (Tab. 7.2.2).

**Tab. 7.2.2:** Thickness and density of gamma-attenuation calibration liner (GC/GKG) filled with stair-shaped block of aluminium in water. Density of aluminium: 2.71 g cm$^{-3}$, density of water: 0.998 g cm$^{-3}$.

| Aluminium Thickness [cm] | Average Density [g cm$^{-3}$] | Av. Den. * Thickness [g cm$^{-2}$] |
|---|---|---|
| 10.00 | 2.40 | 29.35 |
| 9.01 | 2.26 | 27.65 |
| 8.01 | 2.12 | 25.94 |
| 7.01 | 1.98 | 24.22 |
| 6.00 | 1.84 | 22.49 |
| 5.01 | 1.70 | 20.80 |
| 4.00 | 1.56 | 19.08 |
| 3.01 | 1.42 | 17.37 |
| 2.00 | 1.28 | 15.64 |
| 1.01 | 1.14 | 13.96 |
| 0.00 | 0.998 | 12.23 |

To calculate density from gamma counts, GEOTEK-MSCL processing software module was used (www.geotek.co.uk), which applies the following function:

ln (GA) = A (GD * X)$^2$ + B (GD * X) +C;

with GA = Gamma Attenuation (raw data, cps);

X = Sediment thickness (see above);

A, B, C = constants.

For calibration, A, B and C were determined empirically two times during the cruise by logging a standard core consisting of different proportions of aluminum and water as described in Best and Gunn (1999). The data of the standard stair-shaped blocks of aluminum logged in a GC liner filled with water are given in Table 7.2.3.

**Tab. 7.2.3:** Parameter used for calibration of P-Wave Velocity (PTO) and Wet-Bulk Density (A,B,C) during PS118 (see equations under *Density* and *Velocity* in text).

| Core No. | PTO | A | B | C |
|---|---|---|---|---|
| PS118_5-2 | 20.4 | -0.0002 | -0.0576 | 10.08 |
| PS118_8-3 | 20.4 | -0.0002 | -0.0576 | 10.08 |
| PS118_9-9 | 20.4 | -0.0002 | -0.0576 | 10.08 |
| PS118_10-2 | 20.4 | -0.0002 | -0.0576 | 10.08 |
| PS118_25-1 | 20.0 | -0.0002 | -0.0572 | 10.076 |
| PS118_38-4 | 20.3 | -0.0002 | -0.0572 | 10.076 |
| PS118_38-7 | 20.1 | -0.0002 | -0.0572 | 10.076 |
| PS118_48-3 | 20.1 | -0.0002 | -0.0572 | 10.076 |
| PS118_62-4 | 19.6 | -0.0002 | -0.0572 | 10.076 |
| PS118_63-1 | 20.0 | -0.0002 | -0.0572 | 10.076 |
| PS118_64-1 | 20.0 | -0.0002 | -0.0572 | 10.076 |
| PS118_65-1 | 20.0 | -0.0002 | -0.0572 | 10.076 |
| PS118_66-1 | 20.0 | -0.0002 | -0.0572 | 10.076 |
| PS118_75-2 | 20.0 | -0.0002 | -0.0572 | 10.076 |
| PS118_78-1 | 20.0 | -0.0002 | -0.0572 | 10.076 |
| PS118_79-1 | 20.0 | -0.0002 | -0.0572 | 10.076 |

Also, postprocessing included WBD corrections for liner sections affected by end caps (see -Density above):

$WBD_{corr} = WBD + ((ct-x)/(x/100)*WBD/100-0.005)$

Ct is the measured core thickness at end caps, x is the mean core thickness between the end caps and 0.005 is the empirical effect on core density caused by additional gamma ray absorption of plastic caps. This correction has been fully applied for all post-processed GC (Tab. 7.1.3).

*Porosity*

Fractional Porosity (FP) is the ratio of the total volume over the volume of the pores filled with water. FP determined by MSCL-logging is not an independent data-acquisition parameter, but can be calculated from the WBD using the GEOTEK processing software module as follows:

$FP = (dg - WBD) / (dg - dw);$

with dg = grain density (2.7 g cm$^{-3}$);

dw = pore-water density (1.03 g cm$^{-3}$).

This approach includes the assumption that grain density and pore-water density are constant as given above.

*Temperature*

Temperature (T) was measured as room temperature in air on top of the logging bench in the laboratory. The cores were stored for 24 hours in the laboratory before logging in order to allow equilibration with room temperature.

*Velocity*

For determination of sonic velocity across the core the travel time (TT) of ultrasonic pulses (Tab. 7.2.1) are measured which are transmitted and received via rolling transducers (see geometry above). Vp was then calculated using the following equation from the GEOTEK processing software module:

Vp = X / (TT-PTO);

with: X = Sediment Thickness (see above);

TT = total travel time measured between the transducers (raw data in µs);

PTO = P-Wave Travel-time Offset.

The PTO is the travel time through the core liner walls (see geometry above), transducer, electronic delay, and detection offset between the first arrival and second zero-crossing of the received waveform (see GEOTEK Manual for details), where the travel time can be best detected (Fig. 7.2.2).
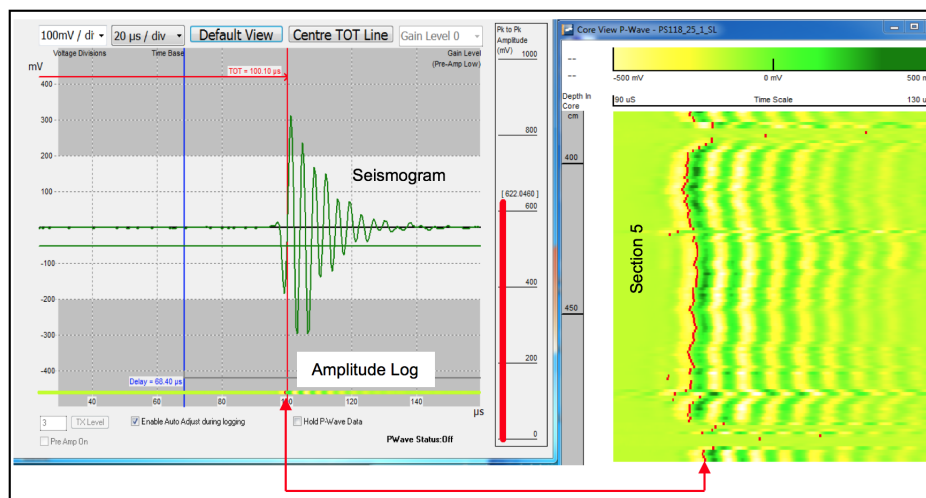


*Fig. 7.2.2: Screenshot of GEOTEK Software display with P-Wave single transmission seismogram (left centre), single transmission amplitude log (left bottom) and transmission-seismogram amplitude logs of core PS118_25-1, Section 5. Red line (left) and dots (right) marked by arrows show pulse arrival detection used during PS118 core logging.*

This travel-time offset was determined using a GC-liner filled with freshwater (Vp = 1483 m s$^{-1}$) logged together with the density standard (see above) and together with all logged cores (Initial Calibration Piece, see GEOTEK Manual for details, also as final calibration piece

below the core). In order to find the correct PTO we used the GEOTEK processing software approaching the correct Vp in water (table-output function) by inputs of different PTO values into the processing panel and repetitive processing until the PTO value was approached to give correct Vp in water (1483 m s$^{-1}$ at 20°C). The PTO values determined during PS118 are presented in Tab. 7.2.3. The Vp amplitudes remained unprocessed in the final data sets.

*Magnetic Susceptibility (MS)*

The specifications of the Bartington MS-2 loop sensor used on board are summarized in Table 7.2.1. The MS-2 meter was set to zero 200 mm before the core reached the MS sensor. Sensor was checked for possible drift above the top and below the bottom of the core by logging a 200 mm long liner filled with water as initial and final calibration piece. Any drift observed, which was larger than 1 or -1, was corrected assuming a linear drift over the entire core length.

$MS_{dc}$ = MS - CD*(Drift/Core Length);

with $MS_{dc}$ = the drift corrected MS;

MS = the MS raw data;

CD = depth in core (raw data, mbsf).

The first processing of data using GEOTEK Software does not change MS data from raw data. In order to calculate volume-specific magnetic susceptibility (VMS) data are corrected for loop-sensor and core diameter as follows:

MS ($10^{-6}$ SI) = measured value ($10^{-5}$ SI) / K-rel * 10

with K-rel empirically determined by GEOTEK (www.geotec.co.uk):

K-rel = $4.8566(d/D)^2$ – 3.0163(d/D) + 0.6448

D is the diameter of the MS-2-meter loop sensor (140 mm) and d is the reference diameter of the core.

**Preliminary results**

Minor gaps of data are at or near the end of individual liner sections. No meaningful Vp data are recorded along the end caps of GC core sections, because the arrival times of the acoustic pulse were not detectable through end caps. The same effect was observed for some core sections between the caps from the eastern shelf of the Antarctic Peninsula. It is assumed that the sediments inside the liners were not in contact with the liner wall and, thus, did not allow sound propagation between transducers. On the other hand, MS and WBD logs provide nearly complete and relatively good Vp records in sediments from the deep sea of the Powell Basin.

Here we present preliminary results of combined MS/WBD logs and cross correlations of WBD and Vp of four cores (Fig. 7.2.3), each of which is somehow representative of pattern from the different sampling areas (Weddell Sea Shelf of the Antarctic Peninsula, intra-shelf basins with high postglacial accumulation as well as pelagic realm and contourites from the abyssal area of the Powell Basin). In all records, MS is somehow positively correlated with WBD indicative of porosity as one controlling factor of MS. However, the overall trends and large fluctuations of MS are clearly superimposed on WBD fluctuations. This suggests that MS is also controlled by individual concentrations of magnetic grains in the sediments independent of porosity.
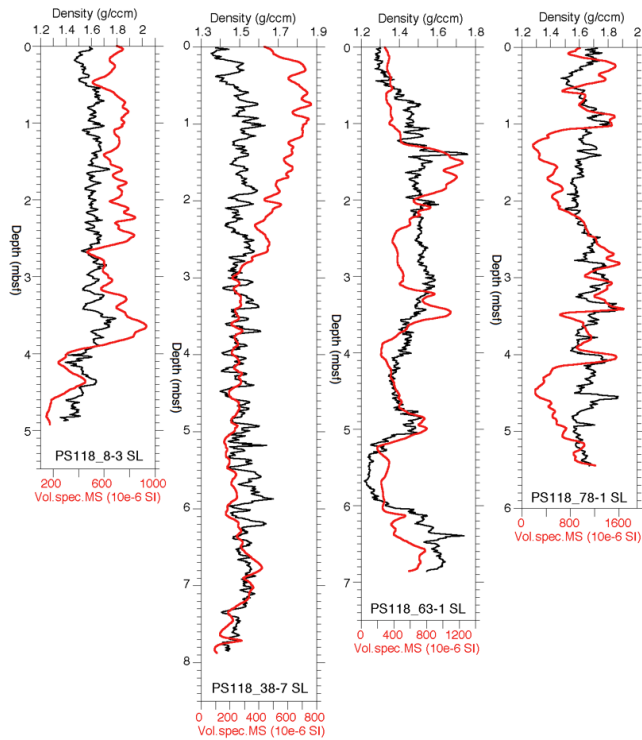
*Fig. 7.2.3: Examples of MSCL data (WBD and MS) of cores 8-3, 38-7, 63-1 and 78-1*

A comparison of WBD and Vp from the cores mentioned above (Fig. 7.2.4) indicates that cores from the different areas and sedimentary environments exhibit different Vp clustering relative to the WBD. This may indicate differences in the cores in terms of content of biogenic opal, carbonate/detrital contents and/or grain size (Weber 1998).

The potential of the records for core correlation, stratigraphy/chronology and core composition needs to be further analysed after the cruise.
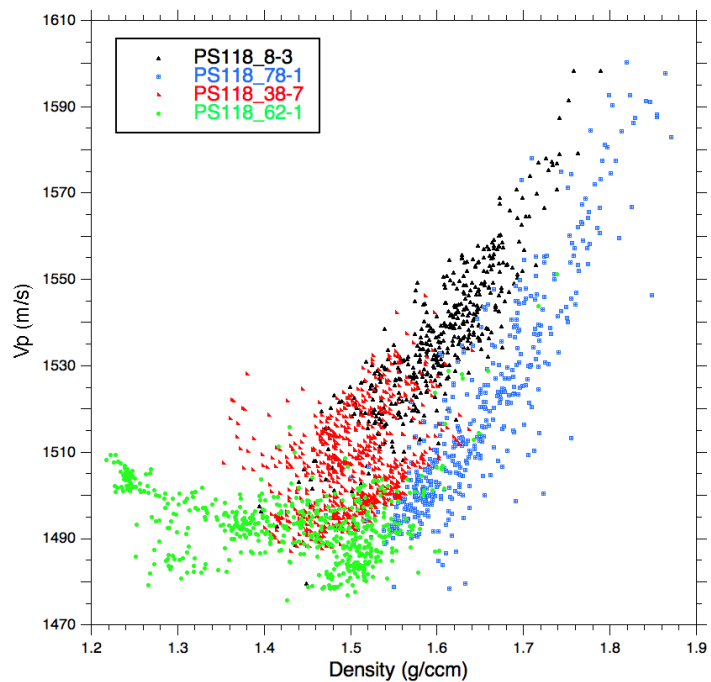


*Fig. 7.2.4: Density / p-wave velocity (Vp) plot of 4 selected cores*

**Data management**

Data acquisition and processing of whole cores went through several steps:

MSCL raw-data acquisition of whole cores using GEOTEK software.

First processing of whole-core data using GEOTEK software. This includes the calculation of core thickness, Vp, and WBD. WBD data have errors along liner caps. MS sensor response remained in raw-data state ($10^{-5}$ SI).

Second processing of whole-core data using software Kaleidagraph ™. This includes a data quality control on calibration sections logged on top and below the bottom of the core (200 mm liner filled with water) and a removal of these data from the core. It also includes a correction of core-section length according to the obtained recovery and cleaning for odd data points. In addition, MS is corrected for sensor drift and MS "tails" above and below top and bottom of cores, respectively, were "mirrored" into the core. These "tails" are related to the magnetic grains in the core and the low depth resolution of MS loop sensor. MS data are then converted to volume-specific susceptibility. WBD of gravity cores are corrected for end-cap errors. All physical properties of the cores of PS118 were fully processed during the cruise.

All data will be available to the shipboard science party for joint publication. In addition, the data are stored as a function of core depth in form of text-files in the World Data Center PANGAEA Data Publisher for the Earth & Environmental Science ([www.pangaea.de](www.pangaea.de)).

## 7.3. Biomarker

**Objectives**

Antarctic sea ice is one of the most variable features on Earth, which makes modelling efforts of sea ice changes challenging. Observational data, such as proxy-based sea ice reconstructions, are therefore a helpful tool for improving numerical models and hence the understanding of past sea ice conditions of Antarctica. Specific organic biomarker lipids (highly branched isoprenoids) can be used to distinguish between different sea surface conditions and give semi-quantitative sea ice estimates. In order to further develop and evaluate the relatively new sea ice proxy IPSO$_{25}$ (Ice Proxy of the Southern Ocean with 25 carbon atoms; Belt et al., 2016), a set of surface sediments (MUC) and sediment cores (GC) were acquired during the expedition. For source identification of the biomarker IPSO$_{25}$, five "dirty ice" samples were additionally collected.

**Work at sea**

In total, nine MUC cores from different locations for biomarker analysis were successfully re-trieved, with core lengths from 28 to 40 cm (Fig. 7.1.1, Tab. 7.1.2). The cores were cut into 1 cm slices and stored fro-zen in combusted glass top vials at -20°C. One archive MUC from each station was wrapped in aluminium foil, put into a tubular plastic foil and also stored at -20°C to permit a possible resampling for biomarker studies.

**Preliminary (expected) results**

Analysis of biomarkers will be carried out in the home laboratory at AWI Bremerhaven, preliminary results can therefore not be presented herein. However, high organic contents in multiple MUCs and high-resolution Holocene sediments, which were retrieved with the GC, provide a promising basis for biomarker analysis.

**Data management**

Except for navigational data of MUC stations, which is managed through D-Ship, no data on biomarkers are produced during the cruise.

## 7.4 Isotope geochemistry

**Objectives**

Seawater radiogenic Nd and Hf isotopes are sensitive and powerful tracers for circulation change and water mass mixing. The actual dissolved seawater Nd and Hf is mainly contributed by the continent runoff. Due to the age difference of the East Antarctica and West Antarctic Peninsula, the water masses within Weddell Sea are supplied by distinct Nd and Hf isotopic signatures from different regions of Antarctic continent. To date previously published southernmost Nd and Hf isotopic seawater data exist only from the NE Weddell Sea (Stichel et al., 2012a; Stichel et al., 2012b), despite the fact that the Southern Weddell Sea is the most important AABW formation area (Orsi et al., 1999). Given its unique circulation scheme and hinterland geology, we expect large regional Nd and Hf isotopic gradients dependent on water mass sourcing, particularly in the Larsen C area where a part of AABW formed. Our aim is to provide a water mass Nd and Hf isotopic budget for the Western Weddell Sea area and better constrain the Weddell Sea Deep Water Nd and Hf isotope signature exported to Southern Ocean areas further north. A related study was carried out by the Marcus Gutjahr and Huang Huang during PS111 along the Ronne-Filcher Ice Shelf.

Dissolved Nd and Hf are incorporated into authigenic Fe-Mn oxyhydroxides in marine sediments and can be extracted using a gentle reductive leaching approach for reconstruction of the circulation change in the past (Gutjahr et al., 2007; Blaser et al., 2016). In fact marine sediments are a mixture of different phases such as carbonates, organic matter, authigenic Fe-Mn oxyhydroxides as well as the terrigenous fraction, each carrying distinct Nd and Hf isotopic signals. While the two studies mentioned above provided strong support for the reliability of this technique in extracting bottom water Nd and Hf isotope compositions from North Atlantic settings, reductive leaching aiming to extract past bottom water isotope signatures was so far not rigorously tested for Antarctic sediments. Such sediments are chemically immature since these were largely only physically weathered during sub-glacial erosion. As a result, any freshly ground sediment is chemically relative reactive potentially releasing terrigenous (i.e. non-seawater derived Nd and Hf) during chemical leaching which may ultimately be offsetting extracted bottom water isotopic information.

While first paleo-records look strikingly promising highlighting strong paleocirculation changes over the two last deglaciations, we further want to demonstrate that bottom water Nd and Hf isotopic compositions are indeed reliably archived in Weddell Sea sediments. To this end, sampling for isotope geochemistry (Nd&Hf isotopes and Rare Earth Element (REE) concentrations) were done on surface sediments, collected by means of the multicorer (MUC). The Nd&Hf isotopes and trace metal concentration of the different sedimentary phases in the MUC samples will be compared. Phases to be assessed comprise (i) the sediment porewater, (ii) authigenic Fe-Mn oxyhydroxides as well as (iii) the residual terrigenous phase. This investigation will also provide crucial information on trace metal cycling in the uppermost few centimetres below the sediment – bottom water interface.

**Work at sea**

*Seawater sampling for Nd and Hf isotope and REE analyses*

The major aim of the isotope geochemistry group was seawater sampling for Nd and Hf isotope as well as REE concentration analyses. Owing to a fantastic CTD sampling program carried out by the oceanography group, we were able to obtain seawater for Nd and Hf isotopic analyses from a total of 16 CTD stations (Tab. 7.4.1, Fig. 7.4.1), sampling a total of 56 individual water samples in various locations. Water depths for seawater samples at each station were usually selected to always include a bottom water sample (usually sampled 10 m above ground), as well as in various water depths marking either water mass end-members or mixtures / transitions of water masses. Since Nd and Hf have a rather long residence time in seawater on the order of 200 to 2,000 years, small-scale variations should only be marginal unless the water masses derived from very different source areas. Besides, a minimum of 20 l of seawater were taken for individual samples since Nd and Hf concentrations are in the picomole range requiring large sample sizes. Samples were filtered with 0.2 µm ACROPAC filters directly from the Niskin bottles into acid-cleaned collapsible containers. Samples were acidified to a pH of 2, Fe chloride solution added and left to equilibrate for at least 24 hours, then the seawater pH was raised to >8 with suprapure ammonia. At this high pH, dissolved Fe precipitates also co-precipitating other trace metals such as Nd and Hf. After a further three days newly formed Fe oxyhydroxides enriched in REE settle at the base of the collapsible containers, about 80-90 % of the supernatant can be siphoned off and discarded. The pre-concentrated Nd aliquots are transferred into smaller sample containers and packed for shipping and further purification and measurements at GEOMAR Kiel. Before sampling of the Nd and Hf isotope aliquot, small (250 ml) aliquots were filtered for REE concentration analyses. These samples were acidified and stored for further analyses at GEOMAR Kiel.

*MUC sampling*

Cores for the isotope geochemical studies were taken from five MUC stations (Tab. 7.4.1, Fig. 7.4.1). One core per site were sampled and then frozen at -20°C and taken home for future work. After arrival of the MUC on board Polarstern during station work, about 8 l of MUC water (i.e. bottom water inside the core liners) of selected cores were collected, filtered (0.2 µm mesh size) and acidified for further Nd and Hf isotopic, as well as REE analyses back at GEOMAR Kiel.
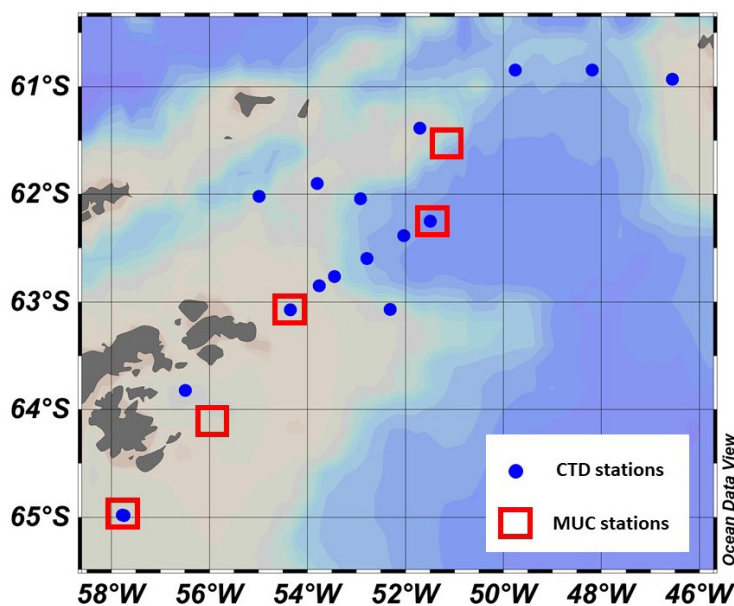


*Fig. 7.4.1: Overview map of all stations covered for the isotope geochemical work of the Marine Geology group during PS118. Multi-core stations are labeled in Fig. 7.1.2. For CTD stations see Oceanography chapter of this report.*

**Tab. 7.4.1:** Summary of all realised stations during PS118 for which isotope geochemical samples have been sampled for further processing at GEOMAR Kiel

| # | Station - Device Operation | DateTime UTC | Device Code | Latitude | Longitude |
|---|---|---|---|---|---|
| A1 | PS118_4-1 | 2019-02-22 18:29 | CTD | 63°49,169' S | 056°28,361' W |
| A2 | PS118_5-1 | 2019-03-04 15:14 | CTD | 64°59,058' S | 057°44,896' W |
| A3 | PS118_13-1 | 2019-03-17 11:18 | CTD | 63°04,088' S | 054°18,766' W |
| A4 | PS118_15-2 | 2019-03-18 18:25 | CTD | 62°00,986' S | 054°59,554' W |
| A5 | PS118_16-1 | 2019-03-18 23:48 | CTD | 61°53,999' S | 053°48,048' W |
| A6 | PS118_21-1 | 2019-03-19 10:07 | CTD | 62°02,445' S | 052°55,126' W |
| A7 | PS118_24-1 | 2019-03-20 00:17 | CTD | 62°15,007' S | 051°30,013' W |
| A8 | PS118_26-1 | 2019-03-20 20:11 | CTD | 62°23,726' S | 052°01,545' W |
| A9 | PS118_28-1 | 2019-03-21 06:06 | CTD | 62°36,279' S | 052°48,150' W |
| A10 | PS118_32-1 | 2019-03-21 21:25 | CTD | 62°45,990' S | 053°26,990' W |
| A11 | PS118_34-1 | 2019-03-22 01:32 | CTD | 62°50,882' S | 053°45,554' W |
| A12 | PS118_38-12 | 2019-03-23 03:33 | CTD | 63°04,259' S | 054°20,130' W |
| A13 | PS118_42-1 | 2019-03-25 13:41 | CTD | 61°23,374' S | 051°42,057' W |
| A14 | PS118_53-1 | 2019-03-27 09:19 | CTD | 60°50,617' S | 049°45,856' W |
| A15 | PS118_59-1 | 2019-03-28 02:09 | CTD | 60°50,781' S | 048°11,739' W |
| A16 | PS118_62-1 | 2019-03-28 13:11 | CTD | 60°55,725' S | 046°33,535' W |
|  |  |  |  |  |  |
| B1 | PS118_5-3 | 2018-02-10 19:05 | frozen MUC | 64°59,022' S | 057°45,108' W |
| B2 | PS118_8-4 | 2018-02-13 00:45 | frozen MUC | 63°58,612' S | 055°54,271' W |
| B3 | PS118_24-2 | 2018-02-20 09:06 | frozen MUC | 62°15,347' S | 051°26,777' W |
| B4 | PS118_38-5 | 2018-02-22 19:46 | frozen MUC | 63°04,945' S | 054°19,773' W |
| B5 | PS118_48-2 | 2018-02-26 13:30 | frozen MUC | 61°34,964' S | 051°08,489' W |

# A1 to A16: Summary of all seawater Nd & Hf isotopes and REE stations

# B1 to B5: Summary of all frozen Multi Core sediment stations

**Preliminary (expected) results**

No results can yet be reported for the geochemical part of the Marine Geology group. Samples were only be pre-processed on Polarstern for further purification and analyses in mandatory clean-room environments at GEOMAR Kiel. Sediment and seawater samples collected within the frame of our project during PS118 will provide a wealth of new insights into Weddell Sea ocean circulation and continental meltwater and sub-glacial input from a radiogenic isotope and dissolved Rare Earth Element perspective. We will produce a first assessment on the regional dissolved Nd and Hf isotopic variation in the West Weddell Sea region and gauge the Nd and Hf isotopic output of Weddell Sea Deep Water into the Southern Ocean from the Powell basin. The sedimentary analyses will highlight in how far reliable bottom water Nd and Hf isotope reconstructions can be made for paleoceanographic studies.

## Data management

Analytical data will be available latest with publication as supplement related to each publication. All datasets will be made citable including a DOI.

## References

Bak Young-Suk, Yoo Kyu-Cheul, Lee Jae Il & Il Yoon Ho (2018) Glacial–interglacial records from sediments in Powell Basin, Antarctica. Antarctic Science, 30, 1-8. doi:10.1017/S0954102018000408.

Belt ST, Smik L, Brown TA, Kim J, Rowland SJ, Allen CS, Gal JK, Shin KH, Lee JI & Taylor KWR (2016) Source identification and distribution reveals the potential of the geochemical Antarctic sea ice proxy IPSO25. Nature Communications, v. 7, p. 12655.

Best AI & Gunn DE (1999) Calibration of marine sediment core loggers for quantitative acoustic impedance studies. Marine Geology, 160, 137-146.

Blaser P, Lippold J, Gutjahr M, Frank N, Link JM & Frank M (2016) Extracting foraminiferal seawater Nd isotope signatures from bulk deep sea sediment by chemical leaching. Chemical Geology, 439, 189-204.

Gutjahr M, Frank M, Stirling, CH, Klemm V, van de Flierdt T & Halliday AN (2007) Reliable extraction of a deepwater trace metal isotope signal from Fe-Mn oxyhydroxide coatings of marine sediments. Chemical Geology, 242, 351-370.

Klages JP, Kuhn G, Hillenbrand CD, Graham AGC, Smith JA, Larter RD, Gohl K & Wacker L (2014) Retreat of the West Antarctic Ice Sheet from the western Amundsen Sea shelf at a pre- or early LGM stage. Quaternary Science Reviews, 91, 1-15.

Kuhn G, Hillenbrand CD, Kasten S, Smith JA, Nitsche FO, Frederichs T, Wiers S, Ehrmann W, Klages JP & Mogollón JM (2017) Evidence for a palaeo-subglacial lake on the Antarctic continental shelf. Nature Communications, 8, 15591. doi:10.1038/NCOMMS15591, hdl:10013/epic.50945.

Orsi AH, Johnson GC & Bullister JL (1999) Circulation, mixing, and production of Antarctic Bottom Water. Progress in Oceanography, 43, 55-109.

Reinardy BTI, Larter RD, Hillenbrand C-D, Murray T & Hiemstra JF, BOOTH AD (2011) Streaming flow of an Antarctic Peninsula palaeo-ice stream, both by basal sliding and deformation of substrate, Journal of Glaciology, 57, No. 204.

Stichel T, Frank M, Rickli J & Haley BA (2012a) The hafnium and neodymium isotope composition of seawater in the Atlantic sector of the Southern Ocean. Earth and Planetary Science Letters, 317-318, 282-294.

Stichel T, Frank M, Rickli J, Hathorne EC, Haley BA, Jeandel C & Pradoux C (2012b) Sources and input mechanisms of hafnium and neodymium in surface waters of the Atlantic sector of the Southern Ocean. Geochimica et Cosmochimica Acta, 94, 22-37.

Weber ME (1998) Estimation of biogenic carbonate and opal by continuous don-destructive measurements in deep sea sediments: applicaton to the eastern Equatorial Pacific. Deep-Sea Reasearch I, 45, 1955-1975.

# 8.    GEOTHERMAL HEAT FLOW

Ricarda Dziadek[1]

Fynn Warnke[1,2], Norbert Kaul[2] (not on board)

[1]AWI

[2]UHB-IUP

**Grant-No. AWI_PS118_03**

## Objectives

The objective of our temperature measurements during *Polarstern* Expedition PS118 was an assessment of the geothermal heat flow in the western Weddell Sea Region, where direct observations of *in-situ* sediment temperatures are entirely absent. The thermal state of polar continental crust plays a crucial role for understanding the stability and height of large ice sheets, the visco-elastic response of the solid-Earth due to unloading, when large ice caps melt and, in turn, the accuracy of future sea level rise prediction. The scientific community repeatedly outlined the importance of better constrained boundary conditions to enhance the accuracy ice sheet model performance for future sea level rise predictions. Regional GHF estimates are based on crustal heat production in the onshore area of the Antarctic Peninsula (Burton-Johnson et al., 2017) and indicate spatial variabilities. Furthermore, locally elevated GHF due to volcanic activity e.g. in the vicinity of James Ross island, could contribute to a latent instability of the West Antarctic Ice Sheet in this region. Temperature measurements in the main target areas were small basins and troughs on the continental shelf, where sediments have accumulated and water column temperatures likely show lesser variation (Dziadek et al., 2017).

## Work at sea

*In-situ* temperature measurements were conducted at 19 stations during *Polarstern* expedition PS118 (see overview Fig. 8.1). Figs 8.2 and 8.3 show a close-up of two temperature transects across the northern Powell Basin and in the western Weddell Sea region. Details for the individual stations, the geographical locations, station ID and deployment type are listed in Table 8.1. We used Miniaturized Temperature Logger (MTL), which are autonomously operating, precision thermometers for deep-sea application to measure *in-situ* temperatures. The housing was designed for an operation depth of up to 6,000 m and sediment penetration. The sampling rate can be adjusted between one second and several minutes, yielding a registration time of 1 hour to 6 months. The MTL are constructed for 0.001 K resolution and 0.1 K precision (Pfender & Villinger, 2002) and were mounted on either the gravity corer or a thermal lance. Schematically represented in Fig. 8.4 are the MTLs details and the probe geometry, where seven MTL are mounted below the weight with a fixed distance. Fig. 8.4 further shows the temperatures recorded by the MTLs during the deployment and penetration phase of station PS118/63-1. In the first stage, the probe is lowered with 1.0 m s$^{-1}$ and the sensors collect the temperature profile of the water column. In the next phase, the winch speed is reduced to 0.8 m s$^{-1}$ and the probe penetrates the sediment. Peak temperatures are seen, due to the frictional heat. We used an up to 10 min steady-time, where the probe rests in the sediment, which allows for the frictional heat to decay and the temperatures to adjust to ambient sediment temperatures. The mean temperature of the stabilization phase is plotted against the depth below sea floor of the sensors to obtain the geothermal gradient. Hence, no absolute penetration depth information of the sensors is required, solemnly their individual distance to each other.
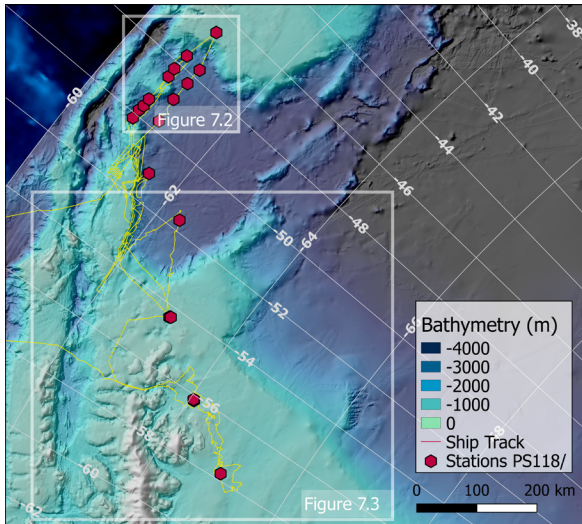
Fig. 8.1: Map shows deployment of Miniaturized Temperature Logger at selected sites in the Weddell Sea region and Powell Basin. We mounted the MTLs at the gravity corer (GC) at selected stations and deployed gradient probes for sediment temperature measurements. For details of the stations see station protocol (Tab. 8.1). Figs. 8.2 and 8.3 show close-ups of temperature transects as well as the station ID for the sites.



Fig. 8.2: Map indicating a transect of in-situ temperature measurements from the western Weddell Sea region into Powell Basin.
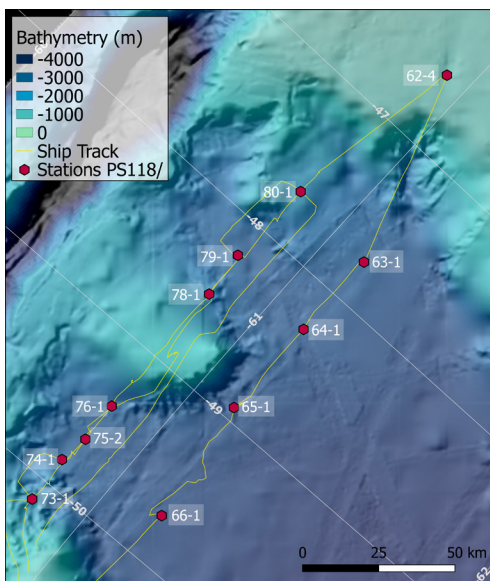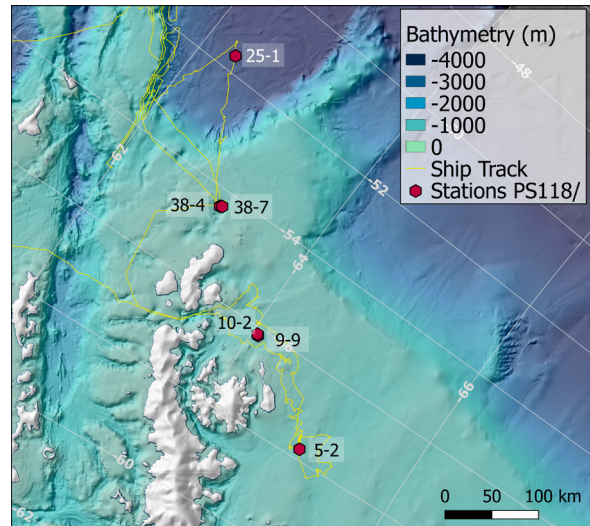


Fig. 8.3: Map showing two in-situ temperature profiles across the northern Powell Basin.

62

The thermal conductivity (k) was measured on whole-round gravity cores taken at the sites listed in Table 8.1. We used a KD2 Pro Thermal Property Analyzer that has an accuracy of ±5% from 0.2 to 2 W m$^{-1}$K$^{-1}$. The 6 cm long sensor applies a very small amount of heat to the needle, which helps to prevent free convection in liquid samples. Because of the sensor's heat pulse, a minimum of 1.5 cm of material parallel to the sensor in all directions was required to minimize errors. The sampling interval along the cores ranged between 10 and 30 cm. The thermal conductivity is temperature dependent and we corrected the influence of ambient laboratory temperatures (~20°C) by estimating the thermal conductivity at 4°C via:

$$k_{Sediment(4°C)} = (k \times k\,^{\varphi}_{Water(4°C)})/(\,k\,^{\varphi}_{Water(20°C)}))$$

This takes into account the porosity of the sediment ($\varphi \approx 0.65$), the thermal conductivity of water at 20°C ($k_{Water(20°C)}$ = 0.6 W mK$^{-1}$) and 4°C ($k_{Water(4°C)}$ = 0.57 W mK$^{-1}$), respectively. Final post-processing will be conducted after the expedition.

**Tab 8.1:** Station protocol of MTL deployments during PS118. Comment section denotes the deployed instrument, where the MTL were mounted on: Gravity Corer (GC) and Thermal Probe (HF). At gravity corer sites thermal conductivity measurements (TC) were conducted on board.

| Date | Station | Latitude ('S) | Longitude ('W) | Comments |
|---|---|---|---|---|
| 2019-03-04 | PS118_005_2 | -64.9855556 | -57.769444 | GC, TC |
| 2019-03-12 | PS118_009_9 | -64.0627778 | -56.1563889 | GC, TC |
| 2019-03-13 | PS118_010_2 | -64.0497222 | -56.1361111 | GC, TC |
| 2019-03-20 | PS118_025_1 | -62.3226667 | -51.6758333 | GC, TC |
| 2019-03-22 | PS118_038_4 | -63.06275 | -54.3495333 | GC, TC |
| 2019-03-22 | PS118_038_7 | -63.0812667 | -54.3276333 | GC, TC |
| 2019-03-26 | PS118_048_3 | -61.54395 | -51.1291667 | GC |
| 2019-03-28 | PS118_062_4 | -60.9289333 | -46.56185 | GC, TC |
| 2019-03-28 | PS118_063_1 | -61.1236833 | -47.7338 | GC, TC |
| 2019-03-29 | PS118_064_1 | -61.1239833 | -48.2835833 | GC, TC |
| 2019-03-29 | PS118_065_1 | -61.1224667 | -48.9201667 | GC, TC |
| 2019-03-29 | PS118_066_1 | -61.1683667 | -49.7056833 | GC, TC |
| 2019-04-01 | PS118_073_1 | -60.8456333 | -50.1339167 | HF |
| 2019-04-01 | PS118_074_1 | -60.8382333 | -49.8366333 | HF |
| 2019-04-01 | PS118_075_2 | -60.8523167 | -49.6517167 | GC, TC |
| 2019-04-01 | PS118_076_1 | -60.8477167 | -49.3972667 | HF |
| 2019-04-02 | PS118_078_1 | -60.8476333 | -48.5034833 | GC, TC |
| 2019-04-02 | PS118_079_1 | -60.835 | -48.2141667 | GC, TC |
| 2019-04-02 | PS118_080_1 | -60.8467 | -47.67625 | HF |

**Preliminary (expected) results**

The on board data processing is exemplarily shown for station PS118_63-1 in Fig. 8.5. *In-situ* temperatures of all sensors are plotted in the graph on the left-hand side together with a close

up of sensor 2. Considering the polynomial fit of the measurements and the ±2δ confidence interval (95%) the temperatures were regarded as stabile. The mean of the stabilization temperatures was then used for plotting the temperature gradient. Assuming a steady-state, one-dimensional heat conduction, constant thermal conductivity (k = 1, applicable for soft, water saturated sediments) and the neglecting radioactive heat production, the geothermal heat flux (Q) can be calculated via the product of thermal conductivity and the temperature gradient.

$$Q = k\ \delta T\ \delta z^{-1} \quad [mW\ m^{-2}]$$

The preliminary geothermal heat flux approximation for this station was 66 mW m$^{-2}$. Detailed data processing will we conducted after the expedition in Bremerhaven. The thermal conductivity will be further constrained by measuring the value directly on split gravity cores taken at the temperature sites.
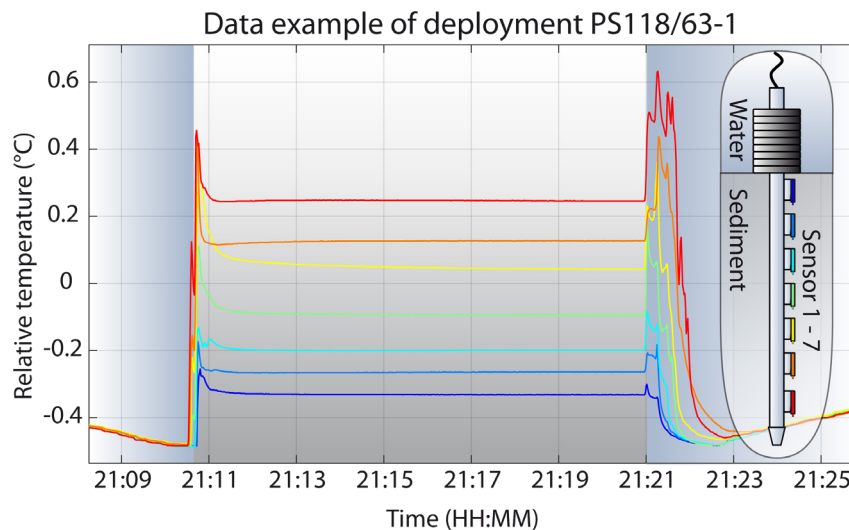


*Fig. 8.4: A schematic representation of the sensor mounting on the gradient probe is shown in the inlet on the right side of the Fig.. The Fig. shows a data example of station PS118_63-1. While entering the sediment frictional heat is generated which then decays, which predominantly depends on the thermal conductivity of the sediment. After ~8 to 10 minutes steady-time the temperature curves have stabilized and temperature gradients can be estimated.*

## Data management

The data sets collected for this study will be available at the World Data Center PANGAEA Data Publisher for Earth & Environmental Science (www.pangaea.de) after publication.
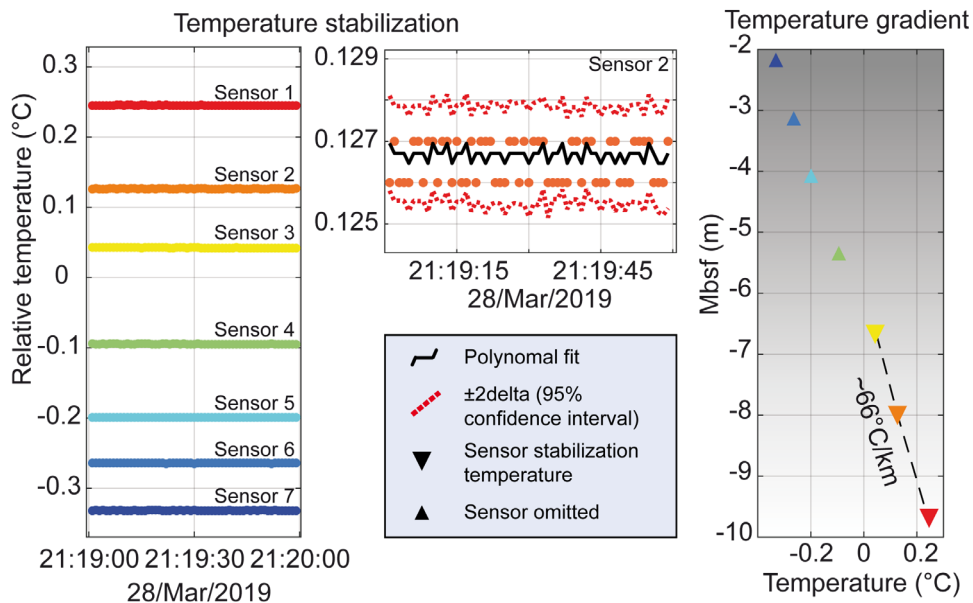
*Fig. 8.5: Example of on-board data quality checking and initial processing*

**References**

Pfender M & Villinger H (2002) Miniaturized data loggers for deep sea sediment temperature gradient measurements, Marine Geology, 186, 557–570.

Burton-Johnson A, Halpin JA, Whittaker JM, Graham FS & Watson SJ (2017) A new heat flux model for the Antarctic Peninsula incorporating spatially variable upper crustal radiogenic heat production, Geophys. Res. Lett., 44(11), 5436–5446.

Dziadek R, Gohl K, Diehl A Kaul N (2017) Geothermal heat flux in the Amundsen Sea sector of West Antarctica: New insights from temperature measurements, depth to the bottom of the magnetic source estimation, and thermal modeling, Geochemistry, Geophys. Geosystems, 2.

# 9.  HYDROACOUSTICS

Simon Dreutter[1], Nina-Marie Lešić[1], Mona Lütjens[2], Fynn Warnke[1], Frank Niessen[1]

[1]AWI
[2]HCU

**Scientific objectives**

Accurate knowledge of the seafloor topography, hence high-resolution bathymetry data, is key basic information necessary to understand many marine processes. It is of particular importance for the interpretation of scientific data in a spatial context. Bathymetry, hence geomorphology, is furthermore a basic parameter for the understanding of the general geological setting of an area and geological processes such as erosion, sediment transport and deposition. Even information on tectonic processes can be inferred from bathymetry. Supplementing the bathymetric data, high-resolution sub-bottom profiler data of the top 10s of meters below the seabed provide information on the sediments at the seafloor and on the lateral extension of sediment successions. This can be used to study depositional environments on larger scales in terms of space and time, of which the uppermost sediments may be sampled.

While world bathymetric maps give the impression of a detailed knowledge of worldwide seafloor topography, most of the world's ocean floor remains unmapped by hydroacoustic systems. In these areas, bathymetry is modelled from satellite altimetry with a corresponding low resolution. Satellite-altimetry derived bathymetry therefore lack the resolution necessary to resolve small- to meso-scale geomorphological features (e.g. sediment waves, glaciogenic features and small seamounts). Ship-borne multibeam data provide bathymetry information in a resolution sufficient to resolve those features.

- Therefore, the main tasks of the bathymetry group on board Polarstern during PS118 were:
- collection of bathymetric data, including calibration and correction of the data for environmental circumstances (sound velocity, systematic errors in bottom detection, etc.)
- post processing and cleaning of the data
- data management for on-site map creation
- The general objectives of sub-bottom profiling during PS118 were:
- to provide the data base for an acoustic facies interpretation indicative for different sedimentary environments
- to obtain different pattern of high-resolution acoustic stratigraphy useful for lateral correlation over shorter and longer distances thereby aiding correlation of sediment cores retrieved during the cruise
- to select coring stations based on acoustic pattern and reflection amplitude

**Work at sea**

*Technical description*

During the PS118 cruise, the bathymetric surveys were conducted with the hull-mounted multibeam echosounder (MBES) Atlas HYDROSWEEP DS3. The HYDROSWEEP is a deep water system for continuous mapping with the full swath potential. It operates on a frequency of ~14 kHz. On *Polarstern*, the MBES transducer arrays are arranged in a Mills cross configuration of 3 m (transmit unit) by 3 m (receive unit). The combined motion, position (Trimble GNSS), and time data comes from an iXBlue Hydrins system and the signal goes directly into the Processing Unit (PU) of the MBES to do real-time motion compensation in Pitch, Roll and Yaw. With a combination of phase and amplitude detection algorithms the PU computes the water depth from the returning backscatter signal. The system can cover a sector of up to 140° with each 70° per side.

The hull-mounted sub-bottom profiling system PARASOUND generates two primary high frequencies (PHF), of which the lower frequency is selectable between 18 and 23.5 kHz transmitting in a narrow beam of 4° at high power. As a result of the non-linear acoustic behavior of water, the so-called "Parametric Effect", two secondary harmonic frequencies are generated, one of which is the difference or secondary low frequency (SLF) and the other the sum or secondary high frequency (SHF) of the two primary frequencies. As a result of the longer wavelength, the difference parametric frequency allows sub-bottom penetration up to 200 m (depending on sediment conditions) with a vertical resolution of about 30 cm. The primary advantage of parametric echosounders is based on the fact that the sediment-penetrating pulse is generated within the narrow beam of the primary frequencies, thereby providing a very high lateral resolution compared to conventional 4 kHz-systems. For vertical beam transmission (conventional) this capability, however, limits good survey results on sea-floor slopes, which are inclined to more than 4° relative to horizontal. The reason is that the energy reflected from the small inclined footprint on the seafloor is out of the lateral range of the receiving transducers in the hull of the vessel. As a consequence, the survey results are poor over longer lateral distances along the slopes of the shelf areas north east of the Antarctic Peninsula forming the transition into the Powell Basin. The technical settings of PARASOUND used during PS118 are summarized in Table 9.1.

In June 2017, the Deep-Sea Sediment Echo Sounder PARASOUND (Teledyne Reson, Bremen, Germany), system PS3-P70, was successfully upgraded to PS3MK2-P70, which includes significant modifications in both hardware and software components. The system was then tested using different settings during cruise PS110 (Niessen 2019). PS118 is one of the first scientific expeditions using the upgraded system intensively. One major modification of the PS3MK2-P70 upgrade is the implementation of the frequency-modulated (chirped) wave for water depth of more than 500 m in addition to the previously used continuous waves. This results in both slight improvement of sediment penetration and vertical resolution.

*Data acquisition and processing*

Data acquisition was carried out throughout the entire cruise, as long as the ship was sailing in international waters. During station work, if not needed, both systems were switched.

The MBES was operated with Atlas Hydromap Control and for online data visualization Teledyne PDS was used. The collected bathymetry was stored in ASD and S7K raw files.

Subsequent data processing was performed using Caris HIPS and SIPS. For generating maps, the data were exported to Quantum GIS in the GeoTIFF raster format.

PARASOUND was also operated with Atlas Hydromap Control and the data was visualized in Atlas Parastore. Acquisition included PHF and SLF data within the working area as summarised in Table 9.2. Both PHF and SLF traces were visualised as online profiles on screen. SLF and PHF profiles (200 m depth window) and online status reports (60 s intervals or shorter) were saved as PNG files.

For the entire period above, and simultaneously with sounding, six different types of PARASOUND data files were stored on hard disc:

• PHF data in ASD format

• PHF data in PS3 format (carrier frequency, lat.lon)

• SLF data in ASD format

• SLF data in PS3 format (carrier frequency, lat.lon)

• Navigation and Auxiliary data (60s intervals) in ASCI format

• PHF and SLF Online "Prints" as A-4 pages in PNG format

• ATLAS PARASTORE 3 settings in XML files

**Tab. 9.1:** Technical Settings of PARASOUND during PS118

| Used Settings | Selected Options | Selected Ranges |
|---|---|---|
| | | |
| Mode of Operation | P-SBP/SBES | PHF, SLF |
| Frequency | PHF | 19.2 kHz |
| | SLF | 3.5 kHz |
| Pulse length | No. of Periods | 2 |
| | Length | 0.5 ms |
| Transmission Source Level | Transmission Power | 100% |
| | Transmission Voltage | 160 V |
| Beam Steering | none | |
| Mode of Transmission | Single Pulse | Auto according to water depth |
| | Quasi-Equidistant | Interval 500-1400 ms |
| Pulse Type | Frequency Modulated (Chirped) | |
| | Continuous Wave | In water depth <500m |
| Pulse Shape | Default | |
| Receiver Band Width | Output Sample Rate (OSR) | 6.1 kHz |
| | Band Width (% of OSR) | 66% |
| Reception Shading | none | |
| System Depth Source | PARASOUND PHF | Fixed Min./Max. Depth Limit |
| | Manual | |
| | HYDROSWEEP DS PHF | Only in Single-Pulse mode |
| Water Velocity | C-Mean | Manual 1500 m/s |
| | C-Keel | System C-keel |
| Data Recording | ASD | Variable, 6.1 kHz |
| | PHF-PS3 | 200 m |
| | SLF-PS3 | 200 m |

**Tab. 9.2:** PARASOUND operation times during PS118 are listed as time window between Time (UTC) switched "On" and "Off".

| Parasound On | | | | | Parasound Off | | | |
|---|---|---|---|---|---|---|---|---|
| Date | Time | Latitude | Longitude | | Date | Time | Latitude | Longitude |
| 20.02.19 | 20:03:03 | 58° 59.067'S | 59° 55.512'W | | 25.02.19 | 12:21:15 | 65° 9.277'S | 57° 10.080'W |
| 25.02.19 | 12:26:00 | 65° 9.522'S | 57° 9.412'W | | 27.02.19 | 12:52:38 | 65° 19.052'S | 57° 57.632'W |
| 27.02.19 | 17:10:00 | 65° 17.037'S | 57° 56.887'W | | 28.02.19 | 23:54:03 | 65° 13.344'S | 57° 55.608'W |
| 01.03.19 | 08:23:00 | 65° 13.654'S | 57° 57.031'W | | 01.03.19 | 10:33:00 | 65° 13.805'S | 57° 57.508'W |
| 01.03.19 | 10:34:00 | 65° 13.802'S | 57° 57.536'W | | 04.03.19 | 20:01:03 | 64° 58.981'S | 57° 45.121'W |
| 04.03.19 | 22:36:00 | 64° 58.208'S | 57° 43.477'W | | 05.03.19 | 13:11:40 | 64° 58.716'S | 57° 46.407'W |
| 05.03.19 | 17:10:03 | 64° 58.439'S | 57° 47.291'W | | 05.03.19 | 17:44:00 | 64° 58.664'S | 57° 48.018'W |
| 05.03.19 | 23:10:00 | 64° 57.568'S | 57° 48.803'W | | 05.03.19 | 23:27:45 | 64° 57.539'S | 57° 48.837'W |
| 06.03.19 | 02:23:01 | 64° 56.933'S | 57° 46.580'W | | 06.03.19 | 10:07:00 | 64° 55.707'S | 57° 49.167'W |
| 06.03.19 | 12:03:00 | 64° 55.568'S | 57° 48.407'W | | 06.03.19 | 14:05:00 | 64° 55.871'S | 57° 48.940'W |
| 06.03.19 | 18:52:01 | 64° 55.215'S | 57° 49.506'W | | 06.03.19 | 20:53:00 | 64° 54.665'S | 57° 49.631'W |
| 08.03.19 | 19:25:30 | 64° 55.000'S | 57° 52.535'W | | 09.03.19 | 10:58:00 | 64° 53.467'S | 57° 52.450'W |
| 09.03.19 | 16:52:06 | 64° 52.581'S | 57° 46.078'W | | 11.03.19 | 10:30:00 | 64° 4.041'S | 55° 54.042'W |
| 11.03.19 | 11:42:00 | 64° 3.215'S | 55° 54.347'W | | 11.03.19 | 18:24:00 | 63° 58.943'S | 55° 54.288'W |
| 11.03.19 | 22:59:02 | 63° 57.723'S | 55° 54.502'W | | 12.03.19 | 09:03:00 | 64° 0.052'S | 55° 57.044'W |
| 12.03.19 | 10:54:00 | 64° 0.612'S | 55° 57.213'W | | 12.03.19 | 13:39:43 | 64° 1.084'S | 55° 54.936'W |
| 12.03.19 | 16:46:00 | 64° 1.315'S | 55° 54.976'W | | 12.03.19 | 16:47:00 | 64° 1.309'S | 55° 54.953'W |
| 12.03.19 | 16:48:00 | 64° 1.315'S | 55° 54.976'W | | 12.03.19 | 16:52:00 | 64° 1.309'S | 55° 54.953'W |
| 12.03.19 | 23:15:00 | 64° 1.181'S | 55° 55.858'W | | 12.03.19 | 23:27:00 | 64° 1.175'S | 55° 55.849'W |
| 13.03.19 | 05:13:01 | 64° 1.427'S | 55° 54.985'W | | 13.03.19 | 11:07:20 | 64° 0.061'S | 55° 58.360'W |
| 13.03.19 | 14:29:00 | 64° 0.093'S | 55° 58.524'W | | 14.03.19 | 04:54:00 | 63° 48.441'S | 55° 45.460'W |
| 14.03.19 | 20:54:00 | 63° 50.773'S | 55° 32.840'W | | 14.03.19 | 21:13:00 | 63° 50.559'S | 55° 32.513'W |
| 14.03.19 | 22:10:00 | 63° 50.304'S | 55° 30.029'W | | 17.03.19 | 11:13:00 | 63° 4.044'S | 54° 18.778'W |
| 17.03.19 | 16:20:00 | 63° 2.985'S | 54° 18.948'W | | 18.03.19 | 17:07:00 | 62° 0.080'S | 55° 0.239'W |
| 18.03.19 | 19:49:02 | 62° 1.389'S | 54° 58.607'W | | 18.03.19 | 23:42:00 | 61° 54.033'S | 53° 48.039'W |
| 19.03.19 | 02:12:02 | 61° 55.144'S | 53° 39.638'W | | 19.03.19 | 02:46:00 | 61° 56.468'S | 53° 31.910'W |
| 19.03.19 | 03:49:00 | 61° 56.445'S | 53° 31.705'W | | 19.03.19 | 04:21:00 | 61° 58.082'S | 53° 22.017'W |
| 19.03.19 | 05:37:02 | 61° 58.631'S | 53° 22.375'W | | 19.03.19 | 06:18:00 | 62° 59.782'S | 53° 9.460'W |
| 19.03.19 | 08:08:01 | 62° 0.860'S | 53° 8.441'W | | 19.03.19 | 10:05:00 | 62° 2.443'S | 52° 55.172'W |
| 19.03.19 | 12:02:03 | 62° 2.328'S | 52° 51.688'W | | 19.03.19 | 13:05:00 | 62° 4.155'S | 52° 41.020'W |
| 19.03.19 | 15:21:00 | 62° 2.695'S | 52° 39.769'W | | 19.03.19 | 16:59:00 | 62° 6.919'S | 52° 22.644'W |
| 19.03.19 | 19:07:00 | 62° 6.937'S | 52° 24.752'W | | 20.03.19 | 00:17:00 | 62° 15.000'S | 51° 30.018'W |

| Parasound On | | | | | Parasound Off | | | |
|---|---|---|---|---|---|---|---|---|
| Date | Time | Latitude | Longitude | | Date | Time | Latitude | Longitude |
| 20.03.19 | 00:18:00 | 62° 15.008'S | 51° 30.012'W | | 20.03.19 | 00:19:00 | 62° 15.015'S | 51° 30.006'W |
| 20.03.19 | 07:56:00 | 62° 14.668'S | 51° 25.050'W | | 20.03.19 | 08:29:00 | 62° 14.550'S | 51° 25.359'W |
| 20.03.19 | 11:19:19 | 62° 14.582'S | 51° 26.689'W | | 20.03.19 | 12:56:00 | 62° 18.888'S | 51° 40.544'W |
| 20.03.19 | 13:02:02 | 62° 18.910'S | 51° 40.598'W | | 20.03.19 | 14:20:06 | 62° 19.365'S | 51° 40.545'W |
| 20.03.19 | 15:46:21 | 62° 19.893'S | 51° 39.581'W | | 20.03.19 | 20:13:00 | 62° 23.701'S | 52 ° 1.545'W |
| 20.03.19 | 22:20:00 | 62° 22.231'S | 52° 3.478'W | | 21.03.19 | 01:24:00 | 62° 30.983'S | 52° 30.274'W |
| 21.03.19 | 03:45:00 | 62° 31.215'S | 52° 30.173'W | | 21.03.19 | 06:08:00 | 62° 36.271'S | 52° 48.129'W |
| 21.03.19 | 08:20:03 | 62° 35.021'S | 52° 47.690'W | | 21.03.19 | 10:23:00 | 62° 39.451'S | 53 ° 1.244'W |
| 21.03.19 | 12:23:01 | 62° 39.183'S | 53° 3.373'W | | 21.03.19 | 13:37:02 | 62° 43.094'S | 53° 17.236'W |
| 21.03.19 | 14:50:00 | 62° 42.778'S | 53° 17.885'W | | 21.03.19 | 19:55:00 | 62° 42.752'S | 53° 15.438'W |
| 21.03.19 | 20:46:00 | 62° 42.578'S | 53° 16.685'W | | 21.03.19 | 21:31:00 | 62° 45.966'S | 53° 26.994'W |
| 21.03.19 | 23:27:00 | 62° 45.481'S | 53° 26.670'W | | 22.03.19 | 00:16:00 | 62°48.403'S | 53°36.109'W |
| 22.03.19 | 00:46:00 | 62°48.188'S | 53°36.024'W | | 22.03.19 | 01:32:00 | 62°50.883'S | 53°45.554'W |
| 22.03.19 | 01:54:00 | 62°50.711'S | 53°45.663'W | | 22.03.19 | 03:13:00 | 62°55.286'S | 54° 1.693'W |
| 22.03.19 | 03:45:00 | 62°55.173'S | 54° 2.077'W | | 22.03.19 | 05:28:00 | 62°59.981'S | 54°19.779'W |
| 22.03.19 | 05:55:00 | 62°59.968'S | 54°19.652'W | | 22.03.19 | 10:29:00 | 63° 4.162'S | 54°18.527'W |
| 22.03.19 | 18:37:00 | 63° 4.293'S | 54°18.050'W | | 22.03.19 | 18:49:00 | 63° 5.021'S | 54°19.377'W |
| 23.03.19 | 06:15:42 | 63° 4.372'S | 54°19.310'W | | 23.03.19 | 17:36:00 | 61°55.917'S | 53°20.540'W |
| 24.03.19 | 10:31:00 | 61°51.551'S | 53°18.464'W | | 25.03.19 | 12:06:00 | 61°19.856'S | 51°50.524'W |
| 25.03.19 | 12:44:10 | 61°19.193'S | 51°50.248'W | | 25.03.19 | 13:41:00 | 61°23.374'S | 51°42.048'W |
| 25.03.19 | 14:19:00 | 61°23.053'S | 51°43.661'W | | 25.03.19 | 15:22:00 | 61°27.222'S | 51°31.906'W |
| 25.03.19 | 16:24:00 | 61°28.136'S | 51°31.292'W | | 25.03.19 | 16:48:00 | 61°29.771'S | 51°25.214'W |
| 25.03.19 | 18:24:00 | 61°30.328'S | 51°24.249'W | | 25.03.19 | 18:54:00 | 61°32.220'S | 51°18.290'W |
| 25.03.19 | 21:09:04 | 61°32.780'S | 51°18.638'W | | 25.03.19 | 22:10:00 | 61°35.783'S | 51° 8.692'W |
| 26.03.19 | 00:46:00 | 61°34.937'S | 51° 8.742'W | | 26.03.19 | 06:55:08 | 61°35.655'S | 51° 8.249'W |
| 26.03.19 | 08:01:02 | 61°36.454'S | 51° 7.848'W | | 26.03.19 | 08:39:00 | 61°36.363'S | 51° 9.679'W |
| 26.03.19 | 10:37:02 | 61°36.479'S | 51° 6.941'W | | 26.03.19 | 11:04:00 | 61°34.925'S | 51° 8.496'W |
| 26.03.19 | 15:49:00 | 61°31.986'S | 51° 8.650'W | | 26.03.19 | 17:08:00 | 61°28.329'S | 51°28.855'W |
| 26.03.19 | 20:18:05 | 61°29.896'S | 51°31.001'W | | 26.03.19 | 20:56:00 | 61°28.864'S | 51°26.878'W |
| 26.03.19 | 22:01:01 | 61°28.154'S | 51°25.628'W | | 27.03.19 | 03:48:00 | 60°50.777'S | 50°11.708'W |
| 27.03.19 | 05:20:00 | 60°50.696'S | 50°12.323'W | | 27.03.19 | 06:01:00 | 60°50.881'S | 50° 0.181'W |
| 27.03.19 | 07:52:00 | 60°51.072'S | 49°59.874'W | | 27.03.19 | 09:14:00 | 60°50.572'S | 49°45.803'W |
| 27.03.19 | 09:36:02 | 60°50.801'S | 49°45.785'W | | 27.03.19 | 11:03:00 | 60°51.475'S | 49°45.841'W |
| 27.03.19 | 11:19:01 | 60°51.475'S | 49°45.814'W | | 27.03.19 | 12:11:00 | 60°50.638'S | 49°36.020'W |

| Parasound On | | | | | Parasound Off | | | |
|---|---|---|---|---|---|---|---|---|
| Date | Time | Latitude | Longitude | | Date | Time | Latitude | Longitude |
| 27.03.19 | 14:25:03 | 60°50.258'S | 49°35.511'W | | 27.03.19 | 15:17:11 | 60°50.669'S | 49°23.609'W |
| 27.03.19 | 17:02:02 | 60°51.038'S | 49°23.748'W | | 27.03.19 | 17:50:00 | 60°50.701'S | 49°11.833'W |
| 27.03.19 | 19:39:00 | 60°50.911'S | 49°12.562'W | | 27.03.19 | 20:30:00 | 60°50.636'S | 49° 0.294'W |
| 27.03.19 | 21:32:00 | 60°50.855'S | 48°59.811'W | | 27.03.19 | 23:02:00 | 60°51.102'S | 48°32.063'W |
| 28.03.19 | 00:50:00 | 60°51.407'S | 48°31.941'W | | 28.03.19 | 02:04:00 | 60°50.744'S | 48°11.669'W |
| 28.03.19 | 04:14:02 | 60°51.302'S | 48°11.781'W | | 28.03.19 | 05:11:00 | 60°50.549'S | 47°53.915'W |
| 28.03.19 | 07:24:00 | 60°51.390'S | 47°54.001'W | | 28.03.19 | 08:42:07 | 60°50.821'S | 47°30.952'W |
| 28.03.19 | 10:18:00 | 60°50.893'S | 47°30.991'W | | 28.03.19 | 13:12:00 | 60°55.737'S | 46°33.523'W |
| 28.03.19 | 15:18:00 | 60°55.901'S | 46°33.796'W | | 28.03.19 | 15:20:00 | 60°55.811'S | 46°33.568'W |
| 28.03.19 | 16:16:00 | 60°55.834'S | 46°34.067'W | | 28.03.19 | 22:26:00 | 61° 7.176'S | 47°44.073'W |
| 28.03.19 | 22:59:03 | 61° 7.017'S | 47°43.442'W | | 29.03.19 | 04:40:00 | 61° 7.441'S | 48°55.252'W |
| 29.03.19 | 06:53:00 | 61° 7.625'S | 48°53.745'W | | 29.03.19 | 12:20:00 | 61°10.021'S | 49°42.482'W |
| 29.03.19 | 14:53:04 | 61°10.114'S | 49°42.355'W | | 31.03.19 | 01:23:00 | 61°11.496'S | 50°59.174'W |
| 31.03.19 | 15:40:01 | 61°11.437'S | 51° 5.821'W | | 31.03.19 | 18:32:00 | 61° 4.720'S | 51°46.345'W |
| 31.03.19 | 20:59:00 | 61° ´4.603'S | 51°47.031'W | | 03.04.19 | 19:42:00 | 61°13.883'S | 50°43.339'W |
| 04.04.19 | 09:28:01 | 61°11.431'S | 50°43.957'W | | 04.04.19 | 13:55:00 | 61°13.452'S | 52°28.309'W |
| 04.04.19 | 15:11:01 | 61°12.782'S | 52°30.809'W | | 05.04.19 | 14:52:00 | 57°40.230'S | 60° 4.296'W |

One system crash has occurred during the cruise due to a Windows failure for no obvious reasons. Only a few minutes of data storage were lost. During the cruise, the SLF PS3 files that were stored with latitude/longitude projection and carrier-frequency mode to enable the Import of the data in IHS Kingdom. The PS3 data were converted into SEG-Y files using the PS32SGY converter (Hanno Keil, University of Bremen). The new SEG-Y files covered a time period of 4 hours, instead of the 10 minute files produced by PARASTORE. A MATLAB script was used to divide the navigational data and the SEG-Y data and then these coupled files were imported into IHS Kingdom to allow further investigation the sub-bottom data.

*Sound velocity profiles*

For best survey results with correct depths, the CTD (Conductivity, Temperature, Depth) casts, performed by the Oceanographic working group were used to measure the water sound velocity in the different depths. This is essential, as the acoustic signal travels down the water column from the transducer to the seafloor and back to the surface through several different layers of water masses with each a different sound velocity. The sound velocity is influenced by density and compressibility, both depending on pressure, temperature and salinity. Wrong or outdated sound velocity profiles lead to refraction errors and reduced data quality. The CTD measures conductivity, temperature, and depth in the water column while it is lowered to the seafloor. From these parameters, the sound velocity is calculated. The sound velocity profiles obtained by the CTD were immediately processed and applied within the MBES for correct beamforming during the survey. Throughout PS118, a total of 62 sound velocity profiles (SVP) were applied on the collected MBES data. 49 SVPs were retrieved from conventional

CTD stations and five SVPs came from Underway CTD (UCTD) measurements, collected while steaming. Additionally, two Ice CTD profiles were used and for opportunistic transit measurements, synthetic SVPs were generated from the World Ocean Atlas 2013 (e.g. in the Drake Passage).

**Preliminary results**

*Bathymetry*

Throughout the cruise a continuous recording of data was achieved. During 44 days of survey, a track length of 4,228 nm (7,831 km) was surveyed by the swath bathymetry system. The raw data volume of the HYDROSWEEP is 245 GB with 1,623 separate files. Figure 9.1 shows the generated bathymetry grid of the main research area of PS118. Next to the underway data recording, seven dedicated bathymetric surveys were conducted.
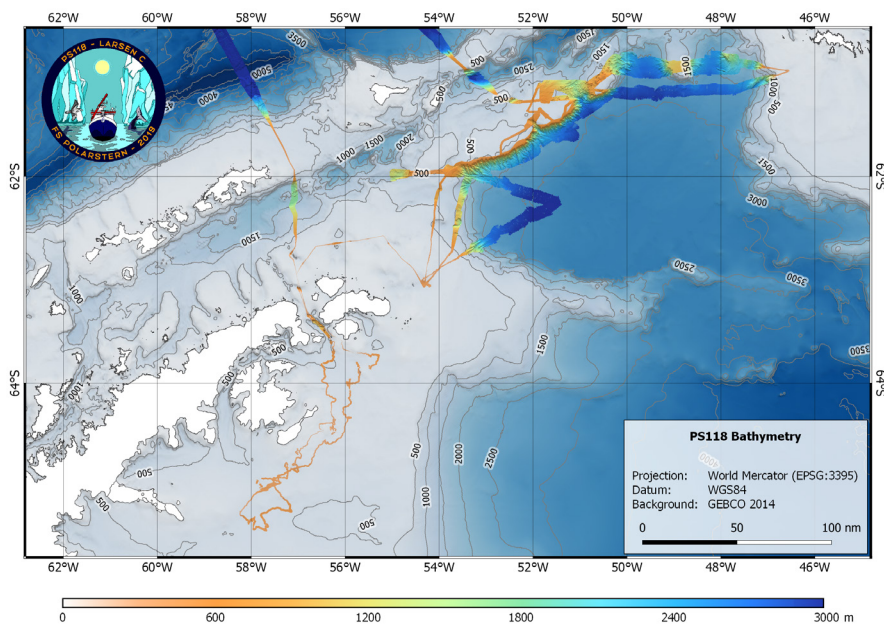


*Fig. 9.1: Overview on the bathymetric data acquired within the PS118 research area*

*Tectonic Margin*

One of the main targets for an extended bathymetric survey in the Powell Basin was the northwestern margin build up by a SW-NE orientated tectonic ridge (Fig. 9.2). The ridge exhibits water depths (WD) of about 500 m below sea surface and a shelf edge at approx. 600 m WD.

To characterize the margin area, four hydroacoustic surveys were conducted. The first survey (PS118_14-1; ~1500 km² coverage) was located at the southwestern end of the tectonic margin. Preliminary results show a distinct morphological step of about 200 m, trending SW-NE, on the shelf. The margin itself is characterized by numerous incisions perpendicular to the ridge, which are up to 500 m deep. Those large-scale incisions are connected to additional smaller, elongated depressions forming a channel-like tributary network. Adjacent to the slope-limited channel-like structures, an approx. 50 m deep and 500 m wide channel structure in water depths between 2,200 and 2,600 m is visible.

The second survey (PS118_40-1; ~2,100 km²) was located adjacent to the northeast. That area generally shows similar morphological structures as described for the first survey area. In contrast, some more channel-like structures, originating from the toe of the slope into the basin, were imaged. Due to variable sea ice coverage, the deeper parts of those structures could not be surveyed. Additionally, a large-scale shelf-incising canyon was mapped, exhibiting an overall SE orientation and depths between 400 and 1,000 m relative to the surrounding shelf. Survey PS118_47-1 (~1,000 km²) covers mainly the deep-water (>2,000 m WD) areas southeast of the incised slope and shows comparable morphological features as previously described.

Covering both the slope northwest of survey area PS118_47-1 and the adjacent margin with a 20 km wide opening between two ridges, survey area PS118_68-1 (~1,300 km²) exhibits different morphological structures. Incising channels occur predominantly on the southwestern slope of the opening, while the northeastern slope appears to be more hummocky. Numerous, almost round features are present at the seafloor, varying between a few 100 m and up to 2,000 m in diameter. Some of those features appear with a doughnut-shaped geometry featuring a distinct depression at their center. They are generally elevated from the surrounding seafloor.

Survey speed of the vessel for the described area varied between 5 and 10 kn, depending on the sea state and requirements regarding along track resolution.
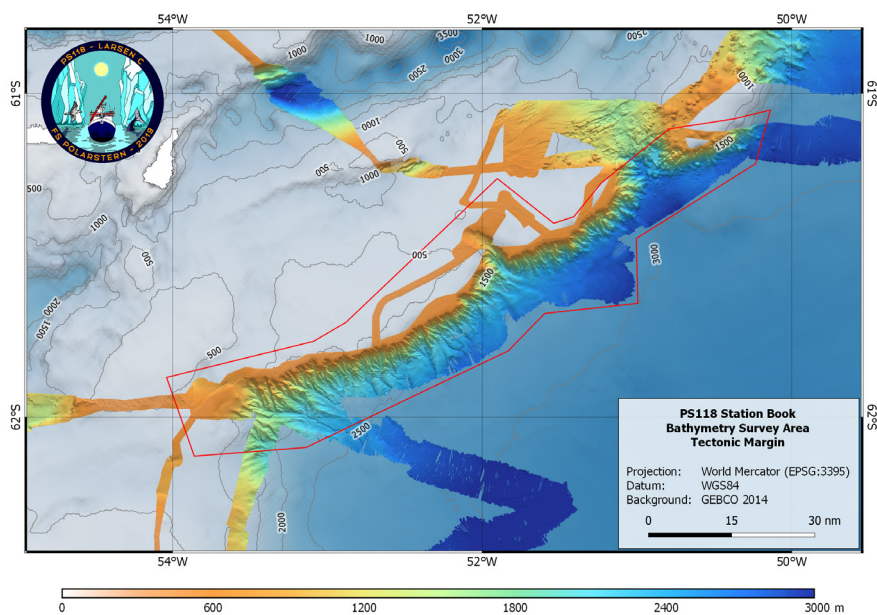


*Fig. 9.2: Bathymetric data acquired along the tectonic margin along the NW of the Powell Basin*

## Lander Site

The second bathymetry survey (PS118_37-1) was conducted on 22 March 2019 between 06:15 and 10:26 UTC (Fig. 9.3). The survey took place on the marginal shelf southwest of Powell Basin. Bathymetric data was used to characterize the habitat of the Lander site (deployment station PS118_13-2). Within four hours and a mean survey speed of 4 kn, 140 km² terrain was mapped. The depth ranges between 273 m and 479 m with a mean depth of 392 m.
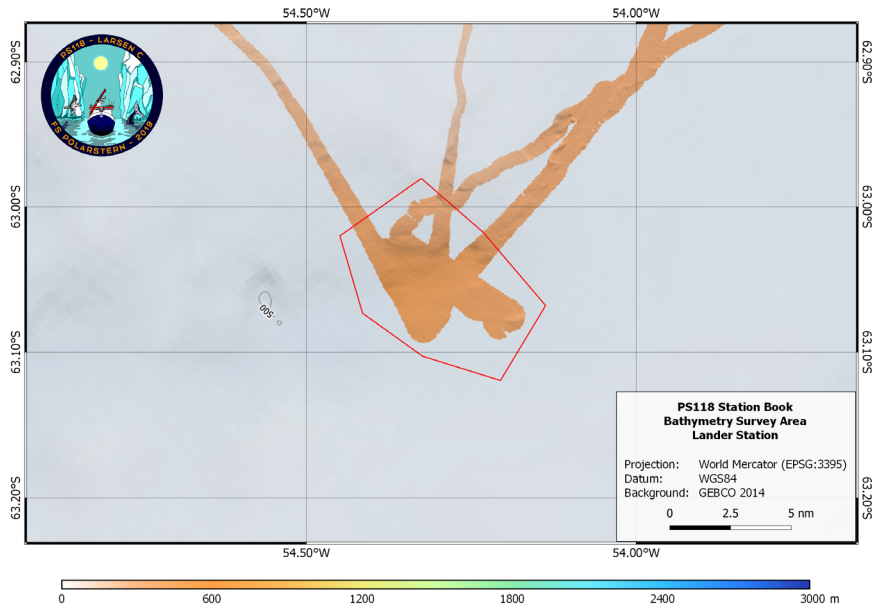
*Fig. 9.3: Bathymetric data acquired on the Lander Site (PS118_37-1)*

*Weather Standby*

Bathymetry Survey PS118_67-1 replaced station work with heavy gear due to stormy conditions between 29th of March 2019 20:06 UTC and 30th of March 03:54 UTC (Fig. 9.4). With a mean survey speed of 7.5 kn, the bathymetric survey was conducted on a shallow shelf region in the North of the Powell Basin's tectonic margin. The surveyed area covers approx. 450 km² with a mean water depth of 796 m, minimum depth of 527 m and maximum depth of 1201 m. The
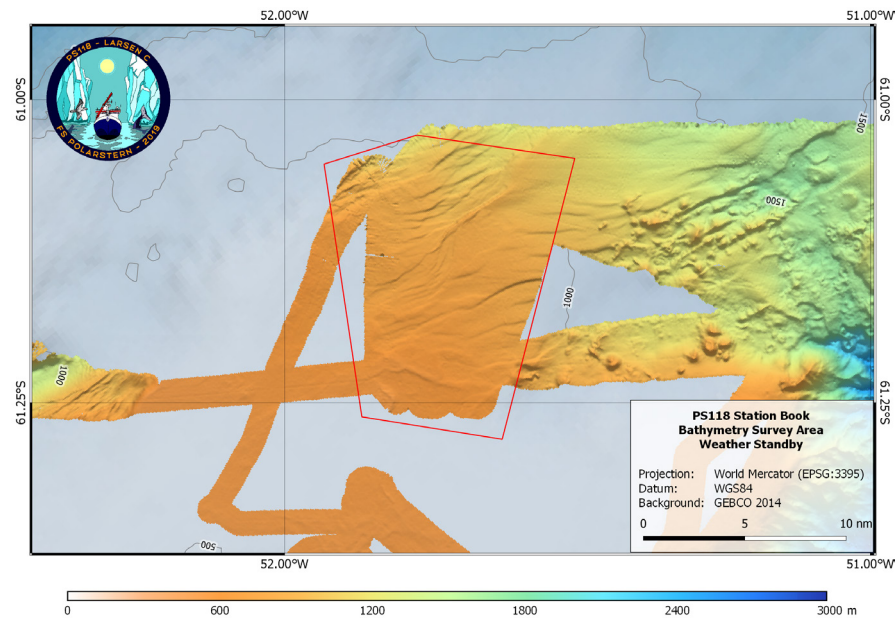


area shows only minor topography and features channel-like sedimentary structures.

*Fig. 9.4: Bathymetric data acquired during weather standby (PS118_67-1)*

*Nina's Route*

Bathymetry Survey PS118_72-1 between 31st of March 2019 21:14 UTC and 1st of April 06:49 UTC aims to connect Survey PS118_67-1 and the underway data acquired during Oceanography and Geology transects (Fig. 9.5). With a mean survey speed of 6.7 kn, approx. 809 km$^2$ were covered, collecting data on shallow shelf areas (minimum depth 524 m) with features of supposedly volcanic origin, on the shelf break and abyssal plain (maximum depth 2,271 m) with a mean depth of 1,244 m.
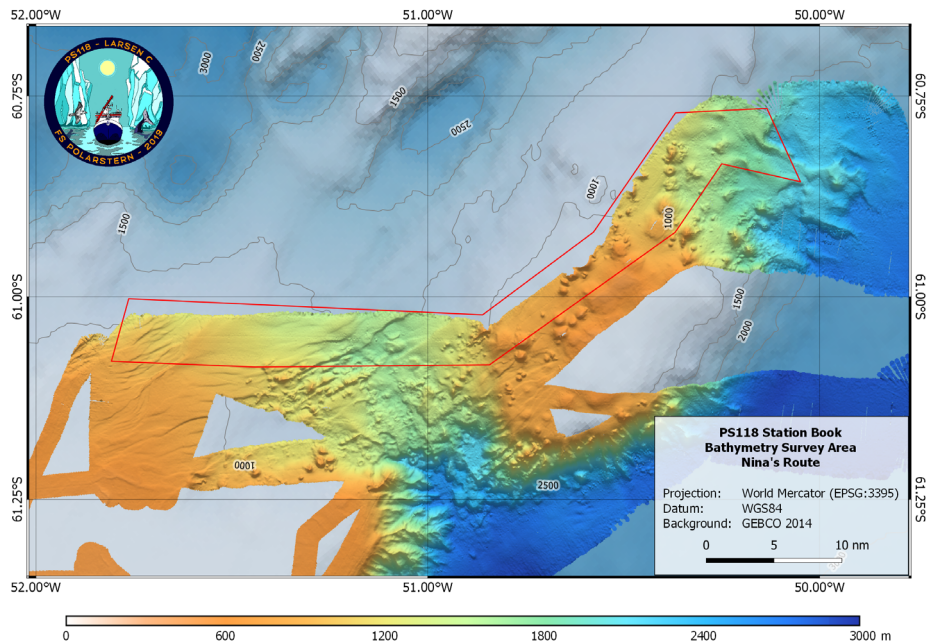


*Fig. 9.5: Bathymetric data acquired during Nina's Route (PS118_72-1)*

*PARASOUND*

Results of PARASOUND data mainly include site survey data for coring locations of PS118 and are described in the Marine Geology chapter (7.2) of this report.

**Data management**

Bathymetric data collected during PS118 will be stored in the World Data Center PANGAEA Data Publisher for Earth & Environmental Science (www.pangaea.de) at the AWI. Furthermore, the data will be provided to mapping projects and included in regional data compilations such as IBCSO (International Bathymetric Chart of the Southern Ocean) and GEBCO (General Bathymetric Chart of the Ocean). Bathymetric data will also be provided to the Nippon Foundation – GEBCO Seabed 2030 Project. All PARASOUND data will be transferred to AWI after the cruise and stored in the data base of the IT section. Once georeferenced, the data will be linked for external accessibility to the data base PANGAEA.

**References**

Niessen F (2019) The Expedition PS110 of the Research Vessel POLARSTERN to the Atlantic Ocean in 2017/2018. Berichte zur Polar- und Meeresforschung = Reports on Polar and Marine Research 730, 26p. Alfred-Wegener-Institut, Helmholtz-Zentrum für Polar- und Meeresforschung, Bremerhaven, Germany. DOI: https://doi.org/10.2312/BzPM_0730_2019.

# 10. OCEANOGRAPHIC CONDITIONS IN THE NORTHWESTERN WEDDELL SEA AND POWELL BASIN

Markus Janout[1], Gillian Damerell[2], Theresa Diener[1], Jens Hölemann[1], Aaron Röhler[3], Yanxin Wang[2], Kevin Wiegand[1], Jonathan Wiskandt[1], Oliver Huhn[3] (not on board)

[1]AWI
[2]University of East Anglia
[3]UHB-IUP

**Grant-No. AWI_PS118_02**

**Grant-No. AWI_PS118_12**

**Grant-No. AWI_PS118_14**

## Background

The disintegration of ice shelves Larsen A in 1995 and Larsen B in 2002 left Larsen C as the last remaining ice shelf in the western Weddell Sea. However, the recent calving of a massive portion of Larsen C in 2016 suggests that further changes are to be expected there as well with likely impacts on the dynamics of adjacent glacier systems and the West Antarctic ice sheet in general. Some Antarctic regions feature dramatic sub-ice shelf melt rates due to the interaction of warm water masses with the ice shelves. Ice shelf-ocean interaction at Larsen and the regional oceanography is poorly understood due to difficult access because thick ice generally accumulates on the western Weddell Sea shelf. The main objectives of the oceanography activities during PS118 aim to improve the general understanding on ocean circulation, water masses and physical mechanisms, to assess the ocean's role in the decay of the ice sheets, and to understand whether retreating ice shelves may change water mass formation and ocean circulation.

Water masses formed along the ice shelf margins of the Weddell Sea are regionally important and contribute to the global ocean circulation. High salinity shelf water (HSSW) forms in polynyas on the continental shelves and is characterized by high salinity and temperatures near the surface freezing point (Nicholls et al., 2009). When HSSW sinks to greater depths, its temperature is above the local freezing point and upon entering the cavities below the ice shelves, HSSW can cause melt at the underside of the ice shelf. During this stage, HSSW cools and freshens due to ice melt and exits the cavity as a supercooled (<-1.9°C) water mass termed Ice shelf water (ISW). These shelf-formed water masses (ISW and HSSW) along with the warmer waters that originate from the deeper Weddell Sea (modified warm deep water; MWDW) characterize the regions' water masses, and PS118 aims at understanding their distribution and further pathways. Anthropogenic transient trace gases (chlorofluorocarbons, CFCs) allow for estimating the time scales of the transport and the renewal and ventilation of deep oceanic water masses. As CFCs enter the ocean by gas exchange with the atmosphere, their evolution is determined on first order by the temporal increase in the atmosphere and subsequently by entrainment and advection in the ocean interior. Combining CFC-based time scales with noble gas and multi-parameter analysis allows to assess basal melt rates and the glacial melt water induced water mass transformation rates (Huhn et al., 2008). The shelf-formed dense water masses then exit the region, partly by flowing down the slope and partly following the continental slope northward due to the impact of the earth rotation. ISW

and HSSW are the major source waters for Antarctic Bottom Water (AABW), the densest water mass that is found in the global ocean with major significance for the global overturning circulation (Foldvik et al., 2004). The Weddell Sea is bounded by complex topography on nearly all sides, and feature only few pathways for deep waters to reach the northern ocean basins. The Powell Basin is a small but deep basin (>3,000 m) with complex bathymetry and the northern extension for currents and water masses found along the western Weddell Sea continental slope. The Basin features strong fronts along the continental slope (Thomspson & Heywood, 2008), and deep water (>1,000 m) export pathways of slope waters (Meijers et al., 2016). Overall, we still lack a thorough understanding of the Basin's currents, water masses, and northward pathways, which can be improved by help of shipboard CTD and glider surveys such as described by Azaneu et al. (2017).

This expedition is closely connected to the ongoing activities in the southern, central and northwestern Weddell Sea, as it connects the sea ice and water mass source regions in Filchner and Ronne with the through-flow area of the Larsen continental shelf and its northern pathway at the tip of the Antarctic Peninsula. Sampling strategies and data analysis will benefit from the knowledge gained during previous Polarstern expeditions (ISPOL, PS96, PS111, PS117). The planned fieldwork included traditional oceanographic sampling methods (CTD, ADCP) complemented by more specialized methods (microstructure measurements, sea gliders, autonomous drift systems), designed to achieve a regional-scale hydrographic overview guided by the bathymetric surveys, as well as to understand the smaller-scale processes that are important for water mass transformation, vertical fluxes, and bio-physical ecosystem processes.

**Specific objectives**

- Specify the physical properties controlling the flow and water mass formation on the western Weddell Sea shelf and slope using CTD and glider surveys

- Determine the temporal variability of the hydrography and tracer distribution on the continental shelf and slope with regard to Ice Shelf Water outflow, Antarctic Bottom Water formation, Modified Warm Deep Water inflow, and High Salinity Shelf Water spreading

- Re-visit some previously occupied hydrographic stations on the western Weddell Sea continental shelf and slope for a new snapshot of the dominant water masses

- Provide an improved estimate of glacial melt water inventories and basal melt rates for the western Weddell Sea (Larsen Ice Shelf) to deduce temporal trends in the future

- Determine vertical fluxes of heat and nutrients in the western Weddell Sea

- Understand the role of canyons in guiding dense water masses off the shelf

- Utilize tracers (stable noble gas isotopes [$^3$He, $^4$He, Ne]) to quantify subglacial meltwater drainage and ice shelf basal melting

- Utilize tracers to quantify Antarctic Bottom Water formation (transient trace gases [CFCs] to identify transit time scales and formation rates)

- Survey hydrographic conditions on the shelf, slope and deep basin of the Powell Basin

- Identify and survey the major outflow passages in the Powell Basin

**Work at sea**

Upon entering the study region on the north-western Weddell Sea shelf through the Antarctic Sound, the expedition faced severe ice conditions, which significantly hampered the progress and limited the options to proceed with the sampling programme. Forced by the sea ice conditions, the PS118 expedition was separated into two regional legs: the Weddell Sea shelf and the Powell Basin.

The oceanographic activities on the western Weddell Sea shelf were limited to only 5 ship-borne CTD casts, and 7 helicopter-based ice stations (see Fig. 10.1 for locations and Table 10.1 and 10.2 for station details).
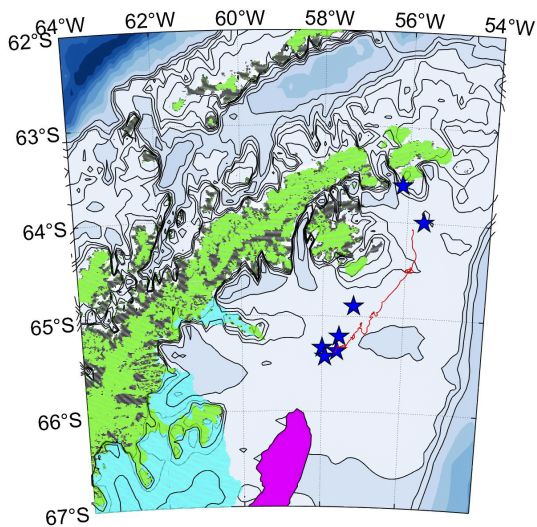
Fig. 10.1: Map of the north-western Weddell Sea shelf. The stars show the locations of the ice-based CTD stations, the magenta object outlines the approximate location and shape of the A68 iceberg during the time of sampling. The red line shows the northward drifter track.
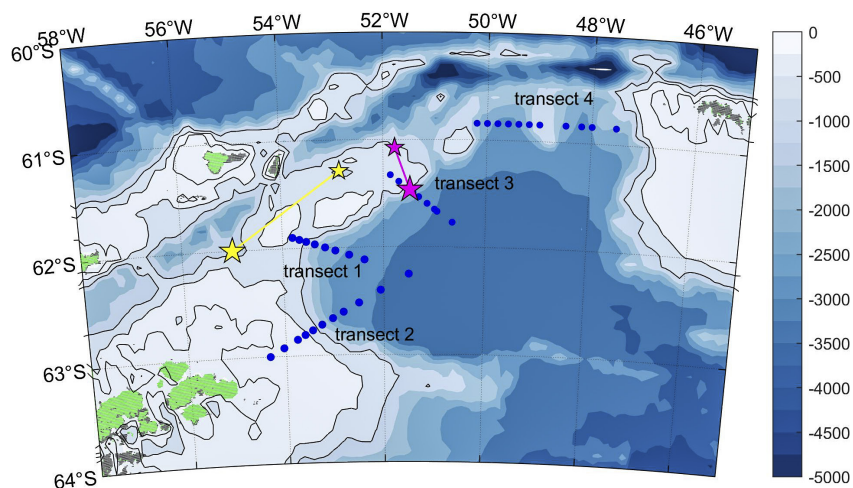
Fig. 10.2: Map of the Powell Basin showing the CTD stations (blue dots) organized in four transects. The big and small stars show the glider deployment and recovery locations of Bella (yellow) and Marlin (magenta), respectively.

**Tab. 10.1:** Shipboard CTD stations occupied during PS118

| Profile | Station | Cast | Date | Time | Latitude | Longitude | Pressure max [dbar] |
|---|---|---|---|---|---|---|---|
| 1 | PS118_004 | 1 | 2019-02-22 | 18:30:03 | 63°49.172' S | 056°28.377' W | 512 |
| 2 | PS118_005 | 1 | 2019-03-04 | 15:15:45 | 64°59.050' S | 057°44.900' W | 424 |
| 3 | PS118_006 | 1 | 2019-03-05 | 12:12:54 | 64°58.801' S | 057°46.634' W | 418 |
| 4 | PS118_008 | 2 | 2019-03-11 | 16:26:29 | 63°59.959' S | 055°54.394' W | 404 |
| 5 | PS118_010 | 1 | 2019-03-13 | 11:42:05 | 64°00.174' S | 055°58.571' W | 407 |
| 6 | PS118_011 | 1 | 2019-03-13 | 18:22:19 | 63°54.000' S | 055°40.561' W | 233 |
| 7 | PS118_012 | 1 | 2019-03-14 | 06:46:58 | 63°48.339' S | 055°44.729' W | 449 |
| 8 | PS118_013 | 1 | 2019-03-17 | 11:19:10 | 63°04.087' S | 054°18.766' W | 415 |
| 9 | PS118_015 | 2 | 2019-03-18 | 18:28:22 | 62°01.011' S | 054°59.499' W | 1469 |
| 10 | PS118_016 | 1 | 2019-03-18 | 23:48:15 | 61°53.999' S | 053°48.046' W | 829 |
| 11 | PS118_017 | 1 | 2019-03-19 | 01:36:01 | 61°55.208' S | 053°39.840' W | 581 |
| 12 | PS118_018 | 1 | 2019-03-19 | 02:52:17 | 61°56.445' S | 053°31.967' W | 979 |
| 13 | PS118_019 | 1 | 2019-03-19 | 04:28:53 | 61°58.091' S | 053°22.143' W | 1448 |
| 14 | PS118_020 | 1 | 2019-03-19 | 06:23:15 | 61°59.868' S | 053°09.468' W | 2188 |
| 15 | PS118_021 | 1 | 2019-03-19 | 10:08:10 | 62°02.445' S | 052°55.126' W | 2518 |
| 16 | PS118_022 | 1 | 2019-03-19 | 13:18:42 | 62°03.974' S | 052°40.654' W | 2639 |
| 17 | PS118_023 | 1 | 2019-03-19 | 17:05:55 | 62°06.876' S | 052°22.745' W | 2814 |
| 18 | PS118_024 | 1 | 2019-03-20 | 00:18:18 | 62°15.010' S | 051°30.011' W | 3259 |
| 19 | PS118_024 | 4 | 2019-03-20 | 08:45:36 | 62°14.539' S | 051°25.529' W | 3278 |
| 20 | PS118_026 | 1 | 2019-03-20 | 20:11:14 | 62°23.724' S | 052°01.545' W | 3037 |
| 21 | PS118_027 | 1 | 2019-03-21 | 01:31:54 | 62°30.987' S | 052°30.313' W | 2902 |
| 22 | PS118_028 | 1 | 2019-03-21 | 06:11:28 | 62°36.218' S | 052°48.095' W | 2791 |
| 23 | PS118_029 | 1 | 2019-03-21 | 10:29:28 | 62°39.445' S | 053°01.290' W | 2400 |
| 24 | PS118_030 | 1 | 2019-03-21 | 13:39:33 | 62°43.078' S | 053°17.250' W | 1364 |
| 25 | PS118_032 | 1 | 2019-03-21 | 21:27:36 | 62°45.990' S | 053°16.020' W | 878 |
| 26 | PS118_033 | 1 | 2019-03-22 | 00:21:42 | 62°48.397' S | 053°36.158' W | 402 |
| 27 | PS118_034 | 1 | 2019-03-22 | 01:32:51 | 63°50.874' S | 053°45.555' W | 283 |
| 28 | PS118_035 | 1 | 2019-03-22 | 03:17:01 | 63°55.250' S | 054°01.736' W | 296 |
| 29 | PS118_036 | 1 | 2019-03-22 | 05:33:33 | 62°59.978' S | 053°19.727' W | 293 |
| 30 | PS118_038 | 1 | 2019-03-22 | 11:44:28 | 63°04.440' S | 054°21.349' W | 438 |
| 31 | PS118_038 | 12 | 2019-03-23 | 03:35:26 | 63°04.261' S | 054°20.137' W | 424 |
| 32 | PS118_041 | 1 | 2019-03-25 | 12:11:47 | 61°19.821' S | 051°50.451' W | 536 |
| 33 | PS118_042 | 1 | 2019-03-25 | 13:42:16 | 61°23.375' S | 051°42.073' W | 528 |
| 34 | PS118_043 | 1 | 2019-03-25 | 15:23:46 | 61°27.229' S | 051°31.948' W | 622 |
| 35 | PS118_044 | 1 | 2019-03-25 | 16:55:41 | 61°29.866' S | 051°25.221' W | 1992 |
| 36 | PS118_045 | 1 | 2019-03-25 | 19:08:55 | 61°32.335' S | 051°18.337' W | 2725 |
| 37 | PS118_046 | 1 | 2019-03-25 | 22:22:38 | 61°35.790' S | 051°08.456' W | 2879 |
| 38 | PS118_049 | 2 | 2019-03-26 | 18:12:51 | 61°28.666' S | 051°30.427' W | 1218 |
| 39 | PS118_051 | 1 | 2019-03-27 | 03:50:29 | 60°50.785' S | 050°11.704' W | 1881 |
| 40 | PS118_052 | 1 | 2019-03-27 | 06:09:21 | 60°50.886' S | 050°00.125' W | 2137 |

| Profile | Station | Cast | Date | Time | Latitude | Longitude | Pressure max [dbar] |
|---|---|---|---|---|---|---|---|
| 41 | PS118_053 | 1 | 2019-03-27 | 09:19:52 | 60°50.620' S | 049°45.852' W | 2612 |
| 42 | PS118_054 | 1 | 2019-03-27 | 12:22:31 | 60°50.591' S | 049°35.791' W | 2671 |
| 43 | PS118_055 | 1 | 2019-03-27 | 15:13:30 | 60°50.684' S | 049°23.711' W | 2524 |
| 44 | PS118_056 | 1 | 2019-03-27 | 18:04:47 | 60°50.647' S | 049°11.826' W | 1868 |
| 45 | PS118_057 | 1 | 2019-03-27 | 20:34:14 | 60°50.652' S | 049°00.315' W | 1094 |
| 46 | PS118_058 | 1 | 2019-03-27 | 23:15:31 | 60°51.114' S | 048°32.064' W | 2054 |
| 47 | PS118_059 | 1 | 2019-03-28 | 02:10:08 | 60°50.783' S | 048°11.739' W | 2608 |
| 48 | PS118_060 | 1 | 2019-03-28 | 05:21:44 | 60°50.726' S | 047°53.833' W | 2218 |
| 49 | PS118_061 | 1 | 2019-03-28 | 08:47:48 | 60°50.812' S | 047°31.063' W | 1947 |
| 50 | PS118_062 | 1 | 2019-03-28 | 13:12:04 | 60°55.737' S | 046°33.522' W | 324 |
| 51 | PS118_071 | 2 | 2019-03-31 | 20:01:09 | 61°04.677' S | 051°46.059' W | 862 |
| 52 | PS118_082 | 2 | 2019-04-04 | 14:15:55 | 61°13.484' S | 052°28.889' W | 971 |

**Tab. 10.2:** Ice-based CTD stations

| Profile | Station | Casts | Date | Time | Latitude | Longitude | Depth [m] |
|---|---|---|---|---|---|---|---|
| | | | | | | | |
| 1 | PS118_20190224_oce1 | 1 | 2019-02-24 | 15:55 | 64°53.508'S | 57°14.160'W | 390 |
| 2 | PS118_20190226_oce2 | 1 | 2019-02-26 | 15:44 | 65°19.932'S | 58°00.036'W | 460 |
| 3 | PS118_20190301_oce3 | 1 | 2019-03-01 | 17:12 | 65°12.744'S | 57°34.820'W | 468 |
| 4 | PS118_20190302_oce4 | 1 | 2019-03-02 | 17:44 | 65°25.482'S | 57°55.789'W | 423 |
| 5 | PS118_20190308_oce5 | 1 | 2019-03-08 | 16:24 | 65°21.870'S | 57°37.956'W | 401 |
| 6 | PS118_20190312_oce6 | 6 | 2019-03-12 | 17:57 | 63°59.718'S | 55°36.348'W | 353 |
| 7 | PS118_20190316_oce7 | 3 | 2019-03-16 | 18:29 | 63°36.852'S | 56°08.739'W | 94 |

**Tab. 10.3:** MSS station locations

| Profile | Station | Cast | Date | Time | Latitude | Longitude |
|---|---|---|---|---|---|---|
| | | | | | | |
| 1 | PS118_031 | 1,2 | 2019-03-21 | 19:54:20 | 62°42.758' S | 053°15.443' W |
| 2 | PS118_032 | 2,3,4 | 2019-03-21 | 22:34:31 | 62°45.732' S | 053°27.379' W |
| 3 | PS118_049 | 3,4,5 | 2019-03-26 | 19:21:48 | 61°29.092' S | 051°30.890' W |
| 4 | PS118_050 | 1,2 | 2019-03-26 | 20:57:46 | 61°28.858' S | 051°26.896' W |

The overall number of shipboard CTD casts during PS118 amounted to 52, with the majority of them organized in four oceanographic shelf-to-basin transects in the Powell Basin (Fig. 10.2). The shipboard CTD system consists of a Seabird 911+ CTD (SN 937) attached to a carousel (SBE32, SN 718) with 24 Niskin bottles of 12 l capacity. The system included (a) two sensor pairs for conductivity (SBE4, SN 3590, SN 3570) and temperature (SBE 3, SN 5112, SN 5115),

(b) one high precision pressure sensor Digiquartz 410K-134 (SN 937), (c) one oxygen sensor (SBE43, SN 1834), (d) one transmissometer (Wetlab C-Star, SN 1198), (e) one fluorometer (Wetlab FLRTD, SN 1853), and (f) one altimeter (Benthos PSA-916, SN 47768). Additionally an upward and downward looking ADCP (LADCP Workhorse Monitor WHM 300 SN 23292, SN 23293) was mounted on the carousel. Calibration of the conductivity and temperature sensors was performed prior to the cruise at Seabird Electronics. The accuracy of the temperature sensors amounts to 2 mK. The readings for the pressure sensor are better than 1dbar. Conductivity was corrected using salinity measurements from water samples. IAPSO Standard Seawater from the P-series P160 (K15 = 0.99983, practical salinity 34.993) was used. A total of 64 water samples were measured using an Optimare Precision Salinometer (OPS SN 006). Based on the water sample correction, salinity was measured to an accuracy of 0.002. The salinity will be corrected following post-cruise calibration of the sensors at the manufacturer. Underway temperature and salinity at 11m depth were recorded with the ship's SBE 21/ SBE 38 thermosalinograph (TSG). The TSG salinity values were corrected against salinometer-based salinity measurements.

The workflow during the ice-based CTD stations generally started with drilling a hole through the sea ice with a 10-inch motorized ice auger. We then lowered a Seabird 19plusV2 CTD though the hole from the surface to the bottom. The CTD was attached to a thin but extremely durable spectra line, which was spooled onto a hand-powered winch (Fig. 10.3). The lowering speed was approximately 0.25-0.5 m/s, which resulted in a vertical resolution of ~10 cm. The accuracy of the SBE19plusV2 is 2 mK and 0.003 for temperature and salinity, respectively.



*Fig. 10.3: Operation of the ice-based CTD through an ice hole*

The southernmost ice station was located ~50 km north of A68. During ice station 5 (Tab. 10.2), we deployed one ice-based drifter (see Fig. 10.1 for location and drifter track). The system was designed by Pacific Gyre and carried a 400 m tether on which we installed two Seabird SBE37 (temperature and salinity at 50 m and 350 m depth) and one SBE39 Seabird temperature logger (390 m depth). The surface unit (Fig. 10.4) additionally included sensors for sea level pressure and air temperature and samples transmits all parameters along with coordinates in 15-minute intervals to the data server. The drifter system can operate for up to two years and will provide valuable information regarding the spatial and temporal variability of the water characteristics in this remote region.

On four stations, we operated a microstructure profiler (MSS, manufactured by Sea&Sun, see Table 10.3 for locations), which measures the standard hydrographic parameters (CTD), optical backscatter, and fluorescence in addition to small-scale velocity shear. The MSS samples with high-frequency (1024 Hz) and can hence provide a fine-scale resolution of the water column (on the order of millimetres), which is sufficient to resolve small eddies and turbulence and to quantify vertical flux rates. Unfortunately, the cable of the MSS was severed during the operation at MSS station 4, which led to the loss of the instrument and marked the end of the MSS measurements during PS118.

The lander deployed by the Bentho-pelagic processes-group (see Richter et al., chapter 6) recorded additional oceanographic data (current velocities and temperature and salinity), and may provide a base for interdisciplinary data analysis.

*Fig. 10.4: Picture of the ice-deployed surface unit of the drifter*

**Work at sea-tracer oceanography**

The tracer oceanography sample collection during PS118 amounted to 130 water samples at 13 stations for stable noble gas isotopes ($^3$He, $^4$He, Ne) and 160 samples at 16 stations for transient tracers (chlorofluorocarbons, SF6, CFC-12). The water samples for helium isotopes and neon were stored from the CTD/water bottle system into gas-tight copper tubes, which were immediately sealed from both sides. The noble gas samples will later be analysed in the IUP Bremen noble gas mass spectrometry lab. The copper tube water samples are processed in a first step with an ultra-high vacuum gas extraction system. Sample gases are transferred via water vapour into a glass ampoule kept at liquid nitrogen temperature. For analysis of the noble gas, isotopes the glass ampoules are connected to a fully automated ultra-high vacuum mass spectrometric system equipped with a two-stage cryogenic trap system. The system is regularly calibrated with atmospheric air standards (reproducibility better ±0.2 %). Also measurement of blanks and linearity are done. Additionally, we sampled 43 seawater samples and 4 snow samples for tritium analysis. This enables us to correct the $^3$He measurements for $^3$He from tritium decay, even if the oceanic and atmospheric concentrations are expected to be low or even negligible.

For the transient tracers (CFC-12 and SF6) water samples from the CTD/water bottle system were collected into 200 ml glass ampoules and are flame-sealed after a CFC-free headspace of pure nitrogen had been applied. The CFC-12 and SF6 samples are later analysed in the TRACER-laboratory at the IUP Bremen. The determination of CFC-12 and SF6 concentration will be accomplished by purge and trap sample pre-treatment followed by gas chromatographic (GC) separation on a capillary column and electron capture detection (ECD). The amount of CFC-12 and SF6 degassing into the headspace will be accounted for during the measurement procedure in the lab. The system will be calibrated by analysing several different volumes of a known standard gas. Additionally the blank of the system will be analysed regularly.

All samples will be shipped home after the expedition and will be analysed in the UHB-IUP noble gas and tracer laboratories. The measurements are expected to be completed within ~one year after the expedition, and will undergo a careful data quality check at the IUP Bremen.

**Work at sea-glider oceanography**

Seagliders are autonomous profiling vehicles, which can carry a variety of scientific sensors to a maximum depth of 1000 m. Vertical movement is provided through altering the glider's

buoyancy by pumping oil between an internal and external reservoir, which alters the density of the glider. External fixed wings allow alterations to the glider's pitch to translate the vertical motion into motion at an angle, generally around 25-30° to the horizontal, thus providing forward motion. The direction of travel is controlled by rolling the glider to turn (similar to how airplanes turn). The flight behaviour is controlled by the on-board processor, which will direct the flight towards target locations given by the user, and also take scientific measurements as directed. When the glider surfaces (approximately every 4 hours if profiling to 1000 m) data from that dive is transmitted over the Iridium satellite network to the base station computer on land, and new instructions can be sent including target locations and depths, and sampling strategy. Details of the sensors on each glider, and their deployment and recovery locations, are given in Table 10.4. Both gliders were deployed without incident from the ship's starboard crane using a 'rigid rope' – a rope sheathed in non-flexible plastic pipe. This prevents the rope wrapping around the antenna, which could cause damage.

**Tab. 10.4:** Glider sensors and details of the deployments and recoveries. All times are in UTC

| Glider | SG558 | SG613 |
|---|---|---|
| Sensors | Seabird CT sail S/N 190 measuring conductivity and temperature.<br><br>Wetlabs triplet Ecopuck S/N 879 measuring optical backscatter and chlorophyll fluorescence.<br><br>Biospherical Instruments PAR sensor S/N 50143 measuring photosynthetically active radiation (light). | Seabird CT sail S/N 114 measuring conductivity and temperature.<br><br>Rockland Scientific Instruments microstructure logger and pods, S/N 001, carrying shear probe S/N M1684 and fast thermistor S/N T1482. |
| Deployment date | 18/03/2019 17:24 | 26/03/2019 17:12 |
| Deployment location | 62° 00.154' S, 55° 00.016' W | 61° 28.349' S, 51° 28.859' W |
| Recovery date | 04/04/2019 14:05 | 31/03/2019 19:12 |
| Recovery location | 61° 13.459 S, 52° 28.539 W | 61° 04.565' S, 51° 46.552' W |
| Number of dives | 209 | 58 |

After the first few dives, Marlin began to experience some communication problems such as incomplete communications (e.g., new instructions were sent to Marlin but data from the previous dive was not successfully transmitted to the base station), or even missing entire communication sessions. Communication problems can be caused by a damaged antenna, malfunctioning modem, or pump problems, which can mean the glider does not fully surface at the end of the dive. Additionally, dive 14 aborted on 28th March because it exceeding the maximum depth. This could also be caused by problems with the buoyancy pump (e.g., oil leaking into internal reservoir increasing the glider's density), or a malfunctioning pressure sensor (i.e., the glider did not actually exceed the maximum depth but the pressure sensor reported deeper depths than were actually achieved). These problems are mission critical and could lead to total loss of the glider, so the decision was taken to recover as soon as possible. Unfortunately, inclement weather prevented recovery for several days, so the decision was

taken to resume diving as the glider would be in danger of further damage if it remained on the surface during storm conditions. Shallow dives place less strain on the pump than full depth dives so the target depth was limited to 200 m. Marlin was recovered successfully on 31st March by using a small boat to place a rope loop around the lifting point, which was then attached to the ship's crane to lift the glider on board. No damage was visible, but problems with the pump, pressure sensor or modem cannot be diagnosed by visual inspection alone so further testing will await Marlin's return to the UK. Bella was recovered without incident using the recovery pole and hoop method, which is more appropriate for slightly rougher seas.

## Preliminary (expected) results

### *Western Weddell Sea shelf*

The first half of the expedition included the attempt to reach the Larsen C region in order to characterize the hydrographic properties and relevant physical exchange processes. The conditions on the western Weddell Sea shelf were overall dominated by heavy ice cover during the sampling period. All surface waters were at the freezing point (~-1.8°C) in a 20-40 m-deep mixed surface layer. Below the mixed layer, the temperature showed a narrow maximum before decreasing again toward the freezing point. The sharp upper-layer gradients suggest modification of the surface waters during sea ice melt. Most of the occupied stations were ice-free one-to-two months before PS118, and surface-warmed waters could have been subject to ice melt (cooling and freshening) following the northward expansion of the Weddell Sea ice cover. Despite the considerable distance to Larsen C, some of the southernmost stations showed an influence of the ice shelf manifested in near-bottom water temperatures of -1.92°C (Fig. 10.5). These temperatures are slightly below the surface freezing point at the respective salinities, which can only result from further cooling underneath the ice shelf. Considering that only two of the profiles showed remnants of ISW indicates that the distribution and propagation of ISW on the western Weddell Sea shelf is patchy and variable. Additional information derives from the ice-based drifter, which also indicates highly variable temperature and salinity characteristics including those of MWDW and ISW.
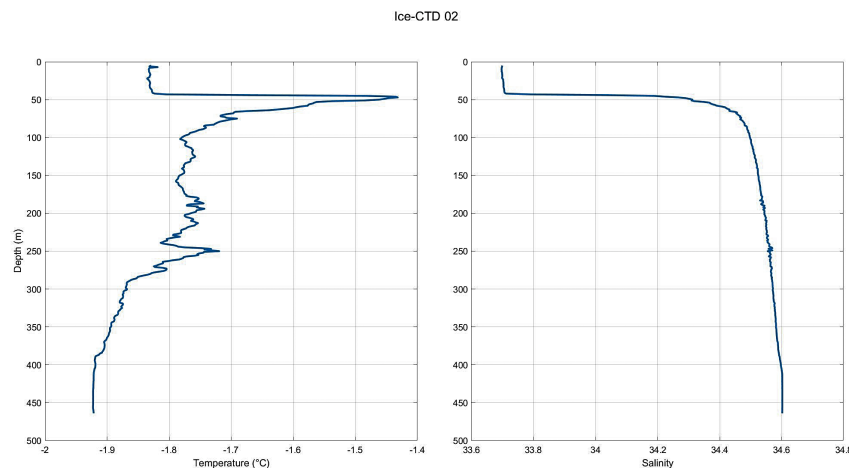


*Fig. 10.5: Salinity and temperature profile from ice station PS118_20190226_oce2*

*Powell Basin*

Major oceanographic activities during the second half from 17th March until the end of scientific activities on 4th April concentrated on hydrographic transects to map the fronts and dominant currents above the continental slope as well as to characterize major outflow passages. The Powell Basin is the northward extension of the western Weddell Sea and through-flow region for some Antarctic waters to the northern ocean basins. The shelf-to-basin CTD transects are characterized by cold and fresh waters in the shallower regions north of the peninsula and over the South Scotia Ridge on the western boundary of the Powell Basin. The steep continental slope features the steep Antarctic slope front between the warm (T>0°C) and saline (>34.65) warm deep water (WDW) and the colder and fresher shallower/shelf waters (Fig. 10.6 and 10.7). Near-freezing temperatures were only found near the surface in parts of the southernmost transects, which were partly ice-covered during the time of occupation. The densest and most saline waters were found at the basin ends of transects 1 and 2 at depths >3000 m, with AABW characteristics of temperature and salinity of 33.65 and -0.9°C, respectively (Fig. 10.8). The lowered-ADCP data requires careful post-cruise processing, and will later provide additional insights regarding current velocities and the ocean circulation in the Powell Basin as well as the transport of waters along the Antarctic Slope Front. The water mass characterization from the shipboard CTD measurements will be complemented and refined by the high-resolution CTD data from the glider surveys. Fig.s 10.9 and 10.10 show the gliders' temperature and salinity data from Marlin and Bella respectively. The deployment location of Bella was inspired by Thompson et al., (2009), who observed a standing eddy centred around a shoal at approximately 62°S, 54°W. However, their work was completed using surface drifters, which provide no information about water mass characteristics below the surface. Recent satellite altimetry suggests the eddy is located further east along the South Scotia Ridge. The objective for Bella was to complete a transect from 62°S, 55°W to 61°S, 52°W, which would go across both possible locations for the eddy and allow characterization of the water masses present.
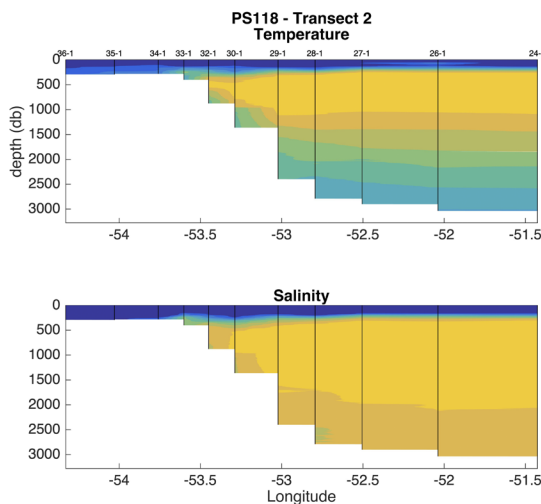


*Fig. 10.6: Temperature (top) and salinity (bottom) shelf-to-basin cross-section at transect 2. Vertical lines show the station locations, station numbers are provided in the top of the upper panel.*
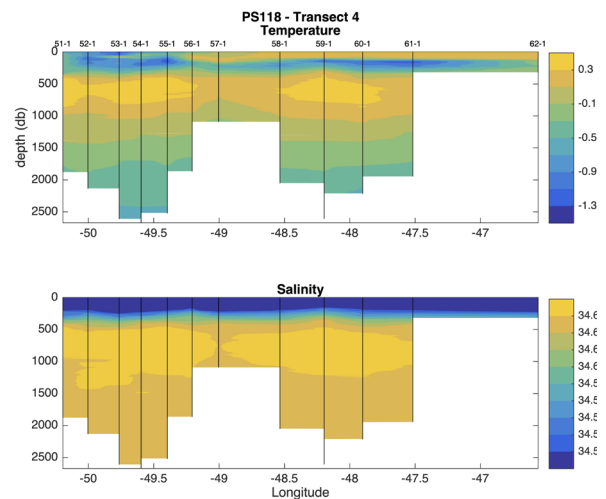
*Fig. 10.7: Same as Fig. 10.6, except for transect 4*
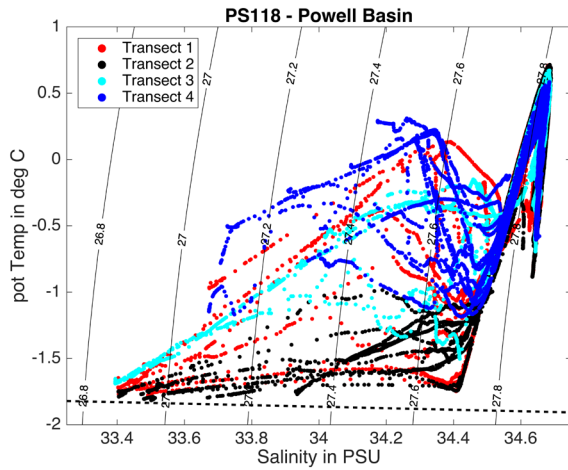
*Fig. 10.8: Temperature-salinity diagram from the Powell Basin CTD profiles. The colours indicate the different transects, contour lines show density (sigma-t in kg m$^{-3}$) lines.*
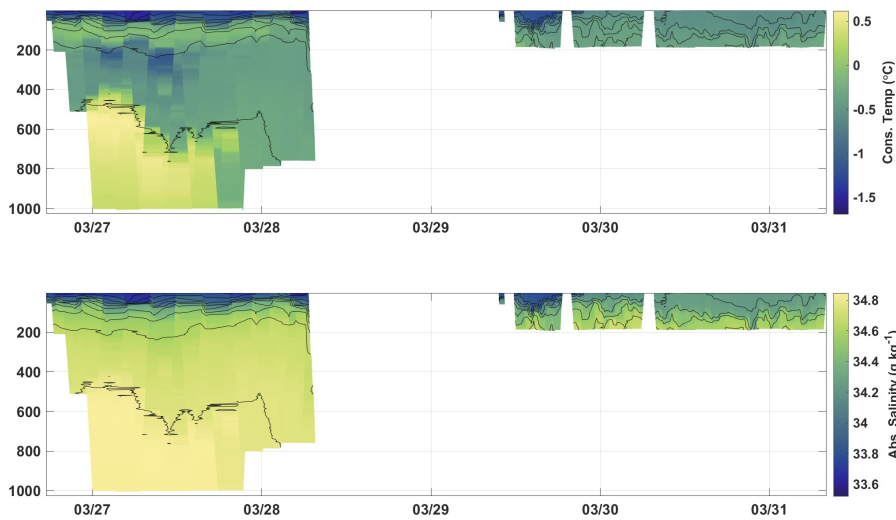


*Fig. 10.9: Temperature (top) and Salinity (bottom) measured by SG613 (Marlin). Thin black lines are density contours. During the period from 28$^{th}$ March to 29$^{th}$ March with no data, Marlin was drifting at the surface while decisions were taken over how best to preserve it until recovery. The remaining portion of the data was taken during the 200 m dives until recovery.*
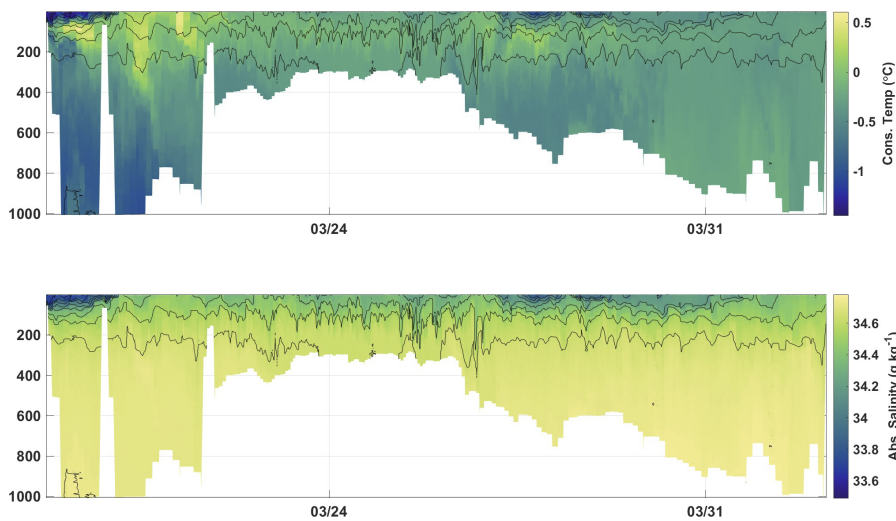


*Fig. 10.10: Temperature (top) and Salinity (bottom) measured by SG558 (Bella) until 1$^{st}$ April. Thin black lines are density contours.*

**Preliminary (expected) results – tracer oceanography**

As soon as the measured data are available, we will use the stable noble gas data ($^3$He, $^4$He, Ne) to quantify the GMW inventories. The transient tracer (CFC, SF6) data will be used to determine the time scales of circulation and residence to assess the formation rates of GMW (basal melting rates) and the related WSDW and WSBW formation and to estimate the anthropogenic carbon content. We will combine our new data set with available historic tracer data to assess possible temporal variability of transit times and carbon content. Overall, we expect valuable insights from the tracer data regarding the role of ice shelf-ocean interaction and the contribution of shelf-formed water masses on the deep waters of the Powell Basin.

**Data management**

All oceanographic data sets were either calibrated on board or will be calibrated after return of the sensors from the manufacturer at the Alfred Wegener Institute. After quality control, they will be published in peer-reviewed journals and/or in the World Data Center PANGAEA Data Publisher for Earth & Environmental Science (www.pangaea.de) for public use.

All gas tracer data will be carefully quality controlled and published on the PANGAEA data base as soon as available (approximately one year after the cruise) and published in a peer-reviewed journal. Our cooperation partners will receive the data as soon as the final data set is available.

All glider data will be published in peer-reviewed journals and made public once available (approximately one year after the cruise) on either the PANGEA data base or through the British Oceanographic Data Centre, which has prior experience managing glider data. Our cooperation partners will receive the data as soon as the final data set is available.

**References**

Azaneu M, Heywood KJ, Queste BY & Thompson AF (2017) Variability of the Antarctic Slope Current system in the northwesternWeddell Sea. Journal of Physical Oceanography, 47(12), 2977–2997.

Foldvik A, Gammelsrød T, Østerhus S, Fahrbach E, Rohardt G, Schröder M, Nicholls K, Padman L &, Woodgate R (2004) Ice shelf water overflow and bottom water formation in the southern Weddell Sea J. Geophyas. Res. Oceans, 109 (C2), C02015, doi:10.1029/2003JC002008.

Huhn O, Hellmer H, Rhein M, Roether W, Rodehacke C, Schodlok M & Schröder M (2008) Evidence of deep and bottom water formation in the western Weddell Sea. Deep-Sea Research II, 55/8-9, 1098-1116, doi:10.1016/j.dsr2.2007.12.015.

Meijers AJS, Meredith MP, Abrahamsen EP, Morales Maqueda MA, Jones DC & Naveira Garabato AC (2016) Winddriven export of Weddell Sea slope water. J. Geophys Res Oceans, 121, 7530–7546, https://doi.org/10.1002/2016JC011757.

Nicholls K, Østerhus S, Makinson K, Gammelsrød T & Fahrbach E (2009) Ice-ocean processes over the continental shelf of the Southern Weddell Sea, Antarctica: A review. Reviews of Geophysics, 47 (3), 1-23, doi:10.1029/2007RG000250.

Talley L (2013) Closure of the global overturning circulation through the Indian, Pacific, and Southern Oceans: Schematics and transports Oceanography, 26, 80–97, https://doi.org/10.5670/oceanog.2013.07.

Thompson AF & Heywood K J (2008) Frontal structure and transport in the northwestern Weddell Sea Deep Sea Research, Part I,55(10),1229–1251.

Thompson AF, Heywood KJ, Thorpe SE, Renner AHH & Trasvina A (2009) Surface circulation at the tip of the Antarctic Peninsula from drifters. Journal of Physical Oceanography, 39, 3-26.

# 11. BENTHIC HABITAT MAPPING AND BENTHIC MACROECOLOGICAL STUDIES WITH THE OCEAN FLOOR OBSERVATION AND BATHYMETRY SYSTEM (OFOBS)

Autun Purser[1], Laura Hehemann[1], Axel Nordhausen[2], Simon Dreutter[1] Ulrich Hoge[1], Julian Gutt[1], Dieter Piepenburg[1], Caspar Kraan[1] (not on board)

[1]AWI
[2]MPI

**Grant-No. AWI_PS118_09**

## Objectives

### General

The main aim of the Benthic Habitat Mapping group was to survey the seafloor with visual and hydroacoustic systems to generate high spatial resolution maps of the seafloor ecosystems visited during PS118, and to collect data of sufficient quality to support the estimation of distributions and abundances of various encountered fauna across these ecosystems.

The initial aim of the cruise was to investigate the seafloor recently uncovered by the breakoff of the A68 iceberg from the Larsen C ice shelf, and/or the changing seafloor communities exposed by similar ice breakoffs of sections of the Larsen A (1995) and Larsen B (2002) shelves (Shepherd et al., 2003; Wendel & Kumar 2017). Unfortunately, ice conditions prevented Polarstern reaching any of these survey targets during PS118. Because of this, the focus of the cruise shifted to opportunistic surveying of the Weddell Sea Seafloor and a northward heading transect (coinciding with an ice cover related surface productivity gradient) into the Powell Basin, with deployments made at several locations of contrasting depths and topographical structure.
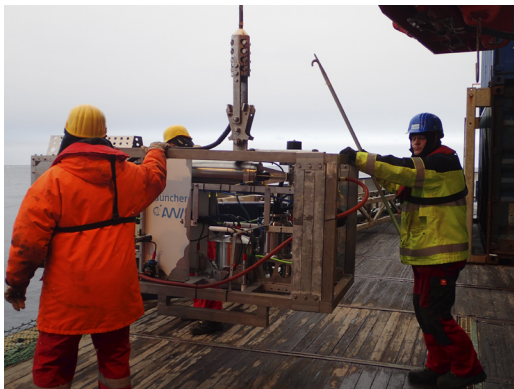


*Fig. 11.1: The OFOBS sled being deployed in the Powell Basin (Image: Autun Purser)*

The recently developed Ocean Floor Observation and Bathymetry System (Purser et al., 2018), Fig. 11.1 was used to carry out the habitat mapping work during PS118. The system incorporates the same still and video camera systems used extensively in Antarctica in the past (e.g. Gutt et al., 2013) during PS81 and Cape et al. (2014) during PS96. The use of the same camera systems allows for easy comparison with results collected during these previous cruises. A dual band Edgetech sidescan sonar is also mounted on the sled to allow high-resolution seafloor structure data to be collected from a swath ~100 m in diameter (given an operational height of 2.5 m). The OFOBS system also includes a much improved navigation system based around the integration of a PHINS inertial navigation system with a POSIDONIA beacon and a DVL dynamic velocity logger system. This navigation system allows all data collected by the OFOBS to be accurately placed spatially, for production of habitat and fauna distribution maps.

**Work at sea**

The OFOBS is a towed underwater camera system equipped with both a high-resolution photo-camera (iSiTEC, CANON EOS 5D Mark III) and a high-definition video-camera (iSiTEC, Sony FCB-H11). The cameras are mounted on a steel frame (140L x 92W x 135H cm), together with two strobe lights (iSiTEC UW-Blitz 250, TTL driven), three laser pointers at a distance of 50 cm from each other that were used to estimate the size of seafloor structures, four LED lights, and a USBL positioning system (Posidonia) to track the position of the OFOS during deployments.

The sidescan bathymetry sonar is an interferometric Edgetech 2205 AUV/ROV MPES (Multi Phase Echosounder) with two sidescan frequencies (230 kHz & 540 kHz) for different range and resolution achievements. The transducers additionally hold a bathymetric receive array to calculate bathymetric 2.5D data in the range of the 540 kHz sidescan sonar with around 800 data points per ping.

The OFOBS system was deployed during PS118 at 11 locations (Tab. 11.1, Fig. 11.2).

**Tab. 11.1:** Locations and details of all OFOBS deployments made during PS118

| Station | Date | In water | Seafloor start | Seafloor end | on deck | Timer images | Hotkey Images | PiCam images |
|---|---|---|---|---|---|---|---|---|
| PS118_6-9a | 2019-03-06 | 03:58 | 04:24 | 04:31 | 04:44 | 25 | 0 | 0 |
| PS118_6-9b | 2019-03-06 | 04:49 | 05:01 | 09:33 | 09:53 | 1372 | 90 | 3044 |
| PS118_7-1 | 2019-03-06 | 19:00 | 19:25 | 20:08 | 20:43 | 259 | 28 | 274 |
| PS118_8-1 | 2019-03-11 | 11:50 | 12:02 | 15:45 | 16:05 | 893 | 74 | 745 |
| PS118_9-1 | 2019-03-12 | 05:39 | 06:00 | 06:51 | 07:08 | 396 | 4 | 561 |
| PS118_11-2 | 2019-03-13 | 19:48 | 20:14 | 22:25 | 22:26 | 711 | 7 | 907 |
| PS118_12-12 | 2019-03-15 | 01:11 | 01:28 | 05:55 | 06:10 | 1642 | 5 | 5499 |
| PS118_38-13 | 2019-03-23 | 04:40 | 05:01 | 06:31 | 06:40 | 443 | 11 | 2636 |
| PS118_39-1 | 2019-03-23 | 18:10 | 18:46 | 09:56 | 10:17 | 3796 | 140 | 5714 |
| PS118_69_1-2 | 2019-03-31 | 01:30 | 01:52 | 16:00 | 16:38 | 2876 | 68 | 0 |
| PS118_77-1 | 2019-04-01 | 20:46 | 21:08 | 21:48 | 22:14 | 323 | 16 | 0 |
| PS118_81-1 | 2019-04-03 | 20:41 | 21:24 | 09:31 | 10:00 | 2406 | 73 | 0 |
| | | | TOTALS | | | 15142 | 516 | 19380 |
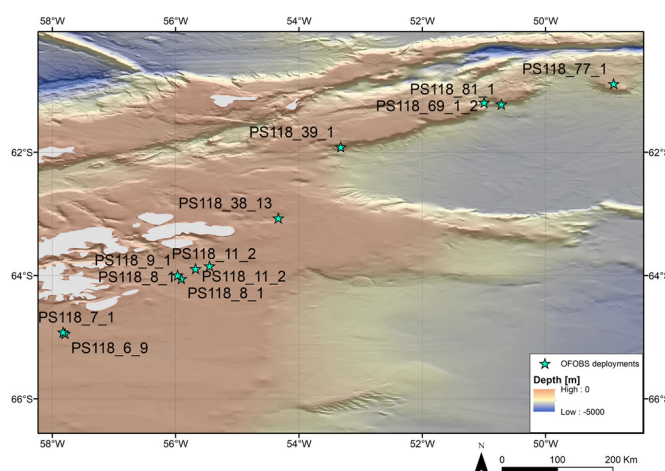


*Fig. 11.2: Overview map of OFOBS deployments made during PS118*

**Preliminary (expected) results**

Video, hydroacoustic and still image data were collected from and altitude of 1.5-2.5 m throughout each deployment. Contrasting regions of soft sediment covered and complex rocky topography were surveyed along a north-south productivity gradient.

Deployment tracks and example images from each deployment are given below.

OFOBS Deployment PS118_6-9
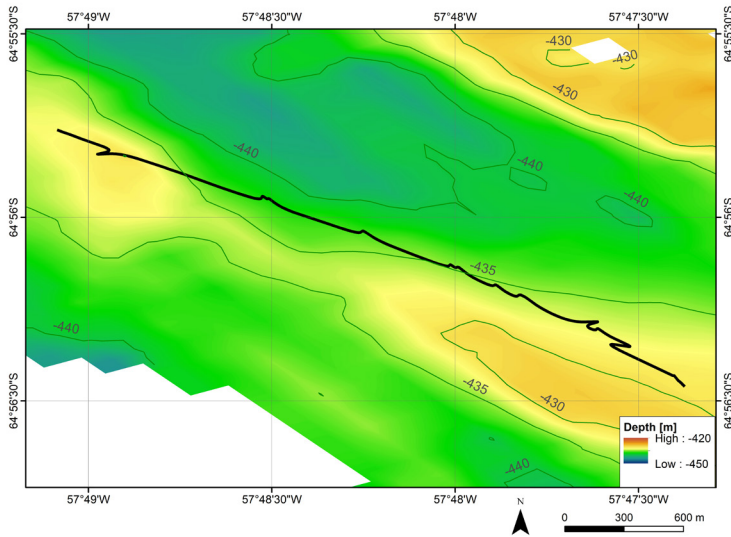


Fig. 11.3: Deployment track of OFOBS, station PS118_6-9



Fig. 11.4: Typical seafloor image taken with OFOBS still camera during station PS118_6-9 deployment

OFOBS Deployment PS118_7-1
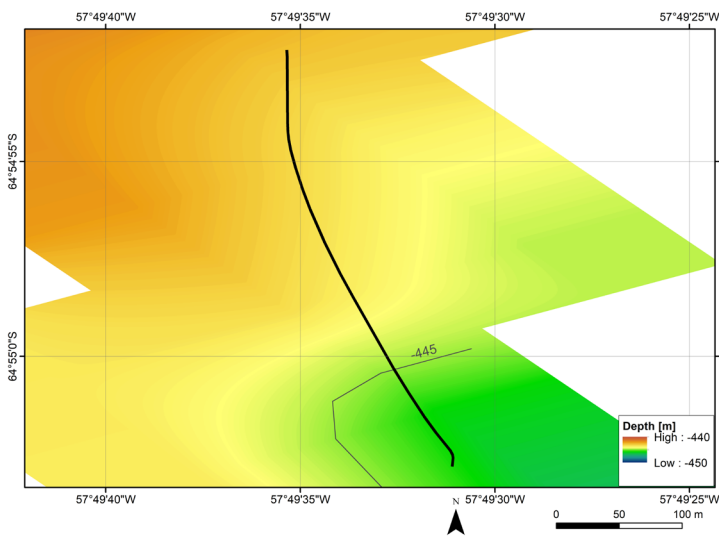


Fig. 11.5: Deployment track of OFOBS, station PS118_7-1



Fig. 11.6. Typical seafloor image taken with OFOBS still camera during station PS118_7-1 deployment

90

*OFOBS Deployment PS118_8-1*
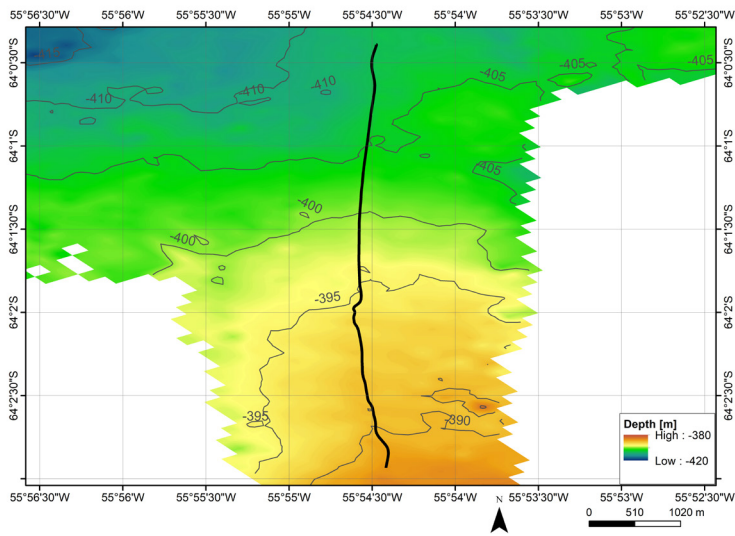


*Fig. 11.7: Deployment track of OFOBS, station PS118_8-1*
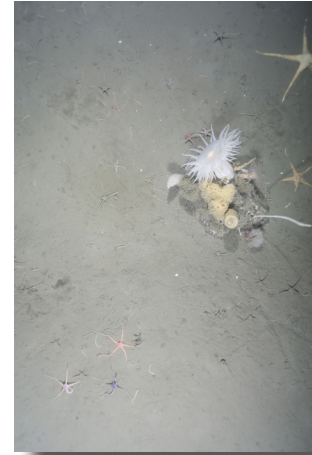


*Fig. 11.8: Typical seafloor image taken with OFOBS still camera during station PS118_8-1 deployment*

*OFOBS Deployment PS118_9-1*
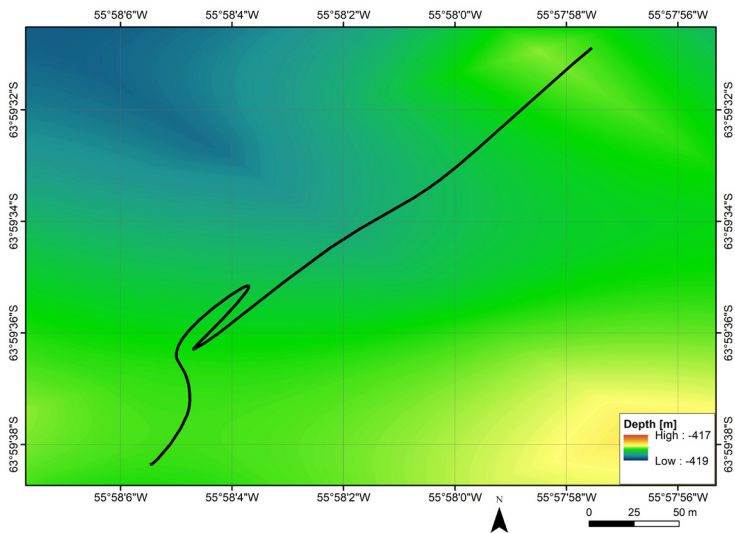


*Fig. 11.9: Deployment track of OFOBS, station PS118_9-1*



*Fig. 11.10: Typical seafloor image taken with OFOBS still camera during station PS118_9-1 deployment*

*OFOBS Deployment PS118_11-2*
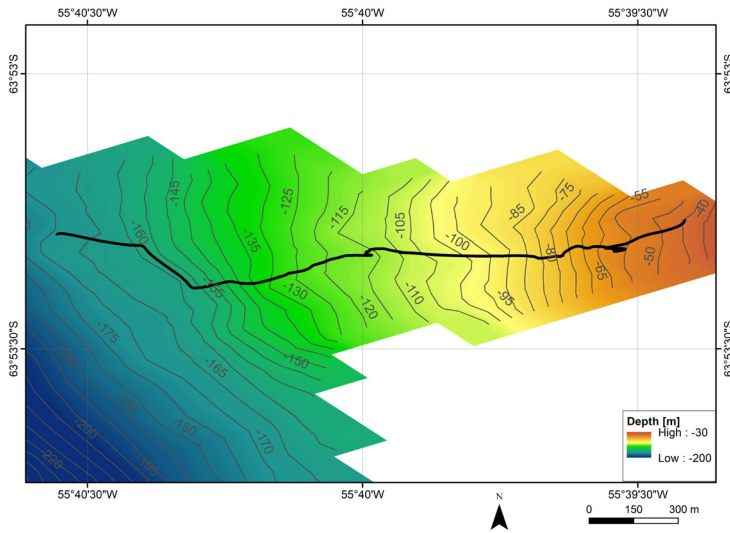


Fig. 11.11: Deployment track of OFOBS, station PS118_11-2



Fig. 11.12: Typical seafloor image taken with OFOBS still camera during station PS118_11-2 deployment

*OFOBS Deployment PS118_12-2*
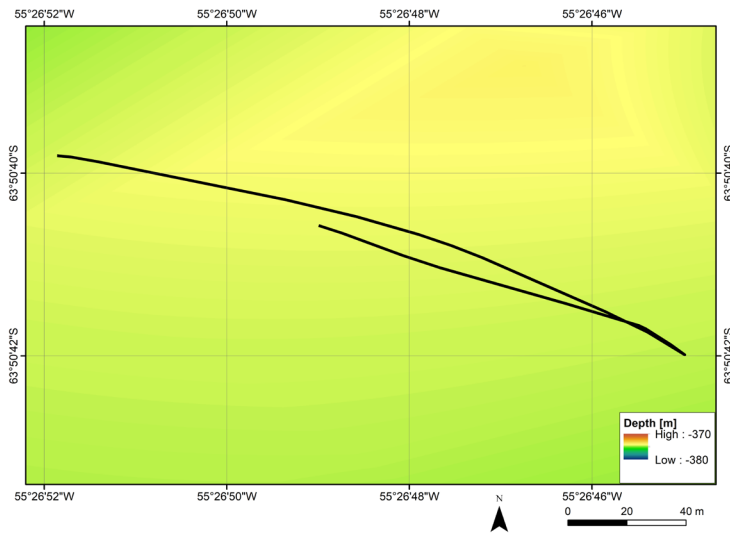


Fig. 11.13: Deployment track of OFOBS, station PS118_12-2
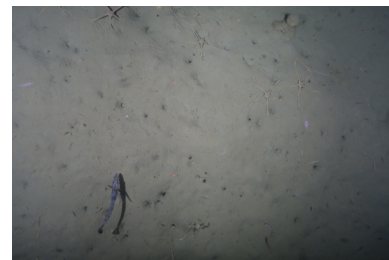


Fig. 11.14: Typical seafloor image taken with OFOBS still camera during station PS118_12-2 deployment

*OFOBS Deployment PS118_38-13*
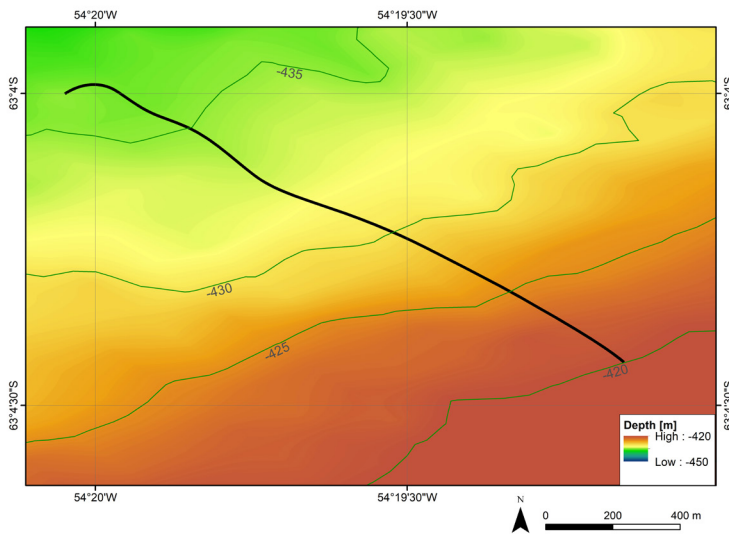


Fig. 11.15: Deployment track of OFOBS, station PS118_38-13



Fig. 11.16: Typical seafloor image taken with OFOBS still camera during station PS118_38-13 deployment

*OFOBS Deployment PS118_39-1*
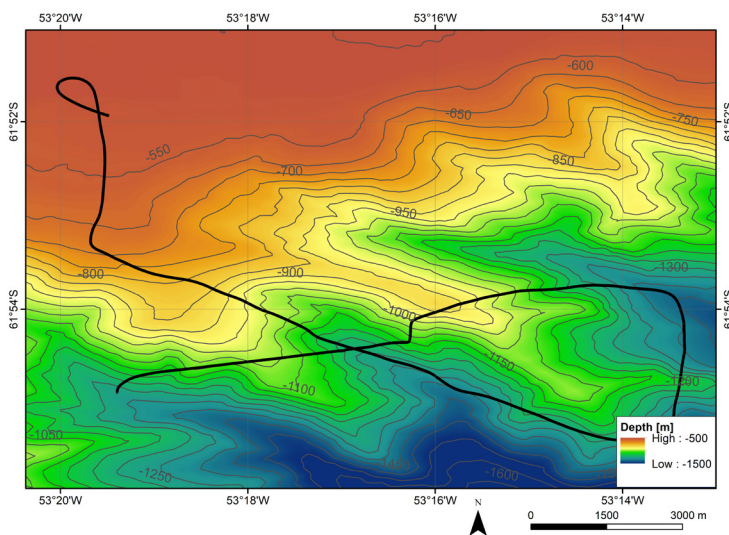


Fig. 11.17: Deployment track of OFOBS, station PS118_39-1
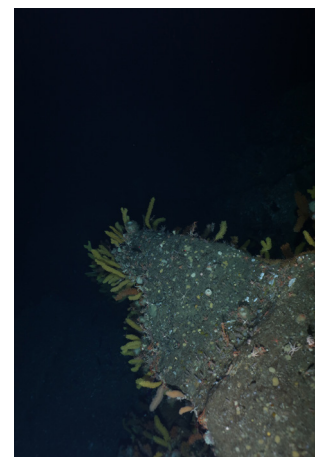


Fig. 11.18: Typical seafloor image taken with OFOBS still camera during station PS118_39-1 deployment

*OFOBS Deployment PS118_69-1*
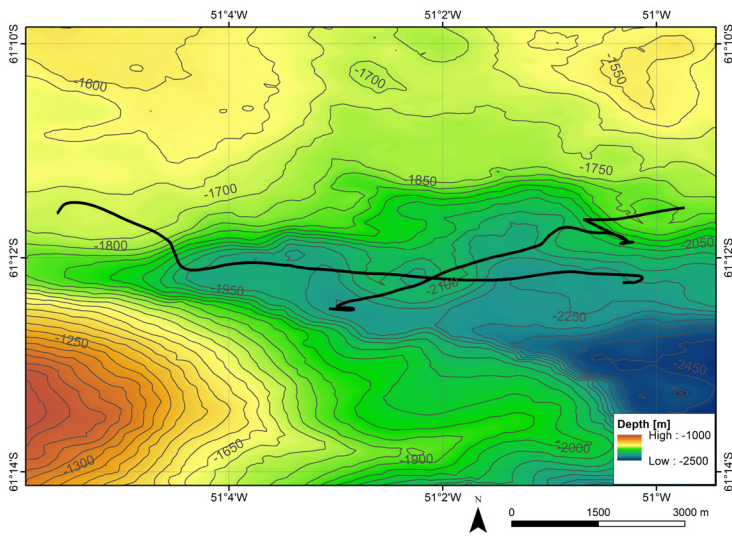


Fig. 10.19: Deployment track of OFOBS, station PS118_69-1



Fig. 11.20: Typical seafloor image taken with OFOBS still camera during station PS118_69-1 deployment

*OFOBS Deployment PS118_77-1*
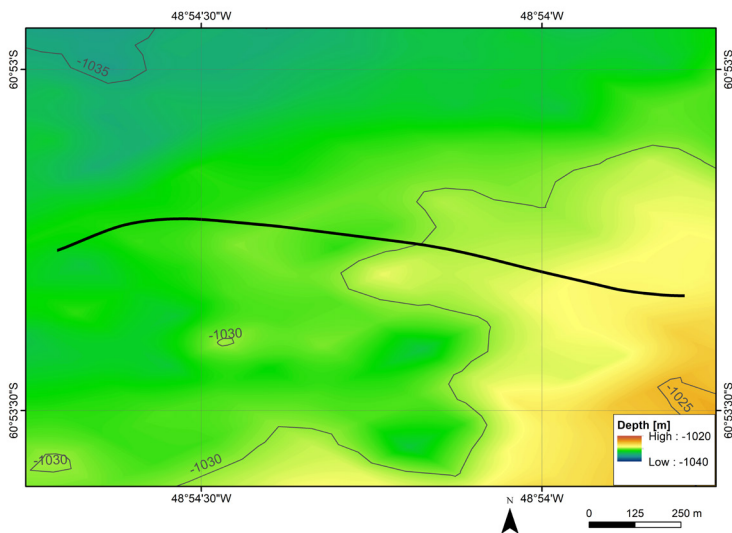


Fig. 11.21: Deployment track of OFOBS, station PS118_77-1



Fig. 11.22: Typical seafloor image taken with OFOBS still camera during station PS118_77-1 deployment

*OFOBS Deployment PS118_81-1*
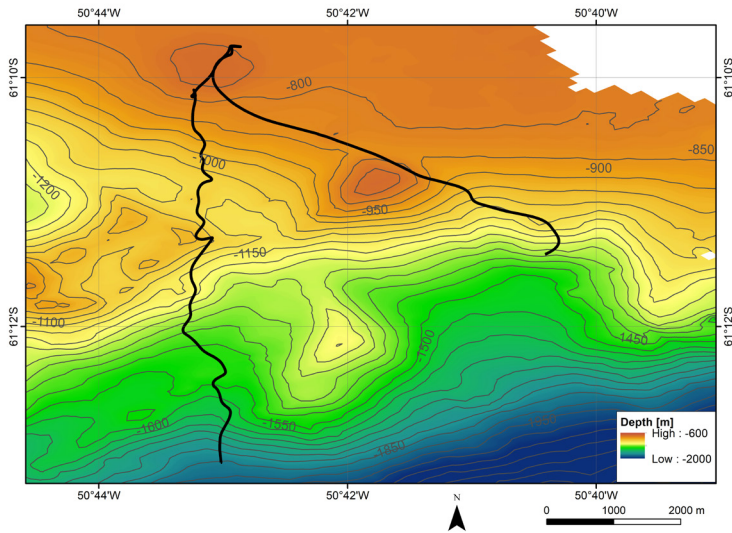


Fig. 11.23: Deployment track of OFOBS, station PS118_81-1
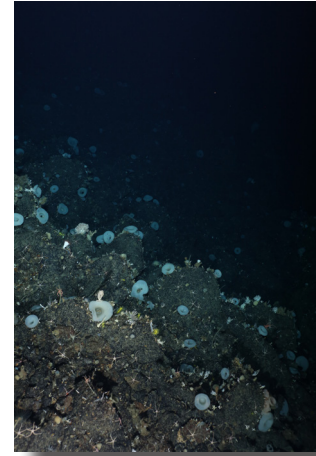


Fig. 11.24: Typical seafloor image taken with OFOBS still camera during station PS118_81-1 deployment

The acoustic data collected during PS118 is still being processed, though examples of high and low freguency sidescan sonar data collected during station PS118_11 are given below. (Fig. 11.25 and Fig. 11.26)
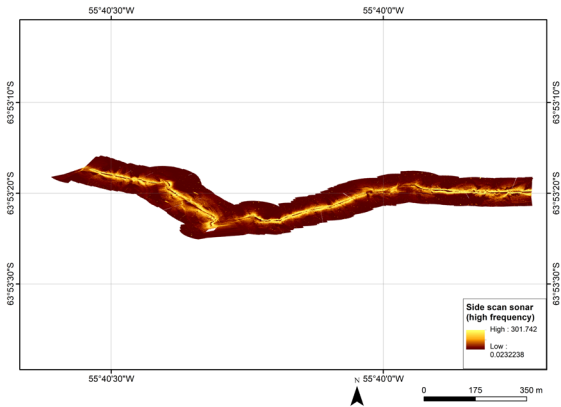


Fig. 11.25: High frequency sonar data collected during PS118_11
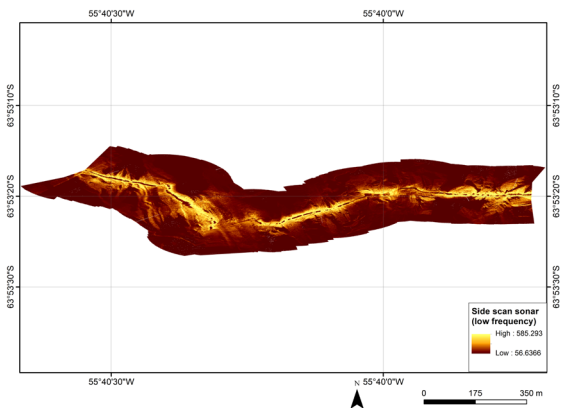


Fig. 11.26: Low frequency sonar data collected during PS118_11

## Data management

*Habitat mapping*

All raw video and image data will be uploaded to the World Data Center PANGAEA Data Publisher for Earth & Environmental Science (www.pangaea.de) within 6 months of cruise completion, and made fully open-access within two years of cruise completion, or earlier following scientific paper publication. All acoustic data will likewise be placed in PANGAEA, following geo-referencing within two years of cruise completion. Derived terrain variable maps will be made open access on PANGAEA following use in scientific papers or two years after cruise completion.

*Macroecological studies*

Faunistic data will be will be publicly available in PANGAEA at latest one year after the cruise, as well as in AntaBIF (Antarctic Biodiversity Information Facility; formerly SCAR-MarBIN), as soon as studies on macro- and megabenthic classification, quantification and identification are finished.

## References

Boetius A & Purser A (2017) The expedition of the research vessel POLARSTERN to the Arctic Ocean in 2016. Berichte zur Polar- und Meeresforschung, 706.

Cape MR, Vernet M, Kahru M & Spreen G (2014) Polynya dynamics drive primary production in the Larsen A and B embayments following ice shelf collapse. Journal of Geophysical Research, 119, 572-594.

Gutt JM, Cape M, Dimmler W, Fillinger L, Isla E, Lieb V, Lundälv T & Pulcher C (2013) Shifts in Antarctic megabenthic structure after ice-shelf disintegration in the Larsen area east of the Antarctic Peninsula. Polar Biology, 36, 895-906.

Gutt JM, Alvaro MC, Barco A, Böhmer A, Bracher A, David B, de Ridder C, et al. (2016) Macroepibenthic communities at the tip of the Antarctic Peninsula, an ecological survey at different spatial scales. Polar Biology, 39, 829–849.

Purser A, Marcon Y, Dreutter S, Hoge U, Sablotny B, Hehemann L, Lemburg J, Dorschel B, Biebow H & Boetius A (2018) OFOBS – Ocean Floor Observation and Bathymetry System: A new towed camera / sonar system for deep sea exploration and survey. IEEE Journal of Oceanic Engineering. DOI: 10.1109/JOE.2018.2794095.

Shepherd A, Wingham DJ, Payne T & Skvarca P (2003) Larsen ice shelf has progressively thinned. Science, 203, 856-859.

Wendel J & Kumar M (2017) Six points of perspective on Larcen C's huge new iceberg. EOS, 98, DOI: 10.1029/2017EO077735.

# 12. SEA ICE

Christian Haas[1], Stefanie Arndt[1], Ilka Peeken[1],
Erika Allhusen[1],
Juliane Müller[1] (not on board), Georgi Laukert[2]
(not on board), Petra Heil[3] (not on board), Ken
Golden[4] (not on board), David Morison[4] (not on
board)

[1]AWI
[2]Geomar
[3]Australian Antarctic Division (AAD)
[4]University Utah

**Objectives**

In contrast to sea ice in the Arctic, the extent of Antarctic sea ice has increased by 3.0 % per decade in summer and by 0.9 % per decade in winter since 1979 (e.g., Parkinson and Cavalieri, 2012; Simmonds, 2015). However, there is large interannual variability and there are large regional differences. In particular, sea-ice extent in the Weddell Sea has slightly declined during winter, but strongly increased during summer (Turner et al., 2014; Hobbs et al., 2016), leading to increasing amounts of thick, second-year ice. While Antarctic-wide changes of sea-ice extent and in particular variations in the Ross, Amundsen, and Bellingshausen Seas have been linked to variations of stratospheric circulation related to ozone depletion, and its imprints on surface winds (e.g., Turner et al., 2009; Thompson et al., 2011) or to the freshening of the Southern Ocean due to increased bottom melt of ice shelves (e.g., Bintanja et al., 2013), there is little understanding of the underlying reasons for the observed changes specifically in the Weddell Sea. Interpretation is further hampered by a lack of observational data of ice drift and thickness required for better model development, interpretation, and prediction. The study region of PS118, i.e. the western Weddell Sea, is a key region in this regard, as it is the region hosting the remaining sea ice during summer. Therefore, PS118 provides unique opportunities to better study the thickness, properties, and drift in this region to unravel the causes of increased summer ice extent and the special role of the Weddell Sea's sea ice cover in Antarctica. One of the key questions is if ice extent has increased due to increased advection of ice to the North, or due to increased ice thickness that protects the ice from early melt.

The planned work builds on previous work carried out by early *Polarstern* cruises in the 1990s (e.g. Lange and Eicken, 1991), as well as during the ISPOL (Hellmer et al., 2008; Haas et al., 2008) and WWOS cruises (Haas et al., 2009; Tan et al., 2012) in 2004 and 2006, respectively. Ice thickness and satellite radar data showed the presence of variable ice types depending on their origin, age, and oceanic regime, which also had distinctly different thickness distributions. Some of the perennial ice in the West was thicker than 3 m and rivaled the thickest ice in the Antarctic. There were no other ice thickness observations since then, except for an airborne survey of snow thickness by NASA (Kwok and Maksym, 2014).

It is therefore the aim of the sea-ice physics' project on "Sea ice properties and processes in the western Weddell Sea" (WedIce) during PS118 to continue ice thickness observations and radar remote sensing and to compare them with results from earlier cruises to detect and quantify potential change. The thickness of different ice regimes will also be related to different oceanic regimes with different magnitudes of ocean heat flux (Hellmer et al., 2011). Due to the timing of

PS118 in February to April, results will represent end-of-summer minimum ice conditions and will help to explain the area and amount of ice surviving the summer. This will provide important background information on the state of sea ice in the Weddell Sea and the reasons for its long-term changes. As the ship will pass from the open water through the Marginal Ice Zone (MIZ) into the closed pack ice zone, it will also be possible to observe meridional and zonal gradients of ice thinning and snow melt representing the changing influence of atmospheric and oceanic melt processes (Rabenstein et al., 2010).

Another important component of the sea ice mass balance is the accumulation and metamorphism of snow (Massom et al., 2001; Haas et al., 2001). Thaw-freeze events and snow metamorphism can be detected by satellite microwave observations (Haas, 2001; Arndt et al., 2016), thus providing valuable insights into the timing and change of melt onset related to changing atmospheric conditions. Melt onset is also related to ice thickness because earlier and stronger surface melt will accelerate overall thinning. During PS118, we plan to validate satellite microwave retrievals of metamorphic snow and to investigate, if regional gradients in the intensity of metamorphism can be detected by satellite microwave sensors.

One consequence of downward heat flux and snow thaw is the percolation of melt water to the snow-ice interface and the formation of gap layers, continuous or highly porous layers in the upper ice filled with seawater or slush and high concentrations of algae and other micro-organisms (Thomas et al., 1998; Haas et al., 2001; Kattner et al., 2004; Ackley et al., 2008). The relationships between the thickness and biomass and other biogeochemical properties of gap layers and the overlying superimposed ice and degree of snow metamorphism have never been investigated. Therefore, the WedIce projects aims to focus also on such interdisciplinary studies, given that we expect strong gradients in experienced melt conditions during summer across the marginal ice zone. In addition, the seeding potential of this biomass for the underlying water is studied. Further studies from the Arctic show that sea ice is a sink and transport vehicle for microplastic (Peeken et al. 2018) and currently nothing is known about the microplastic contamination in Southern Ocean sea ice. Thus, PS 118 will be used to collect sea ice cores from the investigation area to set a baseline for any possible contamination.

**Tab. 12.1:** Pangaea labels as used for sea-ice measurements during PS118 and the respective parameters associated to the measurements

| PANGAEA label | Description |
|---|---|
| **Ship based** | |
| ICEOBS | Ice Observations from ship bridge (along track) |
| Helicopter based | |
| AEM | Airborne EM ice thickness profiler (EM-Bird) |
| Field measurements | |
| SIT | Manual sea-ice thickness drilling |
| SPIT | Snow pit |
| SMP | SnowMicroPen |
| SDMP | Snow depth measured with Magna Probe (SnowHydro) |
| GEM | Ground electromagnetic sounding (GEM-2, Geophex) |
| | |
| Ice Cores | |
| CORE-ARC-MP | Archive  / Microplastic core |

| PANGAEA label | Description |
| --- | --- |
| CORE-BIO | Parameters:  Nutrients, fractionated Chla (>10µm, <10µm), marker pigments, species, DNA (Illumina sequencing ), POC/PON & natural ^{13}C and 15N  isotopes, biogenic silica |
| CORE-DNA | Parameters: Illumina sequencing  (DNA), marker pigments, species, POC/PON & natural 13C and 15N  isotopes,   biogenic silica, |
| CORE-MEIO | Parameters: Meiofauna |
| CORE-NEO | Parameters: Trace elements and their isotopes |
| CORE-TEX | Parameters: Texture, Salinity, Oxygen isotopes |
| CORE-IP25 | Parameters: IPSO-25 |
|  |  |
| ICE |  |
| ICE | Sampling of Slush, Nilas, Brown ice |
|  |  |
| Water sampling |  |
| WATER-GAP | Gap water  for biological varibales, Parameters:  Nutrients, fractionated Chla (>10µm, <10µm), marker pigments, species, DNA, POC/PON & natural 13C and 15N  isotopes, biogenic silica |
| WATER-NEO-GAP | Gap water for trace elements and their isotopes |
| WATER-UIW | Under-ice water for biological varibales, Parameters:  Nutrients, fractionated Chla (>10µm, <10µm), marker pigments, species, DNA, POC/PON & natural 13C and 15N  isotopes, biogenic silica |
| WATER-NEO-UIW | Under-ice water for trace elements and their isotopes |
|  |  |
| Snow- sampling |  |
| Snow | Snow collection;  for biological varibales, Parameters:   trace elements and their isotopes; Oxygen isotopes |
|  |  |
| Buoys |  |
| BUOY-SVP | Surface Velocity Profiler |

**Tab. 12.2:** List of all sea-ice stations within the WedIce project during PS118. Abbreviations for the used gear are in accordance to the labels given in Table 12.1. Explicit label names for each gear at the respective station are given in the following sub chapters. Ice stations accompanied by the physical oceanography group (OCE) are also marked.

| Station | Date | Time [UTC], start | Latitude [min], start | Longitude [min], start | Time [UTC], end | Latitude [min], end | Longitude [min], end | SIT | SPIT | SMP | SDMP | GEM | CORE | water | Snow | ICE | OCE |
|---|---|---|---|---|---|---|---|---|---|---|---|---|---|---|---|---|---|
| PS118_20190222_1 | 2019-02-22 | 15:08 | -63.7983 | -56.3203 | 20:08 | -63.7923 | -56.3400 | X | X | X | X | X | X | X | | | |
| PS118_20190223_2 | 2019-02-23 | 16:41 | -64.3531 | -56.3845 | 20:34 | -64.3664 | -56.4385 | X | X | X | X | X | X | X | X | | |
| PS118_20190224_3 | 2019-02-24 | 13:52 | -64.8925 | -57.2419 | 17:59 | -64.8909 | -57.2381 | X | X | X | X | X | X | | | X | X |
| PS118_20190226_4 | 2019-02-26 | 14:33 | -65.3356 | -58.0064 | 19:00 | -65.3290 | -58.0000 | X | X | X | X | X | X | X | | | X |
| PS118_20190301_5 | 2019-03-01 | 15:31 | -65.2120 | -57.5799 | 19:04 | -65.2117 | -57.5752 | X | X | X | X | X | X | X | X | | X |
| PS118_20190302_6 | 2019-03-02 | 16:41 | -65.4258 | -57.9284 | 19:54 | -65.4207 | -57.9272 | X | X | X | X | X | X | X | | | X |
| PS118_20190304_7 | 2019-03-04 | 14:12 | -64.9777 | -57.6797 | 17:30 | -64.9782 | -57.6576 | X | X | X | X | | X | X | | | |
| PS118_20190307_8 | 2019-03-07 | 16:07 | -64.8969 | -57.8070 | 19:09 | -64.8962 | -57.8165 | X | X | X | X | X | X | X | X | | |
| PS118_20190312_9 | 2019-03-12 | 16:11 | -63.9949 | -55.6063 | 20:22 | -63.9952 | -55.6112 | X | X | X | X | X | X | X | X | | X |
| PS118_20190313_10 | 2019-03-13 | 17:15 | -63.9149 | -55.6765 | 21:16 | -63.9075 | -55.6675 | X | X | X | X | X | X | X | X | X | |
| PS118_20190314_11 | 2019-03-14 | 15:05 | -63.8378 | -55.6659 | 15:48 | -63.8378 | -55.6659 | | X | | | | | | | X | |
| PS118_20190315_12 | 2019-03-15 | 10:57 | -63.7953 | -55.4618 | 13:14 | -63.8027 | -55.4440 | X | X | | X | X | X | X | X | | |
| PS118_20190316_13 | 2019-03-16 | 17:50 | -63.6142 | -56.1457 | 20:19 | -63.6141 | -56.1456 | X | X | | X | X | X | X | X | | X |
| PS118_20190321_14 | 2019-03-21 | 17:38 | -62.7414 | -53.0511 | 18:29 | -62.7404 | -53.0448 | | | | | | X | X | X | | |
| PS118_20190322_15 | 2019-03-22 | 17:01 | -63.0950 | -54.2931 | 19:30 | -63.0972 | -54.2956 | X | X | | | X | X | X | X | | X |
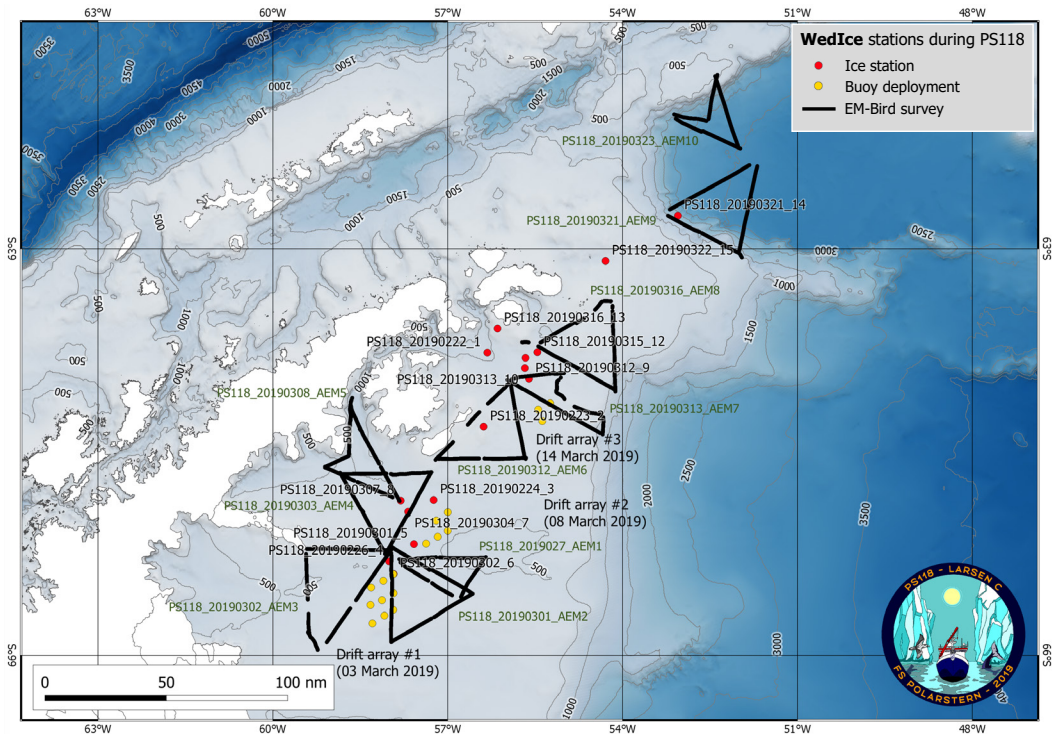
*Fig. 12.1: Overview of all sampling activities within the WedIce project during P118. Red dots denote ice stations, yellow dots the initial position of the deployed buoys and black lines the EM-Bird survey tracks. Not shown here: Hourly observations of sea ice conditions along the cruise track.*

## 12.1    Airborne ice thickness measurements

### Objectives

Ice thickness is one of the most important state variable of sea ice and an important environmental parameter of the study region. The objective of the airborne ice thickness surveys was to characterise the ice thickness variability of the study region and to interpret it in terms of origin and developmental history of the ice. That information is important for the validation of numerical sea ice models and for process studies of ice-ocean-atmosphere-interaction in the western Weddell Sea. Results will also be used for the validation of satellite ice thickness retrievals and interpretation of satellite radar images. The presented surveys are the first to be carried out in the study region since the Ice Station Polarstern (ISPOL) drift station in 2004/05, and the Winter Weddell Outflow Study (WWOS) in 2006. Results will therefore allow to observe potential decadal ice thickness changes that may have occurred in the last 13+ years.

### Work at sea

We used the helicopter-borne frequency-domain electromagnetic induction (HEM) sounding system Rosie to measure total sea-ice thickness (ice thickness plus snow depth) along helicopter flight tracks. The 4 m long instrument, the EM-Bird, is towed on a 20 m long cable underneath the helicopter and measures the sea-ice thickness in a height of 10-15 m above the surface. A laser altimeter and laser scanner are integrated in the EM-Bird system, measuring the distance to the surface in a 30 m wide, 2D swath along the flight track. Besides its role for sea ice thickness calculation, the laser data and accompanying DGPS receivers allow the retrieval of snow freeboard and surface roughness and accordingly ridge density and distribution.

101

In total, we carried out three test flights and 10 successful HEM surveys in the vicinity of the cruise track, each approximately 120 nm long. These are summarized in Table 12.3 and Figs. 12.1 and 12.2.

**Tab. 12.3:** Overview of all conducted EM-Bird flights. The position indicates the starting point of the respective profile flight.

| Flight No. | Date | Time [UTC] | Latitude [min] | Longitude [min] | Mean thick-ness [m] | St. dev. [m] | Modal thick-ness [m] |
|---|---|---|---|---|---|---|---|
| PS118_20190224_AEM_TEST | 2019-02-24 | 19:22 | -64.8689 | -57.5151 | | | |
| PS118_20190227_AEM_TEST | 2019-02-27 | 13:58 | -65.3117 | -57.9580 | | | |
| PS118_20190227_AEM1 | 2019-02-27 | 15:15 | -65.3026 | -57.9532 | 3.15 | 1.31 | 2.5 |
| PS118_20190301_AEM2 | 2019-03-01 | 20:13 | -65.2378 | -57.9648 | 3.38 | 1.59 | 2.7 |
| PS118_20190302_AEM3 | 2019-03-02 | 13:14 | -65.2548 | -57.9691 | 4.12 | 1.87 | 3.9 |
| PS118_20190303_AEM4 | 2019-03-03 | 16:04 | -65.2794 | -58.0620 | 3.16 | 1.66 | 2.5 |
| PS118_20190308_AEM5 | 2019-03-08 | 13:09 | -64.8974 | -57.8293 | 3.61 | 2.71 | 2.5 |
| PS118_20190312_AEM6 | 2019-03-12 | 12:47 | -64.0199 | -55.9313 | 2.78 | 1.36 | 2.5 |
| PS118_20190313_AEM7 | 2019-03-13 | 14:26 | -64.0026 | -55.9768 | 3.04 | 2.01 | 1.4 |
| PS118_20190316_AEM8 | 2019-03-16 | 14:07 | -63.7393 | -55.4725 | 2.63 | 1.62 | 1.8 |
| PS118_20190321_AEM9 | 2019-03-21 | 14:42 | -62.7195 | -53.2876 | 1.62 | 1.05 | 1.1 |
| PS118_20190323_AEM_TEST | 2019-03-23 | 16:41 | -62.0857 | -53.4333 | | | |
| PS118_20190323_AEM10 | 2019-03-23 | 18:33 | -61.9148 | -53.3234 | 1.93 | 1.53 | 0.9 |

**Preliminary (expected) results**

Fig. 12.2 shows the location of all ice thickness surveys. They covered the region from the outer MIZ in the north to the compact pack ice in the Larsen B region, north of iceberg A68 in the south. As can be observed from satellite SAR imagery, the study region was characterised by the presence of at least three different ice regimes of heavily deformed ice near the coast and A68, a band of younger, thinner, less deformed ice originating from the Ronne Ice Shelf east of that, and older, strongly deformed, thick ice originating from the south-eastern Weddell Sea in the very east.

Overall, very thick and compact ice was found (Fig. 12.3 and 12.4) which also caused the icebreaking challenges for *Polarstern*. Mean total (ice plus snow) thicknesses ranged from 3.15 m ±1.31 m to 4.12 m ±1.87 m in the south to 1.62 m ±1.05 m in the north (Tab. 12.3). Modal thickness decreased from 3.9 m in the south to 0.9 m in the north. Note that ice thicknesses were very variable along each flight, with thick second and third year ice coexisting with various classes of thinner first-year ice. In the MIZ, floes larger than three meters existed frequently, despite the overall small mean thickness.
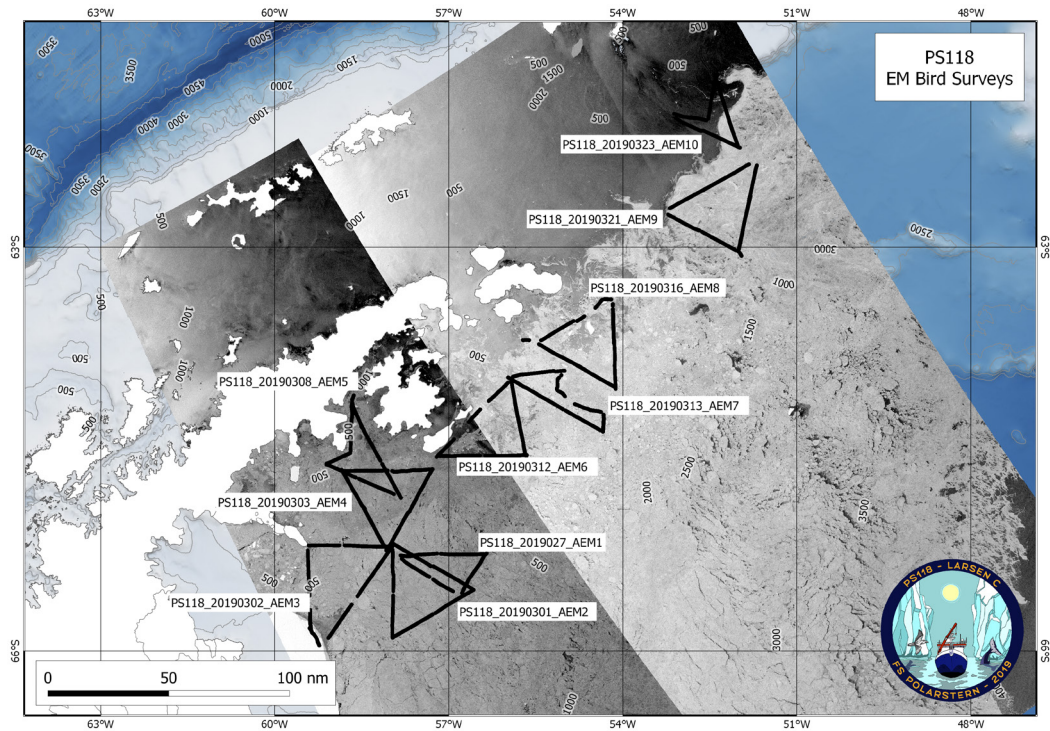
*Fig. 12.2: Overview map of all EM-Bird flights. Background: Sentinel-1 images recorded on 24 March 2019 at 23:33 and 26 March 2019 at 23:20*
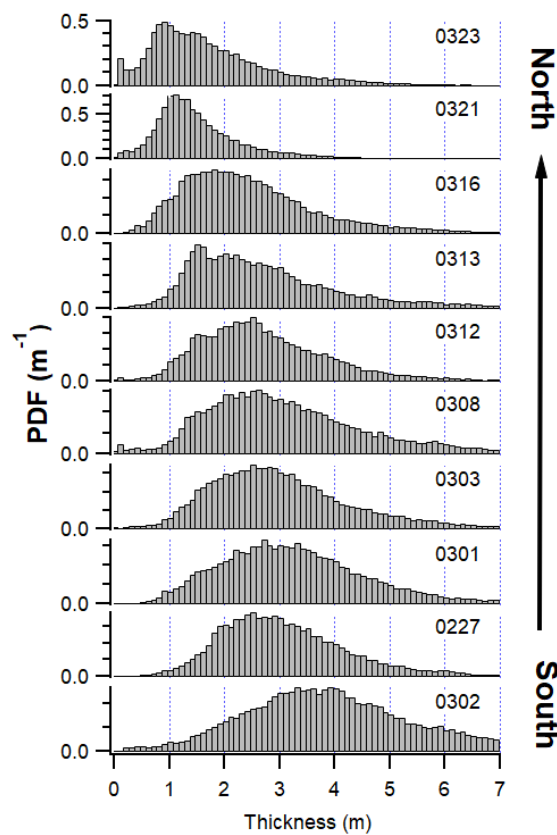


*Fig. 12.3: Ice thickness distributions of all flights, from the south (bottom) to the north (top)*
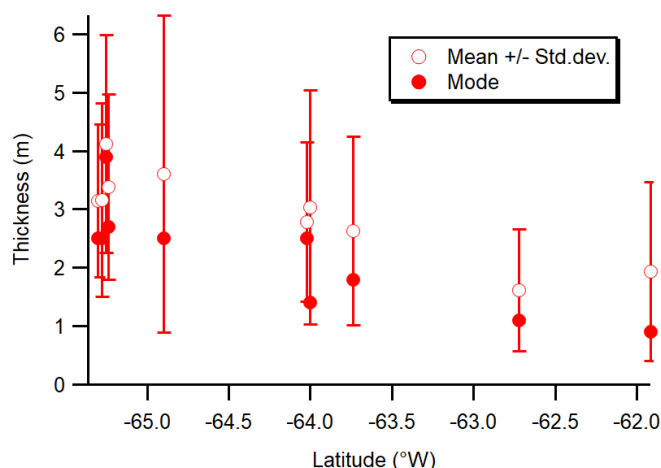
*Fig. 12.4: Ice thickness versus latitude, showing the strong regional gradient between the heavily deformed, compact pack ice in the south and the thinner, looser ice in the MIZ*

**Data management**

The sea-ice thickness data will be released following final processing after the cruise or depending on the completion of competing obligations (e.g. PhD projects), upon publication as soon as the data are available and quality-assessed. Data submission will be to the PANGAEA database.

## 12.2    Sea-ice and snow transect measurements

**Objectives**

The thickness of Antarctic sea ice and its snow cover is one of the most important parameters in terms of total mass and energy balance, but sea-ice thickness datasets are sparse. In addition, there are rarely data sets that combine high-resolution thickness information and high spatial coverage. Therefore, snow depths and sea-ice thicknesses are measured simultaneously on transect lines on the ice floes.

The final data sets are used to classify other conducted measurements on the floe in the general ice floe characteristics. In addition, both sea-ice thickness and snow depth data will be used for validation of satellite remote sensing data products.

**Work at sea**

Total sea-ice thickness (ice thickness plus snow depth) was measured on the ice during transect measurements with a ground-based multi-frequency electromagnetic induction instrument (GEM-2, Geophex Ltd.). The instrument was mounted on a modified plastic sled and pulled over the snow surface. A GPS-equipped Magna Probe (Snow Hydro, Fairbanks, AK, USA) was operated simultaneously in order to obtain snow depth along the GEM-2 tracks. Snow depth measurements were taken every 1.5 to 2.5 m along the track.

Combined sea-ice and snow thickness measurements were conducted on 11 floes, while a single snow-depth transect was performed at station PS118_20190304_7. All transect measurements are summarized in Table 12.4.

**Tab. 12.4:** List of all snow and (total) sea-ice thickness (sea-ice thickness + snow depth) transect measurements during PS118. At station PS118_20190304_7, sea-ice thickness measurements did not take place. Modal values were given only for dominant modes in the respective data set. Abbreviations (according to Table 12.1): SDMP – Snow depth measured with Magna Probe (snow depth transect), GEM – Ground electromagnetic sounding (sea-ice thickness transect).

| Station | Label SDMP | Label GEM | Date | Time [UTC], start | Latitude [min], start | Longitude [min], start | Time [UTC], end | Latitude [min], end | Longitude [min], end | Profil length [m] | Snow depth [mean, cm] | Snow depth [mode, cm] | Total ice thickness [mean, cm] | Total ice thickness [mode 1, cm] | Total ice thickness [mode 2, cm] |
|---|---|---|---|---|---|---|---|---|---|---|---|---|---|---|---|
| PS118_20190222_1 | PS118_20190222_1-3_SDMP | PS118_20190222_1-4_GEM | 2019-02-22 | 18:59 | -63.7985 | -56.3427 | 19:12 | -63.7977 | -56.3434 | 405.0 | 33 ± 22 | 25 | 241 ± 35 | 240 | - |
| PS118_20190223_2 | PS118_20190223_2-3_SDMP | PS118_20190223_2-4_GEM | 2019-02-23 | 19:22 | -64.3589 | -56.4188 | 19:42 | -64.3606 | -56.4241 | 484.8 | 32 ± 21 | 15 | 247 ± 62 | 190 | 250 |
| PS118_20190224_3 | PS118_20190224_3-3_SDMP | PS118_20190224_3-4_GEM | 2019-02-24 | 16:52 | -64.8918 | -57.2358 | 17:07 | -64.8916 | -57.2359 | 358.1 | 20 ± 14 | 5 | 183 ± 66 | 240 | 100 |
| PS118_20190226_4 | PS118_20190226_4-3_SDMP | PS118_20190226_4-4_GEM | 2019-02-26 | 18:00 | -65.3304 | -57.9982 | 18:20 | -65.3299 | -57.9978 | 373.5 | 46 ± 29 | 30 | 408 ± 203 | - | - |
| PS118_20190301_5 | PS118_20190301_5-3_SDMP | PS118_20190301_5-4_GEM | 2019-03-01 | 17:59 | -65.2120 | -57.5786 | 15:30 | -65.2117 | -57.5772 | 793.8 | 36 ± 18 | 20 | 242 ± 48 | 220 | - |
| PS118_20190302_6 | PS118_20190302_6-3_SDMP | PS118_20190302_6-4_GEM | 2019-03-02 | 18:46 | -65.4229 | -57.9294 | 19:19 | -65.4216 | -57.9283 | 811.3 | 35 ± 18 | 20 | 268 ± 78 | 190 | - |
| PS118_20190304_7 | PS118_20190304_7-3_SDMP | - | 2019-03-04 | 15:55 | -64.9800 | -57.6676 | 16:24 | -64.9798 | -57.6646 | 704.3 | 18 ± 12 | 10 | - | - | - |
| PS118_20190307_8 | PS118_20190307_8-3_SDMP | PS118_20190307_8-4_GEM | 2019-03-07 | 18:21 | -64.8974 | -57.8127 | 18:54 | -64.8972 | -57.8149 | 942.4 | 23 ± 14 | 20 | 208 ± 77 | 130 | 180 |
| PS118_20190312_9 | PS118_20190312_9-3_SDMP | PS118_20190312_9-4_GEM | 2019-03-12 | 18:37 | -63.9960 | -55.6057 | 19:35 | -63.9959 | -55.6081 | 1181.2 | 21 ± 20 | 10 | 238 ± 92 | 130 | 270 |
| PS118_20190313_10 | PS118_20190313_10-3_SDMP | PS118_20190313_10-4_GEM | 2019-03-13 | 19:32 | -63.9091 | -55.6684 | 20:05 | -63.9075 | -55.6676 | 825.2 | 5 ± 6 | 0 | 150 ± 48 | 90 | 160 |
| PS118_20190315_12 | PS118_20190315_12-3_SDMP | PS118_20190315_12-4_GEM | 2019-03-15 | 15:28 | -63.8008 | -55.4506 | 15:49 | -63.8021 | -55.4465 | 422.3 | 26 ± 21 | 0 | 246 ± 79 | 160 | 240 |
| PS118_20190316_13 | PS118_20190316_13-3_SDMP | PS118_20190316_13-4_GEM | 2019-03-16 | 19:00 | -63.6143 | -56.1461 | 19:21 | -63.6143 | -56.1461 | 663.4 | 21 ± 17 | 5 | 207 ± 75 | 250 | 60 |

**Preliminary (expected) results**

Table 12.4 and Fig. 12.5 summarize all conducted snow depth and total sea-ice thickness transect measurements during PS118. Taking all data into account, a mean total sea-ice thickness of 234 ±96 cm with a mean snow depth of 26 ±21 cm was observed. The 11 combined snow and sea-ice thickness transects show a similar distributions where thinner and level sea ice is accompanied by a thinner snow layer, and vice versa. Thus, mean snow depth of all sampled stations ranged from 5 ±6 cm (PS118_20190313_10) to 46 ±29 cm (PS118_20190226_4). At the same stations, averaged minimum and maximum sea-ice thicknesses of 150 ±48 cm and 408 ±203 cm, respectively, were measured.

However, it must be considered that the transects across the floe might cover different proportions of level and ridged sea-ice areas. Thus, PS118_20180226_4 indicates a rather wide and equally distributed value range in both snow depth and sea-ice thickness. This indicates a balanced transect line in level and ridged ice regimes. In contrast, PS118_20190301_5 shows a rather narrow thickness range of 48 cm around a mean value of 242 cm revealing that the respective transect was mainly conducted on level ice. In a next step, it is therefore crucial to distinguish between level and ridged ice regimes in order to increase the quality of the given statistics and associated results.
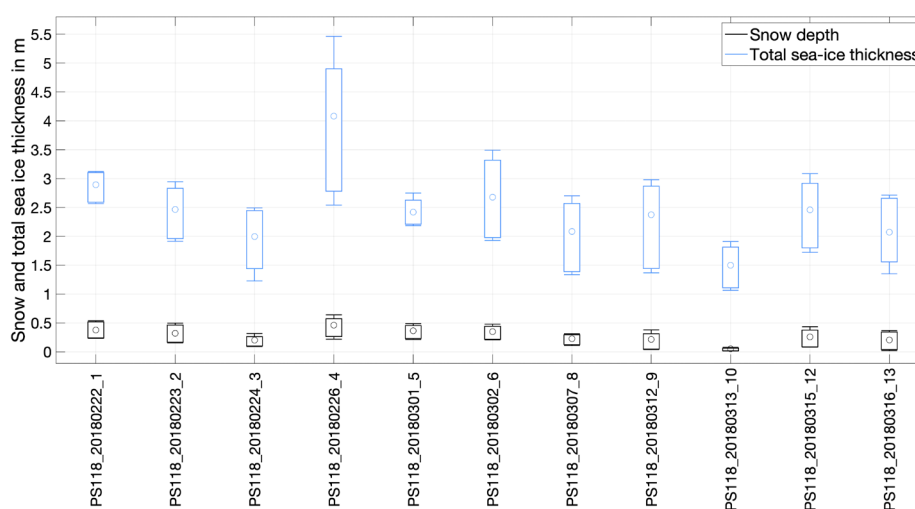


*Fig. 12.5: Summary of all combined snow depth (MagnaProbe, blue) and total sea-ice thickness (GEM, black) measurements conducted during PS118. Boxes are the first and third quartiles. Whiskers display the 20- and 80-percentiles. Circles indicate mean values.*

**Data management**

The sea-ice thickness and snow depth transect data will be released following final processing after the cruise or depending on the completion of competing obligations (e.g. PhD projects), upon publication as soon as the data are available and quality-assessed. Data submission will be to the World Data Center PANGAEA Data Publisher for Earth & Environmental Science (www.pangaea.de).

## 12.3   Physical and biological properties of sea ice

**Objectives**

Summer thaw-freeze cycles in the snow and upper ice layers result in strong, destructive snow metamorphism, and eventually in the formation of superimposed ice and gap layers. These gap layers receive comparable high light and are thus known to be highly productive regions within the ice. While metamorphic snow was studied in snow pits and with lateral profiling methods (Section 12.4), different ice types indicative of specific ice developmental histories including the transformation from snow to ice, and the porosity and state of ice deterioration can only be observed from ice cores. In addition, ice cores are the easiest way to measure bio-geochemical ice properties and to determine the sea ice biomass and other biogeochemical variables, which can be put into context of the physical ice observations. Ice cores are sectioned according to these physical properties and compared with gap and under ice water allowing to distinguish the exchange processes of species and biogeochemical parameters within the ice and the underlying ocean.

**Work at sea**

A regular ice station for biogeochemical sampling involved the collection of sea ice cores, the sampling of gap water and seawater directly under the ice (Tab. 12.5). Up to 10 ice cores were collected at each ice station. Some of them were only taken for the upper <60 cm. These surface cores were sampled to obtain a larger data set of development of superimposed ice and further properties of the surface layer. Whenever possible, these surface cores were combined with cores for other biogeochemical variables as DNA, IPSO-25 (Tab. 12.5). Occasionally other ice types like Nilas or brown ice were taken (Tab. 12.5). Cores for trace elements (NEO) and their isotopes and archive/microplastic (ARC-MP) were stored in core bags after retrieval and kept frozen at -20°C. For the isotopes additional snow under ice and gap water samples were taken (Tab. 12.5). Bottom and brown ice sections were further sampled at several stations for meiofauna (MEIO) and the biomarker IPSO-25 (IP25). Cores for biological variables (BIO) were usually sectioned into a top, above and below gap, 1 to 4 middle and a 10-14 cm bottom section (Fig. 12.6). Ice samples were transferred to the cool container (5°C) for sea ice melting. From all melted ice core sections, the volume and the salinity was determined and water samples were taken for nutrients and cell counts (qualitatively). The remaining water was divided for filtering the following parameters: size-fractionate chlorophyll a (>10  µm; <10 µm), marker pigments, particulate biogenic silicate, particulate organic carbon and nitrogen (POC, PON) and the isotopic composition of POC and PON ($\delta^{13}$CPOC and $\delta^{15}$NPON; Tab. 12.1). If high biomass was present, additional Illumina sequencing (DNA) samples were taken from the BIO core. For DNA, usually well colored ice core sections were taken and in the cool container (5°C) filtered sea water was added to the ice sections to reduce the osmotic shook of the organism and the cores were allowed to melt. Samples for DNA (Illumina sequencing) were filtered on >10 µm, 3-10 µm and 0.2-3 µm filters and sometimes, entire communities were filtered on 0.4 µm. If enough sample was present, additional parameters were taken (Tab. 12.1). All parameters collected for the BIO core were also filtered from the sampled under ice water (UIW) and the gap layer water (GAP).

In collaboration with Moritz Holtappels (AWI) four ice and gap water samples with high biomass were further subjected to productivity measurements using the oxygen optode technique. Samples were transferred to 300 ml glass bottles, with attached optode sensors. and placed in a water bath with -1.5°C (Fig. 12.7). The oxygen concentration was monitored for the four sample bottles simultaneously. The experiment was set to a 12:12 hour dark and light cycle using commercial available plant bulbs. Light intensity was changed with different meshes. Illumination was between 10-80 µE measured in the sample glass bottles using a Waltz ULM

500 PAR sensor. The oxygen respiration measured during the night was subtracted from oxygen production during the light phase to estimate the net primary production. Experiments lasted for three to several days. Subsamples for nutrients, species, marker pigments and POC/PON were taken at the beginning and end of the experiment.

To understand the physical properties of sea ice cores, a total of 21 TEX cores were analysed on board for ice texture and salinity (Tab. 12.5). In the cold laboratory (-20°C) vertical thick sections were produced and their texture was determined visually in polarized light. Ice cores were subsequently cut into up to 15 cm long sections according to their texture, and melted for measurements of vertical profiles of bulk ice salinity. Melted ice samples were further stored for later measurements of $\delta^{18}O$ back in Germany. In addition, snow samples for of $\delta^{18}O$ were taken (Tab. 12.5).
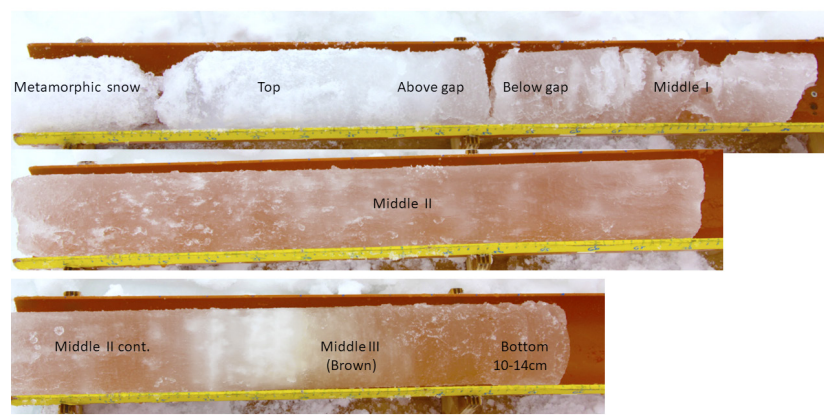


*Fig. 12.6: Example for sea ice core from the surface (upper panel) to the bottom part (lowest panel). Indicated are the usual subsections taken for the BIO core sampling*
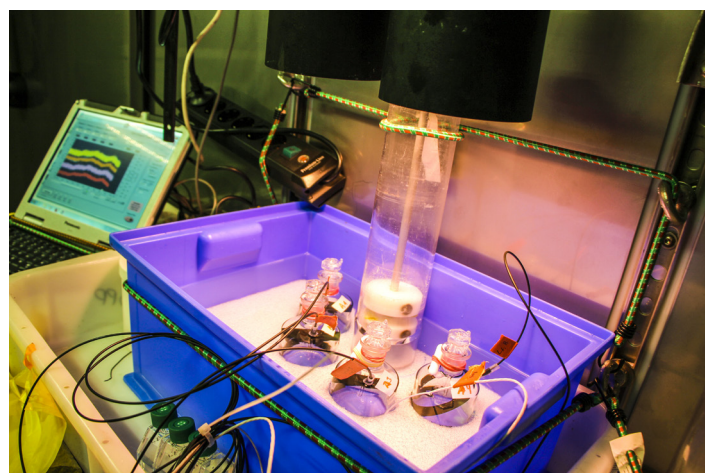


*Fig. 12.7: Incubation set up for oxygen primary production measurements*

**Tab. 12.5:** Overview of all samples collected during the ice station

| Station | Date | Time [UTC], start | Ice cores (CORES-) | | | | | | | | Water sampling (WATER-) | | | | Snow sampling | | ICE |
|---|---|---|---|---|---|---|---|---|---|---|---|---|---|---|---|---|---|
| | | | ARC-MP | BIO | DNA | IP-25 | MEIO | NEO | TEX | Total number of cores | GAP | NEO-GAP | UIW | NEO-UIW | delta-O-18 | NEO | |
| PS118_20190222_1 | 2019-02-22 | 15:08 | 1 | 1 | 1 | | 1 | 1 | 1 | 5 | | | 1 | 1 | | 1 | |
| PS118_20190223_2 | 2019-02-23 | 16:41 | 1 | 3 | | | 1 | 1 | 1 | 7 | | | 1 | 1 | | 1 | |
| PS118_20190224_3 | 2019-02-24 | 13:52 | | 2 | | | | | 1 | 3 | 1 | | | | | | 1 |
| PS118_20190226_4 | 2019-02-26 | 14:33 | | 4 | | | | | 2 | 6 | 1 | | | | | | |
| PS118_20190301_5 | 2019-03-01 | 15:31 | 1 | 1 | 1 | | | 1 | 1 | 5 | 1 | | 1 | 1 | | 1 | |
| PS118_20190302_6 | 2019-03-02 | 16:41 | | 1 | 2 | 1 | 1 | | 2 | 5 | 1 | | 1 | | | | |
| PS118_20190304_7 | 2019-03-04 | 14:12 | | 3 | | 1 | 1 | 2 | 1 | 7 | 1 | | 1 | 1 | | 2 | |
| PS118_20190307_8 | 2019-03-07 | 16:07 | | 2 | | | 1 | 1 | 2 | 7 | 1 | | 1 | 1 | 1 | 1 | |
| PS118_20190312_9 | 2019-03-12 | 16:11 | 1 | 1 | 1 | 1 | 1 | 1 | 1 | 5 | 1 | 1 | 1 | 1 | 1 | 1 | 2 |
| PS118_20190313_10 | 2019-03-13 | 17:15 | | 7 | | | 1 | | 2 | 10 | | | | | | | 5 |
| PS118_20190314_11 | 2019-03-14 | 15:05 | | | | | | | 0 | 0 | | | | | | | |
| PS118_20190315_12 | 2019-03-15 | 10:57 | | 2 | | | | | 1 | 3 | 1 | | 1 | | 1 | | |
| PS118_20190316_13 | 2019-03-16 | 17:50 | | 3 | | | | | 2 | 5 | 1 | | 1 | | 1 | | |
| PS118_20190321_14 | 2019-03-21 | 17:38 | | 1 | | | | | 1 | 2 | 1 | | 1 | | 1 | | |
| PS118_20190322_15 | 2019-03-22 | 17:01 | | 2 | 1 | | 1 | 1 | 3 | 6 | 1 | 1 | 1 | 1 | 1 | 1 | |
| Sum: | | | 4 | 33 | 6 | 3 | 8 | 7 | 21 | 76 | 11 | 2 | 11 | 6 | 6 | 7 | 8 |

**Preliminary (expected) results**

The aim of this study is to understand the variability and biodiversity of the sea ice-associated biomass and the biogeochemical parameters with respect to the physical sea ice properties. This will allow to assess the role of sea-ice biota for the cryo-pelagic, cryo-benthic coupling under different environmental scenarios in the western Weddell Sea from the south to the north. Although a gap layer was found at all ice stations, biomass remained rather low at the southernmost stations. A strong development of biological active gap layers were present towards the end of the cruise (Fig. 12.8), also supported by the primary production measurements. These point measurements will be up scaled with the floe-wide observations (Section 12.2) and set into context with the large-scale EM bird observations (Section 12.1) in order to elucidate the role of sea ice for biological and biogeochemical cycles in the western Weddell Sea.



*Fig. 12.8: Development of high biomass gap layers in the Powell basin region.*

The physical characteristics of the sea ice were already analysed on the ship. In total, 21 cores have been sampled for texture and salinity (Fig. 12.9), while full profiles are available for 4 cores only. The remaining cores cover between 24 to 104 cm of the top part of the ice (excluding snow). Large-grained, polygonal granular texture associated with superimposed ice was identified for all ice floes with an averaged thickness of 12 ±6 cm, ranging from 5 to 24 cm. Considering the top part of all ice cores only (up to 60 cm), superimposed ice therefore accounts for 22 ±11%. Typically, the grain size within the layer decreases with depth. The polygonal granular layer was often underlain by a layer of finer grained orbicular ice making detecting the transition between both layers often rather difficult. It is therefore possible, that the actual proportion of superimposed ice is underestimated. This is also suggested by the measured salinity profiles indicating an averaged thickness of rather salt-free sea ice of 16 ±13 cm. Salt-free ice can be attributed to superimposed ice. In order to certainly quantify the relative and absolute proportion of superimposed ice, additional oxygen isotope analysis will be performed in the lab back home. However, considering the top part of all cores only, fine grained orbicular ice layers account for 49 ±26%, while columnar ice structures account for 16 ±24% only. The residual of 13% can be allocated to a mixture of polygonal, orbicular and columnar ice textures. The results of the texture cores will be put into context of the biological and biogeochemical parameters.
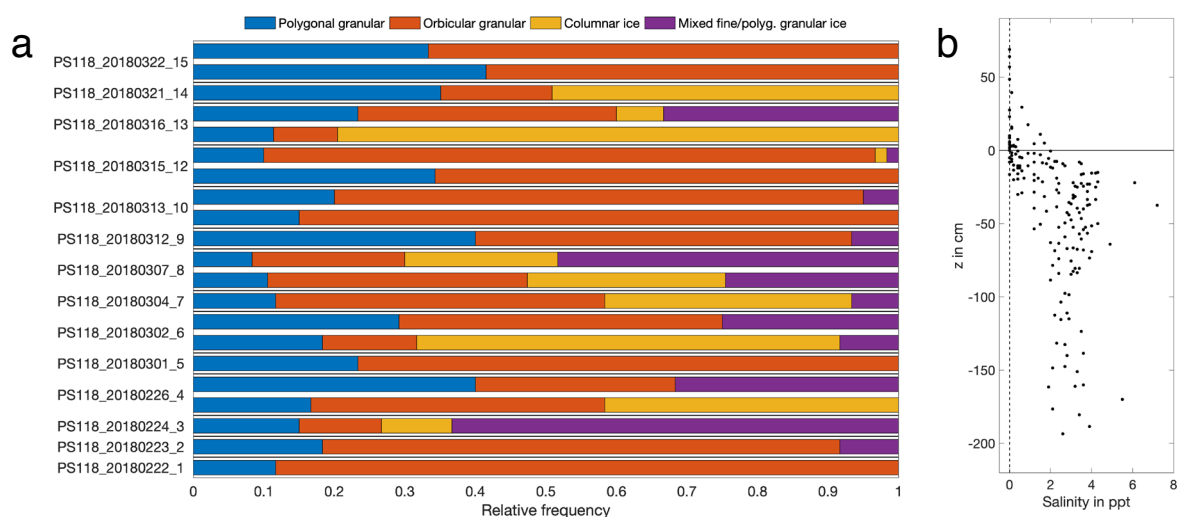
*Fig. 12.9: (a) Overview of the relative proportion of the identified ice types of the top part (up to 60 cm) of all sampled ice cores grouped for the respective ice station. (b) Salinity of all sampled texture cores plotted at center position of individual core segment with respect to the water level (z = 0 cm).*

## Data management

All ice-core data will be released following its analysis in the home laboratories after the cruise or depending on the completion of competing obligations (e.g. PhD projects), upon publication as soon as the data are available and quality-assessed. Data submission will be to the World Data Center PANGAEA Data Publisher for Earth & Environmental Science (www.pangaea.de). DNA data will be deposited in NCBI's Sequence Read Archive.

## 12.4  Physical properties of snow

### Objectives

Physical snow properties are highly variable even on small horizontal scales. These spatial and temporal variations in the snow pack characteristics (e.g. temperature, density, stratigraphy) and their dimension have a crucial impact on the energy and mass budget of Antarctic sea ice. Therefore, the snow pack on different ice floes is characterised in detail.

Snow stratigraphy will be used as ground truth for the interpretation of retrieved snowmelt signatures from passive and active microwave data.

### Work at sea

The work on physical snow properties was performed on 13 of the sampled ice floes. The work can be subdivided in two parts: Snow pits to describe essential physical snow parameters and its stratigraphy, and SnowMicroPen measurements deriving a high-resolution density profile of the prevalent snowpack.

*Snow pits*

Snow pit measurements were taken on the undisturbed shaded working wall of the snow pit.

At first, the temperature was measured every 1 to 5 cm from the top (snow-air interface) to the bottom (snow-ice interface) with a hand-held thermometer (Testo). In a next step, the different layers in the snow pack and their stratigraphic parameters were described. For each layer, the snow grain size and type (e.g. rounded crystals, facetted crystals, depth hoar) is determined by the magnifying glass and a 1 to 3 mm grid card. In addition, every layer was characterised by its hardness with the following categories: fist (F), 4 fingers (4F), 1 finger (1F), pencil (P), and knife (K). Additional measurements of the specific surface area (SSA) of snow were performed with an IceCube. The working principle of the IceCube relies on the relationship between the infrared hemispherical reflectance of snow and its SSA. Afterwards, the density of each layer was measured volumetrically by removing a defined snow block with a density cutter of snow from each layer (density cutter weight: 155 g, volume: 100 ml) and weighting it with a spring scale. In addition, measurements of liquid water content (in Vol. %) were performed with a Denoth probe (SLF) through the di-electrical properties of the snowpack. Denoth probe measurements were performed twice every 2 cm from the top to the bottom.

Overall, 24 snow pits were analyzed on 13 different ice floes. Table 12.7 summarizes the explicit conducted measurements for each snow pit.

*SnowMicroPen*

The SnowMicroPen (SMP) is a high-resolution snow penetrometer. It measures the bonding force between snow grains, with high spatial resolution and high speed. During the measurement, the SMP is pressed down to the snow surface while the rod is driven into the snow pack. A piezoelectric force sensor measures penetration resistance as function of depth. The measured data are displayed on the controller and stored in binary format on a SD card.

During PS118 the SMP was used to perform transect measurements on straight lines with two measurements per meter on distances of up to 43 m.

An overview of all measurements is given in Table 12.7.

**Preliminary (expected) results**

Fig. 12.10 shows a typical snow pit data set from station PS118_20190301_5. The snow pit was sampled in a representative area of the floe with a snow depth of 33.5 cm. The snow pack contained 4 different layers (from top to bottom): soft layer of rounded facetted grains (1), followed by a harder layer of depth hoar (2), and an even harder layer of melt-freeze forms (3). Finally, the bottom layer shows clear superimposed ice (4). Throughout the sampled snowpack the grain sizes increase, which correlated with the strong temperature gradient from -3.4°C (top) to -1.8°C (bottom). Due to clear sky conditions and associated high shortwave solar radiation fluxes, the upper layer is slightly heated up. The given grain type distribution throughout the snowpack is typical for all sampled snow pits during PS118. Thus, melt-freeze forms were the dominant grain type in all snow pits with an averaged relative proportion of 60% (Fig. 12.11) caused by an early beginning and frequently recurrence of thaw-freeze events in the north-western Weddell Sea.

In addition to the traditional snow pit measurements, about 664 valid SnowMicroPen (SMP) measurements were conducted. Those were done, on the one hand, related to all sampled snow pit sites (Fig. 12.10, grey/yellow lines), and, on the other hand, on transect lines with a spacing of 1 m. Fig. 12.12 shows a typical transect line at station PS118_20190301. The measurement site of the transect was chosen as representative for the ice floe with a homogenous surface appearance. Measurements were taken twice at every measurement point. During post-processing, corresponding measurement profiles were averaged. The described melt-forms in the bottom part of the snowpack prevent the SMP to penetrate throughout the entire snow

column as the resistance in those parts is exceeding 40 N and therefore the measurement pole is interrupting the profile. However, the given transects indicates a clearly layered soft snowpack in the top 10 to 15 cm with typical density values between 150 and 350 kg m$^{-3}$. As soon as melt-forms dominate the snowpack, the profile is getting rather heterogenous and highly variable due to different bonding forces and grain transitions in the rather icy layer.

This transect line is therefore an excellent example for the small-scale variability in the vertical profile of an Antarctic summer snowpack.
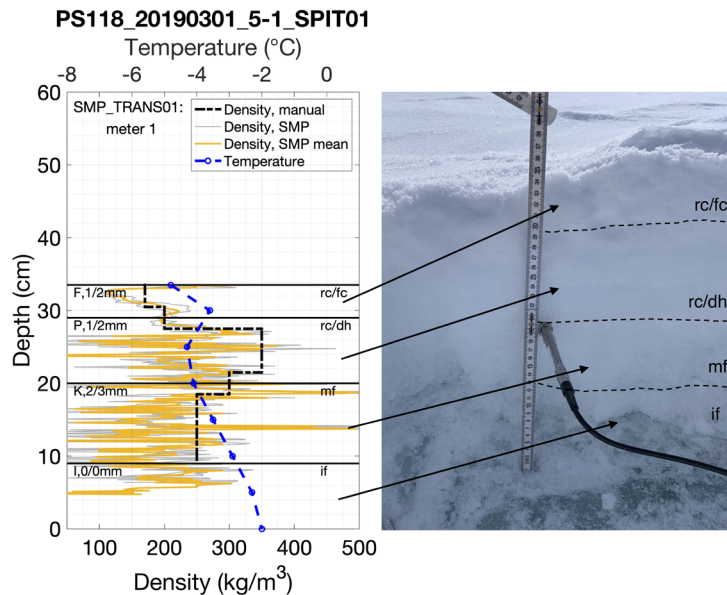


*Fig. 12.10: Example of snow pit analysis from station PS118_20190301_5. Temperature measurements are marked in blue, density measurements with the density cutter in black, and density measurements with the SMP in grey (all) and yellow (average). Horizontal lines indicate the different layer interfaces. Below the lines grain type classifications for the respective layer are given.*
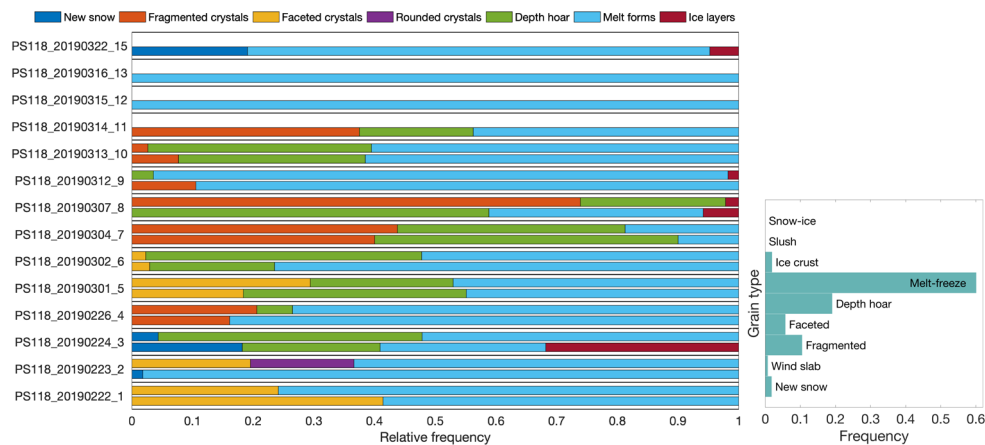


*Fig 12.11: Overview of all conducted snow pit analysis regarding its relative proportion of grain types (left) within each snow pit, and (b) summarized for all snow pits.*
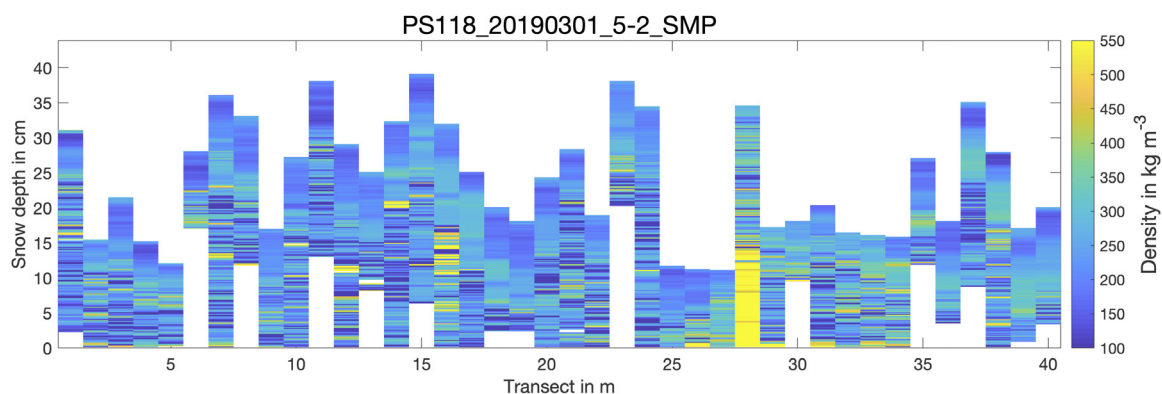
*Fig. 12.12: Example of SMP transect line at station PS118_20190301_5. Plotted density values are calculated mean values of two measurements per profile meter. Missing data in the lower profile part indicate an overload of the instrument due to too high densities.*

**Data management**

Data from all snow pit and SMP measurements will be delivered to the World Data Center PANGAEA Data Publisher for Earth & Environmental Science (www.pangaea.de) within two years after the cruise.

114

**Tab. 12.6:** Overview of all sampled snow pits. Possible conducted measurements are: temperature (TEMP), density (DENS), stratigraphy (STR), specific surface area with IceCube (SSA), and liquid water content with Denoth probe (LWC).

| Station | Label | Date | Time [UTC], start | Time [UTC], end | Latitude [min] | Longitude [min] | Snow depth [cm] | TEMP | DENS | STRAT | SSA | LWC |
|---|---|---|---|---|---|---|---|---|---|---|---|---|
| PS118_20190222_1 | PS118_20190222_1-1_SPIT01 | 2019-02-22 | 16:11 | 17:15 | -63.8000 | -56.3226 | 29 | X | X | X | X | |
| PS118_20190222_1 | PS118_20190222_1-1_SPIT02 | 2019-02-22 | 17:30 | 17:55 | -63.7985 | -56.3287 | 29 | X | X | X | | |
| PS118_20190223_2 | PS118_20190223_2-1_SPIT01 | 2019-02-23 | 17:40 | 18:40 | -64.3542 | -56.3945 | 28 | X | X | X | X | |
| PS118_20190223_2 | PS118_20190223_2-1_SPIT02 | 2019-02-23 | 18:51 | 19:11 | -64.3589 | -56.4191 | 41 | X | X | X | | |
| PS118_20190224_3 | PS118_20190224_3-1_SPIT01 | 2019-02-24 | 14:41 | 15:40 | -64.8926 | -57.2384 | 11 | X | X | X | X | |
| PS118_20190224_3 | PS118_20190224_3-1_SPIT02 | 2019-02-24 | 15:52 | 16:23 | -64.8922 | -57.2363 | 11.5 | X | X | X | | |
| PS118_20190226_4 | PS118_20190226_4-1_SPIT01 | 2019-02-26 | 15:42 | 16:40 | -65.3346 | -58.0028 | 31 | X | X | X | X | |
| PS118_20190226_4 | PS118_20190226_4-1_SPIT02 | 2019-02-26 | 16:51 | 17:23 | -65.3324 | -58.0007 | 34 | X | X | X | | |
| PS118_20190301_5 | PS118_20190301_5-1_SPIT01 | 2019-03-01 | 16:01 | 17:01 | -65.2119 | -57.5800 | 33.5 | X | X | X | X | |
| PS118_20190301_5 | PS118_20190301_5-1_SPIT02 | 2019-03-01 | 17:15 | 17:47 | -65.2117 | -57.5752 | 34 | X | X | X | | |
| PS118_20190302_6 | PS118_20190302_6-1_SPIT01 | 2019-03-02 | 17:05 | 17:53 | -65.4254 | -57.9290 | 19 | X | X | X | X | |
| PS118_20190302_6 | PS118_20190302_6-1_SPIT02 | 2019-03-02 | 18:02 | 18:31 | -65.4240 | -57.9300 | 24 | X | X | X | | |
| PS118_20190304_7 | PS118_20190304_7-1_SPIT01 | 2019-03-04 | 14:42 | 15:20 | -64.9791 | -57.6753 | 13 | X | X | X | X | |
| PS118_20190304_7 | PS118_20190304_7-1_SPIT02 | 2019-03-04 | 15:59 | 16:14 | -64.9782 | -57.6576 | 17 | X | X | X | | |
| PS118_20190307_8 | PS118_20190307_8-1_SPIT01 | 2019-03-07 | 16:40 | 17:23 | -64.8977 | -57.8075 | 8.5 | X | X | X | X | |
| PS118_20190307_8 | PS118_20190307_8-1_SPIT02 | 2019-03-07 | 17:28 | 17:52 | -64.8977 | -57.8100 | 24 | X | X | X | | |
| PS118_20190312_9 | PS118_20190312_9-1_SPIT01 | 2019-03-12 | 16:51 | 17:44 | -63.9996 | -55.6044 | 23 | X | X | X | X | |
| PS118_20190312_9 | PS118_20190312_9-1_SPIT02 | 2019-03-12 | 17:56 | 18:09 | -63.9958 | -55.6046 | 34 | X | | X | | |
| PS118_20190313_10 | PS118_20190313_10-1_SPIT01 | 2019-03-13 | 17:48 | 18:40 | -63.9136 | -55.6733 | 14 | X | X | X | X | |
| PS118_20190313_10 | PS118_20190313_10-1_SPIT02 | 2019-03-13 | 18:51 | 19:12 | -63.9108 | -55.6697 | 21 | X | X | X | | |
| PS118_20190314_11 | PS118_20190314_11-1_SPIT01 | 2019-03-14 | 15:12 | 15:37 | -63.8391 | -55.6607 | 24 | X | X | X | X | |
| PS118_20190315_12 | PS118_20190315_12-1_SPIT01 | 2019-03-15 | 14:24 | 15:01 | -63.7966 | -55.4594 | 25 | X | X | X | | X |
| PS118_20190316_13 | PS118_20190316_13-1_SPIT01 | 2019-03-16 | 17:56 | 18:32 | -63.6144 | -56.1461 | 17.5 | X | X | X | | X |
| PS118_20190322_15 | PS118_20190322_15-1_SPIT01 | 2019-03-22 | 17:25 | 17:40 | -63.0953 | -54.2950 | 20 | X | X | X | | |

**Tab. 12.7:** Overview of all SMP measurements. Start/end time and position indicate the starting/last point of the respective profile line.

| Station | Label | Date | Time [UTC], start | Latitude [min], start | Longitude [min], start | Time [UTC], end | Latitude [min], end | Longitude [min], end | Profile length [m] |
|---|---|---|---|---|---|---|---|---|---|
| PS118_20190222_1 | PS118_20190222_1-2_SMP_TRANS01 | 2019-02-22 | 16:20 | -63.7997 | -56.3231 | 19:14 | -63.7986 | -56.3464 | 41 |
| PS118_20190223_2 | PS118_20190223_2-2_SMP_TRANS01 | 2019-02-23 | 17:56 | -64.3546 | -56.3973 | 18:45 | -64.3564 | -56.4105 | 20 |
| PS118_20190224_3 | PS118_20190224_3-2_SMP_TRANS01 | 2019-02-24 | 15:26 | -64.8924 | -57.2372 | 16:50 | -64.8915 | -57.2352 | 39 |
| PS118_20190226_4 | PS118_20190226_4-2_SMP_TRANS01 | 2019-02-26 | 15:37 | -65.3347 | -58.0029 | 17:46 | -65.3310 | -57.9926 | 43 |
| PS118_20190301_5 | PS118_20190301_5-2_SMP_TRANS01 | 2019-03-01 | 16:26 | -65.2120 | -57.5800 | 18:01 | -65.2118 | -57.5793 | 41 |
| PS118_20190302_6 | PS118_20190302_6-2_SMP_TRANS01 | 2019-03-02 | 17:24 | -65.4250 | -57.9294 | 17:27 | -65.4250 | -57.9294 | 3 |
| PS118_20190304_7 | PS118_20190304_7-2_SMP_TRANS01 | 2019-03-04 | 14:42 | -64.9791 | -57.5756 | 15:24 | -64.9799 | -57.6705 | 23 |
| PS118_20190307_8 | PS118_20190307_8-2_SMP_TRANS01 | 2019-03-07 | 16:47 | -64.8977 | -57.8076 | 18:07 | -64.8978 | -57.8122 | 41 |
| PS118_20190312_9 | PS118_20190312_9-2_SMP_TRANS01 | 2019-03-12 | 17:04 | -63.9957 | -55.6044 | 18:44 | -63.9957 | -55.6053 | 41 |
| PS118_20190313_10 | PS118_20190313_10-2_SMP_TRANS01 | 2019-03-13 | 17:59 | -63.9133 | -55.6730 | 19:29 | -63.9089 | -55.6680 | 41 |

## 12.5    Deployments of autonomous ice tethered platforms (buoys)

**Objectives**

Ice drift and advection are important components of the sea ice mass balance, and depend on winds and currents and on the internal strength of the ice. When the ice cover deforms, open water or pressure ridges can form with consequences for the ice thickness distribution. Better information on the wind and current dependent ice drift and deformation are required to improve the representation of ice deformation and thickness redistribution in numerical sea ice models. In turn, ice deformation also depends on ice thickness which determines the ice's internal strength. In order to study ice drift and deformation we have deployed three buoy arrays in regions of different general ice conditions and thickness observed during our ice thickness surveys (see Section 12.3). These arrays allow to compute the full deformation field, i.e. ice divergence and shear in triangular regions spanned by triplets of buoys.

Beyond the immediate value for our sea ice mass balance research, all buoys report their position together with measurements of surface temperature and partially atmospheric sea level pressure directly into the Global Telecommunication System (GTS) used by weather prediction and atmospheric reanalysis systems. This activity is a contribution to the International Programme for Antarctic Buoys (IPAB) which is coordinated by AWI.

**Work at sea**

Fig. 12.13 and Table 12.8 give an overview about the deployed 17 Surface Velocity Profilers (SVPs). The SVPs have been deployed on the ice as so-called drift arrays. The first drift array consisted of 9 SVPs, the second array of 5 SVPs, and the third array of 3 SVPs. The distance between each drifter in the respective drift array was initially between 5 and 10 nm.

**Preliminary (expected) results**

The SVP buoys will provide information on the sea-ice drift velocity and its seasonal behavior. As soon as the ice floe disintegrates, the SVPs will float in the ocean and will measure ocean currents at the ocean surface.

The first buoy array consisted of 9 buoys and was deployed on 03 March 2019, the second one consisted of 5 buoys deployed on 08 March 2019, and the third consisted of 3 buoys deployed 14 March 2019. Fig. 12.14 shows examples of time series and histograms of drift velocities of the respectively most south-western and north-eastern buoy of the first (2019P86 and 2019P85) and second buoy arrays (2019P87 and 2019P104). Although the buoys were deployed originally only 5 to 10 nm apart from each other in the respective drift array, their drift pattern reveals differences in their actual drift velocities. All four buoys indicate that they experience the same weather and wind patterns as their drift velocity profiles show similar qualitative drift pattern. However, there is a clear gradient towards higher drift velocity from the southwest to the northeast. This might be due to the location of the north-eastern buoys farther away from the coast and nearer to the ice edge resulting in less pressure on the ice. In addition, a strong low-pressure system accompanied by strong wind velocities passing through the area might have been stronger in the northern part of the area than in the southern area.

Over the next months, the buoys will record further data, which will be used to calculate the sea-ice drift and deformation variability in the north-western Weddell Sea.

**Tab. 12.8:** List of all deployed buoys with their initial deployment position and time. Buoy names are identical to their name in www.meereisportal.de, where all data and buoy information is available in real time.

| Station | Label | Date | Time (UTC) | Name | IMEI | Latitude (min) | Longitude (min) |
|---|---|---|---|---|---|---|---|
| PS118_20190303_BUOY1 | PS118_20190303_BUOY1_SVP01 | 2019-03-03 | 19:24 | 2019P86 | 300234067406790 | -65.7765 | -58.2922 |
| PS118_20190303_BUOY1 | PS118_20190303_BUOY1_SVP02 | 2019-03-03 | 19:35 | 2019P96 | 300234067703740 | -65.7216 | -58.0860 |
| PS118_20190303_BUOY1 | PS118_20190303_BUOY1_SVP03 | 2019-03-03 | 19:44 | 2019P95 | 300234067702670 | -65.6803 | -57.9347 |
| PS118_20190303_BUOY1 | PS118_20190303_BUOY1_SVP04 | 2019-03-03 | 19:54 | 2019P97 | 300234067704690 | -65.5626 | -57.9313 |
| PS118_20190303_BUOY1 | PS118_20190303_BUOY1_SVP05 | 2019-03-03 | 20:03 | 2019P84 | 300234067403800 | -65.6118 | -58.1276 |
| PS118_20190303_BUOY1 | PS118_20190303_BUOY1_SVP06 | 2019-03-03 | 20:11 | 2019P94 | 300234067701700 | -65.6460 | -58.3256 |
| PS118_20190303_BUOY1 | PS118_20190303_BUOY1_SVP07 | 2019-03-03 | 20:22 | 2019P_ACED-UT-0006 | 300234065459880 | -65.5227 | -58.3140 |
| PS118_20190303_BUOY1 | PS118_20190303_BUOY1_SVP08 | 2019-03-03 | 20:31 | 2019P98 | 300234067704750 | -65.4743 | -58.1045 |
| PS118_20190303_BUOY1 | PS118_20190303_BUOY1_SVP09 | 2019-03-03 | 20:41 | 2019P85 | 300234067406770 | -65.4272 | -57.9357 |
| PS118_20190308_BUOY2 | PS118_20190308_BUOY2_SVP01 | 2019-03-08 | 18:02 | 2019P87 | 300234067407770 | -65.2087 | -57.3708 |
| PS118_20190308_BUOY2 | PS118_20190308_BUOY2_SVP02 | 2019-03-08 | 18:13 | 2019P99 | 300234067704760 | -65.1592 | -57.1717 |
| PS118_20190308_BUOY2 | PS118_20190308_BUOY2_SVP03 | 2019-03-08 | 18:23 | 2019P100 | 300234067705680 | -65.1159 | -57.0000 |
| PS118_20190308_BUOY2 | PS118_20190308_BUOY2_SVP04 | 2019-03-08 | 18:34 | 2019P104 | 300234067706690 | -64.9811 | -56.9985 |
| PS118_20190308_BUOY2 | PS118_20190308_BUOY2_SVP05 | 2019-03-08 | 18:43 | 2019P89 | 300234067600950 | -65.0424 | -57.1977 |
| PS118_20190314_BUOY3 | PS118_20190314_BUOY3_SVP01 | 2019-03-14 | 12:52 | 2019_AAD_MetOcean_01 | 300234066342920 | -64.3110 | -55.3783 |
| PS118_20190314_BUOY3 | PS118_20190314_BUOY3_SVP02 | 2019-03-14 | 13:05 | 2019_AAD_MetOcean_02 | 300234066349750 | -64.2270 | -55.4480 |
| PS118_20190314_BUOY3 | PS118_20190314_BUOY3_SVP03 | 2019-03-14 | 13:17 | 2019_AAD_MetOcean_03 | 300234066340660 | -64.1783 | -55.2425 |
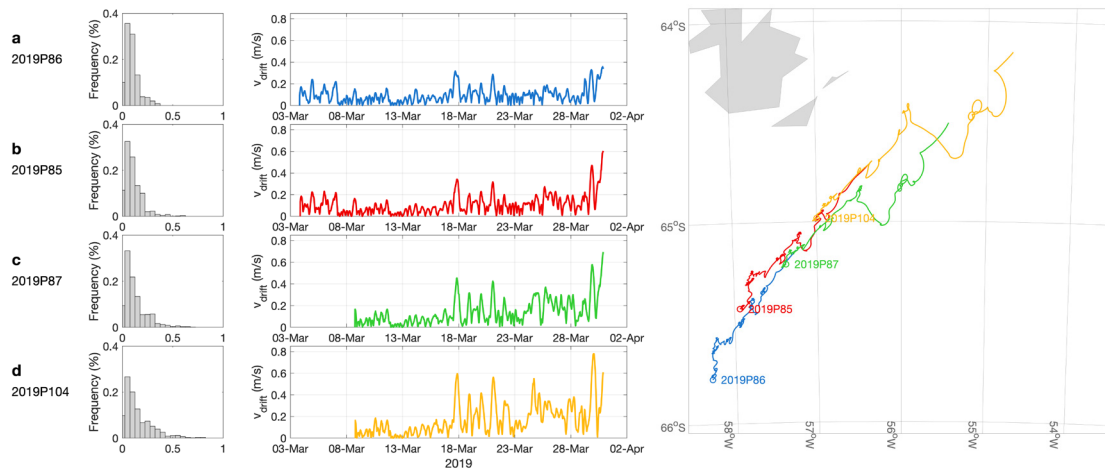
*Fig. 12.14: Histograms and time series of drift velocities of Surface Velocity Profilers (SVPs) of the two buoys of the first (2019P86 and 2019P85) and two buoys of the second buoy array (2019P87 and 2019P104) deployed during PS118. Data are shown until 31 March 2019.*

**Data management**

All buoy positions and raw data are available in near real time through the sea-ice data portal www.meereisportal.de. At the end of their lifetime (end of transmission of data) all data will be finally processed and made available in the World Data Center PANGAEA Data Publisher for Earth & Environmental Science (www.pangaea.de). All SVP report their position and atmospheric pressure directly into the Global Telecommunication System (GTS). Furthermore, all data are exchanged with international partners through the International Program for Antarctic Buoys.

## 12.6    Along track observations of sea ice conditions

**Objectives**

Over the last three decades, ship-based visual observations of the state of the sea ice and its snow cover have been performed over all seasons and serve the best-available observational data set of Antarctic sea ice. The recordings follow the Scientific Committee on Antarctic Research (SCAR) Antarctic Sea Ice Processes and Climate (ASPeCt) protocol and include information on sea-ice concentration, sea-ice thickness and snow depth as well as sea-ice type, surface topography and floe size. These data are combined with information about meteorological conditions as air temperature, wind speed and cloud coverage. This protocol is a useful method to obtain a broad range of characterisation and documentation of different sea-ice states and specific features during the cruise.

**Work at sea**

Every full daytime hour during steaming, sea-ice observations were carried out by trained scientists. The observations follow the ASPeCt protocol (Worby, 1999), with a software following the ASPeCt standard and being provided on a notebook on the ship's bridge. For every observation, pictures were taken in three different directions (portside, ahead, starboard).

Date, time and position of the observation were obtained from the DSHIP system, along with standard meteorological data (current sea temperature, air temperature, true wind speed, true wind direction, visibility). The characterisation of the ice conditions was estimated by taking the average between observations to port side, ahead and to starboard side. Ice thicknesses of tilted floes were estimated by observing a ruler stick attached to the ships starboard side.

**Preliminary (expected) results**

We performed hourly sea-ice observations as soon as we passed the first sea ice on 22 February 2019 at 00:00 UTC at 63°32.872'S/56°22.008'W when going through the Antarctic Sound. The last sea-ice observation was done in the Powell Basin on 29 March 2019 at 11:00 UTC at 61°09.4438'S/49° 28.934'W. Over the time period of 36 days, 136 individual observations were recorded. Sea-ice observations were skipped when the ship was stopped for station work (e.g. CTD, biology/ geology station). Due to limited sight, ice observations are also skipped during civil twilight/night time.

After stopping the official ice observation programme, we crossed again slightly sea-ice covered areas. However, those areas were not considered for further ice observations.

Fig. 12.15 summarizes all conducted sea-ice observations during PS118. The mean sea-ice concentration was calculated as 72.5 % with a mean sea-ice thickness of 1.20 m and 0.27 m snow on top. However, Figure 12.9 indicates that the observed ice classes are a mixture of old multi-year ice and thin new ice classes (e.g. frazil and thin first-year ice). The main ice type in the area, as also known from satellite images, is multi-year ice. Here, we observed a mean ice thickness of 1.67 m with a snow layer of 35 cm on top. These observations slightly underestimate the sea-ice thickness in the area, as we know from our measurements on the sampled ice floes in the same region. This is due to the fact that the track of Polarstern is not going through the typical highly deformed sea-ice but through less compacted and therefore thinner areas.
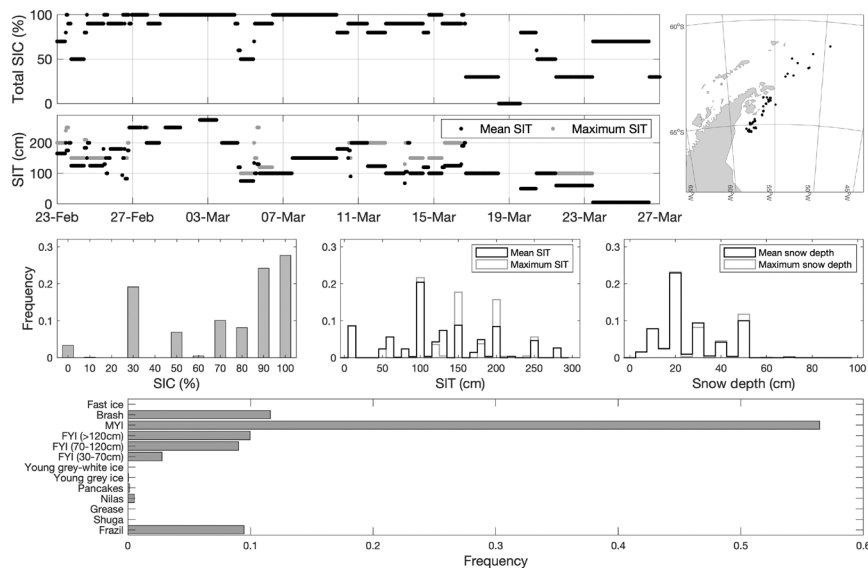


*Fig. 12.15: Overview of all conducted sea-ice observations from the ship's bridge. Total sea-ice concentration (SIC) displays the overall sea-ice concentration around the ship. Sea-ice thickness (SIT) and snow depth data are subdivided into calculated mean (black) and maximum values (grey) per ice observations. Bottom panel displays the overall sea-ice type distribution from all ice observations. Upper right panel displays all locations of ice observations.*

**Data management**

The visual sea-ice observations were already post-processed on board and will be published together with the taken pictures in the World Data Center PANGAEA Data Publisher for Earth & Environmental Science (www.pangaea.de) within two months after the cruise.

## 12.7 Support and use of sea-ice satellite images

**Objectives**

The main objective of the planned extensive support of synthetic aperture radar (SAR) images of sea ice was to assist *R/V Polarstern* through the heavy ice conditions in the western Weddell Sea, and thus give the possibility for an improved route planning towards the iceberg A68 and the entire expedition. Therefore, we defined areas of high interest with corresponding center points in advance for a better assessment of the sea-ice conditions in a time frame of days to weeks.

The provision of Sentinel-1 images (C-Band) was coordinated and supported by Drift&Noise and was displayed through the on-board Mapviewer.

**Work at sea**

We defined 4 main areas of interest for which we wanted to acquire as many Sentinel-1 images as possible for a successful route planning during the cruise. In addition, we defined 21 small areas around the iceberg A68, where we ordered high-resolution Sentinel-1 images. Figure 12.16 gives an overview of all defined centre points.

The data acquisition of Sentinel-1 images started already in end-January 2019, before the expedition started, to track the ongoing changes in our defined areas of interest. Furthermore, Sentinel-1 scenes were acquired and delivered when *Polarstern* was in a Sentinel-1 scene.

During the time on board, 699 scenes were acquired and delivered to the ship between 07 February and 02 April 2019. The delivered scenes can be separated for the defined centre points as follows: 132 scenes at overview 01, 153 scenes at overview 02, 199 scenes at overview 03, 172 scenes at overview 04, and 1in total 112 scenes at position 15, 16, 19 and 20 around the iceberg A68.
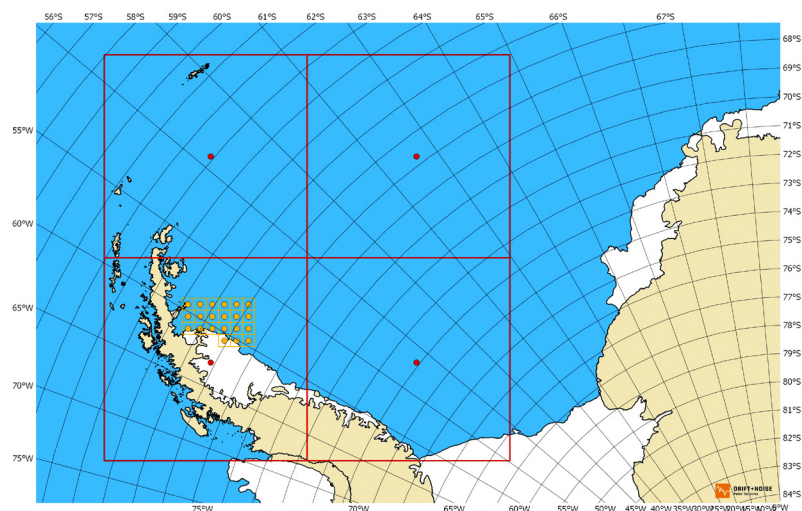


*Fig 12.16: Overview about the defined areas of interests during PS118. Red boxes show the 4 main overview centre points. Small yellow boxes indicate the high-resolution areas in the vicinity of the iceberg A68.*

**Preliminary (expected) results**

The delivered Sentinel-1 data were used for a successful navigation through the ice. Also, the data were used as important background information for the sea-ice group on board to select sampling sites and for preparation of ice-thickness surveys. Thus, the images allowed to identify different dominant ice regimes which were sampled by the EM-Bird surveys.

**Data management**

The near real time Sentinel-1 data were acquired by the European Space Agency (ESA) and were provided through Drift&Noise. The data are freely available for download from their Sentinel-1 Scientific Data Hub SciHub (https://scihub.esa.int/) without any retention period since the day of acquisition.

**References**

Ackley SF, Lewis MJ, Fritsen CH & Xie H (2008) Internal melting in Antarctic sea ice: Development of "gap layers". Geophys. Res. Lett., 35, L11503, doi:10.1029/2008GL033644.

*Arndt S, Nicolaus M, Dierking W & Willmes S (2016) Timing and regional patterns of snowmelt on Antarctic sea ice from passive microwave satellite observations. Journal of Geophysical Research: Oceans, 121(8), 5916–5930, doi: 10.1002/2015JC011504.

Bintanja R, van Oldenborgh G, Drijfhout S, Wouters B & Katsman C (2013) Important role for ocean warming and increased ice-shelf melt in Antarctic sea-ice expansion. Nat. Geosci., 6(5), 376–379, doi:10.1038/ngeo1767.

*Haas C, Thomas DN, Bareiss, J (2001) Surface properties and processes of perennial Antarctic sea ice in summer. Journal of Glaciology, 47(159), 613-625.

*Haas C (2001) The seasonal cycle of ERS scatterometer signatures over perennial Antarctic sea ice and associated surface ice properties and processes. Annals of Glaciology, 33, 69-73.

*Haas C, Nicolaus M, Willmes S, Worby A, Flinspach D (2008) Sea ice and snow thickness and physical properties of an ice floe in the western Weddell Sea and their changes during spring warming. Deep Sea Research II 55(8-9), 963-974.

*Haas C, Friedrich A, Li Z, Nicolaus M, Pfaffling A & Toyota T (2009) Regional variability of sea ice properties and thickness in the northwestern Weddell Sea obtained by in-situ and satellite measurements, In: Peter Lemke. The Expedition of the Research Vessel "Polarstern" to the Antarctic in 2006 (ANT-XXXIII/7). Reports on Polar and Marine Research, 586, 36-74.

*Hellmer HH, Haas C, Schröder M, Dieckmann GS, Spindler M (2008) The ISPOL drift experiment. Deep Sea Research II, 55(8-9), 913-917.

Hellmer HH, Huhn O, Gomis D & Timmermann R (2011) On the freshening of the northwestern Weddell Sea continental shelf. Ocean Sci., 7, 305-316, https://doi.org/10.5194/os-7-305-2011.

Hobbs WR, Massom R, Stammerjohn S, Reid P, Williams G & Meier (2016) A review of recent changes in Southern Ocean sea ice, their drivers and forcings. Global and Planetary Change, 143, 228-250. https://doi.org/10.1016/j.gloplacha.2016.06.008.

*Kattner G, Thomas DN, Haas C, Kennedy H & Dieckmann G (2004). Surface ice and gap layers in Antarctic sea ice: highly productive habitats. Marine ecology-progress series, 277, 1-12.

Kwok R & Maksym T (2014) Snow depth of the Weddell and Bellingshausen sea ice covers from IceBridge surveys in 2010 and 2011: An examination. J Geophys. Res. Oceans, 119, 4141–4167, doi:10.1002/2014JC009943.

Lange MA & Eicken H (1991) The sea ice thickness distribution in the northwestern Weddell Sea. Geophys. Res., 96, 4821- 4837, doi:10.1029/90JC02441.

*Langhorne PJ, Hughes KG, Gough AJ, Smith IJ, Williams MJM, Robinson NJ, Stevens CL, Rack W, Price D, Leonard GH, Mahoney AR, Haas C &Haskell TG (2015) Observed platelet ice distributions in Antarctic sea ice: An index for ocean-ice shelf heat flux. Geophys. Res. Lett., 42, 5442–5451, doi:10.1002/2015GL064508.

*Masso RA, Eicken H, Haas C, Jeffries MO, Drinkwater MR, Sturm M, Worby AP, Wu X Lytle, I Ushio S, Morris K, Reid PA, Warren S & Allison I (2001) Snow on Antarctic sea ice. Reviews of Geophysics, 39(3), 413-445.

Parkinson CL &Cavalieri DJ (2012) Antarctic sea ice variability and trends, 1979–2010. The Cryosphere, 6, 871–880, doi:10.5194/tc-6-871-2012.

*Peeken I, Primpke S, Beyer B, Gütermann J, Katlein C, Krumpen T, Bergmann M, Hehemann L & Gerdts G (2018) Arctic sea ice is an important temporal sink and means of transport for microplastic. Nature Communications, 9, 1505.

*Rabenstein L, Hendricks S, Martin T, Pfaffhuber A & Haas C (2010) Thickness and surface-properties of different sea-ice regimes within the Arctic Trans Polar Drift: data from summers 2001, 2004 and 2007. J Geophys. Res., 115, C12059.

Rott H, Abdel Jaber W, Wuite J, Scheiblauer S, Floricioiu D, van Wessem J M, Nagler T, Miranda N & van den Broeke M R (2017) Changing pattern of ice flow and mass balance for glaciers discharging into the Larsen A and B embayments, Antarctic Peninsula, 2011 to 2016. The Cryosphere Discuss., https://doi.org/10.5194/tc-2017-259.

Simmonds I (2015), Comparing and contrasting the behaviour of Arctic and Antarctic sea ice over the 35 year period 1979-2013. Ann. Glac., 56(69), 18-28, doi: 10.3189/2015AoG69A909.

*Tan B, Li Z, Lu P, Haas C & Nicolaus M (2012) Morphology of sea ice pressure ridges in the northwestern Weddell Sea in winter. J Geophys. Res., 117, C06024, doi:10.1029/2011JC007800.

*Thomas DN, Lara RJ, Haas C, Schnack-Schiel S, Dieckmann B, Kattner G, Nöthig E-M & Mizdalski E (1998) Biological soup within decaying summer sea ice in the Amundsen Sea, Antarctica. Antarctic Research Series AGU, Washington DC,73,161-171.

Thompson DWJ, Solomon S, Kushner PJ, England MH, Grise KM & Karoly DJ (2011) Signatures of the Antarctic ozone hole in Southern Hemisphere surface climate change. Nature Geosci. 4, 741-749, doi:10.1038/ngeo1296.

Turner J, Comiso JC, Marshall GJ, Lachlan-Cope TA, Bracegirdle T, Maksym T, Meredith MP, Wang Z & Orr A (2009) Non-annular atmospheric circulation change induced by stratospheric ozone depletion and its role in the recent increase of Antarctic sea ice extent, Geophys. Res. Lett., 36, L08502, doi:10.1029/2009GL037524.

Turner J, Hosking JS, Bracegirdle TJ, Marshall GJ, Phillips T (2015) Recent changes in Antarctic Sea Ice. Phil. Trans. R Soc. A 373, 20140163. http://dx.doi.org/10.1098/rsta.2014.0163.

# 13. SATELLITE PRODUCTS

Paul Wachter (not on board)                                    DLR

**Grant-No. AWI_PS118_17**

Due to a close cooperation between the Alfred-Wegener Institute (AWI) and the German Aerospace Center (DLR), RV Polarstern was supported by DLR on its cruise PS118 with high-resolution geocoded radar images acquired by the German TerraSAR-X and TanDEM-X satellites. These near real-time (NRT) information products on sea ice conditions in the area of operation assisted Polarstern sailing through the ice covered waters. The satellite data is received at DLR's German Antarctic Receiving Station (GARS) O'Higgins directly after the acquisition and is locally processed in near real-time. Subsequently, just about 60 minutes after the raw data is acquired by the satellite, the information product is transferred via email from GARS O'Higgins to the ship. Such a product is generated up to twice a day. TSX data acquired during the expedition PS118 can be made available for scientific purposes upon request.

During expedition PS118, *Polarstern* experienced severe sea ice conditions in the western Weddell Sea (Fig. 13.1) that eventually prevented research in the target areas on the Larsen continental shelf. Navigation in these conditions relied heavily on helicopter based ice observations and satellite derived sea ice information. The latter were specifically helpful, when weather conditions prevented the use of helicopters. Furthermore, the sea ice data from satellites supported the general cruise planning by providing sea ice information along the planned cruise track beyond the range of helicopters.

The combined use of satellite and helicopter data significantly supported the navigation in severe sea ice conditions. Also at a later phase of expedition PS118 in the sea ice marginal zone in the Powell Basin, satellite derived sea ice information strongly supported the cruise planning especially the planning of hydrographic surveys.
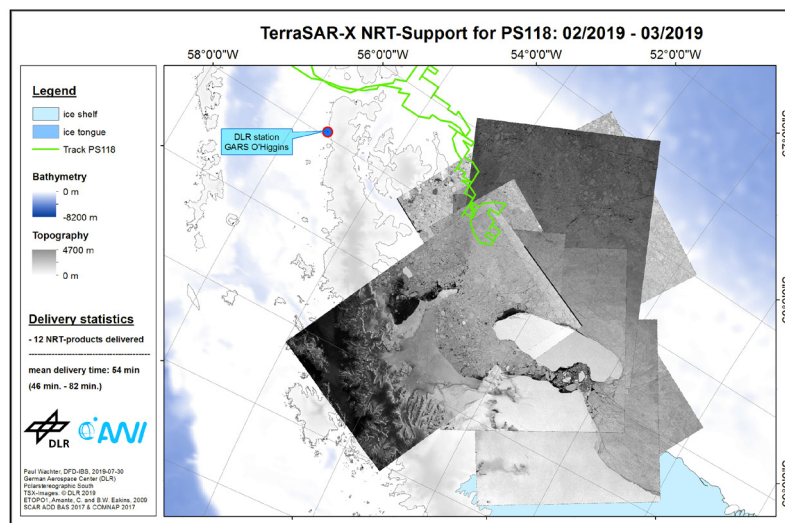


*Fig. 13.1: Overview of TerraSAR-X NRT-Support for PS118.*

# APPENDIX

**A.1    TEILNEHMENDE INSTITUTE / PARTICIPATING INSTITUTIONS**

**A.2    FAHRTTEILNEHMER / CRUISE PARTICIPANTS**

**A.3    SCHIFFSBESATZUNG / SHIP'S CREW**

**A.4    STATIONSLISTE / STATION LIST**

## A.1 TEILNEHMENDE INSTITUTE / PARTICIPATING INSTITUTIONS

|  | Address |
| --- | --- |
| AWI | Alfred-Wegener-Institut<br>Helmholtz-Zentrum für Polar- und Meeresforschung<br>Postfach 120161<br>27515 Bremerhaven<br>Germany |
| BAS | British Antarctic Survey<br>High Cross<br>Madingley Road<br>CAMBRIDGE<br>CB3 0ET<br>United Kingdom |
| Czech Academy of Sciences | Biology Centre, Czech Academy of Sciences<br>Institute of Parasitology<br>Branisovska 1160/31<br>37005 Ceske Budejovice<br>Czech Republic |
| DZMB | Senckenberg am Meer<br>Deutsches Zentrum für Marine Biodiversitätsforschung<br>Südstrand 44<br>26382 Wilhelmshaven<br>Germany |
| DLR | Deutsches Zentrum für Luft- und Raumfahrt e.V.<br>Fernerkundungsdatenzentrum<br>Oberpfaffenhofen<br>82234 Weßling<br>Germany |
| DWD | Deutscher Wetterdienst<br>Geschäftsbereich Wettervorhersage<br>Seeschifffahrtsberatung<br>Bernhard Nocht Str. 76<br>20359 Hamburg<br>Germany |
| GEOMAR | Helmholtz -Zentrum für Ozeanforschung<br>GEOMAR<br>Wischhofstraße 1-3<br>24148 Kiel<br>Germany |

|  | **Address** |
|---|---|
| Goethe University | Goethe-Universität Frankfurt am Main<br>60629 Frankfurt<br>Germany |
| HCU | HafenCity Universität Hamburg<br>Überseeallee 16<br>20457 Hamburg<br>Germany |
| HeliService | HeliService International GmbH<br>Gorch Fock Str. 105<br>26721 Emden<br>Germany |
| KU Leuven | KU Leuven<br>Charles Deberiotstraat 32 - box 2439<br>3000 Leuven<br>Belgium |
| RBNS | Royal Belgian Institute of Natural Sciences<br>Museum of Natural Sciences<br>Vautier Street 29<br>1000 Brussels<br>Belgium |
| SaM-DZMB | Senckenberg am Meer<br>Deutsches Zentrum für Marine Biodiversitätsforschung<br>Südstrand 44<br>26382 Wilhelmshaven<br>Germany |
| Senckenberg | Senckenberg Gesellschaft für Naturforschung<br>Senckenberganlage 25<br>60325 Frankfurt<br>Germany |
| UHB-IUP | Universität Bremen<br>Institut für Umweltphysik<br>Department Ozeanographie<br>Otto-Hahn-Allee 1<br>28359 Bremen<br>Germany |
| ULB | Université libre de Bruxelles<br>Avenue Franklin Roosevelt 50<br>1050 Bruxelles<br>Belgium |

| | Address |
|---|---|
| ULg | Université de Liège<br>Department Oceanologie<br>Quartier Agora Allée du 6 Août 11 Bât. B6c4000<br>Liège<br>Belgium |
| Universität Hamburg | Universität Hamburg<br>Institut für Meereskunde<br>Bundesstraße 53<br>20146 Hamburg<br>Germany |
| University of Aberdeen | University of Aberdeen<br>School of Biological Sciences<br>Tillydrone Avenue<br>Aberdeen<br>AB24 2TZ<br>United Kingdom |
| University of East Anglia | University of East Anglia<br>School of Environmental Sciences<br>Norwich Research Park<br>NR4 7TJ Norwich<br>United Kingdom |
| U of Rostock | Universität Rostock<br>Interdisziplinäre Fakultät<br>Maritime Systeme<br>Albert-Einstein-Str. 21<br>18059 Rostock<br>Germany |
| UoT | The Arctic University of Norway in Tromsø<br>Department of Geosciences<br>Dramsveien 201<br>9037 Tromsø<br>Norway |

## A.2 FAHRTTEILNEHMER / CRUISE PARTICIPANTS

| Name/<br>Last name | Vorname/<br>First name | Institut/<br>Institute | Beruf/<br>Profession | Fachbereich /<br>Discipline |
|---|---|---|---|---|
| Allhusen | Erika | AWI | Technician | Sea Ice Physics |
| Arndt | Stefanie | AWI | Scientist | Sea Ice Physics |
| Baloza | Marwa | AWI | Scientist | Bentho-Pelagic Processes |
| Behrend | Ben | U of Rostock | Student | Biology |
| Bentley | Leroy | Bentley & Mannchen GbR | Media | |
| Brandt | Angelika | Senckenberg | Scientist | Biology |
| Damerell | Gillian | University of East Anglia | Scientist | Oceanography |
| Di Franco | Davide | Senckenberg | Scientist | Biology |
| Diener | Theresa | AWI | Student | Oceanography |
| Dorschel | Boris | AWI | Chief Scientist | Bathymetry |
| Dreutter | Simon | AWI | Scientist | Bathymetry |
| Dziadek | Ricarda | AWI | Scientist | Geophysics |
| Flegontova | Olga | Czech Academy of Sciences | Scientist | Biology |
| Fuchs | Daniel | Heli Service Int | Technician | |
| Gregalis | Jan | Heli Service Int | Technician | |
| Griffiths | Huw | BAS | Scientist | Biology |
| Haas | Christian | AWI | Scientist | Sea Ice Physics |
| Hanisch-Niessen | Sabine | AWI | Scientist | Marine Geology |
| Hehemann | Laura | AWI | Technician | Geophysics |
| Hölemann | Jens | AWI | Scientist | Physical Oceanography |
| Holtappels | Moritz | AWI | Scientist | Bentho-Pelagic Processes |
| Huang | Huang | GEOMAR | Scientist | Chemistry |
| Jager | Harold | Heli Service Int | Chief Pilot | |
| Janout | Markus | AWI | Scientist | Physical Oceanography |
| Jerosch | Kerstin | AWI | Scientist | Functional Ecology |
| Knobelsdorf | Michael | DWD | Scientist | Meteorology |
| Lamping | Nele | AWI | Scientist | Marine Geology |
| Lesic | Nina-Marie | AWI | Student | Bathymetry |
| Lütjens | Mona | AWI | Scientist | Bathymetry |
| Macsween | Kirsten | University of Aberdeen | Scientist | Biology |
| Niessen | Frank | AWI | Scientist | Geophysics |
| Nordhausen | Axel | MPI | Technician | Biology |

| Name/<br>Last name | Vorname/<br>First name | Institut/<br>Institute | Beruf/<br>Profession | Fachbereich /<br>Discipline |
|---|---|---|---|---|
| Owsianowski | Nils | AWI | Engineer | Bentho-Pelagic Processes |
| Peeken | Ilka | AWI | Scientist | Polar Biological Oceanography |
| Piotrowski | Lukas | Heli Service Int | Pilot | |
| Purser | Autun | AWI | Scientist | Deep Sea Ecology and Technology |
| Richter | Claudio | AWI | Scientist | Bentho-Pelagic Processes |
| Rohleder | Christian | DWD | Technician | Meteorology |
| Röhler | Aaron | UHB-IUP | Student | Oceanography |
| Säring | Friederike | U of Rostock | Student | Biology |
| Schreck | Michael | UoT | Scientist | Geology |
| Schröder | Henning | AWI | Engineer | Bentho-Pelagic Processes |
| Veit-Köhler | Gritta | DZMB | Scientist | Biology |
| Verheye | Marie | ULg | Scientist | Biology |
| Volckaert | Filip | KU Leuven | Scientist | Biology |
| Wang | Yanxin | University of East Anglia | Student | Oceanography |
| Warnke | Fynn | AWI | Student | Bathymetry |
| Wiegand | Kevin | Universität Hamburg | Student | Oceanography |
| Wiskandt | Jonathan | AWI | Student | Oceanography |
| Witte | Ursula | University of Aberdeen | Scientist | Biology |
| Wu | Shuzhuang | AWI | Scientist | Marine Geology |

## A.3    SCHIFFSBESATZUNG / SHIP'S CREW

| No. | Name | Rank |
| --- | --- | --- |
| 1. | Wunderlich, Thomas | Master |
| 2. | Grundmann, Uwe | 1.Offc. |
| 3. | Westphal, Henning | Ch.Eng. |
| 4. | Fischer, Tibor | 2.Offc.Lad. |
| 5. | Hering, Igor | 2.Offc. |
| 6. | Peine, Lutz | 2.Offc. |
| 7. | Jaer, Norbert | Doctor |
| 8. | Dr.Hofmann, Jörg | Comm.Offc. |
| 9. | Schnürch, Helmut | 2.Eng. |
| 10. | Brose. Thomas | 2.Eng. |
| 11. | Rusch, Torben | 2.Eng. |
| 12. | Brehme, Andreas | Elec.Tech. |
| 13. | Frank, rhard | Electron. |
| 14. | Markert, Winfried | Electron. |
| 15. | Winter, Andreas | Electron. |
| 16. | Feiertag, Thomas | Electron. |
| 17. | Sedlak, Andreas | Boatsw. |
| 18. | Neisner,Winfried | Carpenter |
| 19. | Clasen, Nils | A.B. |
| 20. | Schröder, Norbert | A.B. |
| 21. | Burzan,Gerd-Ekkehard | A.B. |
| 22. | Hartwig-Labahn, Andreas. | A.B |
| 23. | Fölster, Michael | A.B. |
| 24. | Müller, Steffen | A.B. |
| 25. | Brickmann, Peter | A.B. |
| 26. | Schröder, Horst | A.B. |
| 27. | Beth, Detlef | Storekeep. |
| 28. | Plehn, Markus | Mot-man |
| 29. | Waterstradt, Felix | Mot-man |
| 30. | Krösche, Eckard | Mot-man |
| 31. | Dinse, Horst | Mot-man |
| 32. | Watzel, Bernhard | Mot-man |
| 33. | Meißner, Jörg | Cook |
| 34. | Tupy,Mario | Cooksmate |
| 35. | Martens, Michael | Cooksmate |
| 36. | Wartenberg, Irina | 1.Stwdess |
| 37. | Tscheuschner, Andre | Stwd/KS |
| 38. | Hischke, Peggy | 2.Stwdess |
| 39. | NN | 2.Stwdess |
| 40. | Krause, Tomasz | 2.Steward |

| No. | Name | Rank |
|-----|------|------|
| 41. | Hu, Guo yong | 2.Steward |
| 42. | Chen, Quan Lun | 2.Steward |
| 43. | Ruan, Hui Guang | Laundrym. |
| 44. | Erlenbach, Colin | Trainee 1.LJ |
|     | Krumrei, Benni | Trainee 1.LJ |

# A.4   STATIONSLISTE / STATION LIST

| Station | Date | Time | Latitude | Longitude | Depth [m] | Gear | Action | Comment |
|---|---|---|---|---|---|---|---|---|
| PS118_0_ Underway-1 | 2019-02-20 | 09:15 | -57.92407 | -61.48704 | 2904 | ADCP_150 | profile start | |
| PS118_0_ Underway-1 | 2019-04-05 | 15:00 | -57.64980 | -60.11216 | 3039 | ADCP_150 | profile end | |
| PS118_0_ Underway-3 | 2019-02-20 | 08:56 | -57.89918 | -61.52994 | NA | FBOX | profile start | |
| PS118_0_ Underway-3 | 2019-02-25 | 12:00 | -65.14284 | -57.17910 | 463 | FBOX | profile end | |
| PS118_0_ Underway-3 | 2019-02-27 | 13:36 | -65.31390 | -57.95915 | 454 | FBOX | profile start | |
| PS118_0_ Underway-3 | 2019-02-27 | 17:10 | -65.28410 | -57.94796 | 469 | FBOX | profile end | |
| PS118_0_ Underway-3 | 2019-03-19 | 15:00 | -62.04749 | -52.66433 | 2674 | FBOX | profile start | |
| PS118_0_ Underway-3 | 2019-04-05 | 15:00 | -57.64814 | -60.11549 | 3012 | FBOX | profile end | |
| PS118_0_ Underway-5 | 2019-02-20 | 08:56 | -57.89883 | -61.53069 | NA | PCO2_GO | profile start | |
| PS118_0_ Underway-5 | 2019-02-25 | 12:00 | -65.14284 | -57.17910 | 463 | PCO2_GO | profile end | |
| PS118_0_ Underway-5 | 2019-02-27 | 13:36 | -65.31388 | -57.95914 | 453 | PCO2_GO | profile start | |
| PS118_0_ Underway-5 | 2019-02-27 | 17:10 | -65.28410 | -57.94796 | 469 | PCO2_GO | profile end | |
| PS118_0_ Underway-5 | 2019-03-19 | 15:00 | -62.04749 | -52.66433 | 2674 | PCO2_GO | profile start | |
| PS118_0_ Underway-5 | 2019-04-05 | 15:00 | -57.64767 | -60.11643 | 3012 | PCO2_GO | profile end | |
| PS118_0_ Underway-6 | 2019-02-20 | 08:55 | -57.89832 | -61.53160 | NA | PCO2_SUB | profile start | |
| PS118_0_ Underway-6 | 2019-02-25 | 12:00 | -65.14284 | -57.17910 | 463 | PCO2_SUB | profile end | |
| PS118_0_ Underway-6 | 2019-02-27 | 13:36 | -65.31386 | -57.95913 | 454 | PCO2_SUB | profile start | |
| PS118_0_ Underway-6 | 2019-02-27 | 17:10 | -65.28410 | -57.94796 | 469 | PCO2_SUB | profile end | |
| PS118_0_ Underway-6 | 2019-03-19 | 15:00 | -62.04749 | -52.66433 | 2674 | PCO2_SUB | profile start | |
| PS118_0_ Underway-6 | 2019-04-05 | 15:01 | -57.64709 | -60.11762 | 3012 | PCO2_SUB | profile end | |
| PS118_0_ Underway-8 | 2019-02-20 | 09:02 | -57.90768 | -61.51589 | NA | GRAV | profile start | |

| Station | Date | Time | Latitude | Longitude | Depth [m] | Gear | Action | Comment |
|---|---|---|---|---|---|---|---|---|
| PS118_0_ Underway-8 | 2019-04-05 | 15:00 | -57.64860 | -60.11458 | 3012 | GRAV | profile end | |
| PS118_0_ Underway-9 | 2019-02-20 | 08:55 | -57.89790 | -61.53234 | NA | SVP | profile start | |
| PS118_0_ Underway-9 | 2019-04-05 | 15:01 | -57.64626 | -60.11935 | 3012 | SVP | profile end | |
| PS118_0_ Underway-10 | 2019-02-20 | 08:54 | -57.89733 | -61.53338 | NA | TSG_KEEL | profile start | |
| PS118_0_ Underway-10 | 2019-04-05 | 15:01 | -57.64579 | -60.12033 | 3012 | TSG_KEEL | station end | |
| PS118_0_ Underway-11 | 2019-02-20 | 08:54 | -57.89708 | -61.53389 | NA | TSG_KEEL_2 | profile start | |
| PS118_0_ Underway-11 | 2019-04-05 | 15:01 | -57.64543 | -60.12109 | 3012 | TSG_KEEL_2 | profile end | |
| PS118_0_ Underway-12 | 2019-02-18 | 00:04 | -53.12538 | -70.85843 | 9.7 | WST | profile start | |
| PS118_0_ Underway-12 | 2019-04-08 | 17:50 | -53.18601 | -70.90040 | 12.8 | WST | profile end | |
| PS118_0_ Underway-13 | 2019-02-20 | 09:03 | -57.90864 | -61.51411 | 3240 | MAG | profile start | |
| PS118_0_ Underway-13 | 2019-04-05 | 15:00 | -57.64918 | -60.11342 | 3012 | MAG | profile end | |
| PS118_0_ Underway-14 | 2019-02-20 | 08:50 | -57.89118 | -61.54603 | 1.6 | HS | profile start | |
| PS118_0_ Underway-14 | 2019-04-05 | 15:02 | -57.64487 | -60.12226 | 3012 | HS | profile end | |
| PS118_0_ Underway-15 | 2019-02-22 | 00:00 | -63.54864 | -56.36454 | 708 | ICEOBS | profile start | |
| PS118_0_ Underway-15 | 2019-03-29 | 11:00 | -61.16078 | -49.44588 | 2901 | ICEOBS | profile end | |
| PS118_1-1 | 2019-02-21 | 11:48 | -61.55896 | -57.49172 | 427 | UCTD | station start | |
| PS118_1-1 | 2019-02-21 | 12:13 | -61.63099 | -57.40950 | 414 | UCTD | profile start | |
| PS118_1-1 | 2019-02-21 | 12:16 | -61.63941 | -57.40046 | 420 | UCTD | profile end | |
| PS118_1-1 | 2019-02-21 | 12:22 | -61.65605 | -57.38074 | 407 | UCTD | station end | |
| PS118_2-1 | 2019-02-21 | 14:31 | -62.03498 | -57.08009 | 710 | UCTD | station start | |
| PS118_2-1 | 2019-02-21 | 14:33 | -62.03926 | -57.07976 | 747 | UCTD | profile start | |
| PS118_2-1 | 2019-02-21 | 14:33 | -62.04077 | -57.07973 | 767 | UCTD | profile end | |
| PS118_2-1 | 2019-02-21 | 14:44 | -62.07437 | -57.07961 | 1413 | UCTD | station end | |
| PS118_3-1 | 2019-02-21 | 22:13 | -63.41521 | -56.64180 | 1026 | UCTD | station start | |
| PS118_3-1 | 2019-02-21 | 22:19 | -63.42465 | -56.59974 | 927 | UCTD | profile start | |
| PS118_3-1 | 2019-02-21 | 22:24 | -63.43361 | -56.56802 | 848 | UCTD | profile end | |
| PS118_3-1 | 2019-02-21 | 22:36 | -63.45258 | -56.52951 | 903 | UCTD | station end | |
| PS118_4-1 | 2019-02-22 | 18:29 | -63.81948 | -56.47268 | 534 | CTDOZE | station start | |

| Station | Date | Time | Latitude | Longitude | Depth [m] | Gear | Action | Comment |
|---|---|---|---|---|---|---|---|---|
| PS118_4-1 | 2019-02-22 | 18:45 | -63.81871 | -56.47711 | 534 | CTDOZE | at depth | |
| PS118_4-1 | 2019-02-22 | 19:07 | -63.82105 | -56.48477 | 532 | CTDOZE | station end | |
| PS118_5-1 | 2019-03-04 | 15:14 | -64.98430 | -57.74827 | 448 | CTDOZE | station start | |
| PS118_5-1 | 2019-03-04 | 15:29 | -64.98370 | -57.75156 | 445 | CTDOZE | at depth | |
| PS118_5-1 | 2019-03-04 | 16:03 | -64.98358 | -57.75161 | 444 | CTDOZE | station end | |
| PS118_5-2 | 2019-03-04 | 16:04 | -64.98357 | -57.75147 | 444 | GC | station start | |
| PS118_5-2 | 2019-03-04 | 16:16 | -64.98344 | -57.75113 | 444 | GC | at depth | |
| PS118_5-2 | 2019-03-04 | 16:41 | -64.98358 | -57.75024 | 445 | GC | station end | |
| PS118_5-3 | 2019-03-04 | 18:32 | -64.98370 | -57.75180 | 430 | TVMUC | station start | |
| PS118_5-3 | 2019-03-04 | 19:51 | -64.98335 | -57.75292 | 428 | TVMUC | at depth | |
| PS118_5-3 | 2019-03-04 | 19:52 | -64.98335 | -57.75292 | 428 | TVMUC | profile start | |
| PS118_5-3 | 2019-03-04 | 19:53 | -64.98334 | -57.75292 | 428 | TVMUC | profile end | |
| PS118_5-3 | 2019-03-04 | 20:10 | -64.98226 | -57.75011 | NA | TVMUC | station end | |
| PS118_5-4 | 2019-03-04 | 20:26 | -64.98103 | -57.74684 | NA | TVMUC | station start | |
| PS118_5-4 | 2019-03-04 | 20:43 | -64.97952 | -57.74607 | NA | TVMUC | at depth | |
| PS118_5-4 | 2019-03-04 | 20:43 | -64.97950 | -57.74604 | NA | TVMUC | profile start | |
| PS118_5-4 | 2019-03-04 | 20:44 | -64.97944 | -57.74591 | NA | TVMUC | profile end | |
| PS118_5-4 | 2019-03-04 | 21:00 | -64.97822 | -57.74559 | NA | TVMUC | station end | |
| PS118_5-5 | 2019-03-04 | 22:01 | -64.97284 | -57.73148 | NA | REL | station start | |
| PS118_5-5 | 2019-03-04 | 22:08 | -64.97230 | -57.73008 | NA | REL | at depth | |
| PS118_5-5 | 2019-03-04 | 22:31 | -64.97042 | -57.72512 | NA | REL | station end | |
| PS118_6-1 | 2019-03-05 | 12:10 | -64.98008 | -57.77735 | 440 | CTDOZE | station start | |
| PS118_6-1 | 2019-03-05 | 12:26 | -64.98008 | -57.77600 | NA | CTDOZE | at depth | |
| PS118_6-1 | 2019-03-05 | 12:40 | -64.97955 | -57.77518 | NA | CTDOZE | station end | |
| PS118_6-2 | 2019-03-05 | 13:14 | -64.97859 | -57.77333 | NA | MUC | station start | |
| PS118_6-2 | 2019-03-05 | 13:26 | -64.97873 | -57.77298 | NA | MUC | at depth | |
| PS118_6-2 | 2019-03-05 | 13:43 | -64.97794 | -57.77237 | NA | MUC | station end | |
| PS118_6-3 | 2019-03-05 | 14:12 | -64.97695 | -57.77165 | NA | MUC | station start | |
| PS118_6-3 | 2019-03-05 | 14:30 | -64.97686 | -57.77271 | NA | MUC | at depth | |
| PS118_6-3 | 2019-03-05 | 14:46 | -64.97696 | -57.77420 | NA | MUC | station end | |
| PS118_6-4 | 2019-03-05 | 15:21 | -64.97707 | -57.77789 | NA | MUC | station start | |
| PS118_6-4 | 2019-03-05 | 15:39 | -64.97652 | -57.77934 | NA | MUC | at depth | |
| PS118_6-4 | 2019-03-05 | 15:54 | -64.97611 | -57.78074 | NA | MUC | station end | |
| PS118_6-5 | 2019-03-05 | 16:58 | -64.97383 | -57.78673 | NA | EBS | station start | |
| PS118_6-5 | 2019-03-05 | 17:19 | -64.97360 | -57.78895 | 433 | EBS | at depth | |
| PS118_6-5 | 2019-03-05 | 18:18 | -64.97674 | -57.80400 | NA | EBS | station end | |

| Station | Date | Time | Latitude | Longitude | Depth [m] | Gear | Action | Comment |
|---|---|---|---|---|---|---|---|---|
| PS118_6-6 | 2019-03-05 | 19:07 | -64.97086 | -57.79809 | NA | EBS | station start | |
| PS118_6-6 | 2019-03-05 | 19:27 | -64.97131 | -57.80129 | NA | EBS | at depth | |
| PS118_6-6 | 2019-03-05 | 20:17 | -64.97255 | -57.81045 | NA | EBS | station end | |
| PS118_6-7 | 2019-03-05 | 21:31 | -64.96440 | -57.83635 | NA | AGT | station start | |
| PS118_6-7 | 2019-03-05 | 21:47 | -64.96502 | -57.82639 | NA | AGT | at depth | |
| PS118_6-7 | 2019-03-05 | 22:39 | -64.96273 | -57.80263 | NA | AGT | station end | |
| PS118_6-8 | 2019-03-06 | 00:54 | -64.95339 | -57.79569 | NA | ROV | station start | |
| PS118_6-8 | 2019-03-06 | 01:32 | -64.95108 | -57.78844 | NA | ROV | station end | |
| PS118_6-9 | 2019-03-06 | 03:58 | -64.94140 | -57.78696 | 430 | OFOS | station start | |
| PS118_6-9 | 2019-03-06 | 04:24 | -64.94028 | -57.78883 | 431 | OFOS | at depth | first try, lense dirty |
| PS118_6-9 | 2019-03-06 | 05:01 | -64.93879 | -57.79218 | 432 | OFOS | at depth | second try |
| PS118_6-9 | 2019-03-06 | 05:53 | -64.93650 | -57.79754 | 434 | OFOS | profile start | |
| PS118_6-9 | 2019-03-06 | 09:54 | -64.92861 | -57.81914 | 432 | OFOS | profile end | |
| PS118_6-9 | 2019-03-06 | 09:54 | -64.92861 | -57.81914 | 432 | OFOS | station end | |
| PS118_7-1 | 2019-03-06 | 18:58 | -64.91964 | -57.82511 | 446 | OFOS | station start | |
| PS118_7-1 | 2019-03-06 | 19:25 | -64.91749 | -57.82661 | 446 | OFOS | at depth | |
| PS118_7-1 | 2019-03-06 | 19:30 | -64.91704 | -57.82688 | 446 | OFOS | profile start | |
| PS118_7-1 | 2019-03-06 | 20:08 | -64.91409 | -57.82786 | 444 | OFOS | profile end | |
| PS118_7-1 | 2019-03-06 | 20:45 | -64.91157 | -57.82730 | 441 | OFOS | station end | |
| PS118_8-1 | 2019-03-11 | 11:46 | -64.05250 | -55.90631 | 387 | OFOS | station start | |
| PS118_8-1 | 2019-03-11 | 12:02 | -64.04926 | -55.90769 | 388 | OFOS | at depth | |
| PS118_8-1 | 2019-03-11 | 12:02 | -64.04926 | -55.90769 | 388 | OFOS | profile start | |
| PS118_8-1 | 2019-03-11 | 15:45 | -64.00672 | -55.90743 | 408 | OFOS | profile end | |
| PS118_8-1 | 2019-03-11 | 16:05 | -64.00295 | -55.90724 | 408 | OFOS | station end | |
| PS118_8-2 | 2019-03-11 | 16:25 | -63.99932 | -55.90660 | 410 | CTDOZE | station start | |
| PS118_8-2 | 2019-03-11 | 16:38 | -63.99728 | -55.90609 | 412 | CTDOZE | at depth | |
| PS118_8-2 | 2019-03-11 | 17:09 | -63.99226 | -55.90590 | 412 | CTDOZE | station end | |
| PS118_8-3 | 2019-03-11 | 18:05 | -63.98493 | -55.90522 | 416 | GC | station start | |
| PS118_8-3 | 2019-03-11 | 18:20 | -63.98289 | -55.90492 | 417 | GC | at depth | |
| PS118_8-3 | 2019-03-11 | 18:40 | -63.98023 | -55.90451 | 414 | GC | station end | |
| PS118_8-4 | 2019-03-11 | 19:11 | -63.97687 | -55.90452 | 414 | MUC | station start | |
| PS118_8-4 | 2019-03-11 | 19:27 | -63.97542 | -55.90489 | 414 | MUC | at depth | |
| PS118_8-4 | 2019-03-11 | 19:44 | -63.97397 | -55.90498 | 413 | MUC | station end | |
| PS118_8-5 | 2019-03-11 | 20:04 | -63.97217 | -55.90502 | 413 | MUC | station start | |
| PS118_8-5 | 2019-03-11 | 20:19 | -63.97107 | -55.90537 | 413 | MUC | at depth | |
| PS118_8-5 | 2019-03-11 | 20:32 | -63.97030 | -55.90562 | 414 | MUC | station end | |

| Station | Date | Time | Latitude | Longitude | Depth [m] | Gear | Action | Comment |
|---|---|---|---|---|---|---|---|---|
| PS118_8-6 | 2019-03-11 | 20:48 | -63.96937 | -55.90591 | 414 | MUC | station start | |
| PS118_8-6 | 2019-03-11 | 21:03 | -63.96842 | -55.90640 | 415 | MUC | at depth | |
| PS118_8-6 | 2019-03-11 | 21:17 | -63.96736 | -55.90683 | 415 | MUC | station end | |
| PS118_8-7 | 2019-03-11 | 21:37 | -63.96582 | -55.90743 | 415 | MUC | station start | |
| PS118_8-7 | 2019-03-11 | 21:53 | -63.96470 | -55.90782 | 415 | MUC | at depth | |
| PS118_8-7 | 2019-03-11 | 22:06 | -63.96377 | -55.90801 | 415 | MUC | station end | |
| PS118_8-8 | 2019-03-11 | 22:26 | -63.96282 | -55.90819 | 415 | MUC | station start | |
| PS118_8-8 | 2019-03-11 | 22:40 | -63.96237 | -55.90826 | 415 | MUC | at depth | |
| PS118_8-8 | 2019-03-11 | 22:53 | -63.96201 | -55.90827 | 415 | MUC | station end | |
| PS118_9-1 | 2019-03-12 | 05:17 | -63.99222 | -55.96629 | 419 | OFOS | station start | |
| PS118_9-1 | 2019-03-12 | 06:00 | -63.99222 | -55.96630 | 419 | OFOS | at depth | |
| PS118_9-1 | 2019-03-12 | 06:00 | -63.99222 | -55.96630 | 419 | OFOS | profile start | |
| PS118_9-1 | 2019-03-12 | 06:51 | -63.99441 | -55.96899 | 418 | OFOS | profile end | |
| PS118_9-1 | 2019-03-12 | 07:08 | -63.99391 | -55.96848 | 419 | OFOS | station end | |
| PS118_9-2 | 2019-03-12 | 13:30 | -64.01820 | -55.91511 | 406 | REL | station start | |
| PS118_9-2 | 2019-03-12 | 13:40 | -64.01805 | -55.91564 | 406 | REL | at depth | |
| PS118_9-2 | 2019-03-12 | 13:56 | -64.01793 | -55.91585 | 406 | REL | station end | |
| PS118_9-3 | 2019-03-12 | 13:57 | -64.01793 | -55.91588 | 406 | REL | station start | |
| PS118_9-3 | 2019-03-12 | 13:58 | -64.01793 | -55.91591 | 406 | REL | at depth | |
| PS118_9-3 | 2019-03-12 | 14:03 | -64.01795 | -55.91610 | 406 | REL | station end | |
| PS118_9-4 | 2019-03-12 | 14:24 | -64.01781 | -55.91821 | 406 | EBS | station start | |
| PS118_9-4 | 2019-03-12 | 14:44 | -64.01784 | -55.91836 | 406 | EBS | at depth | |
| PS118_9-4 | 2019-03-12 | 15:32 | -64.01860 | -55.90606 | 404 | EBS | station end | |
| PS118_9-5 | 2019-03-12 | 15:50 | -64.01966 | -55.90140 | 403 | EBS | station start | |
| PS118_9-5 | 2019-03-12 | 16:17 | -64.02053 | -55.90749 | 403 | EBS | at depth | |
| PS118_9-5 | 2019-03-12 | 16:56 | -64.02246 | -55.91502 | 401 | EBS | station end | |
| PS118_9-6 | 2019-03-12 | 17:43 | -64.02380 | -55.91868 | 400 | AGT | station start | |
| PS118_9-6 | 2019-03-12 | 18:00 | -64.02305 | -55.91428 | 400 | AGT | at depth | |
| PS118_9-6 | 2019-03-12 | 18:45 | -64.02178 | -55.90658 | 402 | AGT | station end | |
| PS118_9-7 | 2019-03-12 | 19:08 | -64.02179 | -55.90269 | 401 | AGT | station start | |
| PS118_9-7 | 2019-03-12 | 19:21 | -64.02164 | -55.91101 | 402 | AGT | at depth | |
| PS118_9-7 | 2019-03-12 | 20:04 | -64.02027 | -55.92614 | 403 | AGT | station end | |
| PS118_9-8 | 2019-03-12 | 21:17 | -64.02100 | -55.90906 | 403 | AGT | station start | |
| PS118_9-8 | 2019-03-12 | 21:35 | -64.02054 | -55.92362 | 403 | AGT | at depth | |
| PS118_9-8 | 2019-03-12 | 22:00 | -64.01901 | -55.93310 | 405 | AGT | station end | |
| PS118_9-9 | 2019-03-12 | 23:28 | -64.01952 | -55.93089 | 405 | GC | station start | |

| Station | Date | Time | Latitude | Longitude | Depth [m] | Gear | Action | Comment |
|---------|------|------|----------|-----------|-----------|------|--------|---------|
| PS118_9-9 | 2019-03-12 | 23:42 | -64.01925 | -55.93152 | 405 | GC | at depth | |
| PS118_9-9 | 2019-03-13 | 00:09 | -64.01919 | -55.93087 | 405 | GC | station end | |
| PS118_9-10 | 2019-03-13 | 01:55 | -64.01844 | -55.91864 | 405 | ROV | station start | |
| PS118_9-10 | 2019-03-13 | 02:12 | -64.01837 | -55.91878 | 405 | ROV | at depth | |
| PS118_9-10 | 2019-03-13 | 05:07 | -64.02114 | -55.91679 | 401 | ROV | station end | |
| PS118_10-1 | 2019-03-13 | 11:40 | -64.00288 | -55.97616 | 414 | CTDOZE | station start | |
| PS118_10-1 | 2019-03-13 | 11:55 | -64.00303 | -55.97662 | 414 | CTDOZE | at depth | |
| PS118_10-1 | 2019-03-13 | 12:11 | -64.00320 | -55.97683 | 414 | CTDOZE | station end | |
| PS118_10-2 | 2019-03-13 | 12:28 | -64.00296 | -55.97669 | 414 | GC | station start | |
| PS118_10-2 | 2019-03-13 | 12:41 | -64.00301 | -55.97692 | 414 | GC | at depth | |
| PS118_10-2 | 2019-03-13 | 13:23 | -64.00357 | -55.97750 | 414 | GC | station end | |
| PS118_10-3 | 2019-03-13 | 13:28 | -64.00357 | -55.97737 | 414 | MUC | station start | |
| PS118_10-3 | 2019-03-13 | 14:02 | -64.00250 | -55.97681 | 414 | MUC | at depth | |
| PS118_10-3 | 2019-03-13 | 14:20 | -64.00264 | -55.97682 | 414 | MUC | station end | |
| PS118_11-1 | 2019-03-13 | 18:21 | -63.90002 | -55.67602 | 237 | CTDOZE | station start | |
| PS118_11-1 | 2019-03-13 | 18:33 | -63.89990 | -55.67566 | 234 | CTDOZE | at depth | |
| PS118_11-1 | 2019-03-13 | 18:48 | -63.90017 | -55.67518 | 233 | CTDOZE | station end | |
| PS118_11-2 | 2019-03-13 | 19:40 | -63.88964 | -55.67659 | 179 | OFOS | station start | |
| PS118_11-2 | 2019-03-13 | 20:14 | -63.88864 | -55.67515 | 160 | OFOS | at depth | |
| PS118_11-2 | 2019-03-13 | 22:30 | -63.88781 | -55.65696 | 38.4 | OFOS | station end | |
| PS118_12-1 | 2019-03-14 | 06:44 | -63.80549 | -55.74511 | 457 | CTDOZE | station start | |
| PS118_12-1 | 2019-03-14 | 07:04 | -63.80662 | -55.74433 | 456 | CTDOZE | at depth | |
| PS118_12-1 | 2019-03-14 | 07:23 | -63.80759 | -55.74249 | 455 | CTDOZE | station end | |
| PS118_12-2 | 2019-03-14 | 07:44 | -63.80879 | -55.73985 | 455 | MUC | station start | |
| PS118_12-2 | 2019-03-14 | 07:45 | -63.80895 | -55.73957 | 455 | MUC | at depth | |
| PS118_12-2 | 2019-03-14 | 07:55 | -63.80953 | -55.73706 | 456 | MUC | station end | |
| PS118_12-3 | 2019-03-14 | 08:27 | -63.81161 | -55.73083 | 454 | MUC | station start | |
| PS118_12-3 | 2019-03-14 | 08:40 | -63.81252 | -55.72795 | 453 | MUC | at depth | |
| PS118_12-3 | 2019-03-14 | 08:51 | -63.81290 | -55.72517 | 453 | MUC | station end | |
| PS118_12-4 | 2019-03-14 | 10:00 | -63.81238 | -55.72067 | 453 | MUC | station start | |
| PS118_12-4 | 2019-03-14 | 10:11 | -63.81294 | -55.71909 | 453 | MUC | at depth | |
| PS118_12-4 | 2019-03-14 | 10:25 | -63.81385 | -55.71643 | 454 | MUC | station end | |
| PS118_12-5 | 2019-03-14 | 10:44 | -63.81379 | -55.71370 | 453 | MUC | station start | |
| PS118_12-5 | 2019-03-14 | 10:54 | -63.81397 | -55.71167 | 454 | MUC | at depth | |
| PS118_12-5 | 2019-03-14 | 11:11 | -63.81550 | -55.70771 | 453 | MUC | station end | |
| PS118_12-6 | 2019-03-14 | 11:27 | -63.81615 | -55.70543 | 453 | MUC | station start | |

| Station | Date | Time | Latitude | Longitude | Depth [m] | Gear | Action | Comment |
|---|---|---|---|---|---|---|---|---|
| PS118_12-6 | 2019-03-14 | 11:41 | -63.81654 | -55.70434 | 453 | MUC | at depth | |
| PS118_12-6 | 2019-03-14 | 11:59 | -63.81730 | -55.70141 | 453 | MUC | station end | |
| PS118_12-7 | 2019-03-14 | 13:48 | -63.82330 | -55.67784 | 445 | EBS | station start | |
| PS118_12-7 | 2019-03-14 | 13:50 | -63.82345 | -55.67731 | 445 | EBS | at depth | |
| PS118_12-7 | 2019-03-14 | 14:45 | -63.82467 | -55.67019 | 444 | EBS | station end | |
| PS118_12-8 | 2019-03-14 | 14:46 | -63.82483 | -55.67023 | 444 | ICEBUCKET | station start | |
| PS118_12-8 | 2019-03-14 | 15:01 | -63.82558 | -55.66630 | 443 | ICEBUCKET | station end | |
| PS118_12-9 | 2019-03-14 | 17:08 | -63.82859 | -55.64035 | 438 | EBS | station start | |
| PS118_12-9 | 2019-03-14 | 17:26 | -63.83013 | -55.63331 | 436 | EBS | at depth | |
| PS118_12-9 | 2019-03-14 | 18:09 | -63.83855 | -55.61525 | 425 | EBS | station end | |
| PS118_12-10 | 2019-03-14 | 18:50 | -63.84118 | -55.59727 | 411 | AGT | station start | |
| PS118_12-10 | 2019-03-14 | 19:10 | -63.83744 | -55.58602 | 412 | AGT | at depth | |
| PS118_12-10 | 2019-03-14 | 19:51 | -63.83575 | -55.56843 | 405 | AGT | station end | |
| PS118_12-11 | 2019-03-14 | 20:43 | -63.84700 | -55.55326 | 391 | AGT | station start | |
| PS118_12-11 | 2019-03-14 | 20:58 | -63.84584 | -55.54548 | 393 | AGT | at depth | |
| PS118_12-11 | 2019-03-14 | 21:31 | -63.84148 | -55.53543 | 391 | AGT | station end | |
| PS118_12-12 | 2019-03-15 | 01:08 | -63.84380 | -55.44917 | 379 | OFOS | station start | |
| PS118_12-12 | 2019-03-15 | 01:28 | -63.84416 | -55.44653 | 379 | OFOS | at depth | |
| PS118_12-12 | 2019-03-15 | 06:11 | -63.84424 | -55.44537 | 378 | OFOS | station end | |
| PS118_13-1 | 2019-03-17 | 11:18 | -63.06813 | -54.31278 | 424 | CTDOZE | station start | |
| PS118_13-1 | 2019-03-17 | 11:31 | -63.06863 | -54.31240 | 423 | CTDOZE | at depth | |
| PS118_13-1 | 2019-03-17 | 11:55 | -63.06878 | -54.31258 | 423 | CTDOZE | station end | |
| PS118_13-2 | 2019-03-17 | 12:35 | -63.06882 | -54.31299 | 423 | LAND | station start | |
| PS118_13-2 | 2019-03-17 | 13:36 | -63.06877 | -54.31313 | 424 | LAND | at depth | |
| PS118_13-2 | 2019-03-17 | 13:43 | -63.06867 | -54.31316 | 424 | LAND | station end | |
| PS118_13-3 | 2019-03-17 | 14:01 | -63.05273 | -54.32949 | 447 | MUC | station start | |
| PS118_13-3 | 2019-03-17 | 14:18 | -63.05284 | -54.32953 | 447 | MUC | at depth | |
| PS118_13-3 | 2019-03-17 | 14:33 | -63.05270 | -54.32964 | 447 | MUC | station end | |
| PS118_13-4 | 2019-03-17 | 14:49 | -63.05280 | -54.33000 | 447 | MUC | station start | |
| PS118_13-4 | 2019-03-17 | 15:05 | -63.05330 | -54.32748 | 446 | MUC | at depth | |
| PS118_13-4 | 2019-03-17 | 15:22 | -63.05410 | -54.32224 | 444 | MUC | station end | |
| PS118_13-5 | 2019-03-17 | 15:43 | -63.05423 | -54.31838 | 442 | MUC | station start | |
| PS118_13-5 | 2019-03-17 | 15:58 | -63.05381 | -54.31577 | 440 | MUC | at depth | |
| PS118_13-5 | 2019-03-17 | 16:14 | -63.05349 | -54.31236 | 439 | MUC | station end | |
| PS118_14-1 | 2019-03-17 | 23:00 | -61.99227 | -53.79394 | 559 | HS | station start | |
| PS118_14-1 | 2019-03-17 | 23:00 | -61.99227 | -53.79386 | 559 | HS | profile start | |

| Station | Date | Time | Latitude | Longitude | Depth [m] | Gear | Action | Comment |
|---|---|---|---|---|---|---|---|---|
| PS118_14-1 | 2019-03-18 | 02:02 | -61.92023 | -52.99938 | 2015 | HS | profile end | |
| PS118_14-1 | 2019-03-18 | 02:02 | -61.92022 | -52.99925 | 2015 | HS | station end | |
| PS118_14-2 | 2019-03-18 | 02:02 | -61.92020 | -52.99869 | 2017 | UCTD | station start | |
| PS118_14-2 | 2019-03-18 | 02:12 | -61.91961 | -52.98811 | 2061 | UCTD | at depth | |
| PS118_14-2 | 2019-03-18 | 02:30 | -61.91887 | -52.97346 | 2091 | UCTD | station end | |
| PS118_14-3 | 2019-03-18 | 02:59 | -61.86142 | -52.97032 | 1560 | HS | station start | |
| PS118_14-3 | 2019-03-18 | 03:09 | -61.85078 | -52.99214 | 1104 | HS | profile start | |
| PS118_14-3 | 2019-03-18 | 06:24 | -61.98324 | -53.85419 | 523 | HS | profile end | |
| PS118_14-3 | 2019-03-18 | 06:31 | -61.97267 | -53.84700 | 547 | HS | profile start | |
| PS118_14-3 | 2019-03-18 | 10:11 | -61.81437 | -52.98152 | 506 | HS | profile end | |
| PS118_14-3 | 2019-03-18 | 10:13 | -61.81448 | -52.98602 | 503 | HS | profile start | |
| PS118_14-3 | 2019-03-18 | 13:38 | -61.95974 | -53.88808 | 527 | HS | profile end | |
| PS118_14-3 | 2019-03-18 | 13:39 | -61.96002 | -53.88889 | 526 | HS | station end | |
| PS118_15-1 | 2019-03-18 | 17:12 | -62.00176 | -55.00243 | NA | Glider | station start | |
| PS118_15-1 | 2019-03-18 | 17:21 | -62.00230 | -54.99965 | NA | Glider | station end | |
| PS118_15-2 | 2019-03-18 | 18:25 | -62.01644 | -54.99257 | 556 | CTDOZE | station start | |
| PS118_15-2 | 2019-03-18 | 19:00 | -62.01954 | -54.98186 | 1506 | CTDOZE | at depth | |
| PS118_15-2 | 2019-03-18 | 19:40 | -62.01871 | -54.98025 | 1501 | CTDOZE | station end | |
| PS118_16-1 | 2019-03-18 | 23:48 | -61.89998 | -53.80080 | 823 | CTDOZE | station start | |
| PS118_16-1 | 2019-03-19 | 00:07 | -61.90001 | -53.80267 | 823 | CTDOZE | at depth | |
| PS118_16-1 | 2019-03-19 | 00:28 | -61.90001 | -53.81025 | 864 | CTDOZE | station end | |
| PS118_17-1 | 2019-03-19 | 01:35 | -61.92014 | -53.66396 | 603 | CTDOZE | station start | |
| PS118_17-1 | 2019-03-19 | 01:55 | -61.91946 | -53.66388 | 603 | CTDOZE | at depth | |
| PS118_17-1 | 2019-03-19 | 02:09 | -61.91898 | -53.66432 | 603 | CTDOZE | station end | |
| PS118_18-1 | 2019-03-19 | 02:49 | -61.94094 | -53.53248 | 1020 | CTDOZE | station start | |
| PS118_18-1 | 2019-03-19 | 03:17 | -61.93875 | -53.53334 | 1006 | CTDOZE | at depth | |
| PS118_18-1 | 2019-03-19 | 03:45 | -61.93806 | -53.53307 | 1005 | CTDOZE | station end | |
| PS118_19-1 | 2019-03-19 | 04:21 | -61.96819 | -53.36704 | 1438 | CTDOZE | station start | |
| PS118_19-1 | 2019-03-19 | 05:02 | -61.97165 | -53.37443 | 1484 | CTDOZE | at depth | |
| PS118_19-1 | 2019-03-19 | 05:34 | -61.97642 | -53.37526 | 1638 | CTDOZE | station end | |
| PS118_20-1 | 2019-03-19 | 06:19 | -61.99664 | -53.15779 | 2216 | CTDOZE | station start | |
| PS118_20-1 | 2019-03-19 | 07:10 | -62.00557 | -53.15000 | 2217 | CTDOZE | at depth | |
| PS118_20-1 | 2019-03-19 | 08:06 | -62.01410 | -53.14108 | 2230 | CTDOZE | station end | |
| PS118_21-1 | 2019-03-19 | 10:07 | -62.04076 | -52.91876 | 2514 | CTDOZE | station start | |
| PS118_21-1 | 2019-03-19 | 11:03 | -62.04155 | -52.88979 | 2468 | CTDOZE | at depth | |
| PS118_21-1 | 2019-03-19 | 11:58 | -62.03770 | -52.86604 | 2466 | CTDOZE | station end | |

| Station | Date | Time | Latitude | Longitude | Depth [m] | Gear | Action | Comment |
|---|---|---|---|---|---|---|---|---|
| PS118_22-1 | 2019-03-19 | 13:11 | -62.06772 | -52.68133 | 2604 | CTDOZE | station start | |
| PS118_22-1 | 2019-03-19 | 14:16 | -62.05600 | -52.66616 | 2668 | CTDOZE | at depth | |
| PS118_22-1 | 2019-03-19 | 15:19 | -62.04426 | -52.66472 | 2669 | CTDOZE | station end | |
| PS118_23-1 | 2019-03-19 | 17:02 | -62.11496 | -52.37797 | 2839 | CTDOZE | station start | |
| PS118_23-1 | 2019-03-19 | 18:03 | -62.11331 | -52.39432 | 2831 | CTDOZE | at depth | |
| PS118_23-1 | 2019-03-19 | 19:02 | -62.11557 | -52.41038 | 2826 | CTDOZE | station end | |
| PS118_24-1 | 2019-03-20 | 00:17 | -62.25011 | -51.50022 | 3185 | CTDOZE | station start | |
| PS118_24-1 | 2019-03-20 | 01:25 | -62.25347 | -51.47958 | 3270 | CTDOZE | at depth | |
| PS118_24-1 | 2019-03-20 | 02:45 | -62.25553 | -51.44833 | 3286 | CTDOZE | station end | |
| PS118_24-2 | 2019-03-20 | 02:50 | -62.25579 | -51.44628 | 3287 | MUC | station start | |
| PS118_24-2 | 2019-03-20 | 04:11 | -62.25750 | -51.42800 | 3289 | MUC | at depth | |
| PS118_24-2 | 2019-03-20 | 05:24 | -62.25443 | -51.42121 | 3290 | MUC | station end | |
| PS118_24-3 | 2019-03-20 | 05:25 | -62.25439 | -51.42104 | 3290 | MUC | station start | |
| PS118_24-3 | 2019-03-20 | 06:45 | -62.24878 | -51.40902 | 3295 | MUC | at depth | |
| PS118_24-3 | 2019-03-20 | 08:05 | -62.24325 | -51.41946 | 3297 | MUC | station end | |
| PS118_24-4 | 2019-03-20 | 08:45 | -62.24233 | -51.42541 | 3289 | CTDOZE | station start | |
| PS118_24-4 | 2019-03-20 | 09:55 | -62.24099 | -51.43300 | 3286 | CTDOZE | at depth | |
| PS118_24-4 | 2019-03-20 | 11:16 | -62.24273 | -51.44439 | 3284 | CTDOZE | station end | |
| PS118_25-1 | 2019-03-20 | 13:11 | -62.31620 | -51.67688 | 3199 | GC | station start | |
| PS118_25-1 | 2019-03-20 | 14:16 | -62.32267 | -51.67583 | 3200 | GC | at depth | |
| PS118_25-1 | 2019-03-20 | 16:30 | -62.33670 | -51.63996 | 3155 | GC | station end | |
| PS118_26-1 | 2019-03-20 | 20:11 | -62.39543 | -52.02575 | 3017 | CTDOZE | station start | |
| PS118_26-1 | 2019-03-20 | 21:17 | -62.38216 | -52.03749 | 3061 | CTDOZE | at depth | |
| PS118_26-1 | 2019-03-20 | 22:19 | -62.37049 | -52.05828 | 3003 | CTDOZE | station end | |
| PS118_27-1 | 2019-03-21 | 01:29 | -62.51659 | -52.50484 | NA | CTDOZE | station start | |
| PS118_27-1 | 2019-03-21 | 02:31 | -62.51825 | -52.50795 | 2917 | CTDOZE | at depth | |
| PS118_27-1 | 2019-03-21 | 03:46 | -62.52087 | -52.50268 | 2868 | CTDOZE | station end | |
| PS118_28-1 | 2019-03-21 | 06:06 | -62.60465 | -52.80250 | 2758 | CTDOZE | station start | |
| PS118_28-1 | 2019-03-21 | 07:11 | -62.59404 | -52.79374 | 2809 | CTDOZE | at depth | |
| PS118_28-1 | 2019-03-21 | 08:10 | -62.58499 | -52.79354 | 2808 | CTDOZE | station end | |
| PS118_29-1 | 2019-03-21 | 10:25 | -62.65764 | -53.02079 | 2413 | CTDOZE | station start | |
| PS118_29-1 | 2019-03-21 | 11:22 | -62.65357 | -53.03541 | 2411 | CTDOZE | at depth | |
| PS118_29-1 | 2019-03-21 | 12:18 | -62.65156 | -53.05356 | 2391 | CTDOZE | station end | |
| PS118_30-1 | 2019-03-21 | 13:39 | -62.71796 | -53.28744 | 1387 | CTDOZE | station start | |
| PS118_30-1 | 2019-03-21 | 14:09 | -62.71904 | -53.28947 | 1386 | CTDOZE | at depth | |
| PS118_30-1 | 2019-03-21 | 14:41 | -62.71948 | -53.28743 | 1401 | CTDOZE | station end | |

| Station | Date | Time | Latitude | Longitude | Depth [m] | Gear | Action | Comment |
|---|---|---|---|---|---|---|---|---|
| PS118_31-1 | 2019-03-21 | 19:54 | -62.71265 | -53.25739 | 1712 | MSS | station start | |
| PS118_31-1 | 2019-03-21 | 20:11 | -62.71017 | -53.26069 | 1688 | MSS | at depth | |
| PS118_31-1 | 2019-03-21 | 20:17 | -62.70975 | -53.26240 | 1638 | MSS | station end | |
| PS118_31-2 | 2019-03-21 | 20:18 | -62.70964 | -53.26264 | 1621 | MSS | station start | |
| PS118_31-2 | 2019-03-21 | 20:30 | -62.70912 | -53.26384 | 1541 | MSS | at depth | |
| PS118_31-2 | 2019-03-21 | 20:40 | -62.70796 | -53.26700 | 1525 | MSS | station end | |
| PS118_32-1 | 2019-03-21 | 21:25 | -62.76650 | -53.44983 | 851 | CTDOZE | station start | |
| PS118_32-1 | 2019-03-21 | 21:55 | -62.76301 | -53.44907 | NA | CTDOZE | at depth | |
| PS118_32-1 | 2019-03-21 | 22:20 | -62.76273 | -53.45423 | 880 | CTDOZE | station end | |
| PS118_32-2 | 2019-03-21 | 22:26 | -62.76303 | -53.45624 | 871 | MSS | station start | |
| PS118_32-2 | 2019-03-21 | 22:44 | -62.76082 | -53.45726 | 869 | MSS | at depth | |
| PS118_32-2 | 2019-03-21 | 22:53 | -62.76022 | -53.45499 | 880 | MSS | station end | |
| PS118_32-3 | 2019-03-21 | 22:54 | -62.76015 | -53.45495 | 880 | MSS | station start | |
| PS118_32-3 | 2019-03-21 | 23:00 | -62.75924 | -53.45351 | 888 | MSS | at depth | |
| PS118_32-3 | 2019-03-21 | 23:06 | -62.75780 | -53.45187 | 901 | MSS | station end | |
| PS118_32-4 | 2019-03-21 | 23:08 | -62.75759 | -53.45166 | 902 | MSS | station start | |
| PS118_32-4 | 2019-03-21 | 23:14 | -62.75677 | -53.45080 | 911 | MSS | at depth | |
| PS118_32-4 | 2019-03-21 | 23:22 | -62.75515 | -53.44991 | 930 | MSS | station end | |
| PS118_33-1 | 2019-03-22 | 00:21 | -62.80662 | -53.60267 | 415 | CTDOZE | station start | |
| PS118_33-1 | 2019-03-22 | 00:33 | -62.80441 | -53.60058 | 417 | CTDOZE | at depth | |
| PS118_33-1 | 2019-03-22 | 00:44 | -62.80344 | -53.60158 | 419 | CTDOZE | station end | |
| PS118_34-1 | 2019-03-22 | 01:32 | -62.84802 | -53.75924 | 289 | CTDOZE | station start | |
| PS118_34-1 | 2019-03-22 | 01:42 | -62.84726 | -53.75983 | 285 | CTDOZE | at depth | |
| PS118_34-1 | 2019-03-22 | 01:52 | -62.84578 | -53.76180 | 283 | CTDOZE | station end | |
| PS118_35-1 | 2019-03-22 | 03:16 | -62.92093 | -54.02885 | 292 | CTDOZE | station start | |
| PS118_35-1 | 2019-03-22 | 03:26 | -62.92033 | -54.03146 | 300 | CTDOZE | at depth | |
| PS118_35-1 | 2019-03-22 | 03:49 | -62.91974 | -54.03645 | 301 | CTDOZE | station end | |
| PS118_36-1 | 2019-03-22 | 05:30 | -62.99967 | -54.32925 | 297 | CTDOZE | station start | |
| PS118_36-1 | 2019-03-22 | 05:43 | -62.99980 | -54.32612 | 296 | CTDOZE | at depth | |
| PS118_36-1 | 2019-03-22 | 05:56 | -62.99922 | -54.32757 | 297 | CTDOZE | station end | |
| PS118_37-1 | 2019-03-22 | 06:15 | -63.02215 | -54.35389 | 351 | HS | station start | |
| PS118_37-1 | 2019-03-22 | 10:26 | -63.06823 | -54.30518 | 420 | HS | station end | |
| PS118_38-1 | 2019-03-22 | 11:40 | -63.07513 | -54.35466 | 435 | CTDOZE | station start | |
| PS118_38-1 | 2019-03-22 | 11:57 | -63.07253 | -54.35718 | 445 | CTDOZE | at depth | |
| PS118_38-1 | 2019-03-22 | 12:08 | -63.07111 | -54.35920 | 452 | CTDOZE | station end | |
| PS118_38-2 | 2019-03-22 | 12:43 | -63.08575 | -54.32062 | 412 | MUC | station start | |

| Station | Date | Time | Latitude | Longitude | Depth [m] | Gear | Action | Comment |
|---|---|---|---|---|---|---|---|---|
| PS118_38-2 | 2019-03-22 | 12:58 | -63.08259 | -54.32483 | 414 | MUC | at depth | |
| PS118_38-2 | 2019-03-22 | 13:13 | -63.08083 | -54.32861 | 417 | MUC | station end | |
| PS118_38-3 | 2019-03-22 | 13:27 | -63.07613 | -54.33454 | 425 | MUC | station start | |
| PS118_38-3 | 2019-03-22 | 13:43 | -63.07466 | -54.33709 | 427 | MUC | at depth | |
| PS118_38-3 | 2019-03-22 | 14:05 | -63.07012 | -54.34285 | 438 | MUC | station end | |
| PS118_38-4 | 2019-03-22 | 14:31 | -63.06468 | -54.34813 | 445 | GC | station start | |
| PS118_38-4 | 2019-03-22 | 14:45 | -63.06306 | -54.34952 | 447 | GC | at depth | |
| PS118_38-4 | 2019-03-22 | 15:24 | -63.06515 | -54.34728 | 444 | GC | station end | |
| PS118_38-5 | 2019-03-22 | 16:16 | -63.08241 | -54.32955 | 415 | MUC | station start | |
| PS118_38-5 | 2019-03-22 | 16:36 | -63.08286 | -54.32862 | 415 | MUC | at depth | |
| PS118_38-5 | 2019-03-22 | 16:47 | -63.08253 | -54.32908 | 415 | MUC | station end | |
| PS118_38-6 | 2019-03-22 | 17:21 | -63.06794 | -54.31299 | 423 | LAND | station start | |
| PS118_38-6 | 2019-03-22 | 18:20 | -63.06935 | -54.30300 | 416 | LAND | station end | |
| PS118_38-7 | 2019-03-22 | 19:07 | -63.08319 | -54.32603 | 414 | GC | station start | |
| PS118_38-7 | 2019-03-22 | 19:29 | -63.08109 | -54.32760 | 416 | GC | at depth | |
| PS118_38-7 | 2019-03-22 | 20:17 | -63.07972 | -54.32207 | 415 | GC | station end | |
| PS118_38-8 | 2019-03-22 | 21:04 | -63.08433 | -54.33601 | 421 | EBS | station start | |
| PS118_38-8 | 2019-03-22 | 21:26 | -63.08147 | -54.32628 | 415 | EBS | at depth | |
| PS118_38-8 | 2019-03-22 | 22:11 | -63.07168 | -54.31440 | 422 | EBS | station end | |
| PS118_38-9 | 2019-03-22 | 22:30 | -63.06317 | -54.30932 | 427 | EBS | station start | |
| PS118_38-9 | 2019-03-22 | 22:48 | -63.06325 | -54.31083 | 428 | EBS | at depth | |
| PS118_38-9 | 2019-03-22 | 23:33 | -63.06537 | -54.31255 | 427 | EBS | station end | |
| PS118_38-10 | 2019-03-23 | 00:03 | -63.05399 | -54.31544 | 441 | AGT | station start | |
| PS118_38-10 | 2019-03-23 | 00:21 | -63.05552 | -54.31667 | 442 | AGT | at depth | |
| PS118_38-10 | 2019-03-23 | 01:11 | -63.05270 | -54.32385 | 445 | AGT | station end | |
| PS118_38-11 | 2019-03-23 | 01:46 | -63.07246 | -54.31942 | 423 | AGT | station start | |
| PS118_38-11 | 2019-03-23 | 02:02 | -63.07414 | -54.32314 | 422 | AGT | at depth | |
| PS118_38-11 | 2019-03-23 | 02:41 | -63.07604 | -54.33111 | 421 | AGT | station end | |
| PS118_38-12 | 2019-03-23 | 03:33 | -63.07099 | -54.33550 | 432 | CTDOZE | station start | |
| PS118_38-12 | 2019-03-23 | 03:48 | -63.07108 | -54.33640 | 432 | CTDOZE | at depth | |
| PS118_38-12 | 2019-03-23 | 04:03 | -63.07018 | -54.33700 | 433 | CTDOZE | station end | |
| PS118_38-13 | 2019-03-23 | 04:29 | -63.06733 | -54.33596 | 434 | OFOS | station start | |
| PS118_38-13 | 2019-03-23 | 05:02 | -63.06710 | -54.33396 | 434 | OFOS | at depth | |
| PS118_38-13 | 2019-03-23 | 05:03 | -63.06705 | -54.33387 | 434 | OFOS | profile start | |
| PS118_38-13 | 2019-03-23 | 06:30 | -63.07445 | -54.31912 | 417 | OFOS | profile end | |
| PS118_38-13 | 2019-03-23 | 06:46 | -63.07583 | -54.31638 | 416 | OFOS | station end | |

143

| Station | Date | Time | Latitude | Longitude | Depth [m] | Gear | Action | Comment |
|---|---|---|---|---|---|---|---|---|
| PS118_39-1 | 2019-03-23 | 17:53 | -61.91869 | -53.33028 | 1203 | OFOS | station start | |
| PS118_39-1 | 2019-03-23 | 18:50 | -61.91197 | -53.32342 | 1179 | OFOS | profile start | |
| PS118_39-1 | 2019-03-24 | 09:58 | -61.86661 | -53.32237 | 523 | OFOS | profile end | |
| PS118_39-1 | 2019-03-24 | 10:17 | -61.86448 | -53.31968 | 523 | OFOS | station end | |
| PS118_40-1 | 2019-03-24 | 15:22 | -61.79442 | -52.09052 | 2529 | HS | profile start | |
| PS118_40-1 | 2019-03-25 | 11:41 | -61.32911 | -51.86139 | 541 | HS | profile end | |
| PS118_41-1 | 2019-03-25 | 12:10 | -61.33047 | -51.84085 | NA | CTDOZE | station start | |
| PS118_41-1 | 2019-03-25 | 12:27 | -61.32724 | -51.83770 | 546 | CTDOZE | at depth | |
| PS118_41-1 | 2019-03-25 | 12:41 | -61.32281 | -51.83623 | 549 | CTDOZE | station end | |
| PS118_42-1 | 2019-03-25 | 13:41 | -61.38957 | -51.70094 | 536 | CTDOZE | station start | |
| PS118_42-1 | 2019-03-25 | 13:57 | -61.38565 | -51.71153 | 535 | CTDOZE | at depth | |
| PS118_42-1 | 2019-03-25 | 14:11 | -61.38311 | -51.71936 | 534 | CTDOZE | station end | |
| PS118_43-1 | 2019-03-25 | 15:23 | -61.45382 | -51.53246 | 628 | CTDOZE | station start | |
| PS118_43-1 | 2019-03-25 | 15:40 | -61.45420 | -51.54271 | 627 | CTDOZE | at depth | |
| PS118_43-1 | 2019-03-25 | 16:07 | -61.45675 | -51.55042 | 631 | CTDOZE | station end | |
| PS118_44-1 | 2019-03-25 | 16:54 | -61.49758 | -51.42036 | 1847 | CTDOZE | station start | |
| PS118_44-1 | 2019-03-25 | 17:37 | -61.50261 | -51.42135 | 1997 | CTDOZE | at depth | |
| PS118_44-1 | 2019-03-25 | 18:18 | -61.50568 | -51.41466 | 2060 | CTDOZE | station end | |
| PS118_45-1 | 2019-03-25 | 19:01 | -61.53807 | -51.30476 | 2730 | CTDOZE | station start | |
| PS118_45-1 | 2019-03-25 | 20:05 | -61.54399 | -51.30895 | 2745 | CTDOZE | at depth | |
| PS118_45-1 | 2019-03-25 | 21:03 | -61.54662 | -51.30827 | 2758 | CTDOZE | station end | |
| PS118_46-1 | 2019-03-25 | 22:08 | -61.59645 | -51.14466 | 2849 | CTDOZE | station start | |
| PS118_46-1 | 2019-03-25 | 23:21 | -61.59163 | -51.14287 | 2896 | CTDOZE | at depth | |
| PS118_46-1 | 2019-03-26 | 00:15 | -61.58683 | -51.13793 | 2895 | CTDOZE | station end | |
| PS118_47-1 | 2019-03-26 | 00:30 | -61.58531 | -51.13851 | 2844 | HS | profile start | |
| PS118_47-1 | 2019-03-26 | 06:48 | -61.58710 | -51.15412 | 2837 | HS | profile end | |
| PS118_48-1 | 2019-03-26 | 08:33 | -61.60477 | -51.16286 | 2854 | MUC | station start | |
| PS118_48-1 | 2019-03-26 | 09:21 | -61.61270 | -51.14576 | 2922 | MUC | at depth | |
| PS118_48-1 | 2019-03-26 | 10:24 | -61.61049 | -51.12042 | 2945 | MUC | station end | |
| PS118_48-2 | 2019-03-26 | 11:01 | -61.58273 | -51.14149 | 2838 | MUC | station start | |
| PS118_48-2 | 2019-03-26 | 12:04 | -61.57238 | -51.13311 | 2908 | MUC | at depth | |
| PS118_48-2 | 2019-03-26 | 13:04 | -61.56231 | -51.12890 | 2895 | MUC | station end | |
| PS118_48-3 | 2019-03-26 | 13:43 | -61.55252 | -51.12829 | 2886 | GC | station start | |
| PS118_48-3 | 2019-03-26 | 14:28 | -61.54397 | -51.12910 | 2884 | GC | at depth | |
| PS118_48-3 | 2019-03-26 | 15:52 | -61.53004 | -51.14687 | 2817 | GC | station end | |
| PS118_49-1 | 2019-03-26 | 17:01 | -61.47239 | -51.47908 | 1263 | Glider | station start | |

| Station | Date | Time | Latitude | Longitude | Depth [m] | Gear | Action | Comment |
|---|---|---|---|---|---|---|---|---|
| PS118_49-1 | 2019-03-26 | 18:00 | -61.47617 | -51.50098 | 1225 | Glider | station end | |
| PS118_49-2 | 2019-03-26 | 18:11 | -61.47751 | -51.50663 | 1242 | CTDOZE | station start | |
| PS118_49-2 | 2019-03-26 | 18:40 | -61.48055 | -51.51807 | 1212 | CTDOZE | at depth | |
| PS118_49-2 | 2019-03-26 | 19:15 | -61.48391 | -51.51647 | 1322 | CTDOZE | station end | |
| PS118_49-3 | 2019-03-26 | 19:16 | -61.48408 | -51.51616 | 1352 | MSS | station start | |
| PS118_49-3 | 2019-03-26 | 19:35 | -61.48736 | -51.51304 | 1393 | MSS | at depth | |
| PS118_49-3 | 2019-03-26 | 19:36 | -61.48742 | -51.51311 | 1393 | MSS | station end | |
| PS118_49-4 | 2019-03-26 | 19:42 | -61.49132 | -51.51388 | 1329 | MSS | station start | |
| PS118_49-4 | 2019-03-26 | 19:50 | -61.49132 | -51.51388 | 1329 | MSS | at depth | |
| PS118_49-4 | 2019-03-26 | 19:50 | -61.49132 | -51.51388 | 1329 | MSS | station end | |
| PS118_49-5 | 2019-03-26 | 19:57 | -61.49522 | -51.51258 | 1485 | MSS | station start | |
| PS118_49-5 | 2019-03-26 | 20:05 | -61.49522 | -51.51258 | 1485 | MSS | at depth | |
| PS118_49-5 | 2019-03-26 | 20:13 | -61.49753 | -51.51134 | 1550 | MSS | station end | |
| PS118_50-1 | 2019-03-26 | 20:56 | -61.48102 | -51.44802 | 1590 | MSS | station start | |
| PS118_50-1 | 2019-03-26 | 21:11 | -61.48429 | -51.44548 | 1579 | MSS | at depth | |
| PS118_50-1 | 2019-03-26 | 21:20 | -61.48429 | -51.44548 | 1579 | MSS | station end | |
| PS118_50-2 | 2019-03-26 | 21:22 | -61.48863 | -51.44000 | 1818 | MSS | station start | |
| PS118_50-2 | 2019-03-26 | 21:37 | -61.48863 | -51.44000 | 1818 | MSS | at depth | |
| PS118_50-2 | 2019-03-26 | 21:38 | -61.48875 | -51.43964 | 1824 | MSS | station end | |
| PS118_51-1 | 2019-03-27 | 03:46 | -60.84627 | -50.19488 | 1864 | CTDOZE | station start | |
| PS118_51-1 | 2019-03-27 | 04:32 | -60.84682 | -50.19829 | 1899 | CTDOZE | at depth | |
| PS118_51-1 | 2019-03-27 | 05:18 | -60.84671 | -50.20604 | 1855 | CTDOZE | station end | |
| PS118_52-1 | 2019-03-27 | 06:01 | -60.84804 | -50.00287 | 2077 | CTDOZE | station start | |
| PS118_52-1 | 2019-03-27 | 06:54 | -60.85041 | -50.00329 | 2147 | CTDOZE | at depth | |
| PS118_52-1 | 2019-03-27 | 07:53 | -60.85072 | -49.99767 | 2110 | CTDOZE | station end | |
| PS118_53-1 | 2019-03-27 | 09:19 | -60.84361 | -49.76426 | 1582 | CTDOZE | station start | |
| PS118_53-1 | 2019-03-27 | 10:14 | -60.85177 | -49.76053 | 2599 | CTDOZE | at depth | |
| PS118_53-1 | 2019-03-27 | 11:15 | -60.86003 | -49.76199 | 2645 | CTDOZE | station end | |
| PS118_54-1 | 2019-03-27 | 12:21 | -60.84358 | -49.59614 | 2695 | CTDOZE | station start | |
| PS118_54-1 | 2019-03-27 | 13:17 | -60.84060 | -49.59167 | 2689 | CTDOZE | at depth | |
| PS118_54-1 | 2019-03-27 | 14:23 | -60.83807 | -49.59052 | 2687 | CTDOZE | station end | |
| PS118_55-1 | 2019-03-27 | 15:08 | -60.84546 | -49.39853 | 2529 | CTDOZE | station start | |
| PS118_55-1 | 2019-03-27 | 16:10 | -60.84741 | -49.39072 | 2553 | CTDOZE | at depth | |
| PS118_55-1 | 2019-03-27 | 17:02 | -60.85055 | -49.39557 | 2521 | CTDOZE | station end | |
| PS118_56-1 | 2019-03-27 | 18:04 | -60.84411 | -49.19704 | 1830 | CTDOZE | station start | |
| PS118_56-1 | 2019-03-27 | 18:44 | -60.84420 | -49.20560 | 1903 | CTDOZE | at depth | |

145

| Station | Date | Time | Latitude | Longitude | Depth [m] | Gear | Action | Comment |
|---------|------|------|----------|-----------|-----------|------|--------|---------|
| PS118_56-1 | 2019-03-27 | 19:31 | -60.84780 | -49.20799 | 1939 | CTDOZE | station end | |
| PS118_57-1 | 2019-03-27 | 20:31 | -60.84409 | -49.00525 | 1092 | CTDOZE | station start | |
| PS118_57-1 | 2019-03-27 | 21:00 | -60.84470 | -49.00383 | 1122 | CTDOZE | at depth | |
| PS118_57-1 | 2019-03-27 | 21:26 | -60.84417 | -48.99885 | 1120 | CTDOZE | station end | |
| PS118_58-1 | 2019-03-27 | 23:06 | -60.85190 | -48.53454 | 2074 | CTDOZE | station start | |
| PS118_58-1 | 2019-03-27 | 23:13 | -60.85176 | -48.53393 | 2076 | CTDOZE | station end | |
| PS118_58-1 | 2019-03-27 | 23:15 | -60.85172 | -48.53381 | 2076 | CTDOZE | station start | |
| PS118_58-1 | 2019-03-27 | 23:59 | -60.85388 | -48.53281 | 2090 | CTDOZE | at depth | |
| PS118_58-1 | 2019-03-28 | 00:49 | -60.85662 | -48.53207 | 2109 | CTDOZE | station end | |
| PS118_59-1 | 2019-03-28 | 02:09 | -60.84634 | -48.19564 | 2632 | CTDOZE | station start | |
| PS118_59-1 | 2019-03-28 | 03:04 | -60.85048 | -48.19652 | 2632 | CTDOZE | at depth | |
| PS118_59-1 | 2019-03-28 | 04:13 | -60.85525 | -48.19642 | 2585 | CTDOZE | station end | |
| PS118_60-1 | 2019-03-28 | 05:16 | -60.84454 | -47.89730 | 2179 | CTDOZE | station start | |
| PS118_60-1 | 2019-03-28 | 06:08 | -60.85148 | -47.90093 | 2253 | CTDOZE | at depth | |
| PS118_60-1 | 2019-03-28 | 07:17 | -60.85538 | -47.89946 | 2267 | CTDOZE | station end | |
| PS118_61-1 | 2019-03-28 | 08:46 | -60.84680 | -47.51763 | 1967 | CTDOZE | station start | |
| PS118_61-1 | 2019-03-28 | 09:32 | -60.84989 | -47.51720 | 1973 | CTDOZE | at depth | |
| PS118_61-1 | 2019-03-28 | 10:11 | -60.84981 | -47.51483 | 1959 | CTDOZE | station end | |
| PS118_62-1 | 2019-03-28 | 13:11 | -60.92875 | -46.55891 | 327 | CTDOZE | station start | |
| PS118_62-1 | 2019-03-28 | 13:22 | -60.93071 | -46.55865 | 327 | CTDOZE | at depth | |
| PS118_62-1 | 2019-03-28 | 13:37 | -60.93238 | -46.55996 | 328 | CTDOZE | station end | |
| PS118_62-2 | 2019-03-28 | 13:44 | -60.93328 | -46.55947 | 328 | MUC | station start | |
| PS118_62-2 | 2019-03-28 | 13:57 | -60.93356 | -46.55874 | 329 | MUC | at depth | |
| PS118_62-2 | 2019-03-28 | 14:09 | -60.93405 | -46.55930 | 328 | MUC | station end | |
| PS118_62-3 | 2019-03-28 | 14:20 | -60.93472 | -46.55862 | 328 | MUC | station start | |
| PS118_62-3 | 2019-03-28 | 14:34 | -60.93487 | -46.55807 | 329 | MUC | at depth | |
| PS118_62-3 | 2019-03-28 | 14:57 | -60.93455 | -46.55825 | 327 | MUC | station end | |
| PS118_62-4 | 2019-03-28 | 15:26 | -60.92933 | -46.55934 | 327 | GC | station start | |
| PS118_62-4 | 2019-03-28 | 15:38 | -60.92898 | -46.56180 | 327 | GC | at depth | |
| PS118_62-4 | 2019-03-28 | 16:13 | -60.93031 | -46.56560 | 328 | GC | station end | |
| PS118_63-1 | 2019-03-28 | 20:18 | -61.12551 | -47.74454 | 2633 | GC | station start | |
| PS118_63-1 | 2019-03-28 | 21:11 | -61.12369 | -47.73379 | 2627 | GC | at depth | |
| PS118_63-1 | 2019-03-28 | 22:15 | -61.12110 | -47.74062 | 2623 | GC | station end | |
| PS118_64-1 | 2019-03-29 | 00:58 | -61.12430 | -48.28734 | 2748 | GC | station start | |
| PS118_64-1 | 2019-03-29 | 01:43 | -61.12402 | -48.28354 | 2749 | GC | at depth | |
| PS118_64-1 | 2019-03-29 | 02:41 | -61.12511 | -48.29077 | 2806 | GC | station end | |

| Station | Date | Time | Latitude | Longitude | Depth [m] | Gear | Action | Comment |
|---|---|---|---|---|---|---|---|---|
| PS118_65-1 | 2019-03-29 | 04:45 | -61.12464 | -48.92057 | 2855 | GC | station start | |
| PS118_65-1 | 2019-03-29 | 05:37 | -61.12246 | -48.92018 | 2850 | GC | at depth | |
| PS118_65-1 | 2019-03-29 | 06:47 | -61.12636 | -48.90027 | 2865 | GC | station end | |
| PS118_66-1 | 2019-03-29 | 12:20 | -61.16710 | -49.70795 | 2892 | GC | station start | |
| PS118_66-1 | 2019-03-29 | 13:06 | -61.16833 | -49.70587 | 2944 | GC | at depth | |
| PS118_66-1 | 2019-03-29 | 14:10 | -61.16809 | -49.70394 | 2945 | GC | station end | |
| PS118_67-1 | 2019-03-29 | 20:06 | -61.08233 | -51.55403 | 1011 | HS | station start | |
| PS118_67-1 | 2019-03-29 | 20:06 | -61.08233 | -51.55403 | 1011 | HS | profile start | |
| PS118_67-1 | 2019-03-30 | 05:37 | -61.07450 | -51.87527 | 873 | HS | profile end | |
| PS118_67-1 | 2019-03-30 | 05:40 | -61.07645 | -51.87819 | 881 | HS | station end | |
| PS118_68-1 | 2019-03-30 | 11:27 | -61.34878 | -52.05684 | 534 | HS | station start | |
| PS118_68-1 | 2019-03-30 | 11:27 | -61.34875 | -52.05281 | 531 | HS | profile start | |
| PS118_68-1 | 2019-03-31 | 00:36 | -61.19750 | -50.97617 | 1965 | HS | profile end | |
| PS118_68-1 | 2019-03-31 | 00:37 | -61.19770 | -50.97688 | 1956 | HS | station end | |
| PS118_69-1 | 2019-03-31 | 01:12 | -61.19045 | -50.98376 | 1742 | OFOS | station start | |
| PS118_69-1 | 2019-03-31 | 01:54 | -61.19435 | -50.99961 | 1817 | OFOS | profile start | |
| PS118_69-1 | 2019-03-31 | 08:28 | -61.20894 | -51.04970 | 2152 | OFOS | profile end | |
| PS118_69-1 | 2019-03-31 | 09:32 | -61.20596 | -51.01739 | 2205 | OFOS | station end | |
| PS118_70-1 | 2019-03-31 | 09:49 | -61.20399 | -51.00712 | 2187 | OFOS | station start | |
| PS118_70-1 | 2019-03-31 | 10:43 | -61.20317 | -51.01070 | 2181 | OFOS | at depth | |
| PS118_70-1 | 2019-03-31 | 10:44 | -61.20318 | -51.01096 | 2189 | OFOS | profile start | |
| PS118_70-1 | 2019-03-31 | 15:02 | -61.19061 | -51.09415 | 1666 | OFOS | profile end | |
| PS118_70-1 | 2019-03-31 | 15:38 | -61.19297 | -51.09639 | 1673 | OFOS | station end | |
| PS118_71-1 | 2019-03-31 | 18:50 | -61.07752 | -51.77422 | 890 | Glider | information | |
| PS118_71-1 | 2019-03-31 | 19:17 | -61.07620 | -51.77505 | 896 | Glider | station end | |
| PS118_71-2 | 2019-03-31 | 19:52 | -61.07696 | -51.76951 | 893 | CTDOZE | station start | |
| PS118_71-2 | 2019-03-31 | 20:21 | -61.07737 | -51.77434 | 890 | CTDOZE | at depth | |
| PS118_71-2 | 2019-03-31 | 20:48 | -61.07744 | -51.77916 | 887 | CTDOZE | station end | |
| PS118_72-1 | 2019-03-31 | 21:14 | -61.05268 | -51.73868 | 972 | HS | station start | |
| PS118_72-1 | 2019-03-31 | 21:14 | -61.05265 | -51.73862 | 972 | HS | profile start | |
| PS118_72-1 | 2019-04-01 | 03:03 | -60.84193 | -50.15100 | 1795 | HS | profile end | |
| PS118_72-1 | 2019-04-01 | 06:49 | -60.84611 | -49.83389 | 2489 | HS | station end | |
| PS118_73-1 | 2019-04-01 | 03:22 | -60.84621 | -50.13068 | 1841 | HF | station start | |
| PS118_73-1 | 2019-04-01 | 04:07 | -60.84550 | -50.13358 | 1838 | HF | at depth | |
| PS118_73-1 | 2019-04-01 | 04:58 | -60.84495 | -50.13706 | 1838 | HF | station end | |
| PS118_74-1 | 2019-04-01 | 07:19 | -60.83945 | -49.84085 | 2485 | HF | station start | |

| Station | Date | Time | Latitude | Longitude | Depth [m] | Gear | Action | Comment |
|---------|------|------|----------|-----------|-----------|------|--------|---------|
| PS118_74-1 | 2019-04-01 | 08:13 | -60.83966 | -49.83570 | 2502 | HF | at depth | |
| PS118_74-1 | 2019-04-01 | 09:13 | -60.84049 | -49.83478 | 2499 | HF | station end | |
| PS118_75-1 | 2019-04-01 | 10:13 | -60.85205 | -49.65800 | 2652 | MUC | station start | |
| PS118_75-1 | 2019-04-01 | 11:10 | -60.85266 | -49.65408 | 2643 | MUC | at depth | |
| PS118_75-1 | 2019-04-01 | 12:06 | -60.85285 | -49.65445 | 2647 | MUC | station end | |
| PS118_75-2 | 2019-04-01 | 12:39 | -60.85264 | -49.65167 | 2644 | GC | station start | |
| PS118_75-2 | 2019-04-01 | 13:22 | -60.85233 | -49.65173 | 2653 | GC | at depth | |
| PS118_75-2 | 2019-04-01 | 14:22 | -60.85168 | -49.64607 | 2650 | GC | station end | |
| PS118_76-1 | 2019-04-01 | 15:48 | -60.84675 | -49.39378 | 2508 | HF | station start | |
| PS118_76-1 | 2019-04-01 | 16:44 | -60.84731 | -49.39687 | 2513 | HF | at depth | |
| PS118_76-1 | 2019-04-01 | 17:51 | -60.85101 | -49.39391 | 2503 | HF | station end | |
| PS118_77-1 | 2019-04-01 | 19:33 | -60.89333 | -48.89474 | 1025 | OFOS | station start | |
| PS118_77-1 | 2019-04-01 | 20:11 | -60.88876 | -48.89770 | 1026 | OFOS | at depth | |
| PS118_77-1 | 2019-04-01 | 20:11 | -60.88876 | -48.89776 | 1027 | OFOS | profile start | |
| PS118_77-1 | 2019-04-01 | 20:49 | -60.88677 | -48.90973 | 1032 | OFOS | profile end | |
| PS118_77-1 | 2019-04-01 | 21:15 | -60.88840 | -48.91350 | 1030 | OFOS | station end | |
| PS118_77-2 | 2019-04-01 | 22:34 | -60.88622 | -48.89726 | 1028 | AGT | station start | |
| PS118_77-2 | 2019-04-01 | 23:21 | -60.88278 | -48.91958 | 1036 | AGT | at depth | |
| PS118_77-2 | 2019-04-02 | 00:49 | -60.87825 | -48.95157 | 1048 | AGT | station end | |
| PS118_77-3 | 2019-04-02 | 01:16 | -60.88153 | -48.91736 | 1035 | EBS | station start | |
| PS118_77-3 | 2019-04-02 | 01:57 | -60.88064 | -48.92994 | 1039 | EBS | at depth | |
| PS118_77-3 | 2019-04-02 | 03:09 | -60.87865 | -48.95311 | 1048 | EBS | station end | |
| PS118_78-1 | 2019-04-02 | 05:26 | -60.84683 | -48.50297 | 2071 | GC | station start | |
| PS118_78-1 | 2019-04-02 | 06:11 | -60.84826 | -48.50473 | 2078 | GC | at depth | |
| PS118_78-1 | 2019-04-02 | 07:20 | -60.85136 | -48.48809 | 2122 | GC | station end | |
| PS118_79-1 | 2019-04-02 | 08:57 | -60.84188 | -48.22180 | 2592 | GC | station start | |
| PS118_79-1 | 2019-04-02 | 09:42 | -60.83502 | -48.21402 | 2577 | GC | at depth | |
| PS118_79-1 | 2019-04-02 | 10:49 | -60.82714 | -48.22267 | 2571 | GC | station end | |
| PS118_80-1 | 2019-04-02 | 14:14 | -60.84622 | -47.67684 | 1967 | HF | station start | |
| PS118_80-1 | 2019-04-02 | 14:53 | -60.84671 | -47.67623 | 1969 | HF | at depth | |
| PS118_80-1 | 2019-04-02 | 15:45 | -60.85023 | -47.67792 | 1980 | HF | station end | |
| PS118_81-1 | 2019-04-03 | 19:43 | -61.23123 | -50.72142 | 2255 | OFOS | station start | |
| PS118_81-1 | 2019-04-03 | 20:25 | -61.22689 | -50.71840 | 2147 | OFOS | at depth | |
| PS118_81-1 | 2019-04-03 | 20:25 | -61.22684 | -50.71843 | 2146 | OFOS | profile start | |
| PS118_81-1 | 2019-04-03 | 20:57 | -61.22154 | -50.72022 | 1898 | OFOS | profile end | |
| PS118_81-1 | 2019-04-03 | 21:45 | -61.21158 | -50.71608 | 1528 | OFOS | at depth | |

| Station | Date | Time | Latitude | Longitude | Depth [m] | Gear | Action | Comment |
|---|---|---|---|---|---|---|---|---|
| PS118_81-1 | 2019-04-03 | 21:46 | -61.21129 | -50.71599 | 1526 | OFOS | profile start | |
| PS118_81-1 | 2019-04-04 | 08:32 | -61.18872 | -50.67266 | 1204 | OFOS | profile end | |
| PS118_81-1 | 2019-04-04 | 08:56 | -61.19020 | -50.67325 | 1263 | OFOS | station end | |
| PS118_82-1 | 2019-04-04 | 13:45 | -61.22501 | -52.46028 | 1302 | Glider | station start | |
| PS118_82-1 | 2019-04-04 | 14:08 | -61.22452 | -52.47750 | NA | Glider | station end | |
| PS118_82-2 | 2019-04-04 | 14:15 | -61.22474 | -52.48114 | NA | CTDOZE | station start | |
| PS118_82-2 | 2019-04-04 | 14:39 | -61.22316 | -52.49009 | 1002 | CTDOZE | at depth | |
| PS118_82-2 | 2019-04-04 | 15:00 | -61.22078 | -52.49532 | 1038 | CTDOZE | station end | |

| **Gear abbreviations** | **Gear** |
|---|---|
| ADCP_150 | ADCP 150kHz |
| AFIM | AutoFim |
| AGT | Agassiz Trawl |
| CTDOZE | CTD AWI-OZE |
| EBS | Epibenthossledge |
| FBOX | FerryBox |
| GC | Gravity Corer |
| GRAV | Sea Gravimeter |
| Glider | MAPPA |
| HF | Heat Flow Probe |
| HS | Hydrosweep |
| HVAIR | High Volume Air Sampler |
| ICEBUCKET | Ice fishing |
| ICEOBS | Ice Observation |
| LAND | Lander |
| MAG | Magnetometer |
| MSS | Mikrostruktur Sonde |
| MUC | Multi Corer |
| OFOS | Ocean Floor Observation System |
| PCO2_GO | pCO2 GO |
| PCO2_SUB | pCO2 Subctech |
| REL | Releaser |
| RM | Radiation Measurements |
| ROV | Remotely Operated Vehicle |
| SVP | Sound Velocity Profiler |
| TSG_KEEL | Thermosalinograph Keel |
| TSG_KEEL_2 | Thermosalinograph Keel 2 |
| TVMUC | Video Multi Corer |
| UCTD | Underway CTD |
| WST | Weatherstation |

Die **Berichte zur Polar- und Meeresforschung** (ISSN 1866-3192) werden beginnend mit dem Band 569 (2008) als Open-Access-Publikation herausgegeben. Ein Verzeichnis aller Bände einschließlich der Druckausgaben (ISSN 1618-3193, Band 377-568, von 2000 bis 2008) sowie der früheren **Berichte zur Polarforschung** (ISSN 0176-5027, Band 1-376, von 1981 bis 2000) befindet sich im electronic Publication Information Center **(ePIC)** des Alfred-Wegener-Instituts, Helmholtz-Zentrum für Polar- und Meeresforschung (AWI); see https://epic.awi.de. Durch Auswahl "Reports on Polar- and Marine Research" (via "browse"/"type") wird eine Liste der Publikationen, sortiert nach Bandnummer, innerhalb der absteigenden chronologischen Reihenfolge der Jahrgänge mit Verweis auf das jeweilige pdf-Symbol zum Herunterladen angezeigt.

The **Reports on Polar and Marine Research** (ISSN 1866-3192) are available as open access publications since 2008. A table of all volumes including the printed issues (ISSN 1618-3193, Vol. 377-568, from 2000 until 2008), as well as the earlier **Reports on Polar Research** (ISSN 0176-5027, Vol. 1-376, from 1981 until 2000) is provided by the electronic Publication Information Center **(ePIC)** of the Alfred Wegener Institute, Helmholtz Centre for Polar and Marine Research (AWI); see URL https://epic.awi.de. To generate a list of all Reports, use the URL http://epic.awi.de and select "browse"/ "type" to browse "Reports on Polar and Marine Research". A chronological list in declining order will be presented, and pdf-icons displayed for downloading.

**Zuletzt erschienene Ausgaben:**

**Recently published issues:**

**735 (2019)** The Expedition PS118 of the Research Vessel POLARSTERN to the Weddell Sea in 2019, edited by Boris Dorschel

**734 (2019)** Russian-German Cooperation: Expeditions to Siberia in 2018. Edited by Stefan Kruse, Dmitry Bolshiyanov, Mikhail Grigoriev, Anne Morgenstern, Luidmila Pestryakova, Leonid Tsibizov, Annegret Udke

**733 (2019)** Expeditions to Antarctica: ANT-Land 2018/19 Neumayer Station III, Kohnen Station, Flight Operations and Field Campaigns, edited by Tanja Fromm, Constance Oberdieck, Tim Heitland, Peter Köhler

**732 (2019)** The Expedition PS117 of the Research Vessel POLARSTERN to the Weddell Sea in 2018/2019, edited by Olaf Boebel

**731 (2019)** The Expedition PS116 of the Research Vessel POLARSTERN to the Atlantic Ocean in 2018, edited by Claudia Hanfland and Bjela König

**730 (2019)** The Expedition PS110 of the Research Vessel POLARSTERN to the Atlantic Ocean in 2017/2018, edited by Frank Niessen

**729 (2019)** The Expedition SO261 of the Research Vessel SONNE to the Atacama Trench in the Pacific Ocean in 2018, edited by Frank Wenzhöfer

**728 (2019)** The Expedition PS115/2 of the Research Vessel POLARSTERN to the Arctic Ocean in 2018, edited by Ruediger Stein

**727 (2019)** The Expedition PS115/1 of the Research Vessel POLARSTERN to the Greenland Sea and Wandel Sea in 2018, edited by Volkmar Damm

**726 (2019)** The Expedition PS108 of the Research Vessel POLARSTERN to the Fram Strait and the AWI-HAUSGARTEN in 2017, edited by Frank Wenzhöfer

**ALFRED-WEGENER-INSTITUT**
HELMHOLTZ-ZENTRUM FÜR POLAR-
UND MEERESFORSCHUNG

**BREMERHAVEN**

Am Handelshafen 12
27570 Bremerhaven
Telefon 0471 4831-0
Telefax 0471 4831-1149
www.awi.de

**HELMHOLTZ**